

Functional Characterization of Actin Sequestering Proteins in *Plasmodium berghei*

D i s s e r t a t i o n

Zur Erlangung des akademischen Grades

d o c t o r r e r u m n a t u r a l i u m

(Dr. rer. nat.)

im Fach Biologie

eingereicht an der

Mathematischen-Naturwissenschaftlichen Fakultät I

Der Humboldt-Universität zu Berlin

von

Dipl. Biol. Marion Hliscs

Präsident der Humboldt-Universität zu Berlin

Prof. Dr. Jan-Hendrik Olberts

Dekan der Mathematischen-Naturwissenschaftlichen Fakultät I

Prof. Dr. Andreas Herrmann

1. Gutachter: Prof. Dr. Richard Lucius
2. Gutachter: Prof. Dr. Kai Matuschewski
3. Gutachter: Ph. D., D. Habil. Elena A. Levashina

Tag der mündlichen Prüfung: 17.08.2011

EIDESSTATTLICHE ERKLÄRUNG

Hiermit erkläre ich an Eides statt, die vorliegende Dissertation selbstständig angefertigt und keine anderen als die angegebenen Hilfsmittel verwendet zu haben.

Ich erkläre hiermit, dass ich an keiner anderen Universität ein Prüfungsverfahren beantragt bzw. die Dissertation in dieser oder anderer Form bereits anderweitig als Prüfungsarbeit verwendet oder einer anderen Fakultät als Dissertation vorgelegt habe.

Die vorliegende Arbeit wurde am Max Planck Institut für Infektionsbiologie, Berlin und am Hygiene Institut, Abteilung Parasitologie der Karls-Ruprechts Universität, unter Leitung von Prof. Dr. Kai Matuschewski durchgeführt.

Berlin, den 05.07.2011

Marion Hliscs

ACKNOWLEDGEMENTS

In the first place I would like to express my gratitude my supervisor Prof. Dr. Kai Matuschewski, who gave me the big opportunity to work in his lab. His tremendous and inventive support as well as his great openness regarding new ideas account importantly for my achieved work. He generously provided international congress participation and internship, which were always an exciting challenge and motivated me even more.

I would like to thank Prof. Dr. Richard Lucius for his support as my doctoral thesis supervisor at the Humboldt University and his collaboration and generosity, for using the nice microscope.

I would like to thank Prof. Dr. Michael Lanzer for the opportunity to start my work at the department of parasitology at the hygiene institute of Heidelberg.

I am grateful to Julia Sattler and Herwig Schüler for the great innovative and fruitful collaboration, for sharing knowledge and thoughts as well as antibodies and proteins. I wish we had more time working together.

I would like to thank to Nishith Gupta and Martin Blume for the prosperous collaboration and thereby bringing together research of two apicomplexan parasites.

I would like to thank to Elena Levashina and Guilla Costa for open-mindedness and testing mutant parasites and hopefully continuation of collaboration.

I would like to thank to Marcelo Jacobs-Lorena for kindly providing the CAP380 antibody.

It is a pleasure to thank all present and past members of the Matuschewskis laboratory for motivation, helpfulness and also many funny moments that created a friendly working environment: Katja B., Kaja M., Johanna, Caro, Johannes, Alyssa, Elyzana, Fifi, Jan, Sanketha, Manuel, Taco, Faustin, Diana, Vittoria. Also, a special thanks to Georgina Montagna, Olivier Silvie and Markus Ganter for inspiring discussions and supervision.

I would like to thank Ulrike Abuabed for the nice intricate transmission electron microscope pictures, which really contribute to the understanding what is going on in the parasite.

Additionally, I would like to thank Freddy Frischknecht, who provided the initial steps for working with this interesting parasite, and Stephan Hegge, Michael Kudriashev and Luis Barniol for the great time back in Heidelberg.

A big thank is for my dear friends, whose big support and appreciation over the last time helped me to manage this work; Nadja, Jana, Barbara, Anne, Wiebke, Stine, Katja and Anna.

Martin, I deeply thank you for your appreciation, patience and encouragement over the last time, which helped me to manage this work. I am happily looking forward sharing future plans with you.

From great heart I thank my family Eva and Reiner Hliscs, Thomas with family and Rudolf with family, which always supported me in any condition and their encouragement and love enables me to proceed to and to break new grounds.

SUMMARY

Plasmodium spp. are apicomplexan parasites that rely on an obligate intracellular life-style. They depend on an evolutionary conserved actin-dependent molecular motor machinery that facilitates their motility, host cell invasion and egress. Furthermore parasite actin is implicated in endocytosis during blood stages. However, the molecular mechanisms that are involved in the spatiotemporal regulation of actin-turnover are not yet understood. In this work I report implications of the actin-regulators adenyl cyclase-associated protein (C-CAP), profilin and actin depolymerization factor 1 and 2 (ADF1, ADF2) in distinct and previously unanticipated cellular processes during the life cycle of in the rodent malarial parasite *Plasmodium berghei*. By using a reverse genetic approach I tagged the endogenous *C-CAP* genetic locus to a fluorescent reporter. C-CAPmCherry localizes in the cytosol, which is consistent with its proposed G-actin sequestering activity. Gene deletion demonstrates that the G-actin binding protein C-CAP is entirely dispensable for the pathogenic blood stages and ookinete development. In *in vitro* motility assays *C-cap(-)* ookinetes exhibit a modestly impaired motility that indicates involvement of C-CAP in actin-turnover. Nevertheless, these parasites are able to infect the mosquito host. Unexpectedly however, the *c-cap(-)* mutant fails to complete oocyst maturation. Defects that emerge in this unique extracellular and non-motile replication phase include attenuation of oocysts growth, absence of oocyst compartmentation and impeded nuclear divisions. These findings indicate previously unrecognized functions of the C-CAP protein in the malarial parasites. Successful trans-species complementation with the *C. parvum* *C-CAP* ortholog, rescues the *c-cap(-)* phenotype and proves functional redundancy between apicomplexan CAP proteins. Furthermore, the actin regulator *profilin* fails to rescue the defects of *c-cap(-)* parasites, despite sharing its actin sequestering activity with C-CAP. Taken together, C-CAP is the first G-actin sequestering protein of *Plasmodium* species that is not required for motility but performs essential functions during oocyst maturation instead.

Characterization of the actin regulators profilin, ADF1 and ADF2 revealed dramatic transcriptional down-regulation and the absence of the profilin protein in sporozoites. To test whether G-actin binding proteins interfere with sporozoite functions, I ectopically overexpressed of *profilin* and *C-CAP* stage-specifically in sporozoites. In these recombinant parasites, but not in control lines, demonstrate that overexpression abolishes salivary gland invasion and arrests their lifecycle.

Based on these unexpected findings and the available literature data, I developed a “minimalistic model” for actin regulation in sporozoites that predicts ADF1 as the main actin-turnover regulating factor.

ZUSAMMENFASSUNG

Plasmodien spp. sind einzellige eukaryotische Parasiten, welche sich mittels eines evolutionär konservierten und aktinabhängigen molekularen Motors fortbewegen. Diese spezielle Art der Fortbewegung ermöglicht dem Parasiten einen aktiven Wirtszellein- und -austritt und damit die Etablierung seines pathogenen Lebenszyklusses. Des Weiteren ist bekannt, dass Aktin an der Endozytose in den parasitären Blutstadien beteiligt ist. Die molekularen Mechanismen, welche das Aktinfließgleichgewicht zeitlich und räumlich regulieren, sind bisher für *Plasmodien* nicht vollkommen verstanden.

In dieser Arbeit werden die G-Aktin (globuläres Aktin) bindenden Regulatoren, wie das Cyclase- assoziierte Protein (C-CAP), das Profilin sowie die Aktin depolymerisierenden Faktoren 1 und 2 (ADF1, ADF2) in *Plasmodium berghei* charakterisiert.

Mittels genetischer Geninaktivierung zeige ich, dass das *C-CAP* Gen nicht für die Entwicklung von pathogenen Blutstadien und Ookineten in *P. berghei* notwendig ist. *In vitro* Motilitätsuntersuchungen an Ookineten bestätigen eine verminderte Geschwindigkeit der *c-cap(-)* Mutanten, was auf einen aktinabhängigen Prozess hindeutet. Die Fähigkeit den Wirt (Moskito) zu infizieren wird dadurch jedoch nicht aufgehoben. Mit Hilfe der Mutante kann ich zeigen, dass

C-CAP eine lebensnotwendige Funktion während der Oozystenreifung und Sporozoitenentwicklung in dem invertebraten Wirt besitzt. Die durch den Mangel an C-CAP auftretenden Defekte während der extrazellulären Vermehrungsphase sind eine Verminderung des Oozystenwachstums, das Fehlen der Oozystenkompartimentierung und die unvollständigen finalen Kernteilungen. Diese Ergebnisse deuten auf neue, bisher nicht beschriebene Funktionen, des C-CAP Proteins hin. Die erfolgreiche speziesübergreifende Komplementierung der *c-cap(-)* Defekte mit dem orthologen Gen aus *Cryptosporidium parvum* *CpC-CAP* bestätigt die funktionale Redundanz zwischen beiden Proteinen. Profilin, als ein weiteres G-Aktin bindendes Protein, war hingegen nicht in der Lage die Defekte des *c-cap(-)* Parasiten auszugleichen und zeigt damit deutlich, dass beide Proteine keine funktionellen Redundanzen während des Oocystenwachstums besitzen. Mittels transgener Parasiten welche ein C-CAPmCherry Fusionsprotein exprimieren, wird das C-CAP Protein im Zytoplasma lokalisiert. Erstmals wird mit dieser Arbeit ein G-Aktin bindendes Protein, C-CAP beschrieben, welches eine essentielle Funktion während der Oozystenreifung in *Plasmodium berghei* besitzt.

Im zweiten Teil der Arbeit werden die Aktinregulatoren Profilin, ADF1 und ADF2 eingehender untersucht.

Es wird eine dramatische Abnahme der Profilin und ADF1 Transkripte in Sporozoiten beobachtet. Außerdem wird die Abwesenheit des Profilin Proteins in Sporozoiten nachgewiesen.

Zur Überprüfung des Einflusses von G-Aktin bindenden Proteinen auf die Funktion der Sporozoiten, habe ich *Profilin* und das *C-CAP* spezifisch in diesem Stadium überexprimiert. Diese Parasiten sind nicht in der Lage die Speicheldrüsen des Wirtes zu besiedeln, was eine Unterbrechung des Lebenszykluses hervorruft. Ebenfalls untersuchte Kontrollgruppen zeigen diesen Defekt jedoch nicht.

Aufbauend auf diesen Ergebnissen entwickle ich ein „minimalistisches“ Model zur Beschreibung der Aktinregulation in Sporozoiten, in welchem das ADF1 als regulatorisches Protein im Mittelpunkt steht.

TABLE OF CONTENTS

EIDESSTATTLICHE ERKLÄRUNG

ACKNOWLEDGEMENTS

SUMMARY.....	1
ZUSAMMENFASSUNG	3
TABLE OF CONTENTS.....	5
LIST OF FIGURES	10
LIST OF TABLES	12
LIST OF ABBREVIATIONS.....	13
1. Introduction	17
1.1. Cell motility and the actin cytoskeleton in eukaryotic cells.....	17
1.1.1. Actin biochemistry and polymerization dynamics.....	18
1.1.2. Actin cytoskeleton regulating proteins.....	19
1.1.2.1. Nucleation proteins enhance actin filament elongation	19
1.1.2.2. Capping proteins terminate filament growth.....	20
1.1.2.3. <u>A</u> ctin <u>d</u> epolymerizing <u>f</u> actors (ADF) enhance actin filament disassembly.....	22
1.1.2.4. G-actin binding proteins control actin treadmilling	22
1.1.3. The <u>S</u> uppressor of <u>R</u> AS ^{V19} / <u>c</u> yclase- <u>a</u> ssociate protein Srv2/CAP (CAP)	23
1.2. Apicomplexan parasites and their molecular motor.....	26
1.2.1. The motile stages of <i>Plasmodium</i>	28
1.2.2. Apicomplexan actins and the special case of <i>Plasmodium</i>	29
1.2.3. A minimal repertoire of actin-binding proteins.....	30
1.2.3.1. <i>Plasmodium</i> F-actin binding proteins facilitate actin filament nucleation and stabilization	31
1.2.3.2. <i>Plasmodium</i> G-actin binding proteins control the actin treadmilling process	33
1.2.4. CAP-homology protein in apicomplexan parasites.....	34
1.2.4.1. <i>Cryptosporidium parvum</i> C-CAP (CpC-CAP) sequesters G-actin	35
1.2.4.2. The crystal structure of the apicomplexan <i>Cryptosporidium parvum</i> C-CAP protein.....	35
1.3. Objective of this study:	37

2. Material and Methods.....	39
2.1. Materials.....	39
2.1.1. Biological resources:	39
2.1.2. Laboratory equipment	39
2.1.3. Laboratory materials	41
2.1.3.1. Miscellaneous.....	41
2.1.3.2. Chemicals	42
2.1.4. Commercial Kits	44
2.1.5. Enzymes	44
2.1.6. Media.....	44
2.1.7. Stock and working solutions	45
2.1.8. Buffers	46
2.1.9. Antibodies	47
2.1.9.1. Antibody generation.....	48
2.1.10. Molecular cloning	49
2.1.10.1. <i>Plasmodium</i> target vector.....	49
2.1.10.2. Oligonucleotides for molecular cloning and genotyping	50
2.1.10.3. Oligonucleotides for expression profiling.....	52
2.1.11. Software	52
2.2. Methods.....	53
2.2.1. Microbiological methods.....	53
2.2.1.1. Transformation of <i>Escherichia coli</i> (<i>E. coli</i>)	53
2.2.1.2. Culturing <i>E. coli</i> on agar plates	53
2.2.1.3. Culturing <i>E. coli</i> in liquid medium.....	54
2.2.1.4. Long-term storage of Bacteria.....	54
2.2.2. Molecular biological methods.....	54
2.2.2.1. Polymerase chain reaction (PCR)	54
2.2.2.2. Complementary DNA (cDNA) synthesis by reverse transcription (RT)	55
2.2.2.3. Qualitative real time-PCR (qRT-PCR)	55
2.2.2.4. Quantitative Real Time PCR (qRT-PCR)	55
2.2.2.5. Agarose gel electrophoresis	57
2.2.2.6. DNA purification by ethanol precipitation.....	57
2.2.2.7. DNA purification by gel-extraction (Quiagen)	57
2.2.2.8. DNA purification by PCR purification Kit (Quiagen)	58

2.2.2.9. Determination of DNA concentration	58
2.2.2.10. Vector and Insert preparation	58
2.2.2.11. Ligation of DNA fragments	59
2.2.2.12. Plasmid DNA preparation	59
2.2.2.13. Sequencing of DNA fragments	59
2.2.3. Methods for <i>Plasmodium berghei</i>	59
2.2.3.1. Transfection of <i>Plasmodium berghei</i> parasites	59
2.2.3.2. Transfection schizont culture of <i>P. berghei</i>	60
2.2.3.3. Schizont Isolation	60
2.2.3.4. Transfection of <i>P. berghei</i> schizonts by electroporation	60
2.2.3.5. Positive selection of recombinant parasites	61
2.2.3.6. Long-term storage of blood stage parasites	61
2.2.3.7. Giemsa-stained blood smears and determination of parasitemia	61
2.2.3.8. Preparations of <i>P. berghei</i> blood stage parasites	62
2.2.3.9. Genomic DNA (gDNA) preparations from <i>P. berghei</i>	62
2.2.3.10. Isolation messenger RNA (mRNA) from <i>P. berghei</i>	62
2.2.3.11. Parasite cloning	63
2.2.3.12. Blood stage development / Growth curve analysis of <i>P. berghei</i>	63
2.2.3.13. Exflagellation assay of male gametocytes	63
2.2.3.14. Gametocyte enrichment and purification	63
2.2.3.15. Mosquito infection with <i>P. berghei</i>	64
2.2.3.16. Ookinete culture and purification	64
2.2.3.17. Ookinete indirect immuno fluorescence (IFA)	65
2.2.3.18. Ookinete motility assay	65
2.2.3.19. Ookinete microinjection into the mosquito	66
2.2.3.20. Propagation of <i>Anopheles stephensi</i> mosquitoes	67
2.2.3.21. Mosquito midgut preparation and infectivity determination	67
2.2.3.22. Midgut preparation for electron microscopy (TEM)	67
2.2.3.23. Transmission electron microscopy of midgut-associated oocysts	67
2.2.3.24. Oocyst number and size determination	68
2.2.3.25. Life death assay with SYTOX® Orange on midgut associated oocysts	68
2.2.3.26. IFA on oocysts	68
2.2.3.27. Isolation of midgut and salivary gland associated sporozoites	68
2.2.3.28. Isolation of hemocoel associated sporozoites	69

2.2.3.29. IFA on sporozoite stages	69
2.2.3.30. Sporozoite motility assay	69
2.2.3.31. Transmission of sporozoites to mice and determination of the prepatent period.....	70
2.2.3.32. Propagation of mammalian cells	70
2.2.3.33. Infection of Huh7 <i>cells in vitro</i> / development of exoerythrocytic stages (EEF)	70
2.2.3.34. Fixation of EEFs.....	71
2.2.3.35. Live cell imaging.....	71
2.2.3.36. Sample preparation for western blot (denaturing conditions)	71
2.2.4. Protein biochemical assays.....	72
2.2.4.1. Protein analysis by SDS-PAGE	72
2.2.4.2. Western blot analysis	72
2.2.4.3. Indirect immuno-detection by luminescence	72
3. Results	75
3.1. Characterization of the cyclase-associated protein (C-CAP) in <i>P. berghei</i>	75
3.1.1. Annotation of the <i>Plasmodium C-CAP</i> gene.....	75
3.1.2. Systematic <i>C-CAP</i> gene expression profiling	76
3.1.3. C-CAP is not essential for <i>Plasmodium</i> blood stage development.....	78
3.1.4. Phenotypic analysis of <i>c-cap(-)</i> parasite line	79
3.1.4.1. C-CAP is dispensable for blood stage replication <i>in vivo</i>	79
3.1.4.2. <i>C-cap(-)</i> parasites exhibit reduced ookinete velocity.....	80
3.1.4.3. C-CAP is essential for <i>Plasmodium</i> oocyst development in the mosquito midgut.....	81
3.1.4.4. Expression and localization of the circumsporozoite protein (CSP) and the oocyst capsule protein CAP380 are unaffected by deletion of <i>C-CAP</i> and do not contribute to the maturation phenotype.....	85
3.1.4.5. The oocyst maturation defect in <i>c-cap(-)</i> parasites is independent of ookinete motility	88
3.1.4.6. Transmission Electron Microscopy (TEM) reveals the absence of inner membrane retraction and confirms the DNA segregation defect during oocyst maturation	88
3.1.5. Localization of the C-CAPmCherry fusion protein	93

3.1.5.1. Expression of the C-CAPmCherry fusion protein reverts the <i>c-cap(-)</i> phenotype	94
3.1.5.2. C-CAPmCherry displays cytoplasmic localization during blood stage development	95
3.1.5.3. C-CAPmCherry protein abundance	100
3.1.6. Trans-species complementation with the <i>Cryptosporidium parvum</i>	101
3.1.6.1. Generation of CpC-CAP complementation parasites.....	101
3.1.6.2. <i>Cryptosporidium parvum</i> C-CAP reverts the defects of the <i>Plasmodium berghei</i> C-CAP knockout phenotype.	102
3.1.6.3. Mutagenesis of CpC-CAP	104
3.1.6.4. The CpC-CAP ^{STOP} mutant protein is degraded <i>in vivo</i>	107
3.1.7. Profilin could not rescue the <i>c-cap(-)</i> defects	109
3.2. Characterization of the G-actin binding proteins profilin, actin depolymerizing factor 1 and 2 (ADF1, ADF2) in <i>Plasmodium</i>	112
3.2.1. Gene expression and protein abundance of G-actin binding proteins decrease during sporozoite development in <i>P. berghei</i>	112
3.2.2. Profilin and ADF1 localize to the cytoplasm	115
3.2.2.1. A subpopulation of profilin is localized to the plasma membrane in ookinetes ..	117
3.2.3. Stage-specific overexpression and tagging of <i>P. berghei</i> C-CAP and <i>profilin</i>	118
3.2.3.1. Genetic strategy and generation of parasites with stage-specific overexpression of <i>Flag</i> - tagged C-CAP or <i>profilin</i>	119
3.2.4. Phenotypic analysis of <i>csp/ctrp_flag_c-cap/profilin</i> recombinant parasites.....	122
3.2.4.1. Transgenic parasites that overexpress C-CAP or <i>profilin</i> in the ookinete stage display normal life cycle progression	122
3.2.4.2. Transgenic parasites that overexpress C-CAP or <i>profilin</i> under control of the <i>CSP</i> promoter exhibit ectopic protein expression, resulting in ablated salivary gland invasion of sporozoites	125
4. Discussion	131
4.1. The cellular function of C-CAP in <i>Plasmodium</i>	131
4.1.1. The role of C-CAP during oocyst maturation	133
4.2. C-CAP but not its actin-sequestering activity is essential in oocysts	135
4.2.1. Complementation with <i>Cryptosporidium parvum</i> C-CAP (CpC-CAP).....	135
4.2.2. <i>C-cap(-)</i> mutants can not be complemented by <i>profilin</i>	136
4.3. C-CAP and potential actin-independent processes in oocysts	136

4.4. Conservation of the N-terminal part of C-CAP in <i>Plasmodium</i> parasites	138
4.5. A brief conclusion of C-CAP	138
4.6. The characterization of the G-actin binding proteins profilin, ADF1 and ADF2	139
4.7. The two states of profilin	140
4.8. Overexpression of <i>C-CAP</i> and <i>profilin</i>	141
4.8.1. Overexpression of <i>C-CAP</i> and <i>profilin</i> in ookinetes does not influence the parasite development in mosquitoes.....	142
4.8.2. Ectopic overexpression in sporozoites abolished salivary gland invasion.....	142
4.9. Conclusions and the “minimalistic model” for actin regulation in motile sporozoites.....	143
5. References	145
6. Appendix	159

LIST OF FIGURES

Figure 1: The actin treadmilling model and its regulation by actin-binding proteins.....	21
Figure 2: Srv2/CAP domain organization and atomic structure.	24
Figure 3: The motile extracellular stages of <i>Plasmodium</i> and the molecular motor.....	27
Figure 4: Working model of actin regulation in apicomplexan parasites:	32
Figure 5: CAP-homology proteins in apicomplexan parasites and yeast.....	36
Figure 6: Complete gene annotation of the <i>cyclase-associated</i> gene (<i>C-CAP</i>).	76
Figure 7: Expression profiling of <i>C-CAP</i> transcripts in <i>Plasmodium berghei</i> life cycle stages.	77
Figure 8: Generation of <i>Plasmodium berghei</i> <i>C-CAP</i> gene knockout parasites.	79
Figure 9: <i>P. berghei</i> <i>C-CAP</i> is dispensable for blood stage replication <i>in vivo</i>	80
Figure 10: <i>C-cap(-)</i> ookinetes exhibit reduced velocity.....	81
Figure 12: Oocyst architecture of <i>c-cap(-)</i> mutants.	84
Figure 13: <i>C-cap(-)</i> parasites die during oocyst development.	85
Figure 14: The circumsporozoite protein (CSP) and oocyst capsule protein 380 (CAP380) displaying normal expression and localization in <i>c-cap(-)</i> mutant oocysts.	87
Figure 15: <i>c-cap(-)</i> parasites transmigrate through the midgut epithelium and transform into early oocysts.	89
Figure 16: <i>C-cap(-)</i> oocysts are impaired of membrane retraction and DNA segregation.	91
Figure 17: The membrane retraction process on wild type oocyst.	92
Figure 18: Generation of <i>P. berghei</i> C-CAPmCherry fusion parasites.....	94

Figure 19: C-CAPmCherry is sequentially expressed and exhibits cytoplasmic localization in blood stages.	96
Figure 20: C-CAPmCherry expression and Localization in mosquito stages.....	98
Figure 21: C-CAPmCherry expression and localization in liver stages.....	99
Figure 22: C-CAPmCherry protein abundance.....	100
Figure 23: Trans-species complementation in <i>P. berghei</i> parasites with <i>Cryptosporidium parvum</i> C-CAP.	102
Figure 24: <i>Cryptosporidium parvum</i> C-CAP rescues the <i>c-cap(-)</i> defects.	104
Figure 25: Mutagenesis of the <i>CpC-CAP</i> protein.	105
Figure 26: Generation of mutant <i>Cpc-cap</i> ^{D117A, K118A} and <i>Cpc-cap</i> ^{STOP} parasites.....	106
Figure 27: Phenotypic analysis of <i>Cpc-cap</i> ^{D117A, K118A} and <i>Cpc-cap</i> ^{STOP} parasites.....	107
Figure 28: Protein abundance of <i>CpC-CAP</i> and its mutants <i>in vivo</i>	108
Figure 29: Profilin does not complement the C-CAP function during oocyst maturation.....	111
Figure 30: Gene expression and protein abundance of profilin, actin depolymerizing factor 1(ADF1) and 2 (ADF2).	114
Figure 31: Localization of profilin and ADF1 during life cycle progression of the parasite.	116
Figure 32: Detection of a profilin subpopulation in ookinetes by an anti <i>Toxoplasma gondii</i> profilin antibody.	118
Figure 33: Overview of promoter and gene combinations for generation of recombinant parasites that overexpress <i>C-CAP</i> or <i>profilin</i> under stage-specific promoters.	119
Figure 34: Generation of recombinant parasites expressing <i>Flag</i> -tagged <i>C-CAP</i> and <i>profilin</i> under control of the <i>CTRP</i> or <i>CSP</i> promoters.	121
Figure 35: Localization and protein abundance of the <i>Flag-C-CAP</i> and <i>Flag-profilin</i> fusion proteins expressed under control of the <i>CTRP</i> promoter.	123
Figure 36: Phenotypic analysis of sporozoite development and motility in parasites expressing <i>c-cap</i> and <i>profilin</i> under the <i>CTRP</i> promoter.....	125
Figure 37: Detection of two profilin populations in ookinetes, indicating functional overexpression of the protein under the <i>CTRP</i> and <i>CSP</i> promoter.....	126
Figure 38: Localization and protein abundance of the <i>Flag-C-CAP</i> and <i>Flag-profilin</i> fusion proteins expressed under control of the <i>CSP</i> promoter.....	127
Figure 39: Phenotypic analysis of sporozoite development in parasites with ectopic overexpression of <i>c-cap</i> and <i>profilin</i> under the <i>CSP</i> promoter.	129
Figure 40: The “minimalistic model” for actin regulation in sporozoites.....	144
Figure 41. The circumsporozoite protein (CSP) is expressed in ookinetes.	159

LIST OF TABLES

Table 1. Antibodies with indicated working dilutions and source	47
Table 2. Primer sequences for molecular cloning and genotyping	50
Table 3. Primer sequences for expression profiling	52
Table 4. The conversion factor for different objectives	66
Table 5. Ingredients for preparations of 15 % SDS-PAGE.....	72
Table 6. Ookinete injection does not restore the <i>c-cap(-)</i> defects.....	88

LIST OF ABBREVIATIONS

°C	Celsius degree
μ	micro
μg	microgramm
μl	microliter
μm	micrometer
μM	micromolar
α	alpha, anti
<i>A. stephensi</i>	<i>Anopheles stephensi</i>
aa	amino acids
ADF	actin depolymerization factor
ADP	adenosine diphosphate
ATP	adenosine trisphosphate
β	beta
bp	base pairs
BSA	bovine serum albumin fraction
<i>C. parvum</i>	<i>Cryptosporidium parvum</i>
C-CAP	carboxy-terminal part of (adenylyl) cyclase-associated protein
C-CAP	Gene, genomic locus of C-CAP
c-cap(-)	<i>C-CAP</i> gene deletion mutant parasite
cDNA	complementary deoxyribonucleic acid
Co-IP	Co-immuno precipitation
Cp	<i>Cryptosporidium parvum</i>
CSP	circumsporozoite protein
C-terminal	carboxy terminal
CTRP	circumsporozoite and trap-related protein
Δ	delta, means deletion
DAPI	4',6-diamidino-2-phenylindole
ddH ₂ O	di-distilled water
dhfr/ts	dihydrfolate reductase
DMEM	Dulbecco's Modified Eagle Medium
DMSO	dimethyl sulfoxide

DNA	deoxyribonucleic acid
E. coli	Escherichia coli
EDTA	ethylenediamine-tetraacetate
EEF	exoerythrocytic forms
F-actin	filamentous (polymer) actin
FCS	fetal calf serum
for	forward, sense direction of a gene
γ	gamma
G-actin	globular (monomeric) actin
gamy	gametocytes from <i>P. berghei</i>
GAPDH	glyceraldehyde-3-phosphate dehydrogenase
gDNA	genomic DNA
GFP	green fluorescent protein
HBSS	Hank's Balanced Salt Solution
HFF	Human foreskin fibroblast
hr, hrs	hour, hours
Hsp70	heat shock protein 70
Huh7	Human hepatoma cell line
IFA	indirect immuno fluorescence assay
IMC	inner membrane complex
in vitro	<i>in vivus</i> , in a living organism
in vivo	<i>in vitrum</i> , in a test tube
kb	kilo base pairs
kDa	kilodalton
kg	kilogram
L	liter
m	micro (10^{-6})
M	molar
m	milli (10^{-2})
mero	merozoites from <i>P. berghei</i>
min	minute
ml	milliliter
mRNA	messenger ribonucleic acid
MT	microtubuli

MTOC	microtubule organizing center
MyoA	myosinA
nm	nanometer
NMRI	Naval Medical Research Institute
N-terminal	amino terminal
™	Trademark
ook	ookinetes from <i>P. berghei</i>
ORF	open reading frame
<i>P. berghei</i>	Plasmodium berghei
PAGE	polyacrylamide gelelectrophoresis
Pb	Plasmodium berghei
PBS	phosphate buffered saline
PCR	polymerase chain reaction
Pf	Plasmodium berghei
pH	potentia hydrogenii
PV	parasitophorous vacuole
	quantitative real time reverse transcription polymerase chain reaction
qRT-PCR	
rev	reverse, anti-sense direction of a gene
RNA	ribonucleic acid
rpm	rotation per minute
RT	room temperature
RT-PCR	reverse transcription polymerase chain reaction
Σ	sigma (sum)
<i>S. cerevisiae</i>	Saccharomyces cerevisiae
SDS	sodium dodecyl sulphate
sec	second
spp.	species
spz	sporozoites from <i>P. berghei</i>
Srv2/CAP	Suppressor of RAS ^{V19} / (adenylyl) cyclase-associated protein
<i>T. gondii</i>	Toxoplasma gondii
Taq	Thermus aquaticus
TEMED	N,N,N,N,-tetramethylethylenediamine
Tg	Toxoplasma gondii

TRAP	Thrombospondin-related-adhesive protein
U	Unit, biochemical unit for enzymatic activity
UTR	untranslated region
UV	ultra violets
V	Volt
WB	western blot
WT	wild type
ζ	zeta

1. Introduction

Single cell eukaryotes of the phylum apicomplexa are obligatory intracellular parasites that essentially rely on host cell invasion, egress and transmigration to establish their pathogenic life cycle. *Plasmodium* and other apicomplexan parasites like *Toxoplasma gondii*, or *Cryptosporidium parvum* employ an ancient actin-myosin based molecular motor machinery to facilitate gliding motility and invasion (Baum *et al.*, 2008a; Morrisette and Sibley, 2002; Soldati *et al.*, 2004). This unique machinery clearly distinguishes these parasites from other motile eukaryotic cells that employ filopodia, pseudopodia or cilia and flagella for locomotion.

Interestingly, apicomplexan parasites possess a reduced set of biochemically diverse orthologs of key G-actin regulatory molecules as compared to other eukaryotic cells (Sattler *et al.*, 2011; Schuler and Matuschewski, 2006b). Nevertheless, *Plasmodium* sporozoites exhibit unusually fast gliding motility of up to 150 $\mu\text{m}/\text{min}$ (Vanderberg *et al.*, 1974). These observations suggest that functional characterization of proteins that regulate the actin cytoskeleton in the apicomplexan parasite *Plasmodium berghei* might ultimately help to understand their molecular function and relevance for parasite motility and life cycle progression. To highlight the differences between host and parasite actin and actin-regulating proteins, the introduction will focus first on conventional actin and general regulatory mechanisms, followed by their apicomplexan counterparts.

1.1. Cell motility and the actin cytoskeleton in eukaryotic cells

Cell motility is a fundamental biological process. Free-living cells like amoeba or cells within a multi cellular organism are able to locomote. This includes cell migration during embryogenesis, wound healing, cell response of the innate- and adaptive immune system, morphogenic processes such as neuronal outgrowth and tumor cell metastasis (Wang *et al.*, 2005). The so-called crawling motility is characterized by a cycle of four basic steps: lamellipodial protrusion at the front cell edge, adhesion to the substratum, forward translocation of the cell body and de-adhesion (Pollard and Borisy, 2003). This process is facilitated by the dynamic organization of the actin cytoskeleton. Precisely coordinated polymerization of actin filaments against cellular membranes induces membrane protrusions at the leading edge of the cell and provides the force for active movement (Pollard, 2007; Saarikangas *et al.*, 2010). In contrast, the major components of the cell body, such as the

cytoplasm, nucleus or mitochondria, may follow passively due to mechanical stability and elasticity of the plasma membrane (Svitkina *et al.*, 1997).

The actin cytoskeleton is also a central molecular player in endocytosis (Galletta and Cooper, 2009; Kaksonen *et al.*, 2006), cytokinesis (Oliferenko *et al.*, 2009), intracellular-cargo transport (vesicles, organelles, macro molecular protein complexes and RNA) over short distances (Fagarasanu and Rachubinski, 2007; Pruyne *et al.*, 2004), and maintenance of cell polarity (Martin and Chang, 2006; Vidali *et al.*, 2009). Interestingly, some bacterial and viral pathogens manipulate the host actin cytoskeleton to facilitate cell-to-cell transmission. In contrast, parasites from the phylum apicomplexa employ their own actin-dependent motility for the invasion of host cells.

1.1.1. Actin biochemistry and polymerization dynamics

Actin is the most abundant and a highly conserved protein in eukaryotic cells. It is a globular 42kDa protein, with a characteristic ATPase activity. Under physiological conditions actin exists in two major molecular conformations, the globular actin (G-actin) and the filamentous polymerized actin (F-actin). F-actin filaments are double helical polymers formed by the globular subunits, which are arranged unidirectional giving the filament an important molecular polarity. Subunit addition at both ends is diffusion-limited and therefore the elongation rate is directly proportional to the concentration of G-actin monomers in solution (Drenckhahn and Pollard, 1986; Pollard, 1986). Both filament ends exhibit distinct polymerization properties towards G-actin subunits that are bound to ATP. At the barbed or plus (+) end a low critical concentration of the Mg^{2+} ATP complex (0.1 μM) is sufficient for a high subunit addition rate to elongate the filament. At the pointed or minus (-) end a relatively high critical concentration of the Mg^{2+} ATP (0.7 μM) is needed for G-actin addition and thus results in slow filament growth, respectively (Pollard, 1986; Wegner, 1976). In addition, the intrinsic filament polarity is supported by the intrinsic ATPase activity of actin and leads to filament maturation. After assembly of ATP bound G-actin at the barbed end ATP hydrolysis happened quickly within ~2 seconds (Blanchoin and Pollard, 2002). The residual γ -phosphate remains longer, for ~350 seconds, with the so-called intermediate filaments (ADP-Pi-actin) associated before it finally dissociates (Carrier and Pantaloni, 1986). After phosphate dissociation the ADP-actin subunits adjust their actin- to- actin interfaces to become prone for disassembly at the pointed end (Carrier, 1990; Pollard, 1986). The continuous cycle of actin polymerization, ATP hydrolysis, phosphate dissociation and depolymerization lead to a very slow steady state treadmilling process between monomeric and filamentous actin in the cell.

The filament treadmilling model (Small, 1995) was initially proposed after studying actin filaments *in vitro* (Carlier and Pantaloni, 1997; Pollard, 1986; Wegner, 1976). Pure actin filaments are intrinsically stable at steady state. Polymerization at the (+) end is limited by the dissociation at the (-) end and corresponds to filament growth, totally of $\sim 0.04 \mu\text{m}/\text{min}$ (Pollard and Borisy, 2003). However, motile cells move fast, for example keratocytes ($\sim 10 \mu\text{m}/\text{min}$) or *Plasmodium* sporozoites ($\sim 100 \mu\text{m}/\text{min}$) (Svitkina *et al.*, 1997; Vanderberg, 1974). To expedite the slow intrinsic growth rate of pure actin filaments, cells express a variety of actin cytoskeleton regulatory proteins.

1.1.2. Actin cytoskeleton regulating proteins

Eukaryotic cells express more than 100 accessory proteins regulating the structure and dynamics of the actin filament cytoskeleton in response to external stimuli.

1.1.2.1. Nucleation proteins enhance actin filament elongation

To ensure constant generation of new filaments for the fast, three-dimensional remodeling process, proteins bind to actin filaments and initiate nucleation and promote elongation. Three main mechanisms for de novo actin filament nucleation accomplished by different protein-complexes, named actin related protein 2/3 complex (Arp2/3), formin and spire have been identified.

The Arp2/3 complex initiates actin filament branches along the existing mother actin filament (Machesky *et al.*, 1994; Mahaffy and Pollard, 2006) and creates a highly branched actin network at the leading edge of a cell described as “dendritic nucleation” (Svitkina *et al.*, 1997). Arp 2/3 anchors the pointed end of a new filament in an angle of 70° to the mother filament, while the barbed end grows away from the branch towards the cell membrane (Pollard, 2007; Svitkina and Borisy, 1999; Volkmann *et al.*, 2001). Once activated, the Arp2 and 3 along with one actin monomer constitute a stable trimer that acts as a nucleus to generate a new branch (Pollard, 2007). The main regulators of the Arp2/3 complex are nucleation promoting factors (NPFs) of the Wiskott-Aldrich Syndrome family proteins (WASp) (Machesky *et al.*, 1999; Weaver *et al.*, 2003; Welch and Mullins, 2002) and up stream signaling molecules, such as small guanosine triphosphosphate hydrolases (GTPases) of the Rho-famliy (Cdc42, Rac), the phospholipid phosphatidylinositol 4,5-bisphosphate (PIP₂), profilin, and proteins containing Src homology domain 3 (SH3) (Higgs and Pollard, 2001).

Formins are key regulators for nucleation and elongation of unbranched actin filament bundles (Evangelista *et al.*, 2002; Evangelista *et al.*, 2003; Pruyne *et al.*, 2002). They are most common in filopodia of cells (Waller and Alberts, 2003), in the contractile ring during cytokinesis (Kato *et al.*, 2001; Lee *et al.*, 1999; Tolliday *et al.*, 2001), in stress fibre formations (Tominaga *et al.*, 2000), focal contacts (Riveline *et al.*, 2001) and focal adhesions (Kobiela *et al.*, 2004). The processive association of formin with the growing barbed end precludes capping of the filament and allows constant growing (Kovar *et al.*, 2005; Moseley *et al.*, 2004; Watanabe and Higashida, 2004). All formins contain the formin homology domains 1 and 2 (FH1 and FH2) controlling barbed end growth and specific subcellular localization. The FH1 domain has the capacity to tether multiple profilin-ATP-actin complexes near the barbed end, which accelerates filament elongation rates up to 1.5 μm per second (Higashida *et al.*, 2004; Staiger *et al.*, 2009). The FH2 domain is a stable dimer of donut-shaped structure, that wraps around two actin subunits of a barbed filament end, caps it and confers nucleation activity (Moseley *et al.*, 2004; Otomo *et al.*, 2005; Xu *et al.*, 2004). Formins are also regulated by GTPases of the Rho-family.

Spire uses a completely distinct mechanism for filament nucleation (Quinlan *et al.*, 2005). It first binds four actin monomers through its tandem repeat of four WH2 domains, and then assembles them stereo-specifically into a new filament nucleus (Otto *et al.*, 2000; Quinlan *et al.*, 2005; Wellington *et al.*, 1999). During the elongation process, spire remains associated with the slow growing pointed end (Quinlan *et al.*, 2005). In contrast to Arp2/3 and formin, spire is activated by mitogen-activated protein (MAP) kinases (Otto *et al.*, 2000).

1.1.2.2. Capping proteins terminate filament growth

Filament termination reduces the depletion of the G-actin pool in the cell by steady state polymerization effectively. Capping proteins (CP) are heterodimeric proteins (α -, β -subunits) that bind to the barbed end of a filament and inhibit actin subunit addition and depolymerization, thereby inducing new, short and stiffer polymers.

β -actinin/capping protein (CP) is found ubiquitously in muscle- and non-muscle tissues of metazoa as well as in single cells like *Acantamoeba* and *Plasmodium* (Cooper and Sept, 2008; Isenberg *et al.*, 1980; Maruyama and Obinata, 1965; Schuler and Matuschewski, 2006b). The hetero dimer exhibits typical barbed end-capping function (Bearer, 1991). Elegant biochemical work established that CP is needed for *in vitro* reconstituted actin-based motility (Loisel *et al.*, 1999). Furthermore, CP is a component of the dynactin complex, where it binds and caps the barbed end of the actin-related protein1 (Arp1) mini-filament (Schafer *et al.*,

1994). The CapZ is a sarcomere specific CP isoform in the muscle of vertebrates (Caldwell *et al.*, 1989).

Gelsolin is a calcium-stimulated barbed end-capping as well as severing protein in higher vertebrates (Sun *et al.*, 1999).

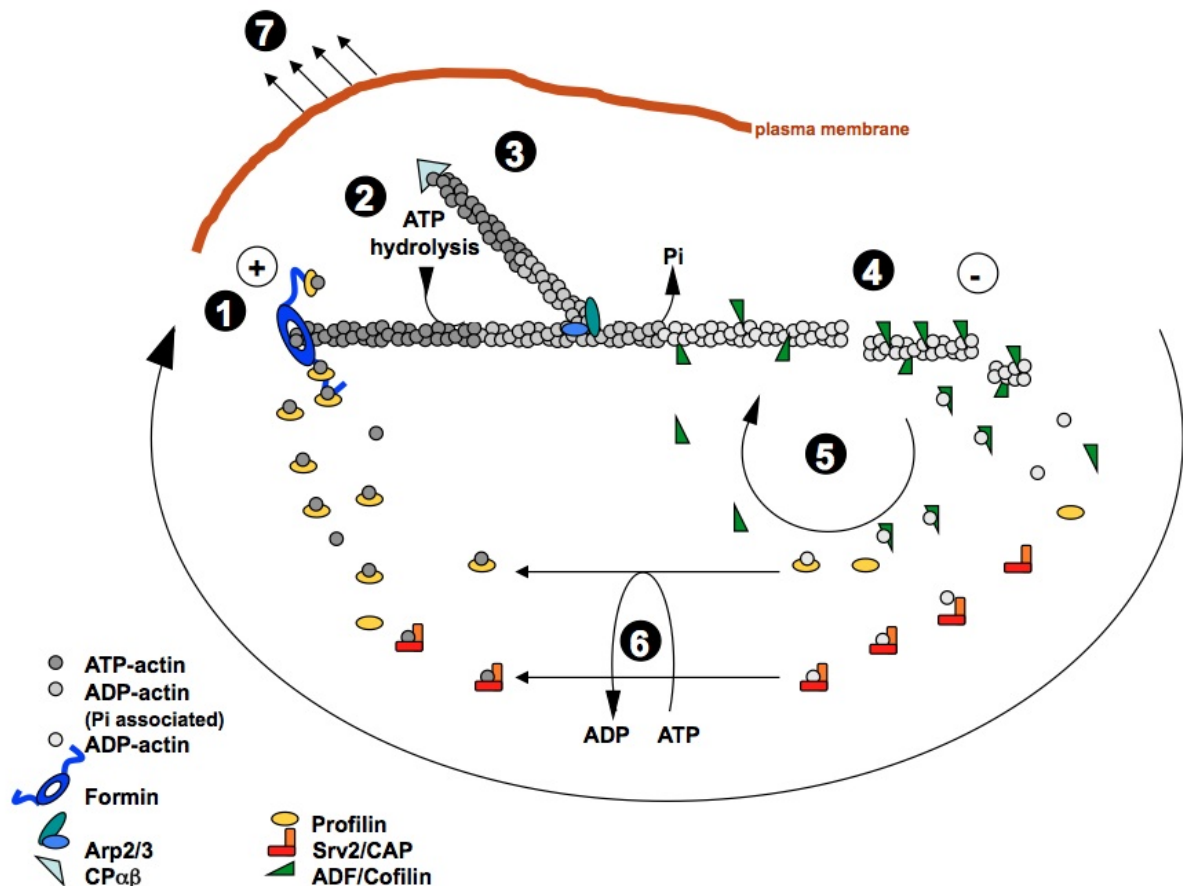


Figure 1: The actin treadmilling model and its regulation by actin-binding proteins.

External signals trigger actin dynamics. **1.)** Actin nucleator proteins formin and the actin-related protein 2/3 complex (Arp2/3) promote and enhance actin polymerization at the barbed end (+) by binding of ATP-actin profilin complexes. **2.)** Branch formation of the mother filament is initiated by the Arp2/3 complex and leads to “dendritic nucleation” the 3 dimensional structures at the leading edge of a motile cell. Furthermore, actin filament maturation is indicated by intrinsic actin ATP-hydrolysis. The phosphate remains associated creating intermediate filaments (light grey circles). After phosphate dissociation the ADP-actin filament (white circles) is prone to dissociation at the pointed end (-). **3.)** Capping proteins (CP, light blue triangle) terminate filament growth and stabilize them. **4.)** Binding of actin depolymerizing factors (ADF/cofilin, green triangle) to ADP-actin filaments induces and enhances debranching and severing of filaments into shorter fragments and ADP-actin monomers. **5.)** G-actin binding proteins like profilin (yellow circle) and the cyclase-associate protein Srv2/CAP (red and yellow angle) interact with ADP-actin and recycle sequestered G-actin. **6.)** Nucleotide exchange of ADP to ATP on actin monomers, is facilitated by profilin and Srv2/CAP. After replenishing the polymerization competent pool of ATP-actin, profilin ATP-actin complexes interact again with the nucleator proteins formin and Arp2/3. **7.)** Constant bending of the actin cytoskeleton facilitates actin incorporation on free barbed ends against the cell membrane and pushes the membrane forward. Thus, resulting in cellular motility. Chart adapted to Pollard *et al.* (2007).

1.1.2.3. Actin depolymerizing factors (ADF) enhance actin filament disassembly

Besides gelsolin, **ADF/cofilin** is a family of ubiquitously small proteins that bind to ADP-actin filaments and promote their disassembly (Bamburg, 1999). Binding of ADF/cofilin proteins promotes dissociation at the pointed end (Blanchoin and Pollard, 1999) thereby changing the twist of the actin helix and accelerating severing into shorter segments (McGough *et al.*, 1997) and eventually into ADP-actin monomers. Subsequent competition of profilin with ADF/cofilin through binding of ADP-G-actin facilitates the nucleotide exchange to ATP (Rosenblatt *et al.*, 1995). This “hand over” mechanism returns ATP-actin into the polymerization competent steady state. Most of the ADF/cofilins are regulated negatively by LIM-kinases that inhibit the interaction with the ADP-actin filaments (Blanchoin *et al.*, 2000). Reactivation by removing the phosphate is due to the specific activity of the *slingshot* phosphatase (Niwa *et al.*, 2002). Phosphorylated ADF/Cofilin can also directly activate phospholipase D1 (PLD1), which is essential for chemotaxis of phagocytotic cells (Han *et al.*, 2007).

1.1.2.4. G-actin binding proteins control actin treadmilling

Proteins that bind to G-actin are the main regulators maintaining the pool of free G-actin. They either influence the nucleotide exchange or sequester the subunits to keep them until they are needed.

Profilin is a small G-actin binding and sequestering protein that plays a central role in all eukaryotic cells (Carlsson *et al.*, 1977). It sequesters actin monomers in a 1:1 complex in unstimulated cells (Goldschmidt-Clermont *et al.*, 1991). One essential function is the acceleration of nucleotide exchange of ADP to ATP on actin subunits, thereby re-generating the pool of ATP-actin (Goldschmidt-Clermont *et al.*, 1992; Mockrin and Korn, 1980; Witke, 2004). The ATP-actin profilin complex binds to formin via the FH1 domain, at the barbed end of the filament, thereby increasing the elongation rate (Kovar *et al.*, 2003; Romero *et al.*, 2004). Apart from the actin buffering capacity, profilin interacts with a plethora (> 50) of different proteins to control the actin network. Profilin interacts with phosphoinositides (PIs) (Chaudhary *et al.*, 1998; Fedorov *et al.*, 1994; Lassing and Lindberg, 1985) that are capable of disrupting the actin-profilin complex and inhibit the monomer sequestering activity (Lassing and Lindberg, 1985). Furthermore, profilins interact with proteins containing poly-L-proline rich stretches, including members that are known for barbed end elongation such as the vasodilator-stimulated phosphoprotein family (Ena/VASP), Wiskott-Aldrich Syndrome protein family (WASP/WAVE), formin and the cyclase associated protein (Srv2/CAP)

(Bertling *et al.*, 2007; Kovar *et al.*, 2003; Reinhard *et al.*, 1995; Watanabe *et al.*, 1997; Witke, 2004). However, the poly-L-proline- binding site on profilin is separated from the actin-binding site. Thus, profilin can integrate signalling events with cytoskeleton rearrangements.

Thymosin- β 4 is a G-actin sequestering protein (Safer and Nachmias, 1994) that binds to ATP-G-actin and blocks actin assembly, nucleation, and growth at both (+/-) ends of the filament and thus preserves G-actin pools.

1.1.3. The Suppressor of RAS^{VAL19}/ cyclase-associate protein Srv2/CAP (CAP)

The Srv2/CAP protein is expressed in all eukaryotic organisms studied thus far. Genetic disruption of Srv2/CAP causes severe defects in actin organization and actin-based processes including cell division, cell motility polarization and endocytosis (Deeks *et al.*, 2007; Hubberstey and Mottillo, 2002). The cyclase-associated protein (Srv2p/CAP) was first identified in *Saccharomyces cerevisiae* as a suppressor of the activated rat sarcoma allele RAS2^{VAL19} (Fedor-Chaiken *et al.*, 1990) and was simultaneously isolated as a component of the adenylyl cyclase complex in yeast (Field *et al.*, 1990). Functional mapping of the 70kDa CAP protein revealed several structural domains indicating a multi-functional protein. The amino-terminal domain of

S. cerevisiae CAP (residues 1-168) is involved in protein-protein interaction and oligomerization (Burkhard *et al.*, 2001; Nishida *et al.*, 1998). The N-terminus binds directly to adenylyl cyclase and facilitates its activation by RAS (Fedor-Chaiken *et al.*, 1990; Field *et al.*, 1990). The adenylyl cyclase-binding domain is not conserved in higher eukaryotes, which implicates diverged functions during evolution (Hubberstey and Mottillo, 2002). Additionally, the specific N-terminal helical domain binds to ADF/cofilin-bound ADP-actin monomers and thereby contributes to ADF/cofilin recycling (Moriyama and Yahara, 2002; Quintero-Monzon *et al.*, 2009). The carboxy-terminal domain (C-CAP), spanning amino acid residues 370 to 526, is highly conserved throughout evolution and is well-characterized for binding to monomeric ADP-actin in a 1:1 stoichiometry, thus suppressing spontaneous actin polymerization (Freeman and Field, 2000; Gieselmann and Mann, 1992; Gottwald *et al.*, 1996; Hubberstey *et al.*, 1996; Mattila *et al.*, 2004). The central region of the CAP comprises the WASp-homology domain (WH2), which binds to ATP-actin and ADP-actin monomers with similar affinities and catalyzes nucleotide exchange on actin, which in turn promotes actin turnover (Chaudhry *et al.*). The WH2 domain is flanked by two poly-proline-rich stretches P1 and P2 separating the C- and the N-terminal domain. The first poly-proline-rich sequence P1 binds to profilin (Bertling *et al.*, 2007; Drees *et al.*, 2001; Lambrechts *et al.*,

1997) and the second P2 region apparently supports interaction with Src homology domain 3 (SH3) domain-containing proteins, such as Abp1, which target CAP to the sites of actin rearrangement (Balcer *et al.*, 2003; Freeman *et al.*, 1996; Lila and Drubin, 1997). Native CAP constitutes a higher order oligomer of 600 kDa comprising 6 molecules of CAP and 6 molecules of actin. Recombinant full length CAP adopts a hexamer via interaction between the N- and the C-terminus. (Balcer *et al.*, 2003; Moriyama and Yahara, 2002).

Initial results in *S. cerevisiae* characterized CAP as a bifunctional protein, since disruption of the C-terminus produced other phenotypes than disruption of the N-terminus. Yeast cells depleted of the C-terminus exhibited nutritional and morphological defects such as the inability to grow on rich medium, sensitivity to nitrogen starvation (Field *et al.*, 1990; Gerst *et al.*, 1991), abnormal large and round cells, random budding pattern, and abnormal actin distribution (Vojtek *et al.*, 1991). These defects could be rescued by overexpression of the C-terminus of CAP on one hand, and by complementation with profilin on the other hand (Goldschmidt-Clermont *et al.*, 1991; Haarer *et al.*, 1993; Vojtek *et al.*, 1991). The ability of profilin to complement the function of the depleted CAP C-terminus in yeast implies a close relationship between both conserved proteins during evolution.

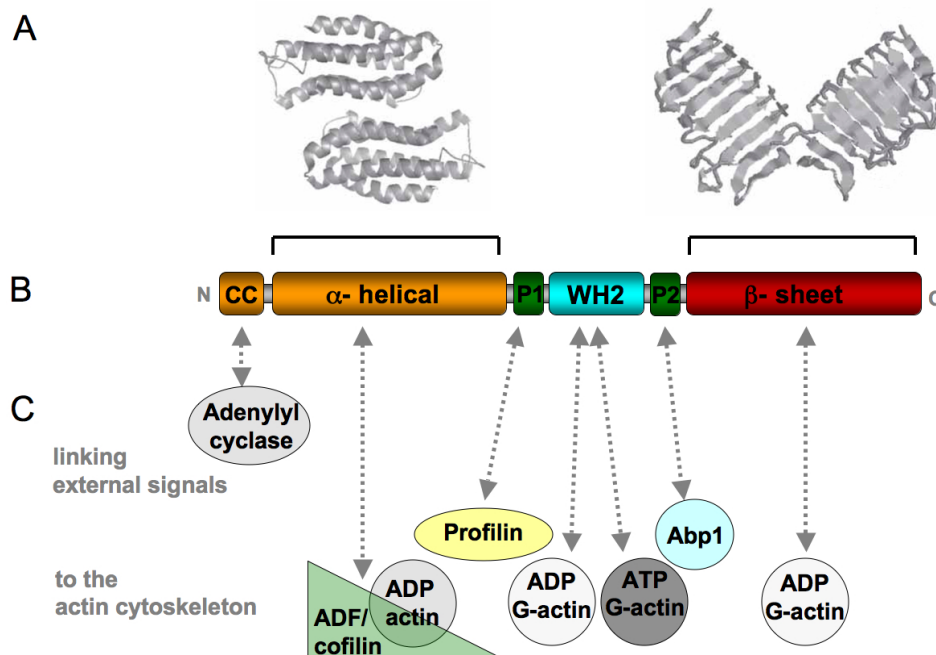


Figure 2: Srv2/CAP domain organization and atomic structure.

(A) X-ray structures of the N-terminal domain (yellow) represented as α -helical and the conserved C-terminal domain (red) as β -sheets. Both domains crystallize as dimers. (B) Domains are colored. CC coiled-coil (yellow); P1 and P2, proline-rich sequences (green); WH2 domain; WASp-homology 2 (blue). The actin-binding domain (red) is also important for dimerization. (C) Dotted arrows indicate direct physical interactions of specific CAP domains with known ligands. Adenylyl cyclase (white circle) interacting with the actin depolymerizing factor (ADF/cofilin, green triangle) and ADP-actin (white circle), profilin (yellow circle), ATP-actin (grey circle), and ADP-actin for nucleotide exchange, Abp1 (blue circle) and ADP-actin. Chart is adapted from Goode *et al.* (2006).

Taking into account the diverse functional domains, CAP provides a “central hub” between external stimuli and the actin cytoskeleton. Recent biochemical work suggests a multi-step mechanism that involves the coordinated interplay of multiple CAP domains (Quintero-Monzon *et al.*, 2009). CAP acts as a crucial binding-platform for actin turnover to convert ADF/cofilin-bound ADP-actin complexes into ATP-actin monomers and replenish the pool of polymerization competent G-actin. During this process, CAP recycles ADF/cofilin for further rounds of filament disassembly and accelerates nucleotide exchange on actin monomers to promote rapid actin turn-over (Chaudhry *et al.*).

The crystal structure of the N-terminus (N-CAP) revealed a coiled-coil domain, which is followed by a dimer of six anti-parallel α -helix bundles (Burkhard *et al.*, 2001; Nishida *et al.*, 1998). The C-terminal actin-binding domain (C-CAP) forms an unusual V-shaped dimer. Each monomer is composed of six coils of right-handed parallel beta-helices, which form an elliptical barrel (Dodatko *et al.*, 2004). The dimerization of C-CAP is facilitated by inter-strand exchange of the last C-terminal β -strands between each monomer (Dodatko *et al.*, 2004). Furthermore, the unique tertiary structure of C-CAP provides a structural model for a wide range of molecules, which includes the C-CAP/cofactor C-like motif (CARP motif). Several cytoskeleton-related proteins including the tubulin binding cofactor C (or tubulin-specific chaperone C) (TBCC), and the X-linked retinitis pigmentosa 2 protein (RP2) belong to this family (Dodatko *et al.*, 2004).

1.2. Apicomplexan parasites and their molecular motor

Apicomplexan parasites constitute a large and diverse group of alveolatan protozoa (Adl *et al.*, 2005) that cause severe diseases in humans, including *Plasmodium* (malaria), *Toxoplasma* (toxoplasmosis), and *Cryptosporidium* (enteritis) and/or life for instance *Theileria* (theileriosis) and *Eimeria* (coccidiosis) (Morrison, 2009). Members of the phylum are auxotrophic and rely on intracellular life style to gain access to host metabolites for survival and replication. Furthermore, this intracellular niche provides a strategy to evade the host defense mechanisms. Importantly, to establish their life cycle extracellular apicomplexan parasites employ gliding motility powered by their unique acto-myosin system, which facilitates invasion, egress out of host cell and transmigration through different tissues (Barragan and Sibley, 2003; Frevert *et al.*, 2005; Matuschewski *et al.*, 2002; Soldati *et al.*, 2004). Here, *Plasmodium* will be discussed. The highly specialized motile and invasive stages of the parasites exhibit a characteristically elongated and polarized cell shape. Their unidirectional movement is dictated by the presence of the apical complex, which contains secretory organelles. Micronemes and rhoptries discharge sequentially a variety of type I transmembrane surface molecules, named TRAP-family proteins (thrombospondin-related anonymous protein) and initiate motility and invasion upon contact with a suitable host cell. Calcium-mediated secretion of micronemal TRAP proteins are critical for (i) receptor recognition, (ii) attachment to the host cell, (iii) establishing a moving junction (MJ) between the host cell and the parasite plasma membrane (Aikawa *et al.*, 1978) and (iv) the formation of the parasitophorous vacuole (PV). The PV constitutes a cellular compartment, which facilitates parasite growth and replication. The elongated parasite shape is built on the subpellicular microtubule scaffold and the alveolata-specific inner membrane complex (IMC). Microtubuli (MT) emerge apically from the microtubuli organizing center (MTOC) and run along 2/3 of the longitudinal axis of the parasite (Morrisette and Roos, 1998). The IMC consists of flattened membranous vesicles between the parasite plasma membrane and the microtubuli skeleton extending beneath the entire surface of the parasite. The unique actin-myosin based molecular motor, which drives parasite motility, is located in the subpellicular space (20 nm) between the IMC and the plasma membrane (Lemgruber *et al.*, 2009; Mann and Beckers, 2001; Morrisette and Sibley, 2002). The current model describes the unconventional myosin A (MyoA) as the major force-generating molecule inside the motor (Heintzelman and Schwartzman, 1997; Matuschewski *et al.*, 2001; Meissner *et al.*, 2002; Siden-Kiamos *et al.*, 2011). MyoA is immobilized to the IMC by its calmodulin-like myosin

light chain and two additional gliding associated proteins (GAP) GAP45 and Gap50 (Bergman *et al.*, 2003; Herm-Goetz *et al.*, 2002; Johnson *et al.*, 2007). The MyoA heads walk along F-actin filaments and create the power stroke. Force transmission from the parasite through the extracellular substratum is facilitated by interaction of actin with a variety of adhesive transmembrane surface molecules of the TRAP-protein family (Sultan *et al.*, 1997). The function of aldolase tetramers, which bind to F-actin and the cytoplasmic tail of TRAP (Buscaglia *et al.*, 2003; Buscaglia *et al.*, 2007; Jewett and Sibley, 2003), seem to play a role as an intermediate scaffold. Depending on the motility mode aldolase functions as an energy supplier or a cytoskeleton-bridging molecule (Starnes *et al.*, 2009). Finally, upon transferring these complexes along the parasite body, the adhesive proteins are cleaved by a protease and shed in a trail left behind the gliding parasite. Whereas the main motor components are known (Daher and Soldati-Favre, 2009) the overall spatiotemporal regulation of the molecular motor is still unclear. Thus far, regulation of the parasite motility can occur at different levels, including sensing of external triggers, energy supply, trafficking, processing of the motor components, and tight regulation of the actin cytoskeleton (Baum *et al.*, 2006a; Baum *et al.*, 2008a; Schuler and Matuschewski, 2006a). Likewise, additional molecules for sensing and connecting external stimuli to the actin cytoskeleton may exist.

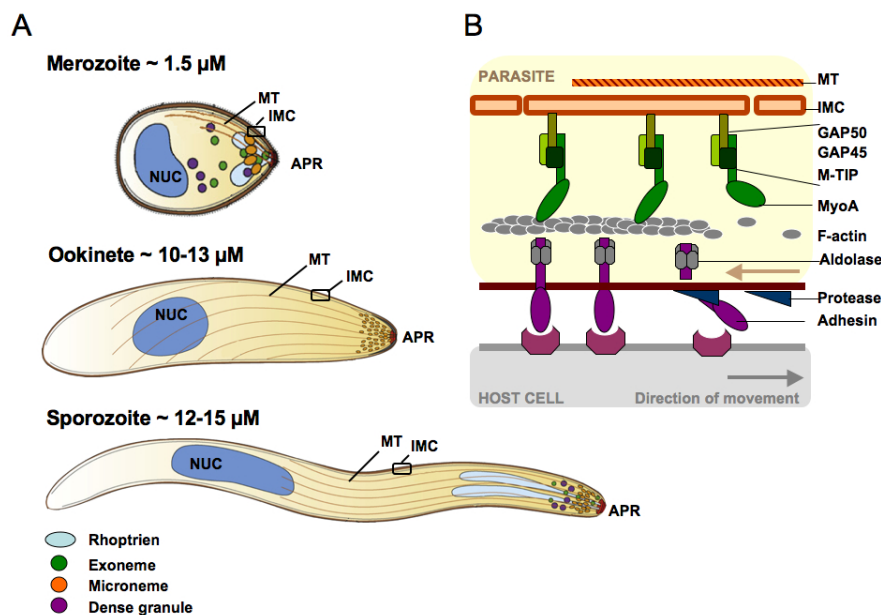


Figure 3: The motile extracellular stages of *Plasmodium* and the molecular motor.

(A) Comparative cell morphology between merozoites, ookinete and sporozoite. Shown are conserved secretory organelles that are central for invasion and motility: rhoptries (light blue), exonemes (green), micronemes (orange) and dens granula (purple). The polarized cell shape is predicted by additional structures: subpellicular microtubuli (MT), nuclei (NUC), inner membrane complex (IMC) and the apical polar rings (APR). **(B)** The molecular motor is located between the IMC and the parasite plasma- membrane. MyosinA (MyoA) is immobilized at the IMC via GAP50, GAP45 and MTIP

proteins. MyoA binds to F-actin and its ATP dependent head activity moves actin backward. Aldolase tetramers are thought to connect the F-actin with transmembrane adhesin molecules and further to host cell receptors, thereby transducing the generated force through the surface of the parasite. Disengagement of the entire complex involves protease activity, shedding the adhesions from the surface and disconnecting host- cell attachment. This chart is modified after Baum *et al.* (2008).

1.2.1. The motile stages of *Plasmodium*

The motile *Plasmodium* stages, termed merozoites, ookinetes, and sporozoites use the common mechanism of the acto-myosin motor for motility and invasion (Baum *et al.*, 2006b).

Merozoites invade erythrocytes of the vertebrate host to establish the asexual replication cycle (Sherman, 1985).

Ookinetes, which emerge after uptake of the sexual stages during a blood meal by the definite host, the Anopheline mosquito, also employ the typical features. Secretion of chitinase and membrane-attack ookinete perforin protein (MAOP) facilitates penetration of the peritrophic membrane (Dessens *et al.*, 1999; Dessens *et al.*, 2001; Kadota *et al.*, 2004). Additional secretion of micronemal proteins like, CDPK3 (calcium dependent protein kinase 3) (Ishino *et al.*, 2006; Siden-Kiamos *et al.*, 2006a), CTRP (circumsporozoite and TRAP-related protein) (Dessens *et al.*, 1999; Yuda *et al.*, 1999) facilitates migration through the midgut epithelium. This process is one of the major bottlenecks during the parasite life cycle. Thereafter, one successful ookinete transformed into an oocyst produces thousands of infective sporozoites.

Sporozoites exhibit an outstanding motility capacity. First, midgut sporozoites actively egress out of the oocyst via an ECP protease (egress cystein protease)- driven process (Aly and Matuschewski, 2005). They have to breach the basal lamina to enter the hemocoel, from where sporozoites invade the salivary glands of the mosquito (Pimenta *et al.*, 1994; Vaughan *et al.*, 1992). They remain motile in the cavity and ducts of the salivary glands for several days (Frischknecht *et al.*, 2004). After injection of sporozoites into the skin of the vertebrate host, they employ active movement to enter the dermal blood vessel where they are passively transported by the circulation system to the liver sinusoids (Amino *et al.*, 2006; Vanderberg and Frevert, 2004). After adhesion to the sinusoid epithelium, sporozoites gain access to the liver parenchyma by migrating through the Kupffer cells (Amino *et al.*, 2006; Frevert *et al.*, 2005; Pradel and Frevert, 2001). Finally, sporozoites traverse through several hepatocytes, before they invade the final hepatocyte for replication (Amino *et al.*, 2006; Mota *et al.*, 2001; Pradel and Frevert, 2001; Silvie *et al.*, 2008).

A detailed understanding of the regulatory processes that triggers the complex developmental program opens new avenues to develop potent malaria intervention strategies.

1.2.2. Apicomplexan actins and the special case of *Plasmodium*

Besides the actomyosin motor complex, gliding motility and invasion of apicomplexan parasites essentially relying on filamentous actin. Actin modifying agents, such as cytochalasins and Jasplakinolide (JAS), have been used extensively to elucidate microfilament functions. Cytochalasins inhibit actin polymerization (Cooper, 1987), whereas Jasplakinolide promotes filament nucleation and stabilization (Bubb *et al.*, 1994). Despite their distinct molecular functions, both drugs inhibited parasite invasion into host cells and influenced the motility in *Plasmodium knowlesi* and *falciparum*, in *Toxoplasma gondii* and *Cryptosporidium parvum* (Dobrowolski and Sibley, 1996; Field *et al.*, 1993; Forney *et al.*, 1998; Miller *et al.*, 1979; Russell and Sinden, 1981; Shaw and Tilney, 1999). Although actin is present in the parasites at relatively high cytosolic levels (8-10 μ M) the vast majority (70 - 90 %) appears to be in the monomeric state (Dobrowolski and Sibley, 1997; Field *et al.*, 1993). Apparently, the dynamics of the apicomplexan microfilament system differ fundamentally from the well-understood turnover in other eukaryotic cells.

Apicomplexan actin has been localized by immunoelectron microscopy primarily to the apical end of the parasite and in the space between the plasma membrane and the inner membrane complex in *Toxoplasma* tachyzoites and *Plasmodium* merozoites (Cintra and De Souza, 1985; Dobrowolski and Sibley, 1997; Shaw and Tilney, 1999; Yasuda *et al.*, 1988). However, visualization of actin filaments in motile unfixed stages of *Plasmodium* or *Toxoplasma* failed thus far (Bannister and Mitchell, 1995; Cintra and De Souza, 1985; Kudryashev *et al.*). Only Jasplakinolide treatment facilitated the detection of actin-like filament in *Toxoplasma* in a random manner underneath the plasma membrane (Wetzel *et al.*, 2003). The most prominent effect of JAS treatment in *Toxoplasma* and *Plasmodium* is the induction of an apical membrane-bound protrusion filled with extensive amounts of parallel-aligned filamentous actin structures that are expelled by the parasite (Mizuno *et al.*, 2002; Shaw and Tilney, 1999). This feature is reminiscent of the acrosomal process of invertebrate sperm (Tilney and Inoue, 1985). However, whether the filament organization as visualized by JAS treatment reflects the natural state remains a matter of debate. In addition to the role in invasion and motility, actin is also required for intracellular growth as indicated by Jas-inhibited abrogation of vesicle maturation during ingestion of nutrients by *P. falciparum* blood stages (Smythe and Ayscough, 2006).

All apicomplexan parasites harbor one conventional actin gene, termed *actinI*, whereas the genus of *Plasmodium* encodes a second actin isoform, termed *actinII* (Gardner *et al.*, 2002; Wesseling *et al.*, 1989). Both actin isoforms share approximately 83 % sequence identity with

homologues from yeast or vertebrate sources and thereby constitute a distinct subfamily within conventional actins (Gardner *et al.*, 2002; Schuler and Matuschewski, 2006b; Wesseling *et al.*, 1989). *ActinI* is ubiquitously expressed throughout the *Plasmodium* life cycle and represents the most abundant isoform. In contrast, *actinII* expression is restricted to gametocytes and the protein plays a specific role during exflagellation of male gametocytes (Siden-Kiamos *et al.*, unpublished).

Less than 5 % of the parasite actin could be detected in the filamentous form in fractionation assays. Microscopic observations and biochemical analysis of actin filaments revealed their short size (~100nm), instability, and a low polymerization rate *in vivo* and *in vitro* (Sahoo *et al.*, 2006; Schmitz *et al.*, ; Schmitz *et al.*, 2005; Schuler *et al.*, 2005b; Wetzel *et al.*, 2003). The formation of short filaments appears to be an inherent property of apicomplexan actin molecules and correlates with distinct amino acid substitutions. These substitutions are likely to weaken the intra-molecular interactions between actin subunits, thus leading to decreased filament nucleation and increased filament instability. Also, posttranslational modifications on actin such as acetylation and methylation may alter the polymerization state of the filament (Schmitz *et al.*, 2005). It was shown that *Plasmodium falciparum* actin lacks the methylation on histidine 73, which is supposed to favor the ADP binding open state of actin, increasing filament instability (Schmitz *et al.*, 2005). In addition, significant differences between parasite orthologs can be expected.

Surprisingly, the parasite moves at the same speed as muscle-actin filament contraction, indicating a role for regulatory actin-binding proteins (Schuler and Matuschewski, 2006a, b). However, the characterized set of apicomplexan actin-binding proteins does not sufficiently explain the unusual actin dynamics of the parasites. It will therefore be critical to learn more about their specific properties in the parasite (Baum *et al.*, 2006a; Baum *et al.*, 2008a; Schuler and Matuschewski, 2006b).

1.2.3. A minimal repertoire of actin-binding proteins

The availability of several apicomplexan genomes (Abrahamsen *et al.*, 2004; Gardner *et al.*, 2002) facilitated homology searches of microfilament proteins and revealed a strikingly small repertoire of actin-binding and actin-regulating proteins (Baum *et al.*, 2006a; Gordon and Sibley, 2005; Schuler and Matuschewski, 2006b). Many of the proteins that are considered key regulators in yeast and higher eukaryotic cells are absent in apicomplexan genomes (Baum *et al.*, 2006a; Schuler and Matuschewski, 2006b). Examples are, the filament nucleation and branching Arp2/3 complex, along with the nucleator spire and its known

regulators WASP/WAVE, Verprolin/WIP and Abp1. Almost no filament bundling and crosslinking proteins like actinin, filamin, spectrin or tropomyosin-related proteins have been identified. Moreover, proteins with capping and severing activity, like gelsolin and β -thymosin, appear absent from apicomplexan genomes. Where orthologs exist they often exhibit prominent structural differences (Sattler *et al.*).

1.2.3.1. *Plasmodium* F-actin binding proteins facilitate actin filament nucleation and stabilization

The intrinsic instable nature of *Plasmodium* actin filaments implying important roles for actin nucleation and stabilizing factors.

Formin-homolog proteins are the only identified proteins with barbed end nucleation capacity to create unbranched actin filaments (Evangelista *et al.*, 2002; Evangelista *et al.*, 2003). Apicomplexan genomes encode between two to four formin-homology domain 2 (FH2) containing proteins. Apart from the FH2 domain, these proteins appear less conserved. The formin-homology domain 1 (FH1) domain is rudimentary and contains only two instead of four proline rich stretches for binding to profilin-actin complexes. Other regulatory domains such as the Rho GTPase-binding domain, the self-regulatory Diaphanous autoinhibitory domain (DAD), and the dimerization motif have not been identified (Schuler and Matuschewski, 2006b). This raises the question whether apicomplexan formins are able to form dimers as the described orthologs and how they are regulated.

The three *Plasmodium falciparum* formins are termed formin1, formin2 and MISFIT and have been characterized previously (Baum *et al.*, 2008b; Bushell *et al.*, 2009). Formin1 is expressed in late blood stages and appears to be essential in blood stages (Baum *et al.*, 2008b). The apical localization and dynamic signal migration with the moving junction between the invading merozoite and the host suggests a role in invasion. *In vitro* studies revealed competent barbed end nucleator activity of formin1 with heterologous chicken actin. Contrary to formin1, formin2 expression peaks at mid trophozoite stage and the proteins localizes to the cytoplasm indicating a non-overlapping roles (Baum *et al.*, 2008b). The formin-like protein MISFIT contains the characteristic FH2 domain and the auto-regulatory (DAD) domain. It localizes to the nuclei in microgametes, zygotes and ookinetes. Gene deletion of MISFIT established a male-inherited role in ookinete-to-oocyst formation (Bushell *et al.*, 2009). *Toxoplasma gondii* formins exhibit similar actin-binding and nucleation capacity (Daher *et al.*). Interestingly, no interaction with profilin could be detected, suggesting an FH1 domain independent pathway for actin assembly in *Toxoplasma* (Daher *et al.*). In contrast to *Plasmodium* both formins localize in the periphery of the replicating and invading parasite.

Coronin represents the only candidate for an F-actin bundling protein in these parasites (Gandhi and Goode, 2008). *Plasmodium* encodes a single copy gene that contains the WH40-repeat. The microtubule-binding domain of canonical coronins is absent in the parasite ortholog. Nevertheless, the majority of actin-binding residues are conserved between species and biochemical assays revealed that *Plasmodium* coronin binds to immobilized F-actin (Tardieux *et al.*, 1998).

Capping protein (CP) is encoded by two single gene copies in the apicomplexan genome and constitutes a heterodimeric protein of an α - and a β -subunit (Gardner *et al.*, 2002; Morrisette and Sibley, 2002). Like its conventional orthologs, the recombinant *P. berghei* capping protein (CP α/β) displayed barbed end capping activity on heterologous actin filaments *in vitro* (Ganter *et al.*, 2009) and as shown in *P. knowlesi* whole cell extracts (Tardieux *et al.*, 1998). The β -subunit transcripts were identified as upregulated in sporozoites (UIS17), but are also expressed in all motile stages of *P. berghei*. Gene deletion of the β -subunit established the essential role for sporozoite motility and transmission in *P. berghei*. Likewise, ookinete motility was also reduced in CP β knockout parasites (Ganter *et al.*, 2009).

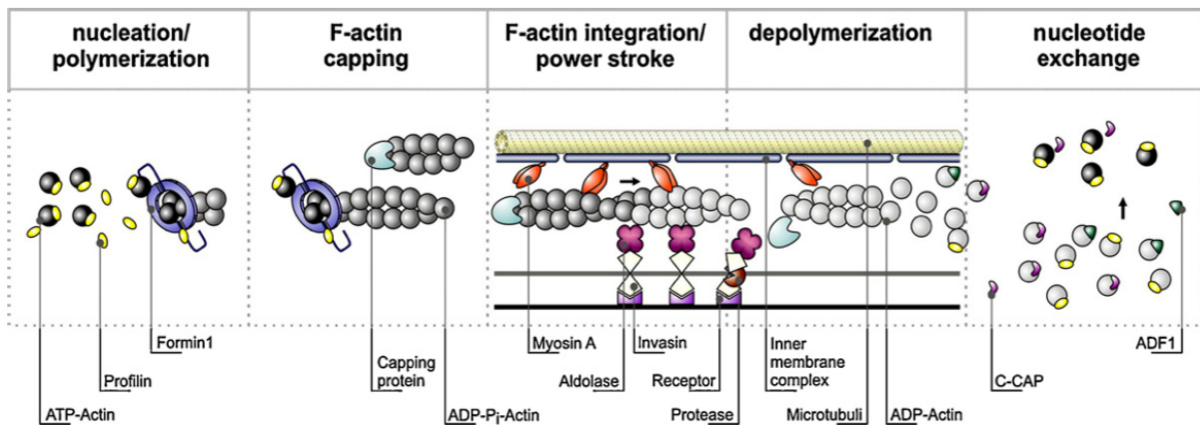


Figure 4: Working model of actin regulation in apicomplexan parasites:

The *Plasmodium* motor machinery is placed between the inner membrane complex (IMC), and the parasite plasma membrane. It is thought that nucleation/polymerization is initiated and promoted by fomin1 and its interaction with profilin- bound ATP-actin complexes at the barbed end of the actin filament. Filament elongation by formin is facilitated by progressive adding of actin monomers to the growing end. Short actin stubs are capped and thereby stabilized by the capping protein (CP). During the power stroke, F-actin is moved by the action of myosinA (MyoA) heads. The driving force is than translocated through the parasite plasma membrane by interaction of actin with transmembrane surface proteins (invasins) via aldolase tetramers, and binding to extracellular target- cell receptors. Backward translocation of F-actin bound invasions result in forward movement of the parasite, respectively. The depolymerization of ADP-actin filaments is enhanced by the intrinsic instability of the actin filaments and through the action of actin depolymerization factors (ADF). While the G-actin sequestering proteins C-CAP likely keeps ADP-actin monomers in an unpolymerized form, ADF1 promotes nucleotide exchange on actin monomers and stimulates the fast replenishment of polymerizable ATP-actin pool.

1.2.3.2. *Plasmodium* G-actin binding proteins control the actin treadmilling process

The combination of high levels of monomeric actin in apicomplexan parasite cells (Dobrowolski and Sibley, 1997; Field *et al.*, 1993) with the intrinsic instability of actin filaments (Sahoo *et al.*, 2006; Schmitz *et al.*; Schmitz *et al.*, 2005; Schuler *et al.*, 2005b) indicates important functions for G-actin binding proteins in apicomplexan parasites. However, therefore it is not surprising that G-actin binders show significant structural and functional differences to their canonical orthologs in other phyla (Sattler *et al.*).

Profilin is an actin-sequestering protein that contributes to replenishing the pool of polymerization competent ATP-actin (Carlsson *et al.*, 1977; Jockusch *et al.*, 2007), and, together with formin, it enhances the actin polymerization rate at the barbed end in most eukaryotic cells. However, apicomplexa encode some of the most divergent members of the profilin family (Kursula *et al.*, 2008). Biochemical properties, such as binding and sequestration of actin monomers, binding to proline-rich sequences and binding to phosphoinositides justifies the classification as profilin (Kursula *et al.*, 2008). The crystal structure confirmed an overall conserved profilin core fold. Interestingly, a unique mini domain that is shared by all apicomplexa extends from the protein surface and probably enlarges the actin-binding interface. In *Plasmodium*, this structure is even more pronounced by an extra, mobile, acidic loop, but interaction partners remain unknown (Kursula *et al.*, 2008). Reverse genetics in *Plasmodium berghei* revealed that profilin is essential during blood stage development, and, therefore more studies are needed to dissect its detailed *in vivo* function. Conditional gene disruption in *Toxoplasma gondii* demonstrates, that profilin is essential for gliding motility, host cell invasion and egress but is not required for intracellular growth (Plattner *et al.*, 2008). Similar to *Plasmodium*, *T. gondii* profilin sequesters monomeric actin (Plattner *et al.*, 2008). The role of profilin in parasite actin regulation is still not clear. Whether parasite profilin stimulates nucleotide exchange on monomeric ADP-actin and interacts with formin for filament elongation has not been established (Sattler *et al.*, 2010).

Actin depolymerizing factors 1 and 2 (ADF1, ADF2) belong to the ADF/cofilin superfamily (AC) and are characterized by a dual binding and severing activity on pointed ends of F-actin, as well as binding and sequestration of monomeric ADP-actin, to regulate actin turnover (Bamburg, 1999). All apicomplexa typically encode one *ADF* gene (*ADF1*), whereas *Plasmodium* encodes two isoforms, termed *ADF1* and *ADF2*. The major and constitutively expressed *ADF1* is essential in *P. berghei* blood stages (Schuler *et al.*, 2005a), whereas *ADF2* seems to be very low expressed throughout the life cycle and gene deletion

resulted only in minor effects during sporozoite development (Doi *et al.*). Sequence alignment of apicomplexan ADFs with other members of the AC family revealed a generally conserved G-actin binding site in both ADF isoforms, whereas the F-actin binding regions exhibit large deviations (Huttu *et al.*, 2010; Schuler *et al.*, 2005a). Biochemical analysis showed that both ADF1 and ADF2 bind to monomeric actin and accelerate nucleotide exchange on ADP-actin, a property usually associated with profilin. However, apicomplexan ADFs exhibit marked differences in structure and its F-actin binding properties as compared to conventional ADFs (Schuler *et al.*, 2005a). Strikingly, recent studies suggest that ADF1 is able to sever actin filaments, despite of its unusually reduced F-actin binding loop *in vitro* and is required for rapid turnover of filaments in *T. gondii* and *P. falciparum* (Mehta and Sibley 2011; Wong *et al.*, 2011). ADF2, which exhibits a pronounced F-actin binding loop is proposed to display conventional AC protein activities (Sattler *et al.*, 2011; Schuler *et al.*, 2005a; Wong *et al.*, 2011). However, the physiological role for both isoforms remains enigmatic in *Plasmodium*. Recent studies on *Toxoplasma gondii* ADF revealed similar biochemical functions such as monomer sequestration (Mehta and Sibley, 2011). Parasites with suppressed *TgADF* exhibited reduced and aberrant patterns of motility, which led to severe defects in invasion and egress of host cells (Mehta and Sibley). Also, signaling that regulates ADFs in apicomplexa seem to differ from their orthologs. LIM kinases and slingshot phosphatases which usually would regulate the “on” and “off” state of ADFs are absent in the apicomplexan genome (Gardner *et al.*, 2002; Schuler and Matuschewski, 2006b). Possibly, the phosphocofilin regulator 14-3.3 ζ (Gohla and Bokoch, 2002) and the cofilin phosphatase chronophin (Gohla *et al.*, 2005) can complement this regulatory function. Another potential regulation mechanism may involve binding of ADFs to phosphatidylinositol 4,5-bisphosphate (PIP₂) (Yonezawa *et al.*, 1990).

1.2.4. CAP-homology protein in apicomplexan parasites

CAP protein homologues were identified in the apicomplexan genome, using the bio-informatics software tool basic local alignment search tool (BLAST) and the highly conserved C-terminal Srv2/CAP amino acid sequence as template (Schuler and Matuschewski, 2006b). Interestingly, these CAP proteins are truncated and consist of the highly conserved C-terminal domain, only. The N-terminal part of the CAP protein, which contains the adenylyl cyclase-binding domain and the WH2 domain, appears to be missing in apicomplexan genomes. In contrast to the CAP proteins found in *Plasmodium*, which completely lack the WH2 domain and both proline rich stretches, CAP proteins from *Toxoplasma gondii* and *Cryptosporidium*

parvum contain short N-terminal extensions with significant homology to the WH2 domain of *S. cerevisiae* Srv2p/CAP Proteins. This single domain structure is classified as PFAM family PF08603 and appears to be restricted to protozoa. Still, the overall sequence similarity of apicomplexan C-CAP proteins amounts to 70 %. C-terminal amino acid residues specific for actin binding are strictly conserved between the eukaryotic species and argue for similar functions of the proteins.

1.2.4.1. *Cryptosporidium parvum* C-CAP (CpC-CAP) sequesters G-actin

The biochemical function of the recombinant *Cryptosporidium parvum* C-CAP protein was investigated recently and revealed CpC-CAP as the strongest G-actin sequestering proteins in apicomplexan parasites discovered thus far (Julia Sattler, dissertation, Hliscs et al., 2010). CpC-CAP was able to bind to monomeric actin via complex formation. The apparent affinity of CpC-CAP-actin interaction of $0.78 \pm 0.17 \mu\text{M}$, is in agreement with previous studies in yeast (Mattila et al., 2004). This capacity identified the apicomplexan CpC-CAP as a potent actin sequestering protein. Furthermore, CpC-CAP formed dimers with a predicted molecular mass of 38.7 kDa in solution. The lack of the N-terminus in apicomplexan C-CAP proteins seems to be responsible for the absence of higher molecular C-CAP complexes under physiological conditions (Balcer et al., 2003; Hliscs et al., 2010; Moriyama and Yahara, 2002).

1.2.4.2. The crystal structure of the apicomplexan *Cryptosporidium parvum* C-CAP protein

The crystal structure of *C. parvum* was solved by a structural genomics platform (Vedadi et al., 2007). The C-terminal segment of *C. parvum* C-CAP is similar to the structure of *S. cerevisiae* Srv2/C-CAP and human CAP (Dodatko et al., 2004). The monomer displays the similar right-handed β -helical fold consisting of 6 individual β -helical turns. The dimerization takes place by domain swapping. This crystal structures highlights the conservation of the C-terminal actin-binding domain in different CAP proteins during evolution and suggests their functional homology.

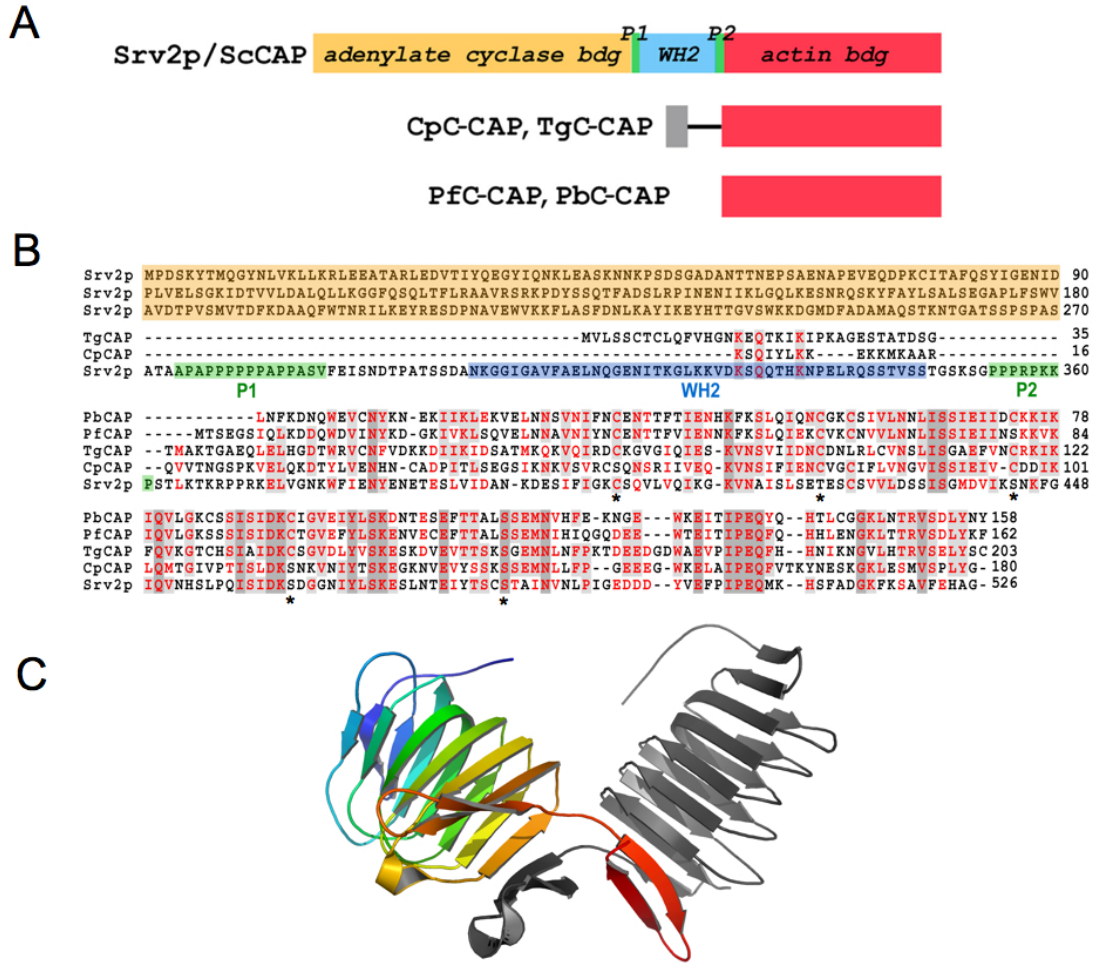


Figure 5: CAP-homology proteins in apicomplexan parasites and yeast.

(A) Protein domain model. Yeast Srv2p/CAP consists of an N-terminal adenylyl cyclase binding domain (orange), an intermitted WH2 homology domain flanked by two proline- rich sequences (blue and green), and a C-terminal actin- binding domain (red). Apicomplexan CAP orthologs from *Toxoplasma gondii* and *Cryptosporidium parvum* contain N-terminal extensions with significant homology to the WH2 domain of the yeast ortholog (grey), whereas *Plasmodium berghei* and *P. falciparum* does not. (B) Sequence alignment of CAP homology proteins from *S. cerevisiae* (Srv2p/ScCAP; gi 6324191), *T. gondii* (TgCAP; gi 211961913), *C. parvum* (CpCAP; gi 66357652), *P. berghei* (PbCAP; gi 68074593), and *P. falciparum* (PfCAP; gi 124505741). Color shading as in A. Residues involved in the internal Cys/Ser ladder (marked by asterisks) are highly conserved cross species. (C) Crystal structure of *C. parvum* C-CAP: overview of the CpC-CAP dimer (colored draft depicts 1 monomer and grey the second monomer). Each β -helical monomer contributes by swapping the last C-terminal β -helical turn to dimerization.

1.3. Objective of this study:

Plasmodium and other apicomplexan parasites employ a unique actin-dependent gliding motility machinery for host cell invasion that is critical to their pathogenic life cycle and transmission. The *Plasmodium* genome encodes a very divergent actin with unusual dynamic properties and only a very limited and structurally diverse repertoire of classical actin-binding proteins as compared to other eukaryotic cells. The underlying molecular mechanisms of how G-actin binding proteins manage to regulate the spatiotemporal actin-organization and turnover are not yet understood.

The adenylyl cyclase-associated protein (Srv2/CAP) was first identified in *Saccharomyces cerevisiae* and constitutes a crucial hub for the binding of diverse actin regulators. It links external stimuli to the reorganization of the actin cytoskeleton. *Plasmodium* parasites express only a truncated, but highly conserved, C-terminal domain of the CAP protein (C-CAP) that confers G-actin sequestering activity.

The aim of this study is the functional characterization of the *PbC-CAP* during the life cycle of *Plasmodium berghei*, employing genetic and molecular biological approaches.

Previous results demonstrate, vital roles for *profilin* and the *actin depolymerization factor 1* (*ADF1*) in blood stages, which precluded further functional analysis based on experimental genetics.

In order to shed light on the cellular roles of these G-actin binding proteins, their transcript expression and proteins abundance needs to be characterized.

2. Material and Methods

2.1. Materials

2.1.1. Biological resources:

Mus musculus:

Naval Medical Research Institute (NMRI) mice	Charles River Laboratories, Germany
C57/Bl6	Charles River Laboratories, Germany

Anopheles stephensi

Nijmegen, Netherlands

Plasmodium bergeri ANKA-GFP-507cl

(Janse *et al.*, 2006a)

Plasmodium bergeri ANKA

Toxoplasma gondii tachyzoites (RH *hxgprt*-)

Huh7 human hepatoma cells

E.coli XL-1blue

Stratagene, Germany

TOP 10 cells

Invitrogen, Germany

2.1.2. Laboratory equipment

Agarose gel casting apparatus, Horizon11-14

Whatman

Amixa Electroporator

Amixa, Germany

Centrifuges:

Bench centrifuge, 5424

Eppendorf, Germany

Megafuge1.OR

Heraeus

Cooled bench centrifuge 5415R

Eppendorf, Hamburg

Electrophoresis power supply

Amersham Pharmacia Biotech

Freezer -20 °C

Liebherr, Germany

Freezer -80 °C, ThermoScientific

Heraeus, Germany

Gel documentation system, Gel Doc 2000

BIORAD, Germany

Heating block, Thermo Scientific

Eppendorf, Germany

Incubators:

Incubator, for cells, Thermo scientific	Heraeus, Germany
Incubator, for <i>P. berghei</i> transfection	Mytrom, Germany
Incubator for bacteria, Thermo scientific	Heraeus, Germany
Incubator, Shaker for bacteria, Innova40	Brunswick Scientific
Incubator for Mosquitoes	Mytrom, Germany

Microscopes:

Binoculars, M80, MZ10F	Leica, Germany
Leica DM2500	Leica, Germany
Confocal laser scanning microscope, LSM510	Zeiss, Germany
Confocal laser scanning microscope, TSP-SP1	Leica, Germany
Apotome Imager.Z2	Zeiss, Germany
Axiovert, 200M, with XL-3 incubator	Zeiss, Germany
Micropipette (Gilson)	Abimed, Germany
Mosquito adults cage	BioQuip Products Inc, USA
Nanodrop ND 1000	peQLab, Germany
Neubauer counting chamber	Marienfeld, Germany
PCR Thermocycler, MJ-mini	BIORAD, Germany
PCR Thermocycler, StepOnePlus, Realtime PCR	Applied Biosystems, USA
pH-meter	Mettler Toledo, Germany
Photometer, GeneQuant pro	Amersham, Germany
Quarz cuvette	Amersham, Germany
Sterile hood, Herasafe KS12	Heraeus, Germany
Vortex-Genie2	Scientific Industries, USA
Western Blot system, Mini Protean Tetrasystem	BIORAD, Germany
Western Blot detection, FLA 3000 Imager	Fuji, Japan

2.1.3. Laboratory materials

2.1.3.1. Miscellaneous

6-well plate	Greiner bio-one, Germany
24-well plate	Greiner bio-one, Germany
8-well chamber slides, LabTek,	Nunc, Fischer, Germany
8-well glass slides	Medeco, Germany
Cover slips	Roth, Germany
Cryo-freezing tubes	Greiner bio-One, Germany
Electroporation cuvettes	Amaxa, Germany
Eppendorf tubes, 1.5 ml	Eppendorf, Germany
Falcon blue cap (50 mL and 15 mL)	Greiner Bio-One, Germany
Filter paper	Schleier and Schuel, Germany
Forceps	Neolab, Germany
Glass slides, clear	Menzel, Germany
Microscope oil	Zeiss, Germany
Needles, sterile	Braun, Germany
Neubauer counting chamber	Roth, Germany
Nitrocellulose membrane, Hybond	Amersham, Germany
Pasteur pipettes	Roth, Germany
PCR tubes	Greiner Bio-One, Germany
Petri-dishes	Starstedt, Germany
Poly-L-Lysins Coated Cover slips	BD, BioCoad, Belgium
Pipettes tips	Brand GMBH, Germany
PVDF Hybond Membrane	GE, Healthcare, UK
Serological pipettes (10 and 25 mL)	Greiner Bio-One, Germany
Sterile filter (0.2 and 0.4 µm)	Millipore, Ireland
Sterile filtration units (500 mL)	NALGENE®, USA
Syringes, 1ml	Roth, Germany
Syringes, insuline	Braun, Germany
Tissue culture flasks (50 and 250 mL)	Greiner Bio-One, Germany
Whatman™ 3MM paper	Whatman, UK

2.1.3.2. Chemicals

1 kb DNA-Ladder	MBI Fermentas
6 x loading dye	MBI Fermentas
Page Ruler TM (SM0671)	Fermentas, Germany
Agarose	Invitrogen, Germany
Alsever's solution	Sigma-Alrich, Germany
Albumin Fraktion F	Roth, Germany
Ampicillin	Roth, Germany
LB-agar powder (Lennox L Agar)	Invitrogen, Germany
β-Mercaptoethanol	Sigma, Germany
Calcium chloride	Merck, Germany
Cellulose (Carboxymethyl)	Sigma-Aldrich, Germany
Coomasie brilliant blue	Roth, Germany
SYBR Safe DNA Gel stain	Invitrogen, Germany
DMEM-medium	GibcoBRL, Karlsruhe
DMSO (Dimethyl sulphoxide)	Merck, Germany
dNTP-mix	Fermentas, Germany
ECL Western Blotting Reagents	GE Healthcare Europe GmbH
EDTA	Roth, Germany
FCS (Fetal Calf Serum), certified (USA)	Gibco Invitrogen, Germany
FCS	Gibco Invitrogen, Germany
Fluoromount G	Southern Biotec
Fibrous Cellulose Powder	Whathman, United Kingdom
Formaldehyde	Merck, Darmstadt
Gentamycin	Invitrogen, Germany
Giemsa stain	BDH Laboratory Supplies
Glass beads, unwashed	Sigma, Germany
Glucose	Merck, Germany
Glycerol	Roth, Germany
Heparin	Ratiopharm, Germany
Hepes	Merck/Calbiochem, Germany
Hypoxanthine	Sigma-Aldrich, Germany
IPTG	MPI Fermentas

Isofluran	Baxter
Ketamin (10%)	VFW
Matrigel	BD Biosciences, UK
Magnesium shloride	Merck, Germany
Magnesium sulphate	Merck, Germany
Milk Powder	Roth, Germany
NP-40	Sigma, Germany
Nycodence	Axis Shield, Oslo
Para-aminobenzoicacid	Sigma, Germany
Para-formaldehyde	Serva, Germany
PBS, sterile solution	Gibco Invitrogen, Germany
PBS, tablets	Gibco Invitrogen, Germany
PCR-buffer set	Roche
PenicillinStreptomycin, liquid	Invitrogen, Germany
Phenylhydrazine 97%	Sigma-Aldrich, Germany
Power SYBR®Green PCR Master Mix	Applied Biosystems
Protogel, 30%	Biozym/National D
Pyrimethamine	Sigma, Germany
RPMI 1640-medium	GibcoBRL, Germany
Saponin	Sigma, Germany
Sodium acetate	Roth, Germany
Sodium hydorgencarbonate	Roth, Germany
Sodium chloride	Roth, Germany
Sodium dodecyl sulphate (SDS)	Sigma-Aldirch, Germany
SYBR Safe DNA Gel stain	Invitrogen
SYBR, Green PCR Mastermix, Power	Applied Biosystems
TEMED, 99 %	Roth, Germany
TRIS	Roth, Karlsruhe
Trypsin-EDTA	Invitrogen, Germany
Triton X-100	Roth, Germany
Xanturenic acid (4.8-Dihydroxylquinalic acid)	Sigma-Aldrich, Germany

2.1.4. Commercial Kits

DNAse Turbo	Ambion
HiSpeed Plasmid Maxi Kit; Cat. No. 12663	QIAGEN, Germany
Human T Cell Nucleofactor Kit	Lonza, Germany
QIAquick PCR Purification Kit; Cat. No. 28106	QIAGEN, Germany
QIAprep Spin Miniprep Kit; Cat. No. 27106	QIAGEN, Germany
QIAamp DNA-Blood Mini Kit; Cat. No. 51106	QIAGEN, Germany
Rapid Ligation Kit	Roche
RETROscript	Ambion
RNeasy Mini Kit; Cat. No. 74104	QIAGEN, Germany
TOPO TA Cloning Kit (pCR 2.1.-TOPO)	Invitrogen, Germany

2.1.5. Enzymes

Restriction endonucleases	New England Biolabs, Fermentas
T4-DNA-ligase	Fermentas, Germany
Taq DNA polymerase	Fermentas, Germany
Platinum Taq DNA Pol.(HF)	Invitrogen, Germany
Phosphatase	Roche
ProteinaseK	Invitrogen, Germany

2.1.6. Media

RPMI Medium 1640 w/HEPES	Gbico Invitrogen, Germany
DMEM 41966	Gbico Invitrogen, Germany
HBSS	Gbico Invitrogen, Germany
SOC	Invitrogen, Germany

Luria Broth (LB) medium

10 g/l Bacto-tryptone, 5g/l Bacto-yeast extract, 5 g/l NaCl, add to ddH₂O pH 7.5

LB-Agar: LB-Medium, 15 g/l Bacto-agar

Transfection media for *P. berghei*

This media contained 160 ml of RPMI 1640 with 25 mM HEPES and L-Glutamine 2.05 mM (Gibco), 40 ml of heat-inactivated FCS and 50 µl gentamycin (50 mg/ml). The media was filtered sterile.

P. berghei ookinete (incomplete media)

0.425 g NaHCO₃ and 2.5 ml of Penicillin / Streptomycin (5000 U/ml and 5000 µg/ml) were added to 500 ml of RPMI 1640, and the pH was adjusted to 8.0 and the solution was sterile filtered.

P. berghei ookinete (complete media)

Ookinete complete media was prepared from above-mentioned incomplete medium by addition of 10 % heat inactivated FCS, 100 nM hypoxanthine and 50 µM xanthurenic acid. The pH was adjusted to 8.0 prior use.

Hepatocyte cell culture media (Huh7)

DMEM medium: 450 ml DMEM, 50 ml FCS, 5 ml Penicillin/Streptomycin

Mosquito dissecting media

3% Bovine albumin serum in 10 ml RPMI

2.1.7. Stock and working solutions

Antibiotics

Ampicillin 100 mg/mL ampicilin in ddH₂O

Primaquine 60 mg/10 mL primaquine in PBS

Working antibiotic dilution is 1:1000 in LB medium.

P. berghei freezing solution

Freezing-solution (for blood parasites): Glycerol: Alsever's solution (1:9)

Freezing-solution (for hepatocytes): 10 % DMSO, 90 % FCS

This solution was prepared by mixing glycerol and Alsever's solution at 1: 9 ratio. 200 µl of isolated blood were diluted with 100 µl of freezing solution and directly frozen at -80°C

Pyrimethamine stock (100x)

7 mg pyrimethamine was dissolved in 1 ml of DMSO and finally diluted in drinking water. PH was adjusted between 3.5 – 5.5.

Giemsa-stain

10 % Giemsa Solution in H₂O

Glycerin stock for bacteria long-term storage

50% Glycerin in ddH₂O was autoclaved. Finally, 1 ml of the bacteria culture (5ml LB, overnight culture) were mixed with 500ml Glycerin, slowly cooled down on ice and placed into the -80 °C.

Mosquito breeding/feeding solution

Mosquitoes breeding water (for larvae and pupae): 0.1 % sea salt in ddH₂O

Sucrose adults feeding solution: 10 % Sucrose, 0.01 % PABA, add ddH₂O

Nycodenz-stock solution

5 µM Tris pH 7.5 (1 M stock), 3 mM KCL (250 mM stock), 0.3 mM EDTA (0.5 M stock) and 110.4 g Nycodenz (27.6 g/100 ml), were dissolved in 400 ml dH₂O, pack tight light and autoclave the solution. Store at 4°C.

Xanthurenic acid (stock)

Dissolve 51.3 mg Xanthurenic acid in 1ml NaOH (1mol/L) and add 4 ml ddH₂O.

Finally, followed by steril filtration and storage at 4°C.

2.1.8. Buffers

Lysisbuffer for western blot samples

20 mM TrisCl, NaCl 50 Mm, TritonX-100 0.5 %, fill up to vol. 200 ml with ddH₂O and add proteinase inhibitors (PMSF). Store at 4°C.

RIPA buffer

Dissolve 0.87g NaCl in 1 ml Triton, add 12.5 ml 4% deoxycholate, 1 ml SDS, 5 ml 1M Tris pH 8 and 0.2 ml 0.5M EDTA. Add H₂O up to 100 ml.

Electrophoresis-buffer TAE (50x-stock)

Tris 2 M, sodium acetate 250 mM, EDTA 0.5 mM, (pH 7.8)

Electrophoresis-running buffer (5x stock)

25 mM Tris (15.1 g), 250 mM Glycine (94 g), 0.1 % SDS (50 ml, 10 %) to 1L ddH₂O. Use 1:5 dilution in ddH₂O.

Electrophoresis-transfer/-blotting buffer (10x stock)

Add 30 g Tris to 144 g Glycine and dissolve in 1L ddH₂O. Use 100 ml buffer (10x) together with 200 ml EtOH and 700 ml H₂O, cooled.

TBS (20x stock)/ TBS-T

Add 20 mM Tris to 137mM NaCl and dissolve in H₂O, adjust to pH 7.6 and fill up to 1L.

Add 0.05/ 0.1 % Tween 20/NP-40 for TBS-T/TBS-NP40.

Coomassie-destaining buffer

MeOH 10 ml (100 %), acetic acid 30 ml, ddH₂O 60 ml

4 % PFA

Heat 450 ml of ddH₂O up to 60 °C and add 20 g para-formaldehyde powder (Fisher :04042). 5 drops of 2N NaOH (1 drop per 100ml) were added until the solution should cleared. Subsequently, 50 ml of 10x PBS were added the pH was adjusted to pH 7.2. The final volume

Microtubuli stabilization buffer (MTSB) (2x stock)

20 mM MES, 300 mM NaCl, 10 mM EGTA, 10 mM glucose, 10 mM MgCl₂, adjust to pH 6.9.

500ml was filtered and placed on ice in the dark. Solution was stored in aliquots at -20 °C.

Final aliquots can be mixed with 4 % PFA before storage.

2.1.9. Antibodies

Table 1. Antibodies with indicated working dilutions and source

Primary antibody (animal source)	IFA / WB	Source
Anti-PbCSP (mouse)	1: 500 / 1: 2000	(Yoshida <i>et al.</i> , 1981), NYU
Anti-PbHSP70 (mouse)	1: 500 / -	Tsuji M, NYU
Anti-Tubulin monocl.B5-12 (mouse)	1: 300 / 1: 2000	Sigma
Anti-ds red polyclonal (rabbit)	- / 1: 2000	BioZOL
Anti-Flag monoclonal M2 (mouse)	1: 3000 / 1: 3000	Sigma
Anti-Actin (rabbit)	1: 300 / -	ICN
Anti-Actin (rabbit)	1: 300 / -	Sigma
Anti-p28 (mouse)	1: 300 / -	Sinden R.E. (2001), Imperial collage London

Anti-MyosinA (rabbit)	1: 300 / -	Pinder <i>et al.</i> 1997
Anti-CAP380 (rabbit)	1: 1000 / -	Srinivasan <i>et al.</i> (2008s) John Hopkins Hospital, Balimore, USA
Anti-TgProfilin (goat)	1: 300 / 1: 1000	R & D Systems, Inc
Anti-PfProfilin (rabbit)	1: 300 / 1: 1000	Eurogenetec, H. Schöler
Anti-CpCAP (rabbit)	- / 1: 5000	Eurogenetec, J. Sattler
Anti-PbADF1 (rabbit)	1: 300 / 1: 500	Eurogenetec, J. Sattler
Anti-PbADF2 (rabbit)	1: 300 / 1: 500	Eurogenetec, J. Sattler
Secondary antibody	IFA	
Anti-mouse Alexa Fluor 488 (donkey)	1: 3000	Molecular Probes, NL
Anti-mouse Alexa Fluor 546 (donkey)	1: 3000	Molecular Probes, NL
Secondary antibody	WB	
Anti-mouse-IgG-HRP (goat)	1:10000	Amersham, Germany
Anti-rabbit-IgG-HRP (goat)	1:10000	Amersham, Germany
Anti-rat-IgG-HRP (goat)	1:10000	Amersham, Germany
DNA-stain		
Hoechst 33342	1: 1000	Invitrogen, Germany
Draq 5	1: 1000	Axxora
SYTOX® Orange		Molecular Probes, NL
Other stains		
Phalloidin	1: 50	Molecular Probes, NL

2.1.9.1. Antibody generation

A. *Pf*Profilin (Herwig Schöler)

Full-length *Pf*Profilin with an N-terminal hexahistidine tag was expressed in *E. coli* BL21(DE3)RIPL cells and purified by nickel affinity chromatography. 1 mg of purified protein was separated by SDS-PAGE, the profilin band was cut out and sent to Eurogentec. The company immunized two rabbits with 3 x 100 micrograms of this material. The 5370 sera recognized *Pf*profilin as well as the his-tagged protein. The 5371 sera had almost no cross-reactivities (bacterial lysates, rings, trophozoites, and *T.gondii* lysates).

B. *CpCAP*, *PbADF1*, *PbADF2* (Julia Sattler)

Recombinant proteins, *CpCAP*-His-tag, *PbADF1*- and *PbADF2*- GST-tag, were purified with appropriate chromatography, and used for antibody generation in rabbit by Eurogenetec.

2.1.10. Molecular cloning

2.1.10.1. *Plasmodium* target vector

In this study the targeting plasmid vector b3D.DT^H.^D (B3D) or B3D+ was used to replace or target genes in the *Plasmodium berghei* genome. The vector contains a selectable marker (a mutated *Toxoplasma gondii* dihydrofolate reductase thymidylate synthase, *Tgdhfr/ts*), which introduces resistance against pyrimethamine and enables recombinant parasite selection and an ampicillin resistance for selection in *E. coli* during the cloning procedure. Additionally, the B3D + vector contains the 3'UTR of the *P. berghei dhfr/ts*, which confers mRNA stability of the introduced transgene.

The replacement strategy was used, to replace the entire gene (*C-CAP*) by the *Tgdhfr/ts* selectable marker cassette. Gene targeting was facilitated by introduction of the 3' and 5' UTRs (untranslated regions) of the *PbC-CAP* gene into the B3D+, flanking the *Tgdhfr/ts*. Both UTRs facilitate homologous recombination and stable integration into the genomic *PbC-CAP* locus.

The same vector was used to design the complementation plasmid containing the *C. parvum* *C-CAP* and its mutants *CpC-CAP*^{STOP} and *CpC-CAP*^{17/118}, as well as for the complementation with *profilin*. Therefore, the coding sequence of either *CpC-CAPs* or *profilin* were cloned upstream of the 5' UTR of *PbC-CAP*, using it as the endogenous promoter, simultaneously.

The B3D plasmid was employed for overexpression and Flag-tagging of the *PbC-CAP* and *profilin* under the *CSP* and *CTRP* promoters. Therefore, the integration-strategy was chosen. The stage specific promoters were cloned upstream of the Flag-tag and the coding sequence of the gene of interest (goi). Subsequently, the *PbC-CAP* and *profilin* were cloned with their 3'UTR into the B3D vector. Linearization of the plasmid, within the goi sequence facilitated the introduction of a second goi copy into the genome.

For transfection, the replacement vector was linearized by digestion with appropriate endonucleases. Preparative digestion was analyzed by agarose gel electrophoresis, purified and concentrated by ethanol precipitation. Finally, 5- 10 µl DNA were diluted in 10 µl H₂O and used for transfection.

2.1.10.2. Oligonucleotides for molecular cloning and genotyping

Primers were synthesized by eurofines MWG | operon. For molecular cloning, the Platinum-Taq polymerase was used for fragment amplification, and for genotyping on gDNA the Taq-polymerase.

Table 2. Primer sequences for molecular cloning and genotyping

Primer Name (restriction side)		Primer Sequence 5'→3' (restriction side underlined, linker bold)	objective
C-CAP annotation			
B5	CL_Tsplice_rev	CATTTTGTAAATGCACACTTCCC	Gene annotation
B7	CL_Tsplice_for2	GTTACACAAAACATATATTGCGGC	
C-CAP cloning			
B1	CL_5'UTR_for (SacII)	TCC <u>CCGCGG</u> GCTATGGGCACATCAACAATTTATTATTC CC	B3D+ c-cap(-) 5'UTR
B2	CL_5'UTR_rev (NotI)	ATAAGAATGCGGCCGCACTTCTTATGTGGTATTTTCT GGTAAATTGTTTATTCC	
B3	CL_3'UTR_for (HindIII)	CCCAAGCTTCATTTTTTACATGGAAAAATTAGTTC	3'UTR
B4	CL_3'UTR_rev (KpnI)	CGGGGTACCAATATAAAAATTAATAAGGAAAATGG	
C-CAPmCherry tagging			
B6	CL_5'UTR (SacII)	TCC <u>CCGCGG</u> TTTCTCGTTTAGTTATTAATTCATAACTCT AT GTTTTTGTTC	B3D+ 5'UTR+ C- CAP ORF
B8	CL_5'UTR linker (SpeI)	CGGACTAGTTGCTGCTGCTGCTGCTGCTGCTGCATA ATT ATACAAATCCGAAACCCTTGATTTAATTTACCC	
M	C'mCherry_for (SpeI)	CGGACTAGTGTGAGCAAGGGCGAGGAGGATAAC	mCherry
M1	C'mCherry_rev (BamHI)	CGGGATCCTTACTTGTACAGCTCGTCCATGCCGC	
C. parvum C-CAP and mutant cloning			
C1	CpCAP_for (SpeI)	CGGACTAGTAAAAATGAAAGCAGCAAGACAAGTAGTTA CA AATGGTAGT	CpC-CAP and CpC-CAP 117 ORF
C3	CpCAP_rev (BamHI)	CGGGATCCTTATCCATACAATGGAGAAACCATACTTTC TA ATTTGC	
C4	CpCAP_rev STOP (BamHI)	CGGGATCCTTAAATTGCAAGTTCTTCCAGTCACCTTC TTC TTC	CpC-CAP STOP
PbProfilin			
P1	Prf1_for (SpeI)	CGGACTAGTAAAAATGGAAGAATATTCATGGG	Profilin
P2	Prf2_rev (BamHI)	CGGGATCC TTATGCGGCACCTGTATCAGTG	OFR

CTRP/CSP_Flag_C-CAP/profilin overexpression			
T23	CTRP_Prom_for (SacII)	TCC <u>CCGCGG</u> ATATATACCACTTCCTCAAAATGAATAGG	CTRP promoter
T22	CTRP_Prom_rev (SpeI)	GG <u>ACTAGT</u> TGTGTTTTGCTTTGTATTTAAATAGATTA	
T25	CSP_Prom_for (SacII)	TCC <u>CCGCGG</u> ACATAAAAGGGAATATGGAATATACTAGC	CSP promoter
T26	CSP_Prom_rev (SpeI)	GG <u>ACTAGT</u> AAATATATGCGTGTATATATAGATTTTG	
B20	Pbc-cap_for (NotI)	ATAAGAATGCGGCCGCGCTAGCAAACCAAGTAAGTTTATC	C-CAP ORF+3' UTR
B23	Pbc-cap_rev (BamHI)	CGGGATCCGCGCTTCAACTATATAAATGTTCC	
B21	PbPRF_for (NotI)	ATAAGAATGCGGCCGCGAAGAATATTCATGGGAAAATTTTTAAATGAC	Profilin ORF+3' UTR
B22	PbPRF_rev (BamHI)	CGGGATCCGGAATACCCCACTAGCTATGC	
Genotyping			
c-cap(-)			
T9	CL_3UTR_rev_endo	CCGTAATAAGCTTTTTATGAATAAATTATTTATACAAC	3'UTR integration
T8	TgPro_rev	CGCATTATATGAGTTCATTTACACAATCC	
T10	CL_5'UTR_for_endo	GTTTGCGCATTAAGTGTGTGCACATATATATAG	5'UTR
T11	OSUTR_rev	AATTCCGGTGTGAAATACCGCACAGA	integration
ΔC-CAP::C-CAPmCherry			
T16	TmCherry_rev	TTCACGTAGGCCTTGGAGCCGTA	5'UTR
T10	CL_5'UTR_for_endo	GTTTGCGCATTAAGTGTGTGCACATATATATAG	integration
ΔC-CAP:: CpC-CAP/CpC-CAP ^{STOP}			
C3	CpCAP_rev (BamHI)	CGGGATCCTTATCCATACAATGGAGAAACCATACTTTCTA ATTGTC	5'UTR integration
C4	CpCAP_rev STOP (BamHI)	CGGGATCCTTAAATTGCAAGTTCTTCCAGTCACCTTCTTC TTC	
T10	CL_5'UTR_for_endo	GTTTGCGCATTAAGTGTGTGCACATATATATAG	
ΔC-CAP::Pbprofilin			
P2	Prf2_rev (BamHI)	CGGGATCC TTATGCGGCACCTGTATCAGTG	5'UTR
T10	CL_5'UTR_for_endo	GTTTGCGCATTAAGTGTGTGCACATATATATAG	integration
Ctrp/csp_Flag_c-cap/profilin			
T25	Flag_for	GACTACAAAGACCATGACGGTG	
	CTRPpromTestFor	TATATATATTTGTTTTGCTATCTGAGACCG	
	CSPpromTestFor	TTTGATAACCCTCACATAAGACAATCC	
TP1		GGTTGCAGCAAACCTTATCAATGCCTGG	
TP0		GCAAATTTATGCATTTGATCGGCG	

2.1.10.3. Oligonucleotides for expression profiling

Oligonucleotides for RT-PCR and qRT-PCR were designed to amplify a ~200 bp DNA fragment from cDNA. Primers were chosen to span an exon-intron structure, if it was possible.

Table 3. Primer sequences for expression profiling

Gene	Primer Name	Primer sequence 5' → 3'
RT-PCR		
<i>PbHsp70</i>	p41_PBHsp79_for	CATATTGATACGATTATGCAATTTTTATTACGACACTG
	p43_PBHsp70_rev	GTAAGTTTGGCTTTGCTTTTGCCTTAGCC
qRT-PCR		
<i>PbC-CAP</i>	X23_PbCL_for	CAAAGATAATCAATGGGAAGTGTGC
	X24_PbCL_rev	ATTAAAAACAATACTACATTTCCACAG
<i>PbProfilin</i>	X1_Prif_rev	GCGGCACCTGTATCAGTGC
	X2_Prif_for	TAAAGGTTTAGAATATGAAGGACACAG
<i>PbADF1</i>	X3_ADF1_for	TGTGCATATGTTGTTTTTGACGC
	X4_ADF1_rev	CATCTAGGGCACTTCAACAACCG
<i>PbADF2</i>	X5_ADF2_for	TATGCCTATCCCAACTCCTGAAG
	X6_ADF2_rev	GTTCTTCTTCAAATTCATTTATATCACAAAG
<i>GFP</i>	X7_GFP_for	GATGGAAGCGTTCAACTAGCAGACC
	X8_GFP_rev	AGCTGTTACAACTCAAGAAGGACC

2.1.11. Software

DNA sequence analysis was done with the *Clone Manager* or *SerialCloner1-3* software. Primer evaluation was done with *Oligo Calc* (Oligonucleotide Properties Calculator). Protein and DNA sequence alignments were done using mainly *ClustalW* and *Muscle* software. For Image and movie analyzation *ImageJ* was used. Data processing was done with *EXCEL* and *GraphPad Prism V.5.*, *MS Word*, *MS Powerpoint*, *Adope Photoshop*

2.2. Methods

2.2.1. Microbiological methods

2.2.1.1. Transformation of *Escherichia coli* (*E. coli*)

The purpose of this technique is the introduction of foreign DNA, mostly in plasmid conformation, into bacterial cells (*E. coli*). The bacteria cell will replicate the DNA along with its own to produce large DNA quantities. Using a plasmid containing an antibiotic selectable marker, facilitates selection of transformed cells, under antibiotic pressure. “Competent” bacteria will take up the foreign DNA. The *E. coli* strain XL-1 blue (stratagene) was used for final target vector amplification and Top 10 cells (invitrogen) were used for the subcloning procedure into the TOPO™ vector (Invitrogen). A frozen stock of competent *E. coli* (36 µl) was incubated on ice for 10 min. Adding β-mercaptoethanol (0.68 µl) for 10 min on ice, induces permeabilization of the bacteria outer membrane. Subsequently, the ligation reaction was diluted at least 10 times, mixed with the competent bacteria and incubated for 30 min on ice. To induce DNA uptake by *E. coli*, the bacteria need to be exposed to a temperature of 42 °C for 42 sec, called “heat shock”, followed by a incubation, on ice for 2 min. For some bacteria, a preculture step for 1 hr shaking at 37 °C, with 800 ml of LB or SOC medium can be performed. The preculture medium does not contain antibiotics, to enhance the first bacteria growth amplification. The cells were pelleted with 13.000 rpm, for 30 sec and 600 µl of the medium were discharged. To obtain defined bacterial colonies, 200 µl of the transformation suspension was than spread on to LB-agar plates, containing the antibiotic ampicillin and incubated at 37 °C for 16-20 hours. Single colonies growing on the LB-agar plates were picked up for separate liquid cultures. Different bacterial strains rely on distinct transformation protocols, which are described in the manufacturers instruction.

2.2.1.2. Culturing *E. coli* on agar plates

This technique is used to produce discrete colonies containing one clonal *E. coli* population. The bacteria grow on semi-solid surface of the agar-plates, containing antibiotics for selection. The agar plate can be stored at 4 °C, for up to one month.

2.2.1.3. Culturing *E. coli* in liquid medium

Luria Bertani (LB) medium is the universal medium to grow *E. coli* bacteria. It contains peptides, peptones, vitamins, and trace elements that are important for bacteria proliferation. For selection antibiotics are added. Inoculation of single *E. coli* colonies on agar plates or the pre-culture was the most common technique to grow bacteria. For small-scale plasmid purification a 5 ml LB culture was used. For midi- and big-scale DNA purification 50 ml or 250 ml LB culture is sufficient. Bacteria grow shaking with 250 rpm at 37 °C overnight.

2.2.1.4. Long-term storage of Bacteria

500 µl of a 5 ml overnight liquid culture is mixed with 1 ml of 500 µl of 50 % Glycerol, and stored at –80 °C in cryo-vessels.

2.2.2. Molecular biological methods

2.2.2.1. Polymerase chain reaction (PCR)

PCR was used to amplify specific DNA sequences from *P. berghei* wild type genomic DNA or other sources containing template DNA for molecular cloning, gene annotation, diagnostic parasite genotyping or gene expression analysis.

This method is based on the ability of heat stable DNA polymerases to synthesize a new strand of DNA from a template, by usage of primers and deoxynucleotide triphosphates (dNTP). Specific primers, complementary to the three prime end of sense and anti sense target DNA, were used. Primers contained three prime extensions, coding for specific endonuclease restriction sites to facilitate molecular cloning. Repetitive cycles of four steps, (i) the denaturation of double strand (ds) DNA, (ii) primer annealing to template DNA, (iii) new DNA-strand synthesis by the polymerase and (iv) an elongation step to terminate all amplicons, leads to an exponential accumulation of PCR products. 10-50 ng of template DNA was used for one PCR reaction. Platinum Taq-Polymerase was employed for amplification of fragments used for expression cloning and Taq-Polymerase was used for analytical PCR. Due to the high AT content of *Plasmodium* DNA the annealing temperature was typically performed by 55 °C and the extension- temperature was 60 °C instead of the normal temperature (72 °C). PCR composition and conditions were further set according to the primers, polymerase and amplification targets.

Standard PCR program:

Step 1: Denaturation ds DNA	94 °C, 5 min
Step 2: Denaturation ds DNA	94 °C, 30 seconds
Step 3: Annealing primer	55 °C, 30 seconds
Step 4: Extension of new DNA strand	60 °C, two to five minutes
Step 5: Elongation	60 °C, ten minutes
Step 6: Cycling between steps 2-4	30-35 cycles
Step 7: store 4 °C	∞

2.2.2.2. Complementary DNA (cDNA) synthesis by reverse transcription (RT)

This technique uses the ability of the viral DNA polymerizing enzyme Reverse Transcriptase to synthesize cDNA from mRNA for further applications. The cDNA was synthesized following manufacturers instructions of the “RETROscript Kit” (Ambion). Finally, cDNA was stored in aliquots at –20 °C to avoid thawing cycles. Also, cDNA samples were tested by PCR for gDNA contamination. Primers, which discriminate between g- and c- DNA, by spanning an intron, were used to perform standard PCR and subsequent analyses by agarose gel electrophoresis.

2.2.2.3. Qualitative real time-PCR (qRT-PCR)

This technique is used for qualitative gene expression profiling. cDNA samples and appropriate primers were subjected to standard PCR for detection of cDNA/mRNA content. Note, this procedure detects and analyses amplicons only at the end of the PCR, which permit high real time sensitivity due to saturation of PCR amplicon after 35 cycles. A gDNA control was analyzed in parallel.

2.2.2.4. Quantitative Real Time PCR (qRT-PCR)

This technique is used for gene expression profiling through the different life cycle stages of *P. berghei*. It is a PCR based technique, which is used to amplify and simultaneously quantify the targeted DNA molecule. During double strand DNA synthesis the fluorescent nucleic acid marker SYBR green, is incorporated and fluorescence is measured after each cycle. A threshold for detection of fluorescence above the background is determined, and the cycle at which the fluorescence crosses the threshold is called the cycle threshold Ct. Here, relative DNA concentrations are measured during the exponential phase of reaction, by plotting fluorescence against the cycle numbers on a logarithmic scale. Measurements are normalized using the endogenous control.

QRT-PCR was performed on cDNA using the Applied Biosystems StepOnePlus™ Real Time PCR system and Power SYBR® Gene Master mix (Applied Biosystems), according to the manufacturers instructions. QRT-PCR was performed in triplicates with the standard PCR program containing and elongation step for detection of the melting curve:

Sample preparation:

cDNA probe: 10 µl of cDNA diluted in H₂O (1:40)

SYBR probe: 12.5 µl SYBR mix

0.1 µl primer mix

2,4 µl H₂O

final volume: 25 µl

Standard qRT-PCR program: °

Step 1: 95 °C, 15 min

Step 2: 95 °C, 15 sec

Step 3: 55 °C, 15 sec

Step 4: 60 °C, 45 sec

Step 5: 40 cycles between step 2 and 3

Step 6: 60 °C, 45 sec

For determination of the melting curve further steps were added:

Step 7: 95 °C, 15 sec

Step 8: 60 °C, 1 min

Step 9: 95 °C, 15 sec

Transcript abundance was determined using the $2^{-\Delta\Delta Ct}$ method and calculated as followed:

Step 1:

Mean of Ct_{1-3} gene x = $mCt_{gene\ x}$

Mean of Ct_{1-3} normalizer = mCt_{norm}

Step 2:

$\Delta Ct = mCt_{norm} - mCt_{gene\ x}$

Step 3:

Relative mRNA levels = $2^{-\Delta Ct}$

Expression data were normalized using the GFP transgene, which is expressed constitutively under the *EF1 α* promoter (Janse *et al.*, 2006b) or the house keeping gene *gapdh*.

The melting curve and H₂O negative control was analyzed, to exclude gDNA contamination and primer efficacy.

2.2.2.5. Agarose gel electrophoresis

Gel electrophoresis is used to separate DNA molecules, according to their charge, size and conformation. Due to the DNA phosphate backbone, molecules are negatively charged and migrate inside an electric field to the positive pole the (anode). Depending on their length they are transported differentially fast and far through the gel. Gels were prepared from 0.8 – 1 % agarose in 1x TAE buffer. The solution was boiled in a microwave oven to dissolve the agarose and allowed to cool down 50 - 60 °C, before SYBR Safe green (10 µg/100 ml) was added. The DNA samples were loaded in 1x loading dye, additional to the 1 kb ladder and separated by 100 V for 1 hrs. Ultraviolet light was used to visualize the separated DNA molecules in a gel documentation system.

2.2.2.6. DNA purification by ethanol precipitation

To obtain purified and concentrated DNA, mainly for the transfection of parasites, precipitation using sodium acetate and ethanol was used. 0.1 x volume of sodium acetate (pH 4.8) and 2.5 x volume ethanol 100 % were added to the DNA and incubated for 30 min at -80 °C. The precipitated DNA was collected by centrifugation for 10 min at maximum speed (13000 rpm) at 4 °C. The DNA was washed two times with ice-cold ethanol 70 % and centrifuged for 5 min at 4 °C. The air- dried DNA pellet was than dissolved in an appropriate volume of ddH₂O.

2.2.2.7. DNA purification by gel-extraction (Quiagen)

PCR fragments as well as digested vector backbones were purified by gel- extraction. Separation of DNA was performed by agarose gel electrophoresis. Importantly, during cutting the fragment out of the gel, UV-light illumination should be avoided. This could be facilitated by running a reference probe next to the sample where the size is designated, which is than used for orientation in the gel. The exercised gel block containing the sample is further processed under manufactures instructions using the gel extraction kit (Quiagen).

2.2.2.8. DNA purification by PCR purification Kit (Quiagen)

This method is preferentially used for purification of PCR fragments and digestion preparations. DNA fragments with appropriate size (up to 10 kb) can be purified with a silica membrane. Further sample processing was done under manufactures instructions.

2.2.2.9. Determination of DNA concentration

The absorption of UV light by nucleic acids is direct proportional to the concentration of DNA. The UV absorption of DNA is highest at 260 nm. For calculation of DNA concentrations the optical density at 260 nm (OD₂₆₀) is used:

$$(\text{OD}_{260} \times \text{dilution factor} \times 50)/1000 = \text{DNA concentration in } \mu\text{g/ml}.$$

The maximum UV light absorption for proteins is 280 nm, therefore the DNA purity can be calculated as the proportion of OD₂₆₀/OD₂₈₀. Plasmid DNA should have the purity in a range of 1.8 – 2.0. Alternatively the Nanodrop spectrophotometer can be used.

2.2.2.10. Vector and Insert preparation

For cloning the gene/insert of interest into the target vector, first the plasmid and the PCR amplified gene/insert were digested with the respective restriction endonucleases. One unit of endonuclease enzyme corresponds to the amount of enzyme required to digest 1 µg of DNA under optimal conditions, which depend on the optimum temperature and the proper enzyme buffer. The standard endonuclease digestion reaction used for cloning consists of the following:

1-2 µg DNA

1-2 U/ml restriction enzyme

1x BSA (bovine serum albumine, indicated if necessary)

1x Enzyme buffer

ddH₂O/ add to the final volume

DNA digestion can be done simultaneously by two restriction enzymes, if a suitable buffer is available. After digestion the DNA was purified, mainly using the PCR-purification kit or gel extraction kit (Qiagen), and was eluted in water.

Optional, the vector was dephosphorylated for 1hr at 37 °C using the rapid- ligation kit (Roche), to prevent intrinsic vector ligation. Subsequently, dephosphorylated DNA was purified with the PCR-purification kit (Quiagen).

2.2.2.11. Ligation of DNA fragments

The ligation of the digested and dephosphorylated vector with the insert was done with the rapid ligation kit (Roche) at 1: 7 molar ratio (vector: insert). T4-Ligase was added for 20 min at room temperature or at 4 °C overnight, following the manufacturers instructions. Afterwards, the ligation reaction is ready to be transferred into competent bacterial cells. The remainder of the ligation reaction can be kept on ice or frozen at -20 °C.

2.2.2.12. Plasmid DNA preparation

The plasmid isolation from the bacterial cells was done by alkaline lysis. This method lyses the bacterial cell wall and plasma membrane. For precipitation of the proteins, lipids, and genomic DNA, acetic acid was used. The circular plasmids do not precipitate and remain in the soluble supernatant. The "QIAprep Spin Miniprep Kit" (Qiagen), was used to isolate the recombinant plasmids from the 5 ml overnight culture. Finally plasmids were eluted in 50 µl H₂O. A detailed description of the isolation procedure is described in the manufacturers manual. Midi-scale plasmid preparations were done using the MIDI- kit (Quiagen).

2.2.2.13. Sequencing of DNA fragments

Sequencing is an important step to confirm the correct DNA sequence of the transgene, to ensure subsequent functionality and to reduce mice numbers for transfection and subsequent cloning.

Every DNA fragment, which was used for transfection, was send to a company for sequencing (eurofins mwg | operon).

2.2.3. Methods for *Plasmodium berghei*

2.2.3.1. Transfection of *Plasmodium berghei* parasites

During transfection, foreign material, *i.e* DNA, RNA, or proteins were introduced into eukaryotic cells. Stable DNA transfection has been reproducibly established in *P. falciparum* and *P. berghei* (Thathy and Menard, 2002). The transfection in *Plasmodium* was performed using the blood stage parasites. Molecular biology approaches allow gene targeting, gene inactivating or gene modifying by homologous recombination between the introduced transgene and the genomic DNA. Since, *Plasmodium* is haploid for almost all parts of its life cycle a simple gene targeting event is sufficient to generate a loss of function mutant (de Koning-Ward *et al.*, 2000; Menard and Janse, 1997; van Dijk *et al.*, 1995; Waters *et al.*, 1997). A major limitation, however, is the inability to delete genes that are essential for

asexual blood stage growth. Two stable transfection strategies; (i) the integration strategy, where a single crossover occurs to alter the gene of interest, and (ii) the replacement strategy, which needs two crossover events to replace the target gene (de Koning-Ward *et al.*, 2000).

2.2.3.2. Transfection schizont culture of *P. berghei*

Transfection was done in mature schizonts that are capable to infect new erythrocytes after the transfection event. To gain parasites, NRMI mice or Wistar rats were infected by intra-peritoneal injection of the respective *Plasmodium* host strain. In this study the Anka or the Anka-GFP-507cl stain (Janse *et al.* 2006) were used. Animals with 2 to 3 % parasitemia and low gametocyte density were employed for the schizonts culture. The blood was harvested by heart puncture from isofluran-anesthetized animals with heparin-treated syringes. The blood was washed once in 10 ml of pre-warmed transfection media, containing 250 µl heparin/PBS (200 U/ml) and erythrocytes were isolated by centrifugation at 1000 rpm for 8 min at room temperature. The blood pellet was mixed with 50 ml of pre-warmed transfection media and pipetted under the final 100 ml transfection culture in the Erlenmeyer vessel. The culture was incubated for 15- 16 hours at gentle shaking by 77- 80 rpm at 37°C in a mixed gas incubator. The gaseous atmosphere contained 10 % O₂, 5 % CO₂ and 85 % N₂. During this culturing, almost all blood stages mature into late schizonts. The quantity and quality of schizonts can be tested, by making a Giemsa stained blood smear, from the culture.

2.2.3.3. Schizont Isolation

To purify mature schizonts, a 55 % Nycodenz gradient centrifugation was used. 35 ml of the overnight culture is distributed into 4 x 50 ml falcon vessels and 10 ml of the Nycodenz gradient (room temperature) was mounted under the culture. For gradient generation, the culture was then centrifuged for 25 min at 1000 rpm (without brake!) at room temperature. Mature schizonts are accumulated in the brownish interphase ring and were collected with a Pasteur pipette. Schizonts were washed in 30 ml transfections media in two falcon tubes with centrifugation for 10 min at 1000 rpm (without break). The pellet was subsequently suspended in 10- 15 ml media (10 to 30 x 10⁶/ ml schizonts). 1 ml of schizonts per one transfection was sedimented in 1,5 ml eppendorf tubes by centrifugation of 1 min at 13.000 rpm at room temperature.

2.2.3.4. Transfection of *P. berghei* schizonts by electroporation

The electroporation increases the cell plasma membrane permeability by an external electrical field so that the DNA can easily be taken up. The electroporation was facilitated by usage of

the Amaxa electroporator and the U33 program. First, the parasite pellet was resuspended in 100 µl of human T-cell nucleofactor solution and afterwards mixed with the transfection vector. The whole mixture was placed into the transfection cuvette and electroporation was started. Afterwards, 50 µl of fresh transfection media was added and the whole transfection solution was injected intra-venously into two recipient NMRI mice.

2.2.3.5. Positive selection of recombinant parasites

24 hours after transfection the selection pressure was started by the antifolate drug pyrimethamine. Pyrimethamine (70 ng/ml; pH 3.6- 5.0) was added to the drinking water and parasitemia was monitored over a period of six to ten days. Depending on the genetic strategy, mice became positive at different time points. Using the insertion strategy resistant parasites became positive between 5 - 7, and by replacement strategy mice became positive at day 8-12, respectively. Positive blood samples were collected by heart puncture and stored as stabilates, as gDNA for genotyping or were transferred to naïve mice for parasite cloning.

2.2.3.6. Long-term storage of blood stage parasites

Infected blood was mixed with freezing solution in a 1: 2 ratio (100 µl blood with 200 µl freezing solution), and stored in liquid nitrogen for long-term or at -80°C for short-term storage.

2.2.3.7. Giemsa-stained blood smears and determination of parasitemia

Giemsa staining allows the monitoring of red blood cell infection, differentiation between developmental stages and determination of the parasitemia, the percentage of erythrocytes infected with *Plasmodium*. A blood drop was taken from the tail of the mice and smeared onto the glass slide. The air-dried smear was fixed in methanol for 3 - 5 min, and afterwards stained with 10 % Giemsa solution for 10 - 20 min. After the slides were rinsed with H₂O and air-dried, microscopic observation followed. Using the 100x objective (immersion oil) in the bright field microscope, the average number of erythrocytes in two fields was determined. Subsequently, the amount of parasites was counted in 10- 30 fields, with comparable erythrocyte density. Finally, the parasitemia is calculated as follows:

$$\sum \text{ of parasites} / (\sum \text{ of erythrocytes per field} \times \sum \text{ of counted fields}).$$

2.2.3.8. Preparations of *P. berghei* blood stage parasites

The genomic DNA was isolated from blood stage parasites for gene amplification or genotyping of transgene parasite lines. Parasite infected erythrocytes were purified from leukocytes and thrombocytes by running the blood through a column filled with batting, cellulose and glass beads (from the bottom up). The erythrocytes are eluted from the column with 1x PBS and collected in a 15 ml falcon. Erythrocytes were pelleted by centrifugation at 1500 rpm, for 8 min at room temperature. Subsequently, parasites were obtained by erythrocyte lysis, through resuspension of the erythrocyte pellet in 14 ml 0.2 % Saponin/1x PBS. The parasites were pelleted by a following centrifugation of eight minutes at 3000 rpm, room temperature. Parasites were transferred to a 1.5 ml eppendorf tube. Two washing steps, including resuspension of the parasite pellet in 1 ml in 1x PBS and centrifugation at 7000 rpm for 3 min at room temperature were applied. Parasite pellet was dissolved in 200 µl PBS 1x, and stored at -20 °C, or further processed to gDNA for genotyping, or for western blot samples.

2.2.3.9. Genomic DNA (gDNA) preparations from *P. berghei*

Parasites mostly blood stages, dissolved in 200 µl 1x PBS, and stored by -20 °C, were thrown and processed following the manufacturers manual of the “QIAamp DNA-Blood Mini Kit”, (Qiagen). Finally, gDNA is eluted in 200 µl H₂O and stored at -20 °C.

2.2.3.10. Isolation messenger RNA (mRNA) from *P. berghei*

For gene expression analysis or for cloning of genes without introns, mRNA was isolated from different life cycle stages. All parasite stages were treated using the same protocol accordingly to the “RNeasy Mini Kit” manual (Quiagen). Collected parasite cells were kept in 350 µl RTL buffer with 3.5 µl β-Mercaptoethanol, in RNase free tubes and stored at -80 °C. After mRNA isolation, samples were eluted in H₂O and subsequently processed to cDNA. If this was not possible, samples were stored at -80 °C. An additional DNase treatment was applied (Turbo DNase) to ensure purity of mRNA samples. It is important to avoid constant defrosting of the sample, because of mRNA instability. The whole mRNA isolation and processing was done quickly and with usage of filter tips to avoid RNase contamination of the sample.

2.2.3.11. Parasite cloning

Clonal parasite populations were obtained *in vivo* by intravenous injection of limiting dilutions of one parasite into recipient NMRI mice, and calculated as follows:

$$7 \times 10^6 (\sum \text{number of erythrocytes per 1 ml blood}) \times \text{parasitemia} \times 10^{-2} \text{ parasites} \\ = \text{number of parasitized erythrocytes per } \mu\text{l blood.}$$

Blood was collected by heart puncture from mice with < 1 % parasitemia and six to ten fold dilution were made in RPMI (100 μl blood: 900 μl RPMI), on ice. Single parasites were injected intra-venously into NMRI mice and kept under pyrimethamine treatment. Finally, genotyping using specific primers were used to confirm clonality.

2.2.3.12. Blood stage development / Growth curve analysis of *P. berghei*

To determine blood stage development of mutant and wild type parasites *in vivo*, mice were infected intravenously with 1.000 mixed blood stage parasites. Groups of seven NMRI mice were used. Parasitemia was determined by daily microscopic examination of Giemsa- stained blood smears. Growth curve analysis was done, by plotting parasitemia against time of both groups.

2.2.3.13. Exflagellation assay of male gametocytes

The development of male and female gametocytes can be observed using Giemsa-stained blood smears. Furthermore, the exflagellation process of male gametocytes, which normally occurs in the mosquito midgut, can be visualized *ex vivo*. A drop of blood is placed onto a cover slip and examined with the 40x objective in the bright field microscope. The temperature drop of 2 - 5 °C (to room temperature) induces the exflagellation process after ~10 min, *in vitro* (Billker *et al.*, 1997). Analysis of the exflagellation is important in order to characterize the functionality of mutant parasites and obtain an optimal mosquito infection rate.

2.2.3.14. Gametocyte enrichment and purification

In order to gain high gametocyte ratio in the infected mice, mice were treated with 100 μl of phenylhydrazin/NaCl solution (6.82 μl Ph in NaCl) by intra peritoneal injection, one day before infection with *P. berghei*. After infection, parasitemia and exflagellation is monitored daily. At time points (3- 4 days after blood meal) when high exflagellation occurs,

sulfadiazine (12.5 mg/l) is added into the drinking water of mice, freshly. Sulfadiazine efficiently kills all asexual stages, but not gametocytes. At 48 hrs after starting treatment with sulfadiazine, the blood was harvested by heart puncture and run through a column as used for blood stage parasite purification. All steps are performed quickly at high room temperature and 37 °C warm PBS to avoid gametocyte activation. Here, I used PBS only and not the rich medium, because of sample preparation for mRNA or western blot. The gametocytes were isolated from blood by a Nycodenz gradient centrifugation, as described for schizonts purification. The brown interphase ring represents the gametocyte fraction and was collected with Pasteur pipette. One washing step was included with 10 ml 1x PBS and centrifugation by 1.500 rpm for 3 min. The quality of the gametocyte fraction was estimated by a Giemsa-stained smear. The material was further processed to mRNA or western blot samples.

2.2.3.15. Mosquito infection with *P. berghei*

In order to get high infectivity rates, mosquitoes should be 2- 4 days old. Starvation of 4- 8 hrs prior blood meal, can enhance the amount of sucking mosquitoes. Infection was done, by feeding of mosquitoes on narcotized NMRI mice infected with *P. berghei*. Therefore, it is important, that mice exhibit significant exflagellation with 4 to 6 exflagellation centers (one male gametocyte) in the microscopic field (2000-3000 erythrocyte). The infected mouse was placed on top of the mosquito cage for 15 - 30 min. The mice were narcotized with ~100µl ketamin/ xylazinhydrochlorid (depending on the weigh and age of the mice). After blood meal the mosquitoes were placed into the incubator to ensure optimal parasite development.

2.2.3.16. Ookinete culture and purification

Ookinetes from *P. berghei*, which normally occur in the mosquito midgut, can easily be cultured *in vitro*. Fresh blood was harvested from infected NMRI mice. 1 ml of the blood was mixed with 9 ml of the complete ookinete medium (pH 8.0) and cultured for 17- 20 hrs in a small cell culture flask inside the mosquito incubator. For purification the blood was concentrated from the culture by centrifugation with 1.500 rpm for 8 min at room temperature, without break. Depending on the further processing Ookinetes were harvested either with p28 labeled magnetic beads or with 0.17 M NH₄Cl₄ (Ammonium chloride), erythrocyte lysis.

The purification with magnetic beads is fast and easy, but should not be used by subsequent IFA with anti mouse antibodies. The ookinete pellet is transferred into a 2 ml eppendorf tube under dilution with ookinete medium. 3 µl of the p28 labeled beads (p28 is an ookinete specific surface molecule) were added and incubated for 10 min an on rotation wheel at room

temperature. The tube was placed into the magnetic rack and the blood was carefully removed. Two washing steps with adding 1 ml ookinete or 1x PBS are recommended to remove residual blood cells. Finally the ookinetes bound to the magnetic beads can be resolved in appropriate ookinete medium for further processing.

For the Ammonium chloride method, the ookinete pellet was resolved in 50 ml ice cold 0.17M NH_4Cl , and incubated for 30 min on ice, inducing erythrocytes lysis. The ookinetes were pelleted by centrifugation with 1.500 rpm, for 5 min, at room temperature, without break.

Ookinetes were further processed.

Ookinete numbers are determined using the Neubauer counting chamber and calculated as following:

$$\begin{aligned} (\Sigma \text{ ookinetes per 4 field} / 4) \times 10 \times \text{dilution factor} &= \text{numbers of ookinetes} / \mu\text{l} \\ \text{number of ookinetes} / \mu\text{l} \times \text{total volume} &= \Sigma \text{ of ookinetes in the sample} \end{aligned}$$

2.2.3.17. Ookinete indirect immuno fluorescence (IFA)

After standard ookinete culture and purification, ookinetes were mixed with complete ookinete medium and incubated on poly L lysine coated cover slips for 30 min at room temperature. After ookinete settlement, they were directly fixed with 4 % PFA or MTSB/4 % PFA (microtubuli stabilizing buffer), for 10 min, on ice. After removing the fixative, the ookinetes were permeabilized with 0.2 % TritonX-100 in 1x PBS (250 μl /well), for 3 min, at RT. Blocking was done with 3% BSA in 0.2 % TritonX-100 in 1x PBS, for 20- 30 min, at RT. The primary antibody was used by given dilution in 3 % BSA in 0.2 % TritonX-100 in 1x PBS, for 1- 2 hrs at room temperature or at 4 °C overnight. After three washing steps with 1x PBS for 10 min, the secondary antibody with given dilution in 3 % BSA in 0.2 % TritonX-100 in 1x PBS was incubated for 1- 2 hrs at RT, or at 4 °C overnight. After two washing steps with 1x PBS the DNA was stained with Hoechst 33342, Dapi or Draq5 in 1: 1.000 dilution with PBS. Finally the cover slips were mounted onto glass slides with Fluoromount G.

2.2.3.18. Ookinete motility assay

For this ookinete motility assay, ookinetes were cultured and purified under standard conditions using p28 labelled beads. Ookinetes were set in commercially available basement membrane preparation, matrigel. Motility of individual ookinetes was analyzed combined with time- lapse microscopy. Note, that aliquots of matrigel need to be defrosted overnight at 4 °C Purified ookinetes were left in ookinete medium, 20 μl of ookinetes and 20 μl of matrigel, were gently mixed by a cut tip, to avoid bubbles. 6 μl were spotted onto a

microscope cover slip (18 x 18) rimmed with a thin layer of Vaseline. A couple of cover slips were prepared that way, and left at room temperature for 30 min, at 22- 24 °C, for polymerization of the matrigel. The samples were checked for settled ookinetes and fixed erythrocytes, to ensure proper motility. These samples were analyzed with the 63x oil objective in DIC/phase illumination. Time-lapse movies were taken by 1 picture every 5 seconds for 10 minutes. Only ookinetes, which stayed the whole time in the view were used. To track the velocity, the movies were analyzed using the *ImageJ* software and the plugin *manual tracking*. The information about the time between each single picture and the conversion factor (Tab. 4) of each pixel in μm , allows setting of fix points and measuring the distance between each picture. The distance for every ookinete was followed over time. Finally, the velocity was calculated using the *Excel* program as following:

$$v \text{ (velocity)} = s \text{ (distance)} / t \text{ (time)}$$

Table 4. The conversion factor for different objectives

objective	1 pixel equates	1 μm equates
100x	0.0645 μm	15.504 pixel
63x	0.0984 μm	10.163 pixel
40x	0.156 μm	6.41 pixel
25x	0.249 μm	4.016 pixel
10x	0.627 μm	1.595 pixel

2.2.3.19. Ookinete microinjection into the mosquito

Cultured and purified ookinetes were injected into *A. stephensi* female mosquitoes as described earlier (Sinden *et al.*, 2002; Weathersby, 1952). Female mosquitoes (~35) were collected in nets covered cups, at least one day before injection. Ookinets were cultured and purified under standard conditions. Defined numbers were resolved in ookinete medium adequate to 750 ookinetes in 69 nl (nano) of injection volume. In total 1500 ookinetes were injected into one mosquito by two times of 69 nl injection. Mosquitoes were anesthetized with carbon dioxide out on a porous polyethylene pad, coupled to a flow regulator (5 l/ min at the flow body and 1 l/ min at the polyethylene pad). Mosquitoes should be anesthetized not longer that 20 min, for high recovering. The injection was done by a micro injector II

(Drummond Nanoject), into the small round chitin plate at the thorax. Mosquitoes were placed back into the cup and fed and incubated like usually.

2.2.3.20. Propagation of *Anopheles stephensi* mosquitoes

The mosquitoes were raised in a 14 hrs light /10 hrs dark cycle, 75 % humidity and at 28°C or 20°C for uninfected and infected mosquitoes. Mosquitoes were fed with sucrose solution and mosquito breeding solution.

2.2.3.21. Mosquito midgut preparation and infectivity determination

Mosquitoes were sucked out of the cage and collected in a 15 ml falcon tube and are kept on ice to anesthetize them. They were washed once in 70 % ethanol and once in PBS 1x. Dissection takes place in PBS or PRMI under the binocular microscope. With the help of one forceps and one syringe tip the abdomen is gently removed so that the midgut becomes visible. Mosquito midguts can be stored either in PBS or RMPI media, depending on the processing. Infectivity can be easily estimated by GFP fluorescence of the oocysts at day 10 after infection (if the Anka-GFP-507cl strain was used). Also, non-fluorescent oocysts become visible under higher magnification (40x, 100x).

Infectivity is calculated as followed:

$$\text{Infectivity} = (100 / \Sigma \text{ total mosquitoes}) \times \Sigma \text{ of infected mosquitoes}$$

2.2.3.22. Midgut preparation for electron microscopy (TEM)

Two charges of mosquitoes were fed in parallel with WT and the mutant parasites. Mosquitoes were dissected directly in PBS 1x without the washing step in ethanol. Midguts were fixed and stored in 2.5 % glutaraldehyde/PBS (EM grade) at 4 °C.

2.2.3.23. Transmission electron microscopy of midgut-associated oocysts

For fine structural analysis, midguts were fixed with 2.5 % glutardialdehyde, postfixed with 1 % osmiumtetroxide, contrasted with tannic acid and 1 % uranyl acetate. After dehydration samples were embedded in Polybed (Polysciences). After polymerization, specimens were cut at 60 nm slides and contrasted with lead citrate. Specimens were analyzed in a Leo 906E transmissionelectron microscope at 100KV (Zeiss, Oberkochen) using digital camera (Morada; SIS).

2.2.3.24. Oocyst number and size determination

Oocyst numbers were counted at least from 10 infected mosquitoes, using the 10x fluorescence objective and ten randomly selected microscopic fields.

For size determination and microscopic analysis of the architecture, midguts were shortly fixed for 10 min in 4 % PFA, and permeabilized in 0.2 % Triton X100 for 20 min at room temperature. DNA was stained with Hoechst 33342 for 10 min and midguts were subsequently mounted in

40 % glycine/ PBS on glass cover slides. The development of the parasite oocyst was investigated over time using a LSM510 confocal laser-scanning microscope (Zeiss). The oocyst diameter was measured using the LSM510 image observer software.

2.2.3.25. Life death assay with SYTOX® Orange on midgut associated oocysts

Infected midguts were incubated for 10 min at RT in 0.5 μ M SYTOX/PBS and subsequently, mounted in 40 % glycerin solution.

2.2.3.26. IFA on oocysts

Oocysts have a very thick capsule, which is difficult to penetrate. Depending on the question either mild or harsh conditions are needed. Infected midguts were dissected in PBS, washed 1x short in Methanol (-20 °C)(optional), and were fixed in 4 % PFA, for 10 min. The harsh permeabilization was in 1 % Triton X100/ PBS, for 1 hr, at 37°C. After blocking in 3% BSA, 0.2 % triton PBS, three washing steps in PBS 1x, for 10 min followed. The primary and secondary antibodies were used under given dilution in 3 % BSA, 0.2 % triton PBS, for 1- 2 hrs at 37°C. Finally, two washing steps with PBS for 10 min, and incubation with Hoechst 33342 and Draq5 were done. Oocyst IFAs were mounted in Fluoromount G and sealed with nail polish.

2.2.3.27. Isolation of midgut and salivary gland associated sporozoites

Midgut sporozoites were mainly isolated at day 14 after mosquito infection. Salivary gland sporozoites were isolated between days 17 - 21 after infection. At day 14 midguts were isolated as described before and collected on ice in RPMI media containing 3 % BSA. Midguts were smashed extensively and centrifuged with low speed at 800 rpm for 3 min, at 4°C. The supernatant contains the sporozoites and is collected. The difficulty to isolate salivary gland sporozoites is the dissection of the tiny glands, which sit in pairs at the basis of the head. In brief, salivary glands are collected in RPMI with 3 % BSA on ice, smashed and

centrifuged at 800 rpm, for 3 min, at 4 °C. Pelleting of sporozoites is done by centrifugation of 7000 rpm for 3 min at 4 °C. Sporozoite numbers were calculated as described for ookinetes.

2.2.3.28. Isolation of hemocoel associated sporozoites

Hemocoel sporozoites were dissected between days 19 - 25 after mosquito infection.

A glass capillary needs to be stretched under the flame, to become very thin. Mosquitoes were collected and kept on ice. Dry mosquitoes were placed under the binocular. The head, the wing ends and the last two sections of the abdomen were cut off. Using the fine glass capillary filled with RPMI and pushed into the round chitin plate at the thorax, the sporozoites were flushed out of the body cavity. The sporozoites are collected first on a parafilm and later in an eppendorf tube on ice.

2.2.3.29. IFA on sporozoite stages

8-well chamber slides were precoated with 3 % BSA/RPMI for 20 min at 37 °C, in a humid chamber. Sporozoites were dissected in 3 % BSA/RPMI and incubated for 15 min at 37 °C, to let them settle down. Fixation was done with 4 % PFA for 10 min, at RT. After permeabilization with 0.2 % TritonX100 for 15 min at RT, the samples were blocked with 3 % BSA/0.2 % TritonX100/PBS for 20 min at RT. Both antibodies were used under given dilutions in 3 % BSA/ TritonX100/PBS for 1- 2 hrs at RT, or at 4 °C overnight. In between and after antibody incubation samples were washed 3x with PBS 1x for 10 min at RT. Samples were mounted in Fluoromount G.

2.2.3.30. Sporozoite motility assay

The sporozoite motility assay can be performed either by time-lapse microscopy or by IFA.

For the second method, 8-well glass slides were precoated with 3 % BSA/RPMI for 20 min, at 37 °C, in a humid chamber. Isolated sporozoites in 3 % BSA/RPMI were disposed into the wells, and incubated for 20 min at 37 °C in the humid chamber. During this step, sporozoites settle on the bottom and start gliding. In case of the 2-dimensional glass surface, the sporozoite moves directional in circles. During gliding, the adhesive surface proteins like CSP or TRAP are shed by the parasite and can be detected by IFA with appropriate antibodies. Note that the permeabilization step is not necessary in this case.

2.2.3.31. Transmission of sporozoites to mice and determination of the prepatent period

Natural transmission of sporozoites from the mosquito vector to the mammalian host was tested by bite infection of mice by *Plasmodium berghei* infected *Anopheles stephensi* mosquitoes. Injected sporozoites are transported by the blood circulation system to the liver where they invade hepatocytes and develop into exoerythrocytic forms (EEF). After ~68 hr of liver stage development liver merozoites bud from the hepatocyte and merozoites escape into the blood circulation to infect erythrocytes. The prepatent period is the time interval between infection and the first ability to detect the infection by a diagnostic method. In case of *Plasmodium berghei* it normally takes three days after infection to detect first blood stage parasites by Giemsa- stained blood smears. Infection was done usually on C57/Bl6 mice. Mice were anaesthetized with intraperitoneal injection of 80µl ketamin/xylazin and placed 15 - 20 min on top of the mosquito cage.

Infection of mice was done by intravenous (also possible: intradermal or sub dermal) injection of isolated sporozoites. Thereby a defined number of sporozoites in RPMI are injected (1000-10.000 spz.). The prepatent period was estimated by Giemsa-stained blood smear daily.

2.2.3.32. Propagation of mammalian cells

Human hepatoma (Huh7) cells were maintained in collagen pre-coated 24 well plates (3 x10⁵ cells/well), in multi-well plates or in chamber slides, in complete culture medium (DMEM / FCS 10 % / penicillin/streptomycin). Cells were maintained humidified incubator (10 % CO₂, 37 °C).

2.2.3.33. Infection of Huh7 cells *in vitro*/ development of exoerythrocytic stages (EEF)

To study *P. berghei* liver stage development *in vitro*, the human hepatocellular carcinoma cell line (Huh7) was used and infected with isolated salivary gland sporozoites. The development can be followed up to 65 to 72 hours.

For infection, mosquitoes were washed 1x in ethanol and 3x in DMEM media. Sporozoites were isolated and stored in DMEM on ice. For infection, sporozoites were purified and resuspended in DMEM complete. Before infection, Huh7 cells were washed 1x with DMEM complete. Wells were infected with 10.000 sporozoites in 300µl DMEM complete. After settlement for 1 hr at RT in the dark or optional centrifugation for 5 min at 3000 rpm, wells were incubated for 2 hrs at 37 °C with 5 % CO₂. Subsequently wells were washed 3 times with 300 µl HBSS and finally incubated in 300 µl DMEM complete. Medium was changed daily.

2.2.3.34. Fixation of EEFs

After the medium was removed, cells were fixed with 250 µl methanol, which was immediately removed and followed by a second incubation with fresh 250 µl methanol for 10 min at RT. After two washing steps with PBS 1x, cells can be kept at 4 °C or further processed. IFA was done as described for ookinetes, starting with the blocking step. Cells can also be fixed with 4 % PFA, but the cells need to be permeabilized with 0.2 % TritonX100 /PBS before blocking.

2.2.3.35. Live cell imaging

RBCs: infected erythrocytes were diluted with 37 °C warm RPMI media, and incubated on ConcavalinA coated cover slides for 10 min at RT. The slides were washed once and mounted in 40 % glycerin/PBS. Live cell imaging was performed afterwards.

Ookinetes: were kept in complete ookinete medium, placed on the glass slide and covered with a Vaseline rimmed cover slip. Sealing was done with paraffin.

Sporozoites: were also kept in 3 % BSA/RPI medium and handled as described for ookinetes.

EEFs: Cells were washed 1x with DMEM complete. Medium was removed and cells were mounted in one drop (10µl) of 40 % Glycin/ PBS on cover slips. The cover slip was sealed with paraffin. Importantly, do not use Fluoromount G for live cell imaging it is toxic! Difference between the color emergence of the GFP and mCherry channels in blood and ookinete stages are due to the different microscopes, which have been used for live cell imaging.

2.2.3.36. Sample preparation for western blot (denaturing conditions)

All samples regardless of their origin, were treated the same way. Purified stages were properly washed with PBS to avoid contamination, counted and pelleted with maximum speed for 3 min. Pellet, was lysed with appropriate amount of Lysis buffer for 30 min on ice (100.000 sporozoites in 11 µl final vol.). 2x Laemmli buffer was added to the lysate in 1: 1 dilution so that the final sample concentration is 1x Laemmli in 11 µl. Samples were cooked for 5 min at 95 °C, shortly centrifuged, aliquoted into the final loading volume (11 µl), and stored at -20 °C.

2.2.4. Protein biochemical assays

2.2.4.1. Protein analysis by SDS-PAGE

Proteins were analyzed by sodium dodecyl sulfate polyacrylamid gel electrophoresis (SDS-PAGE). Here, the proteins are separated by their molecular weight. The natural protein conformation is destroyed by SDS, and the protein-surface becomes negatively charged, so that the protein migrates inside an electric field. The stacking gel focuses the probes at the same level before chromatographic resolution is started. Proteins are separated by the resolving gel where the pore size determines the migration speed and distance. For all samples a 15 % SDS PAGE was prepared:

Table 5. Ingredients for preparations of 15 % SDS-PAGE

For 2 gels	15 % resolving gel	stacking gel
Protogel polyacrylamide	9.9 ml	2 ml
Tris- HCl buffer	5 ml (1.5 M Tris, pH 8.8)	1.5 ml (1M Tris, pH 6.8)
10 % SDS	200 µl	120 µl
H ₂ O	4.7 ml	8.3 ml
10 % APS	200 µl	120 µl
TEMED	8 µl	12 µl
Total volume (ml)	20 ml	12 ml

The SDS-PAGE was run in electrophoresis buffer for 2 hrs at 100 V at RT. The Gel can be stained with Coomassie for 30 min and vacuum dried, or further processed by western blot analysis.

2.2.4.2. Western blot analysis

After protein separation by SDS-PAGE, proteins were transferred or “blotted” to a PVDF membrane by the “wet blotting” method. Here, the blotting was done under wet conditions in ice cooled transfer buffer for 1 hr at 100 V.

2.2.4.3. Indirect immuno-detection by luminescence

The PVDF membrane was blocked on the shaker in 5 % milk/TBS-T buffer overnight at 4 °C, or for 2 - 3 hrs at RT. The first antibody was diluted in TBS-T 0.1 %, with 1% milk for 2 hrs at RT, or overnight at 4 °C. The blot was washed 3 x with TBS-NP40 0.05 % for 10 min at the shaker, and subsequently incubated with the secondary horseradish peroxidase (HRP)

conjugated antibody diluted in TBS-NP40 0.05 % for 1- 2 hrs at RT, or at 4 °C overnight. Finally, the blot was washed 3x in TBS-NP40 0.1 % and incubated with the ECL-solution and the chemiluminescence was detected in the Fuji LAS3000 detector.

3. Results

3.1. Characterization of the cyclase-associated protein (C-CAP) in *P. berghei*

3.1.1. Annotation of the *Plasmodium C-CAP* gene

Initially, the *Plasmodium berghei C-CAP* gene (old ID: PB_001030.01.0 new ID: PBANKA_020800) was not completely annotated in the PlasmoDB data bank. The first start methionine and the following amino acids were absent in predicted protein sequences as well as the corresponding nucleotide sequence (Fig. 6 C, D). In order to reveal the complete protein sequence and gene architecture, polymerase chain reactions (PCR) were performed on complementary deoxyribonucleic acid (cDNA) from blood stage schizonts with forward primers that anneal in the 5'prime region (B5) of the *C-CAP* gene and a reverse primer in the annotated open reading frame (B7) (Fig. 6A, Tab. 2). PCR using indicated primers yielded an amplicon of 500 base pairs (bp) on genomic DNA (gDNA) and of 250 bp on cDNA, indicating the existence of an intron (Fig. 6 B). The 250 bp PCR fragment was cloned into the TOPO 1.4-Vector for sequencing. Alignment of the sequenced *P. berghei* 250 bp amplicon with the annotated the *Plasmodium falciparum C-CAP* protein sequence identified the missing nucleotides and the corresponding gene structure (Fig. 6 C, D). The *P. berghei C-CAP* gene is encoded by an initial exon of 16 base pairs and a second exon of 470 base pairs, which are separated by an intron of 265 bp. Splicing of the messenger ribonucleic acid (mRNA) resulted in an 486 bp long coding sequence (CDS) for the C-CAP protein of 161 amino acids.

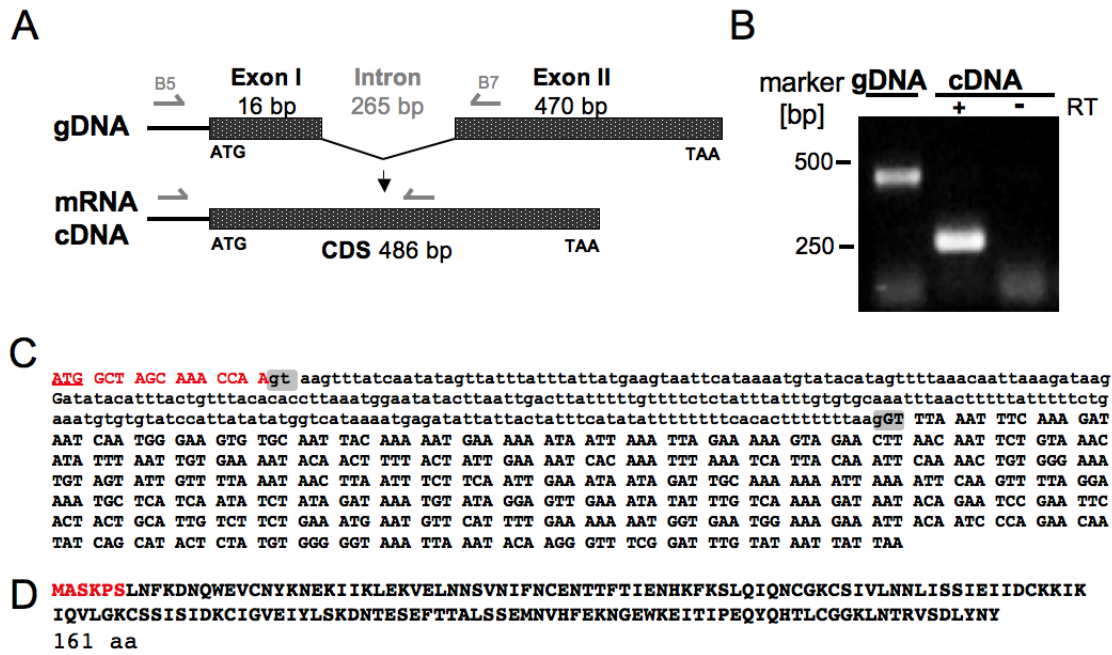


Figure 6: Complete gene annotation of the cyclase-associated gene (C-CAP).

(A) Model of the annotated *C-CAP* gene structure on genomic deoxyribonucleic acid (gDNA), messenger ribonucleic acid (mRNA) and complementary deoxyribonucleic acid (cDNA). The *C-CAP* gene consists of two exons (grey boxes) and one intron. Primer localization and name used for PCR are indicated (grey arrows). (B) PCR amplification of fragments, revealed the existence of an intron on gDNA, which is spliced out on mRNA/cDNA resulting in a short 250 base pair (bp) fragment. (C) The *C-CAP* gene coding sequence (CDS) is shown in big letters indicating the reading frame and the non-coding intron is shown in small letters. Characteristic splice sides are marked in grey. (D) Complete *Plasmodium berghei* C-CAP protein sequence. The newly identified peptide is indicated in red letters.

3.1.2. Systematic *C-CAP* gene expression profiling

To determine the *C-CAP* gene transcript abundance in different stages of the *P. berghei* life cycle, standard qualitative real time (RT)-PCR and quantitative real time (qRT)-PCR were performed. For characterization of blood stage parasites, mixed stages, synchronized rings, trophozoites were obtained *ex vivo* from infected NMRI mice, while synchronized schizonts were prepared from *in vitro* blood cultures. Mosquito stage samples were obtained from *in vitro*-cultured ookinetes, midgut-associated oocysts at day 6 after feeding, and from midgut- and salivary gland associated sporozoites. Liver stage samples were generated *in vitro* from sporozoite-infected Huh7 cells at 24 and 72 hours post infection. The housekeeping gene *Hsp70* was used for qualitative RT-PCR analysis and indicates the abundance of intact cDNA (Fig. 7 A). The constitutive expressed *GFP* gene in the Anka-GFP-507cl host strain (WT) (Janse *et al.* 2006) was used for normalization of *C-CAP* gene expression in quantitative RT-PCR.

Qualitative RT-PCR revealed that *C-CAP* gene transcripts were not abundant in mixed blood stages, rings or trophozoites (not shown). A prominent amount of *C-CAP* mRNA could only

be detected in late stage schizonts and ookinetes. This signal was abolished during sporozoite development, while control gene expression of *Hsp70* was detected in every stage (Fig. 7 A). Quantification by qRT-PCR confirmed that *C-CAP* mRNA was most abundant in late stage schizonts and ookinetes. The *C-CAP* expression decreased in young oocysts at day 6 after infection and was further reduced to background levels during sporozoite development. The lowest mRNA abundance was detected in salivary gland sporozoites. Interestingly, *C-CAP* gene transcription increased again during liver stage development and reached similar levels as detected for blood stage merozoites and ookinetes in liver merosomes at 72 hours after infection.

Taken together, the *C-CAP* gene is differentially expressed during the parasite life cycle in moderate quantities as compared to other G-actin binding proteins (Fig. 30 A-C). The highest expression was detected in merozoites and liver stage schizonts infecting the mammalian host cells, as well as in ookinetes that infect the mosquito midgut. Subsequently, sporozoite development in the invertebrate host is characterized by a drastic decrease of *C-CAP* expression.

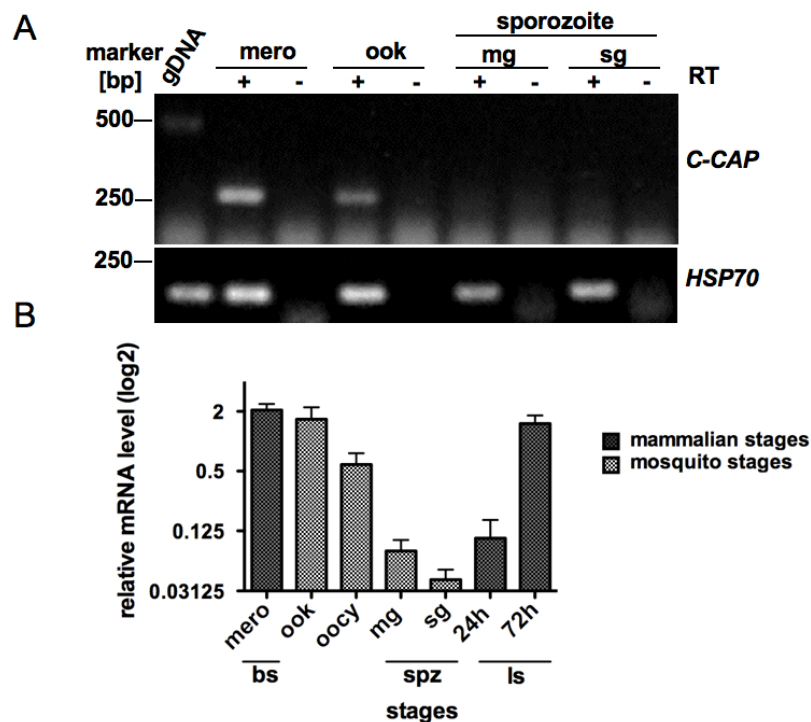


Figure 7: Expression profiling of *C-CAP* transcripts in *Plasmodium berghei* life cycle stages.

(A) *PbC-CAP* and *PbHsp70* transcript expression was monitored with reverse transcriptase chain reaction (RT-PCR) in four parasite stages: blood stage merozoites (mero) that invade erythrocytes, ookinetes (ook) that penetrate the mosquito midgut, and midgut (mg) and salivary gland (sg) sporozoites. Transcript amplification was detected in the presence (+) but not in the absence (-) of reverse transcriptase (RT). WT genomic DNA (gDNA) was loaded as control to show proper splicing of the *C-CAP* transcripts. (B) Quantitative real-time RT-PCR experiments were performed using

samples as indicated below. Transcript levels were normalized to green fluorescent protein (GFP), which is expressed as a transgene under the control of the constitutive *EF1 α* promoter and expression levels are plotted as mean of (n) independent experiments (\pm standard error of the mean, SEM). Samples: blood stage merozoites (BS mero, n= 21), ookinetes (ook, n= 18), oocyst at day 6 after infection (oocy, n= 3), sporozoites (spz) derived from midguts (mg, n= 9) and salivary glands (sg, n= 11) and liver stage parasites (LS) at 24 h (n= 3) and 72h (n= 3) after infection.

3.1.3. C-CAP is not essential for *Plasmodium* blood stage development

To systematically study the *in vivo* function of *C-CAP*, the endogenous gene locus was targeted by a gene replacement strategy. The targeting plasmid b3D.DT^H.^D+ contained the 5'UTR and the 3'UTR of the *C-CAP* gene to facilitate integration into the *C-CAP* genomic locus via double crossover homologous recombination and simultaneously deletion of the endogenous *C-CAP* gene. The introduction of the positive selectable marker *Toxoplasma gondii* dihydrofolate reductase (*Tgdhfr/ts*) into the *C-CAP* open reading frame should thus abolish *C-CAP* expression (Fig. 8 A). Homologous fragments were amplified from gDNA by PCR with specific primers for the 5'UTR (B1/ B2, Tab. 2) and 3'UTR (B3/ B4, Tab. 2) and ligated into the targeting plasmid. 10 μ g of the *KpnI* and *SacII* linearized plasmid were transfected into gradient purified schizonts of the pyrimethamine-sensitive and GFP expressing *P. berghei* Anka strain (Janse *et al.*, 2006). After pyrimethamine selection the parasites were cloned by limiting dilutions and genotyped by PCR.

Genotyping of two independent *c-cap*(-) lines confirmed successful integration of the *Tgdhfr/ts* resistance cassette flanked by 5'UTR and 3'UTR, into the host strain. PCR with recombination specific primer combinations for 5'UTR (T10/T11, Tab. 2) and 3'UTR (T8/T9, Tab. 2) integration resulted in amplification of 2317 kb (5'test) and 1025 kb (3'test) long fragments in *c-cap*(-) parasites but not in wild type parasites, confirming the integration into the genomic *C-CAP* locus (Fig. 8 B). The wild type *C-CAP* gene locus was detected as a fragment of 2752 kb (*WT*) size in parental parasites, but not in *c-cap*(-) parasites (Fig. 8 B). This confirmed the clonality of the two parasite populations. Furthermore, RT-PCR demonstrated the complete absence of corresponding transcripts in the *c-cap*(-) knockout parasites thus confirming the successful disruption of *C-CAP* gene expression (Fig. 8 C). The expression of *P. berghei* glyceraldehyde 3-phosphate dehydrogenase (*GAPDH*) remained unaffected (Fig. 8 C).

In summary, the gene deletion of *C-CAP* is feasible in blood stages and resulted in viable parasites. C-CAP is thus not essential in *P. berghei* blood stages.

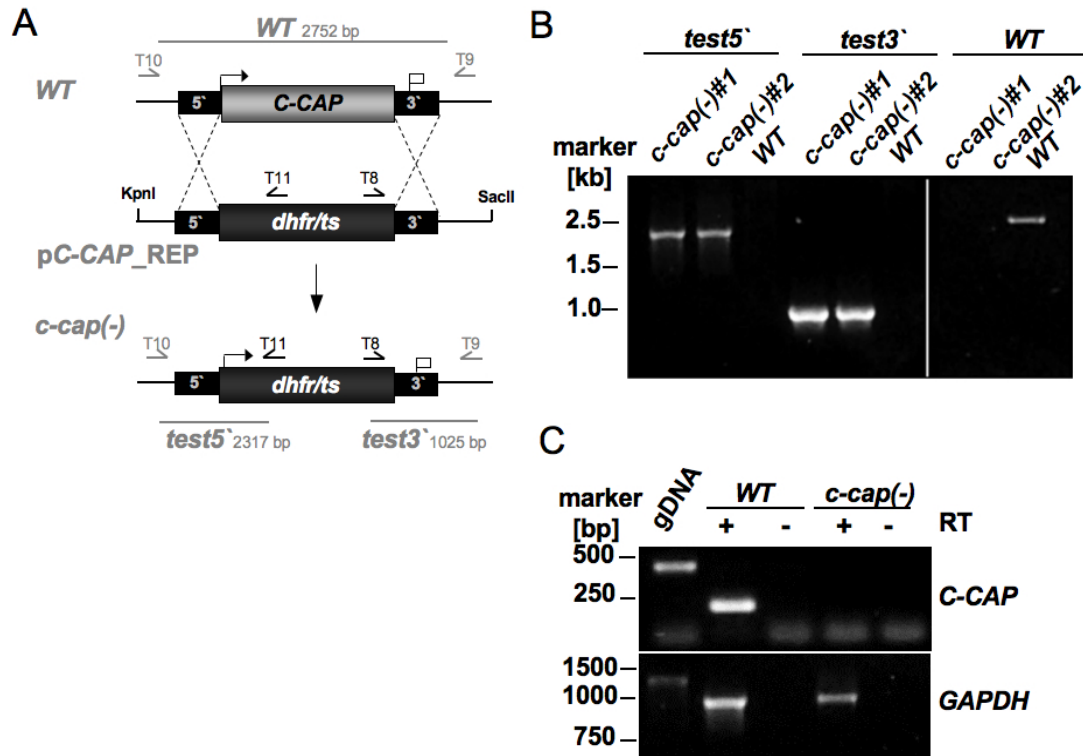


Figure 8: Generation of *Plasmodium berghei* *C-CAP* gene knockout parasites.

(A) Gene replacement strategy for the generation of the *P. berghei* *c-cap(-)* knockout parasites. The wild type (WT) *C-CAP* genomic locus is targeted with a *SacII/KpnI*-linearized replacement plasmid containing the 5'- and 3'-untranslated regions of the *C-CAP* open reading frame (ORF) and the *Toxoplasma gondii* dihydrofolate reductase (*Tgdhfr/ts*)-positive selectable marker. Upon a double crossover event, the *C-CAP* ORF is replaced by the selection marker cassette. Recombination-specific primer combinations are indicated by arrows and expected fragments by line. Primers shown in black hybridize with the vector backbone and primers (grey) hybridize to genomic DNA (gDNA) outside of the *C-CAP* ORF. (B) Genotyping of *c-cap(-)* parasites using PCR with specific primers as indicated in A, confirmed the specific 5' test integration with primers (T10, T11) and 3' test integration with primers (T8, T9) and the absence of residual wild type parasites (WT, T9, T10) in the two clonal *c-cap(-)* lines. (C) Depletion of *C-CAP* transcripts in *c-cap(-)* knockout parasites. Complementary DNA (cDNA) from WT and *c-cap(-)* blood stage merozoites was amplified by 35 PCR cycles with primers indicated in A and confirmed the absence of *C-CAP* transcripts in *c-cap(-)* parasites. Genomic DNA (gDNA) was used to control the cDNA purity.

3.1.4. Phenotypic analysis of *c-cap(-)* parasite line

3.1.4.1. *C-CAP* is dispensable for blood stage replication *in vivo*

To characterize the importance of *C-CAP* during life cycle progression, the proliferation of *c-cap(-)* parasites through blood stages was analyzed. To test if *c-cap(-)* parasites display a minor growth or invasion defect during asexual replication groups of 7 recipient mice were inoculated with 1000 RBCs infected with mixed blood stages of *c-cap(-)* and parental wild type parasites. The parasitemia was monitored daily by Giemsa-stained blood smears.

The growth rate of the *c-cap(-)* knockout parasites revealed no significant differences during the exponential growth as compared to the parental parasites (Fig. 9). During the plateau phase at day 6 to 7 after infection with *c-cap(-)* parasites, infected mice displayed a significantly reduced parasitemia as compared to WT parasites *in vivo* (Fig. 9). Gametogenesis, giving rise to the sexual reproductive stages of *Plasmodium*, was similar to WT infected mice (data not shown). Male microgametes of the *c-cap(-)* mutants showed the typical exflagellation process after 10-12 min, similar to wild type parasites.

Together, these results indicate normal proliferation and invasion of *c-cap(-)* parasites during their asexual reproduction as well as normal gametogenesis. The tolerated gene deletion implicates a non-essential role during asexual parasite replication and sexual differentiation.

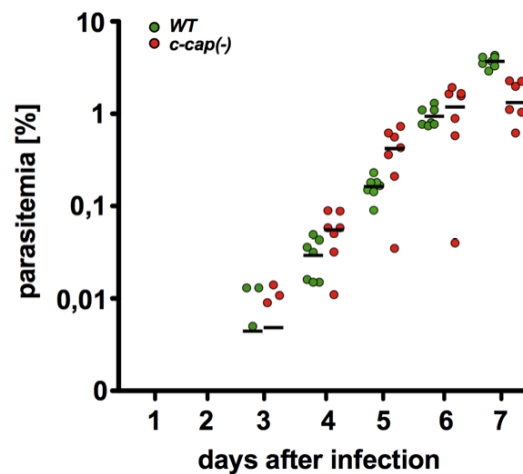


Figure 9: *P. berghei* C-CAP is dispensable for blood stage replication *in vivo*.

C-cap(-) blood stage parasites develop normally in the mammalian host. Asexual blood stage development was determined by intravenous injection of 1000 infected erythrocytes. Parasitemia of recipient animals ($n=7$, each group) was quantified daily by of Giemsa-stained blood smears. Each data point represents the parasitemia of one mouse. Horizontal lines indicate the mean of each group. Values of p were determined with the t test (*, $p < 0.01$; **, $p < 0.001$). All other p values were > 0.01 .

3.1.4.2. *C-cap(-)* parasites exhibit reduced ookinete velocity

Considering the predicted function of C-CAP in regulation of actin polymerization, we further investigated the ookinete motility *in vitro* by video time-lapse microscopy (Moon *et al.*, 2009; Siden-Kiamos *et al.*, 2006b). Purified ookinetes were allowed moving in matrigel and were imaged for 10 min in 6 seconds intervals. The resulting movies were analyzed by manual tracking, and data were used for calculation of the velocity.

The entire pattern of ookinete motility could be observed in *c-cap(-)* and WT parasites as described in (Siden-Kiamos *et al.*, 2006). In both strains, stationary stretching, flexing, axial twirling and a productive migration over distance were observed. To quantify productive

gliding of both strains, the length of migration over time was measured and the calculated velocity was plotted in Figure 10 B. The WT employed an average of velocity of 1.3 $\mu\text{m}/\text{min}$, while the mutant *c-cap(-)* parasites show a significant decrease in velocity to 0.93 $\mu\text{m}/\text{min}$. Taken together these results demonstrate that *c-cap(-)* parasites remain motility competent, but at a reduced speed as compared to WT parasites.

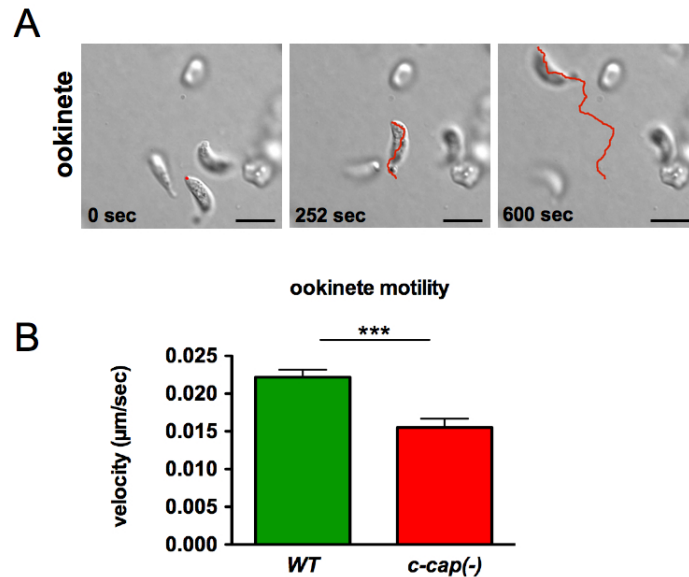


Figure 10: *C-cap(-)* ookinetes exhibit reduced velocity.

(A) Pictures were recorded every 6 seconds and ookinetes motility in matrigel was tracked manually for 10 min by life cell imaging. The red colored line indicates the track of one ookinete. Ookinetes show all typical motility patterns. Scale bar 10 μm (B) Velocity of ookinetes was calculated and means with standard deviation (SDV) was plotted in $\mu\text{m}/\text{sec}$ for *c-cap(-)* (3 movies, parasites $n=9$) and for WT (4 movies, parasites, $n=12$). Note that wild type parasites move significantly faster than *c-cap(-)* parasites. P-values were determined with students t test (***, $p < 0.0003$).

3.1.4.3. C-CAP is essential for *Plasmodium* oocyst development in the mosquito midgut

To study the phenotype of *c-cap(-)* parasites during life cycle progression in the invertebrate host, *Anopheles stephensi* mosquitoes were fed on anesthetized NMRI mice infected with either clonal mutant and wild type parasites as well as mixed parasite populations. The parasite development was monitored over a period of three weeks and the phenotype was analyzed in more than ten independent feedings of *A. stephensi*. Infectivity and oocyst numbers of *c-cap(-)* parasites were estimated from day 4 until day 12 after mosquito feeding and compared to WT (data not shown).

The infectivity of *c-cap(-)* parasites to midguts varies between 7 and 85 % and shows no significant differences to the parental strain (Fig. 11 C), indicating that transmigration and the

initial events of transformation from ookinete to oocyst, were unaffected in the *c-cap(-)* mutants.

However, *c-cap(-)* parasites consistently formed fewer oocysts per infected mosquito midgut as compared to WT parasites (Fig. 11 C). This finding is in good agreement with the observed reduction in ookinete motility.

To further characterize oocyst development in the *c-cap(-)* strain, oocyst diameter was measured in confocal images from day 6 until day 16 post infection. Already at day 6 the quantification of oocyst diameters revealed that *c-cap(-)* oocysts were significantly smaller as compared to WT oocysts and exhibit a size reduction by 20.5 % (Fig. 11 B). More pronounced differences were observed at later time points. At day 16 *c-cap(-)* oocysts grew only to a size of 13 μm in average, while WT oocysts grew up to an average size of 32 μm . This corresponds to a significant size reduction by 60 % in *c-cap(-)* parasites. However, WT as well as *c-cap(-)* oocysts displayed a high degree of variance in oocyst size in each group.

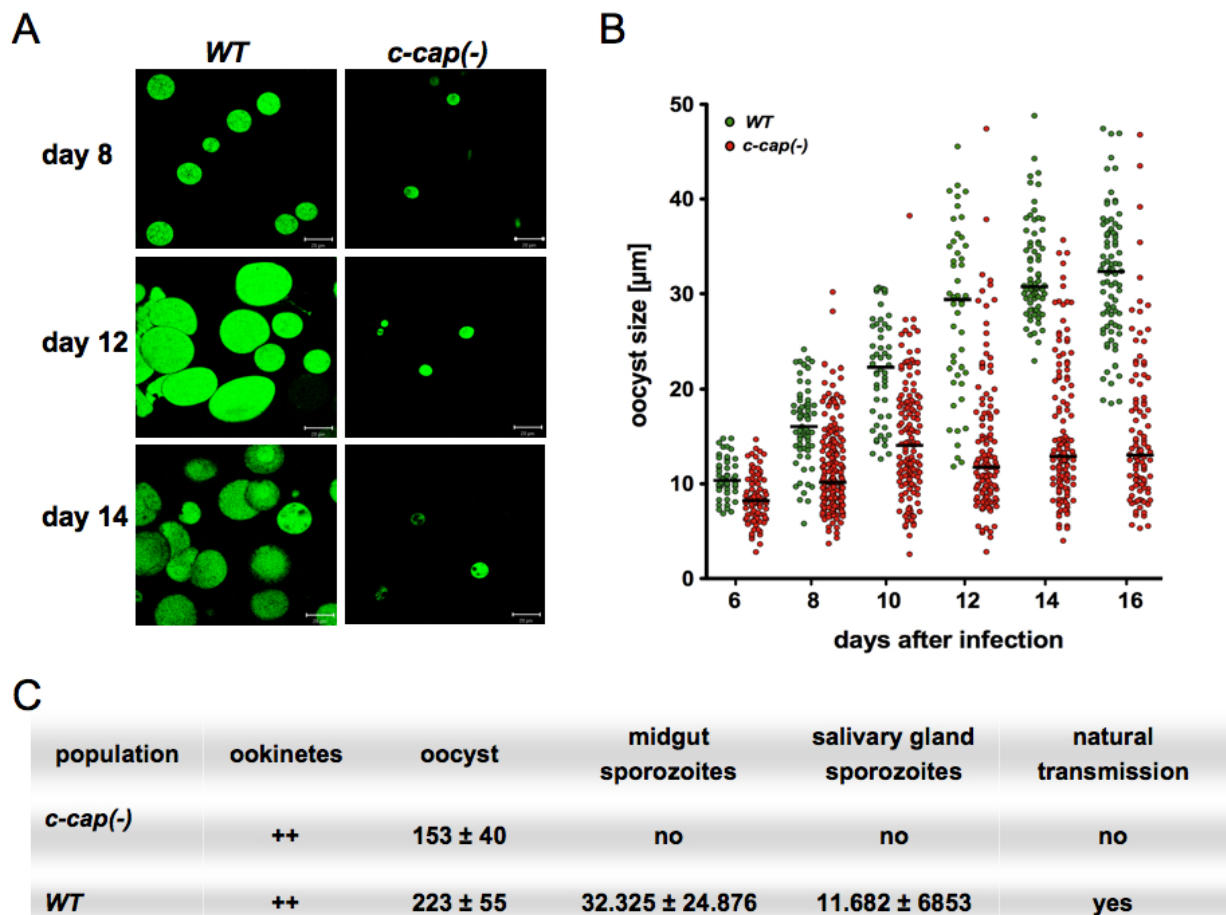


Figure 11: Disruption of *C-CAP* leads to complete attenuation of oocyst development in the mosquito midgut.

(A) *c-cap(-)* oocysts fail to mature. Shown are representative micrographs of GFP-expressing WT and *c-cap(-)* oocysts in the mosquito midgut. The time point after the infectious blood meal is indicated on the left. *C-cap(-)* oocysts were markedly reduced in size and numbers. Scale bars, 20 μm . **(B)**

Quantification of oocyst size during maturation. Shown are oocyst diameters of WT (green) and *c-cap(-)* (red) oocysts over time. WT oocysts display continuous size increase whereas *c-cap(-)* oocysts show impaired growth. Data points represent oocyst diameters from randomly selected oocysts of parasite-infected midguts (n= 12) from six independent feeding experiments for WT and *c-cap(-)*, respectively. Horizontal lines indicate the median oocyst size, $p < 0,0001$. (C) *C-cap(-)* parasites do not develop sporozoites. Characterization of ookinetes, oocysts, midgut- and salivary gland-sporozoites revealed no sporozoite development in *c-cap(-)* parasites in n= 20 independent mosquito infections and as consequence no natural transmission of the parasite to mice (n= 3).

In addition to growth, oocyst development is characterized by multiple rounds of asynchronous mitotic divisions, termed sporogony (Sinden and Garnham, 1973; Sinden, 1974). Parasite DNA condenses, segregates and is distributed into individual budding sporozoites. This process was monitored microscopically using the DNA stain Hoechst 33342. At day 8 to 10 after feeding, WT parasite DNA was detected in multiple condensed loci distributed throughout the oocyst, indicating ongoing mitotic divisions (Fig. 12 A). Despite a reduced size of *c-cap(-)* oocysts, DNA condensation and nuclear division could be observed in *c-cap(-)* oocysts as well. However, the DNA from mutant parasites showed weaker stain, moreover the DNA was distributed to few diffuse nuclei only (Fig. 12 A). The amount of total DNA in *c-cap(-)* parasites corresponds approximately to 4 to 5 rounds of nuclear divisions. Additionally, clear differences were observed at day 14 after feeding. No sporozoite structures and no final DNA segregation steps were detected in *c-cap(-)* parasites (Fig. 12 B). In contrast, WT oocysts contained the typical radially aligned individual sporozoites that mark the final step of daughter cell separation. The DNA was separated into nuclei with each single sporozoite, clearly detected by a highly condensed dot stain with Hoechst 33342. Systematic quantification of sporozoite numbers at day 14 for midgut- and days 17 to 25 for salivary gland- associated sporozoites confirmed the complete absence of sporozoite development in mosquitoes infected with *c-cap(-)* parasites (Fig. 11 C). Natural transmission from *c-cap(-)* infected mosquitoes to C57/Bl6 mice was tested and resulted in absence of blood stage parasitemia and malaria symptoms (Fig. 11 C). In mixed feedings, where *c-cap(-)* and wild type parasites were fed simultaneously to mosquitoes, normal oocyst- and sporozoite development was observed. Furthermore, mixed sporozoites exhibit normal transmission from mosquito to C57/Bl6 mice, with a prepatency of three days, similar to WT transmission. Genotyping of back to mice transmitted parasites, demonstrated still the presence of *c-cap(-)* mutant parasites, by specific detection of the 5'UTR and 3'UTRs.

Taken together, these results demonstrate a stage-specific and essential function of the C-CAP protein during oocyst maturation in the invertebrate host. *C-CAP* gene deletion leads to abrogation of oocyst maturation, indicated by oocyst growth inhibition, incomplete DNA

condensation and separation as well as the complete absence of sporozoite development. In mixed feeding experiments, the *c-cap(-)* defects were restored by functional complementation by the functional wild type *C-CAP* gene locus.

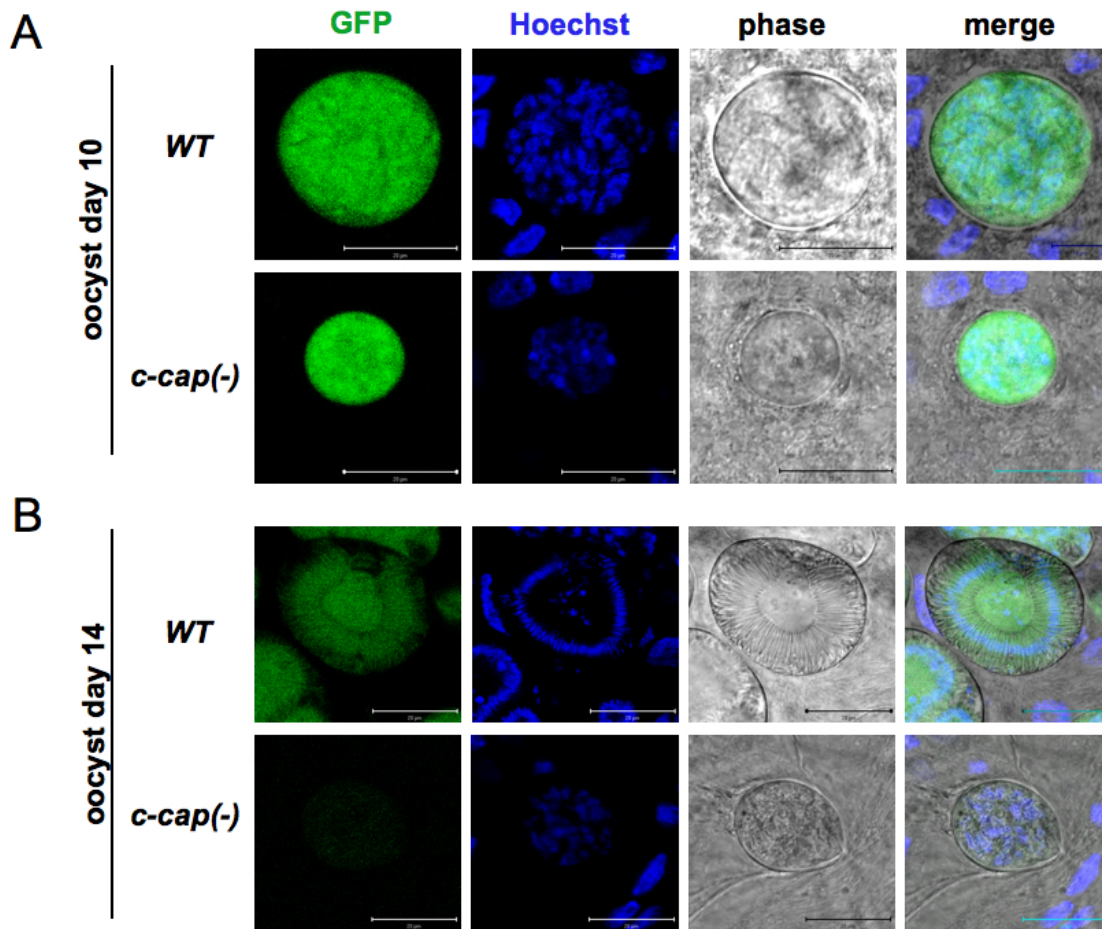


Figure 12: Oocyst architecture of *c-cap(-)* mutants.

Shown are representative micrographs of WT (top) and *c-cap(-)* (bottom) oocysts at day 10 (**A**) and day 14 (**B**). Parasites are visualized by endogenously expressed GFP and parasite nuclei are stained with Hoechst 33342. Note that *c-cap(-)* parasites display impaired DNA segregation and do not contain sporozoites as compared to wild type (B). Scale bars, 20 μm.

Given the fact that *c-cap(-)* oocyst numbers decrease sharply early during infection and oocysts do not mature, a life death assay was performed to examine the fate of these parasites inside the mosquito midgut. SYTOX® Orange stains nucleic acids with high affinity in cells and easily penetrates cells with compromised plasma membranes but does not cross the membranes of viable cells.

Mosquito midguts infected with either WT or *c-cap(-)* parasites were prepared and incubated with SYTOX® Orange followed by microscopic observation.

The mutant *c-cap(-)* oocysts showed internal nucleic acids stain, whereas the dye is clearly excluded from the oocyst in WT parasites (Fig. 13). The SYTOX® Orange stain of *c-cap(-)*

oocysts implicates an increased permeability of the oocyst wall compared to WT and demonstrates their compromised viability.

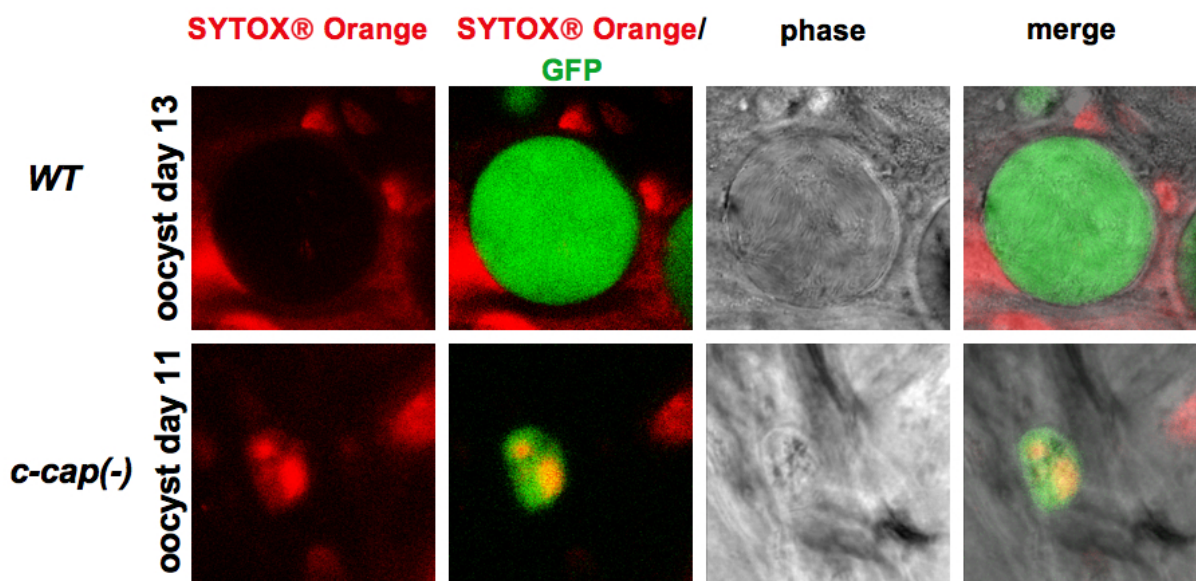


Figure 13: *C-cap(-)* parasites die during oocyst development.

Shown are representative micrographs of living midgut- associated oocysts of WT (top) and *c-cap(-)* (bottom) at day 13 and 11 after mosquito infection, stained in a live/death assay with Cytox® Orange (red). Parasites are visualized by endogenous GFP expression (green). Cytox® Orange is excluded from WT oocysts, whereas it penetrates the oocyst wall in *c-cap(-)* parasites, indicating compromised viability.

3.1.4.4. Expression and localization of the circumsporozoite protein (CSP) and the oocyst capsule protein CAP380 are unaffected by deletion of *C-CAP* and do not contribute to the maturation phenotype.

The circumsporozoite protein (CSP) and the oocyst capsule protein 380 (CAP380) are essential proteins for oocyst maturation and sporozoite development in the mosquito host (Menard *et al.*, 1997; Srinivasan *et al.*, 2008; Thathy *et al.*, 2002). Both proteins localize to the oocyst capsule during oocyst maturation. Initially, the CSP protein resides in the inner cyst membrane and is involved in establishing polarity inside the oocyst; it is thereby essential for sporozoite development. Later in sporogony, CSP will cover the major surface protein of sporozoites and is important for motility and invasion of both the salivary glands of mosquito and hepatocytes of the mammalian host (Coppi *et al.*). Loss of CSP aborts sporozoite development (Menard *et al.*, 1997; Thathy *et al.*, 2002). The CAP380 protein is part of the outer oocyst capsule (Srinivasan *et al.*, 2008). Parasites lacking CAP380 develop only small

oocysts, which are unable to form sporozoites. The similarities between phenotypes of *CSP(-)* and *CAP380(-)* parasites and the

c-cap(-) parasite during oocyst maturation, prompted us to investigate expression and localization of CSP and CAP380 in *c-cap(-)* parasites during oocyst maturation.

Infected midguts were prepared for CSP detection at day 8 and for CAP380 and CSP localization at day 11 after infection for indirect immuno-fluorescence (IFA). Consistent with previous findings (Aly and Matuschewski, 2005; Srinivasan *et al.*, 2008; Thathy *et al.*, 2002) CSP was detected as a ring surrounding the oocyst in both the *c-cap(-)* and in WT parasites (Fig. 14 A). Later on, CSP localization changes from the oocyst wall to the inner content of the cyst in WT and *c-cap(-)* parasites (Fig. 14 B). In WT the CSP decorates the outer membrane of developing sporozoites, whereas in *c-cap(-)* the CSP locates to the syncytium of the undifferentiated oocyst (Fig. 14 B). This result demonstrates that despite of reduced growth and absence of sporozoites in *c-cap(-)* oocysts CSP is correctly expressed and localized in mutants. Thus, the inhibition of sporozoite development in *c-cap(-)* parasites appears to be a CSP-independent process.

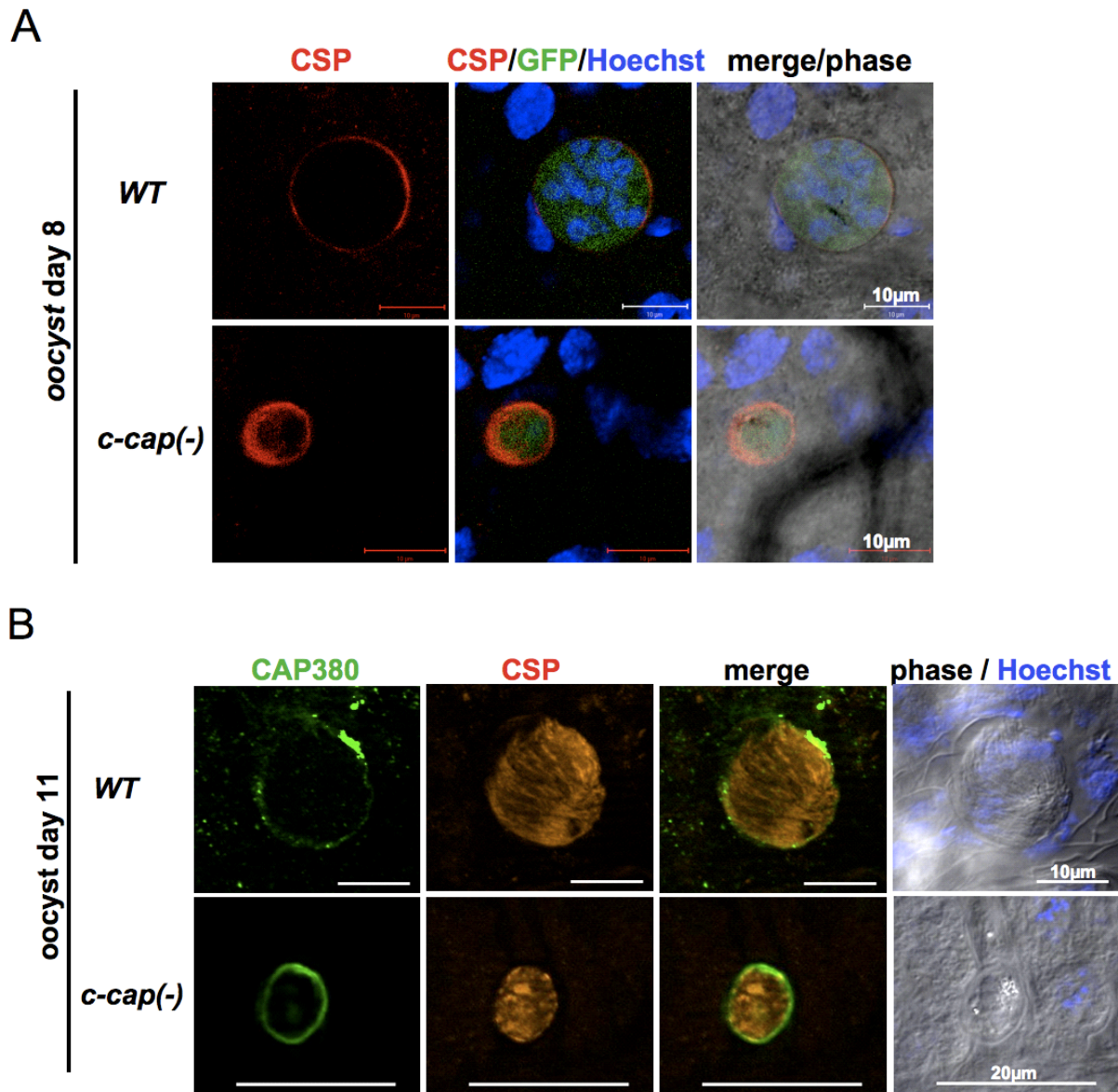


Figure 14: The circumsporozoite protein (CSP) and oocyst capsule protein 380 (CAP380) displaying normal expression and localization in *c-cap(-)* mutant oocysts.

Shown are representative images of indirect immuno-fluorescence assays (IFA) on oocysts at day 8 and 11 after mosquito infection, from WT (top) and *c-cap(-)* parasites (bottom). **(A)** Localization of CSP (red) and parasites (GFP) indicate normal ring staining of CSP on the oocyst capsule in both parasites. **(B)** Localization of CAP380 (green) (Srinivasan *et al.* 2008) and CSP (red) (Aly *et al.* 2005) by IFA on the oocyst at day 11. Localizations are indistinguishable between wild type and *c-cap(-)* parasite lines.

During oocyst development CAP380 localizes to the outer oocyst capsule in wild type and *c-cap(-)* parasites, indicating a normal cyst wall composition. This is consistent with previous findings (Srinivasan *et al.*, 2008). However, despite the normal ring like pattern of CSP and CAP380, both proteins seem to be more prominent in the oocyst wall in *c-cap(-)* as compared to WT. Whether this phenomenon is due to the lack of oocyst wall expansion and absent growth in mutant parasites, needs further analysis. Together, these results show that CAP380

is expressed and localized indistinguishable between wild type and *c-cap(-)* parasites. Thus, C-CAP seems to fulfill an independent function during oocyst maturation.

3.1.4.5. The oocyst maturation defect in *c-cap(-)* parasites is independent of ookinete motility

Because of the reduced ookinete motility of *c-cap(-)*, the next aim was to test whether *c-cap(-)* parasites are able to develop into sporozoites when natural midgut transmigration is bypassed by ookinetes injection into the hemocoel of the mosquitoes.

WT and *c-cap(-)* *in vitro*-generated ookinetes (n= 1500) were microinjected into the mosquito thorax (Sinden *et al.*, 2002; Weathersby, 1952) and development of sporozoites was monitored. Quantification of hemocoel- and salivary gland sporozoites was done 17 and 21 days later (Tab. 6). While substantial sporozoite numbers in WT inoculated mosquitoes were detected, no sporozoites were found in mosquitoes injected with *c-cap(-)* ookinetes. These results confirm that sporozoite development is possible in the hemocoel without mosquito midgut passage and argues for an additional motility independent function of C-CAP during oocyst maturation.

Table 6. Ookinete injection does not restore the *c-cap(-)* defects

population	injected ookinetes / (mosq.)	hemocoel sporozoites / (mosq.)		salivary gland sporozoites / (mosq.)	
		17	21	17	21
<i>c-cap(-)</i>	1500 (1)	no (16)	no (13)	no (16)	no (13)
WT	1500 (1)	3783 (36)	630 (7)	792 (36)	30 (7)

3.1.4.6. Transmission Electron Microscopy (TEM) reveals the absence of inner membrane retraction and confirms the DNA segregation defect during oocyst maturation

To further asses the *c-cap(-)* oocyst maturation defect, the ultra structure of oocysts was investigated by Transmission Electron Microscopy (TEM) on mutant and WT oocysts during day 6, 8, 10 and 12 after infection. Mosquito midguts were dissected in 1x PBS. Highly infected WT and *c-cap(-)* midguts were selected under the fluorescence microscope, fixed and

stored in 2.5 % glutaraldehyde at 4 °C. Further processing of the oocysts for TEM was performed by Ulrike Abuabed from the imaging facility of the Max Planck Institute for Infection Biology, Berlin.

All TEM pictures show the successful settlement of the WT and mutant *c-cap(-)* ookinetes in their developmental niche, between the basal side of epithelial midgut cells and the basal membrane (Fig. 15 A, B). Both parasites transformed successfully from motile ookinetes into young sessile cysts at day 6 after infection. The round spherical body of the cyst is encircled by a thick capsule, and could be detected as dark electron dense material in both parasites (Fig. 15 A, B). The cyst plasma appears as homogeneous electron light material and contains organelles like membrane cisternae from the endoplasmic reticulum or the golgi apparatus, vesicles and condensed DNA material (Fig. 15 A, B). Marked differences between WT and *c-cap(-)* mutant parasites appear at day 6 to 8 after mosquito infection (Fig. 15 A, C).

The *c-cap(-)* oocysts are decreased in size as already recognized during their quantification by fluorescence microscopy (Fig. 11 A, B). At day 8 after infection severe defects are observed in the *c-cap(-)* mutant parasites. In addition to their reduced size, the majority of cysts appears asymmetric and shows strong vacuolization of the cyst plasma (Fig. 15 C).

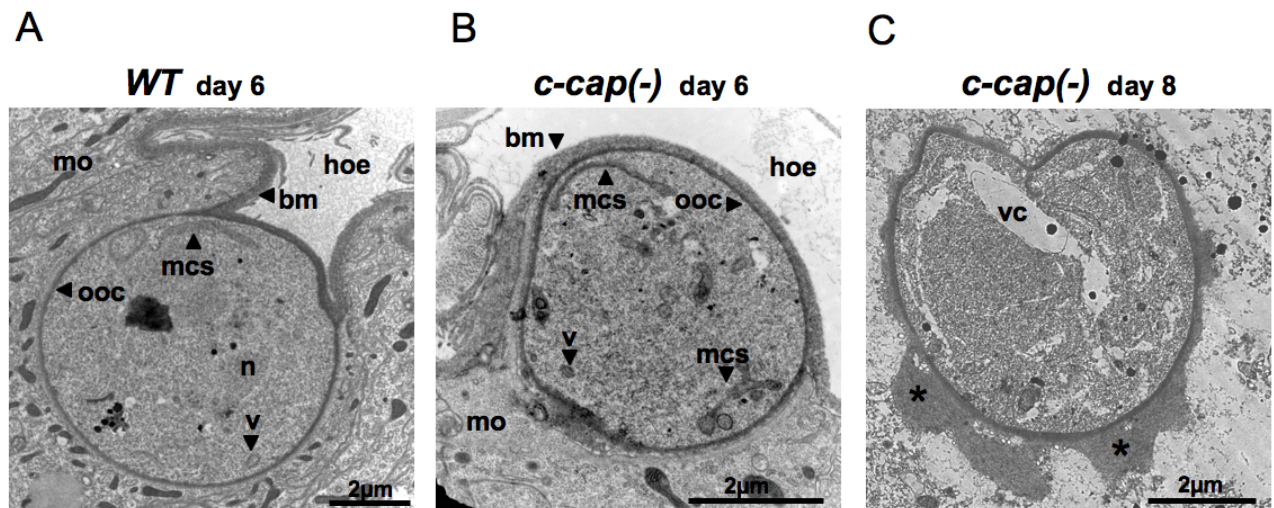


Figure 15: *c-cap(-)* parasites transmigrate through the midgut epithelium and transform into early oocysts.

Shown are representative micrographs of transmission electron microscopy (TEM) on midgut-associated oocysts. **(A)** WT oocyst at day 6 after infection settles extra cellular on the basal side of mosquito midgut cells (mo) and underneath the basal membrane (bm) that separates the cyst from the mosquito hemocoel (hoe). The transforming oocyst is surrounded by a thick electron oocyst capsule (ooc). Electron dense nuclear material (n), membranous cisternae (mcs) and vesicles (v) are detected. **(B)** *c-cap(-)* oocyst at day 6 post infection. Complete settlement, transformation and membranous structures are visible, but oocysts are clearly smaller. **(C)** *c-cap(-)* oocyst at day 8 post infection. Note that high degree of vacuolization (vc) in the cyst cytoplasm, asymmetric shape of oocyst and a disturbed capsule structure (*).

The structure of oocyst capsule develops abnormally as compared to the WT capsule, which is characterized by symmetric thickness of the oocyst wall. In contrast, the *c-cap(-)* parasites possess an asymmetric distributed outer cyst wall, which expands into the mosquito cells (Fig. 15 C). The high degree of vacuolization and the disturbed wall integrity of the cyst indicate an early developmental defect in the majority of the *c-cap(-)* parasites. These findings are in agreement with the results from the life death assay with SYTOX® Orange (Fig. 13).

A proportion of the developmentally arrested *c-cap(-)* mutant parasites persists as immature oocysts in the midgut and survive in the mosquito for up to 27 days. At day 10 after mosquito infection, WT oocysts grew to an average size of 28 μm . The DNA has undergone several mitotic divisions without cytokinesis resulting in a growing multinucleated parasite. In WT parasites the segregated DNA is detected as electron dense compartments in dark grey spots in the cytoplasm (Fig. 16 A). In *c-cap(-)* parasites, however, lesser and larger joined nuclei were detected, indicating that the mutant parasite is impaired in DNA segregation and in potentially other mitotic processes (Fig. 16 C). During WT development the oocyst maturation proceeds with initiation of membrane retraction, which gives rise to subcapsular vacuoles (blastomers) and lead to further compartmentation of the oocyst. This process was detected on oocysts at day 10 after infection (Fig. 16 B, F) and will be highlighted in a following chapter in more detail. However, oocyst membrane retraction or invaginations are never observed in *c-cap(-)* oocysts (Fig. 16 D, I). These defects further intensify through cyst maturation as indicated in TEM pictures at day 12 after infection. Oocysts of WT parasites undergo further compartmentation of the cytoplasm. Subcapsular vacuoles (blastomers) are formed and separate the dividing nuclei with a membrane from the residual oocyst plasma or syncytium (Fig. 16 E). The membrane, which confines the blastomer is detected as an electron dense line in wild type oocysts (Fig. 16 G *). The underlying nuclear foci are further separated from the surrounding blastomer material by a gap. This gap is detected as an electron light area in WT (Fig. 16 G). Compared to WT, the *c-cap(-)* parasites display a lack of cyst compartmentation. The blastomer membrane, that usually encircles the DNA replication sites are entirely absent (Fig. 16 H-J). This is highlighted in detail in Figure 16 J. Here, an abnormal gap appears at the place where usually the electron dense blastomer membrane situates. In addition, the membrane retraction is still absent in *c-cap(-)* mutants (Fig. 16 I). Also, the DNA continues its persistence in few undivided areas, indicating the absence of final mitotic divisions necessary for sporozoite formation (Fig. 16 H).

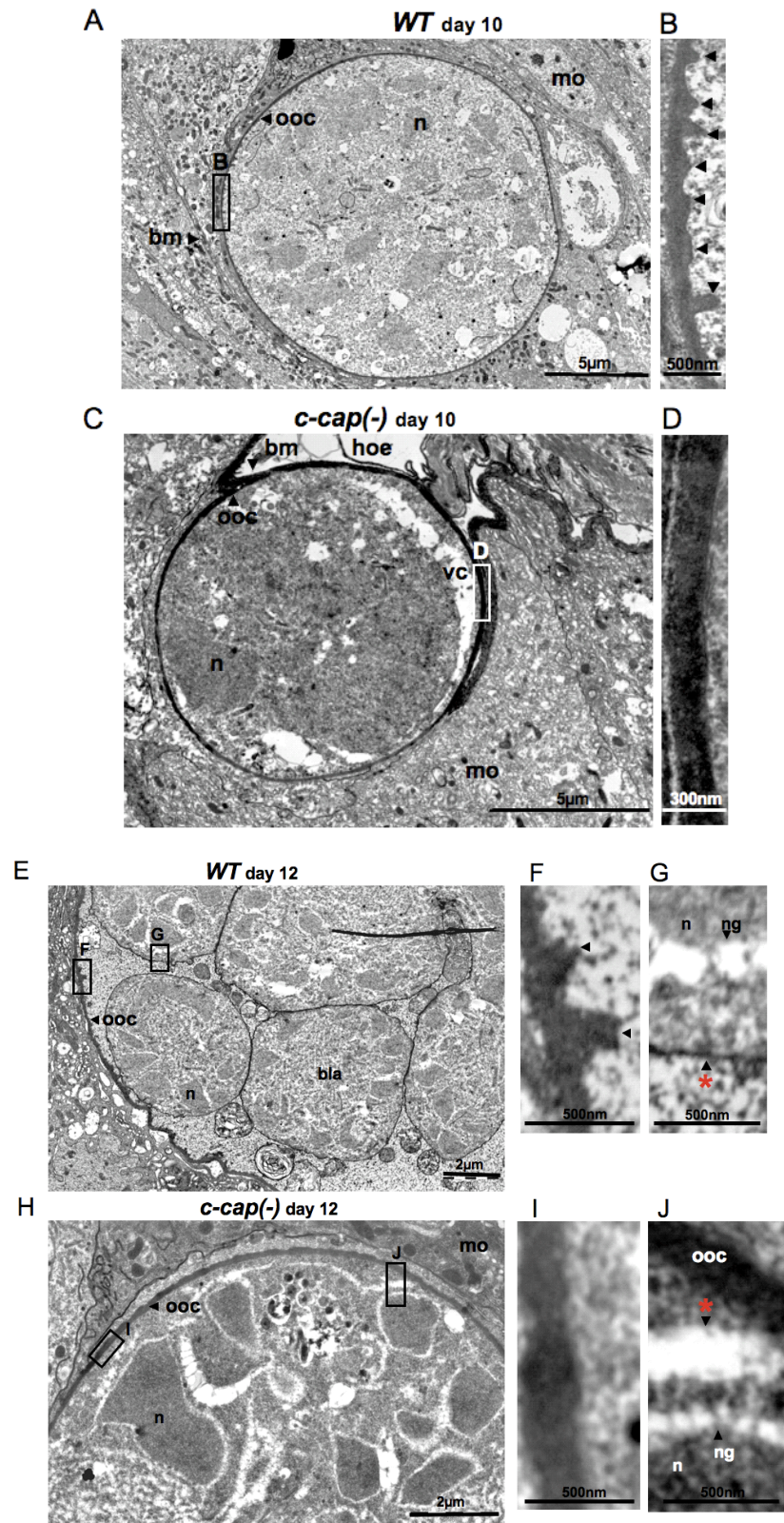


Figure 16: *C-cap(-)* oocysts are impaired of membrane retraction and DNA segregation.

Shown are TEM pictures of oocysts from WT (top A, B) and *c-cap(-)* (bottom C, D) parasites at day 10 (A-D) and day 12 (E-J) post mosquito infection. (A) WT oocyst growth underneath the basal membrane (bm) and extra cellular of the mosquito cell labyrinth (mo). Nuclear material (n) is segregated in small foci through the oocyst plasma. At the oocyst wall (ooc) membrane invaginations are visible (detail (B) arrows). (C) *C-cap(-)* oocysts at day 10 post infection, are located like WT, the nuclear material (n) is less condensed and separated, vacuolization (vc) of the cyst plasma is visible.

(D) Detail of oocyst wall, no membrane invaginations was detected. (E) Detail of a WT oocyst day 12, compartmentation of the cyst plasma into blastomers (bla). Blastomers are filled with condensed nuclei loci (n) and surrounded by a blastomer membrane (blm). (F) Detail of membrane invagination process at the oocyst wall (asterisk). (G) Detail of blastomer membrane (blm, red asterisk), which separates cyst plasma from nuclear material (n) that is encircled by an nuclear gap (ng). (H) Detail of *c-cap(-)* oocyst clearly shows no compartmentation, no blastomers (bla), no blastomer membranes (blm), and the nuclear material (n) is not condensed and not segregated. (I) Detail of oocyst wall, membrane invaginations are absent. (J) Detail of absent blastomere membrane (blm), but the nuclear gap (ng) exists like in WT.

The membrane retraction- or invagination- process in oocysts is highlighted in Figure 17 in more detail. These pictures display the dynamic behavior of the wild type cyst capsule. The inner plasma membrane starts to invaginate at specific sides from the oocyst wall and take along capsule material, indicated by the same dark color of the electron dense capsular substance (Fig. 17 A1). Over time these structures become elongated into the cyst plasma (Fig. 17 A1-3). At one point the structure rounds up to “vesicular bodies” and seem to disconnect from the residual cyst wall (Fig. 17 A4-5). Thus far, it remains elusive if this process reflects an uptake mechanism for nutrient acquisition. However, this unique membrane retraction process was never observed in *c-cap(-)* parasites (Fig. 16 D, I).

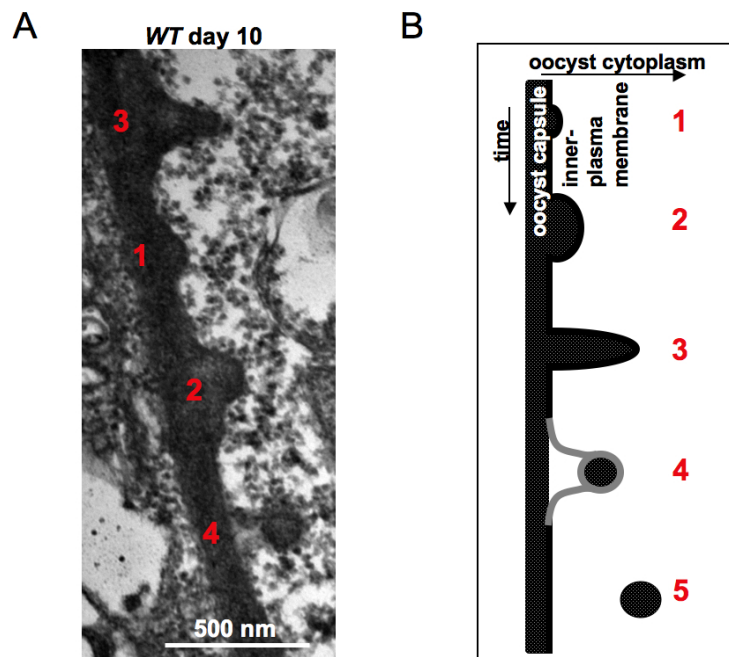


Figure 17: The membrane retraction process on wild type oocyst.

(A) TEM picture of the dynamic behavior of the WT oocyst capsule membrane (dark grey material) at day 10 after infection. Representative occurrence of invaginations, are indicated by numbers (red). (B) Schematic representation of the membrane invagination process in a time dependent manner: (1) initiation of retraction, (2 - 4) elongation into the cyst cytoplasm and (5) final separation of “vesicle-like” bodies from the cyst capsule.

Taken together, the TEM analysis revealed further details of the developmental defects of *c-cap(-)* mutant parasites. *C-cap(-)* parasites are able to transmigrate the midgut epithelium and transform into early oocyst, like wild type parasites. Strikingly, these parasites are significantly smaller and do not develop sporozoites during their lifetime in the mosquito. Two further phenomena were observed. First, the majority of the *c-cap(-)* oocysts undergo an early dying process during oocyst development. They show high degree of vacuolization and disturbed oocyst wall integrity. Second, the persisting parasites fail to accomplish nuclear divisions. The process of inner membrane retraction is absent. The *c-cap(-)* oocysts thus fail to mature and to differentiate, as indicated by the impaired growth and the absence of inner compartments and sporozoites. In conclusion the C-CAP protein has a stage-specific function during oocyst maturation in the mosquito host.

3.1.5. Localization of the C-CAPmCherry fusion protein

The stage-specific C-CAP gene expression and the observed phenotype of the knockout parasites prompted us to examine the exact subcellular localization of the C-CAP protein in *P. berghei*. Therefore, a parasite line expressing a chimeric C-terminal fusion protein of C-CAP and the fluorescent mCherry protein was engineered.

The endogenous *C-CAP* gene was replaced by introducing a *C-CAPmCherry* fusion protein and the pyrimethamine selectable marker *Tgdhfr/ts* cassette by double homologous recombination (Fig. 18 A). Gene replacement was enabled by introduction of 5' and 3' UTRs of the *C-CAP* gene, analogous to the knockout strategy (Fig. 8 A). The *C-CAP* and *mCherry* domains are separated by a short linker peptide sequence of eight alanines to ensure flexibility and functional folding of both domains. Transfection was performed in *P. berghei* Anka-507cl parasite line expressing GFP (Janse *et al.*, 2006). Clonal parasite lines were obtained, by injection of limiting parasite dilutions into mice. For genotyping specific primers for the 5' (T10/T11) and 3' (T8/T9) integration were designed and used for diagnostic PCR (Tab. 2). Successful integration into the 5'UTR and 3'UTR was confirmed by the presence of the predicted amplicons with sizes of 3786 bp (5'test) and 1028 bp (3'test) respectively, in both $\Delta C-CAP::C-CAPmCherry$ parasite lines (Fig. 18 B). No more of these fragments could be detected in WT parasites (Fig. 18 B). Moreover, the specific mCherry integration was verified by amplification of a 2081 bp (5'test mCherry) long fragment in both transgene parasites, using primers (T10/T16, Tab. 2). In WT parasites the genomic *C-CAP* gene locus of 2725 bp was detected with specific primers (T9, T10), while in the $\Delta C-CAP::C-CAPmCherry$ parasite

lines this fragment was not amplified, thus confirming the clonality of the recombinant parasite lines (Fig. 18 B).

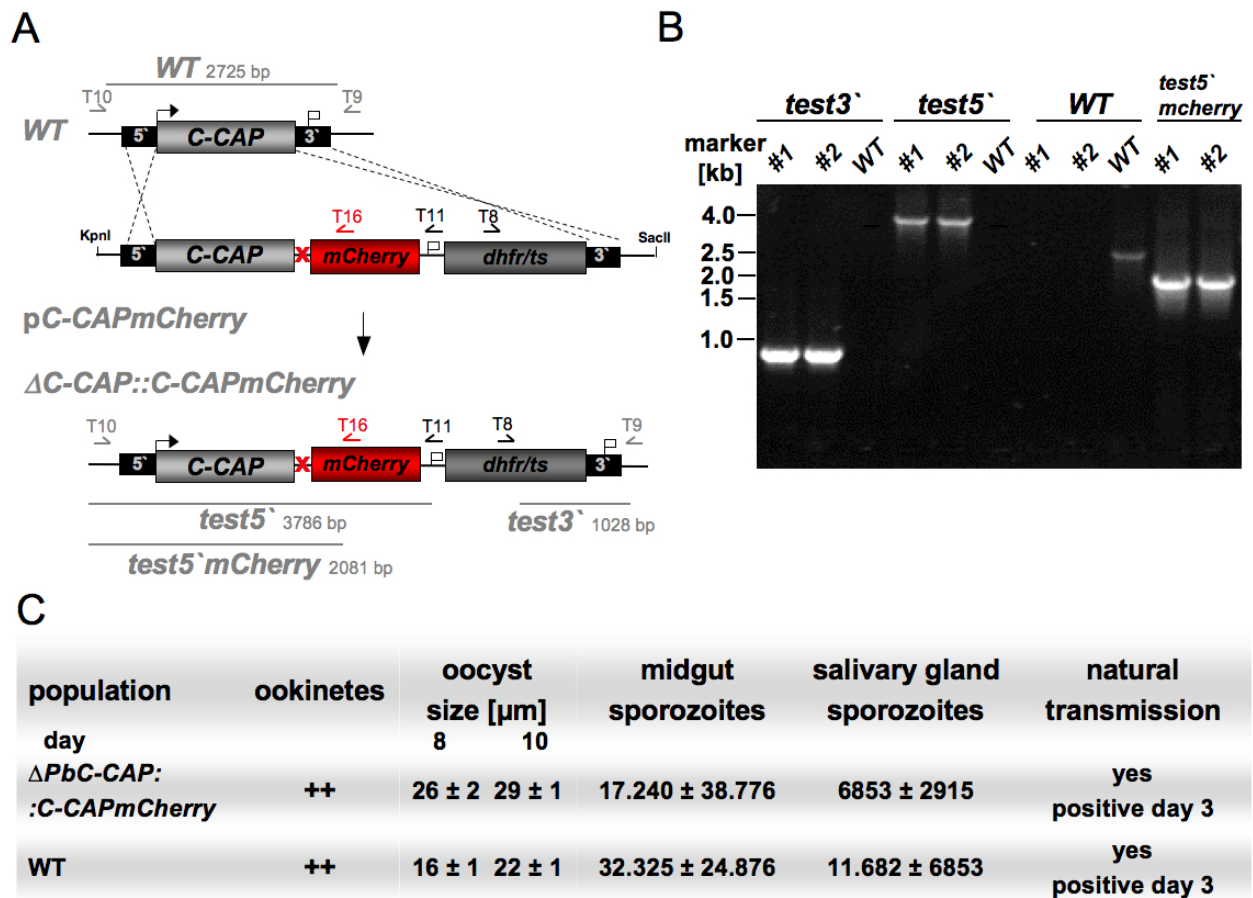


Figure 18: Generation of *P. berghei* C-CAPmCherry fusion parasites.

(A) Gene replacement strategy for the generation of the *P. berghei* *c-capmCherry* parasites. The wild type (WT) *C-CAP* genomic locus is targeted with a *SacII/KpnI* linearized replacement plasmid containing the 5'- and 3'-untranslated regions of the *C-CAP* open reading frame (ORF) and the *T. gondii* *dhfr/ts* positive selectable marker. Upon a double crossover event, the *C-CAPmCherry* ORF and the selection marker cassette are introduced. Replacement-specific test primer combinations are indicated by arrows and expected fragments by line. Black arrows hybridize with the vector backbone; grey arrows hybridize on genomic DNA (gDNA) outside of the *C-CAP* ORF, respectively. (B) Genotyping of $\Delta C-CAP::C-CAPmCherry$ parasites using PCR with specific primers as indicated in A, confirmed the specific 5' test and 3' test fragment integration and the absence of residual WT parasites in the two clonal $\Delta C-CAP::C-CAPmCherry$ lines. Specific mCherry integration was confirmed by positive test 5' mcherry fragment amplification. (C) $\Delta C-CAP::C-CAPmCherry$ parasites complement the *c-cap(-)* phenotype and develop normally through parasite life cycle compared to WT.

3.1.5.1. Expression of the C-CAPmCherry fusion protein reverts the *c-cap(-)* phenotype

After successful integration of the transgene into *P. berghei*, the $\Delta C-CAP::C-CAPmCherry$ parasites were systematically followed through the life cycle to test whether they develop normally. After confirmation of normal blood stage development, seven independent

transmission experiments of the $\Delta C\text{-CAP}::C\text{-CAPmCherry}$ parasite to mosquitoes were performed. The infectivity rates of 31 - 100 % are similar to wild type infections. In one feeding the oocyst size was characterized at days eight and ten after infection. An average size of 26,4 μm and 29.24 μm , which is even larger than compared to WT oocyst, was observed (Fig. 18 C). Normal sporozoite numbers, determined from six independent feedings, were observed at day 14 for midgut associated sporozoites (17.240 ± 38.776 spz./mosq.) and at days 17 to 26 for salivary gland sporozoites (6853 ± 2915 spz./mosq.) (Fig. 18 C). The infectivity of $\Delta C\text{-CAP}::C\text{-CAPmCherry}$ sporozoites from mosquitoes transmitted to mice was confirmed in two independent infection experiments with C57/Bl6 mice by mosquito bite. Blood stage parasitemia was monitored daily by Giemsa stained smears. The prepatency of $\Delta C\text{-CAP}::C\text{-CAPmCherry}$ parasites was three days, which is similar to wild type infections. Taken together the $\Delta C\text{-CAP}::C\text{-CAPmCherry}$ parasites exhibit normal life cycle progression, as compared to WT, and display full complementation of the *c-cap(-)* defects. I therefore conclude that these results confirm fully biochemical activity of the C-CAPmCherry fusion protein.

3.1.5.2. C-CAPmCherry displays cytoplasmic localization during blood stage development

To follow the cellular localization of the C-CAP protein during blood stage development, NMRI mice were infected with the clonal $\Delta C\text{-CAP}::C\text{-CAPmCherry}$ parasites. The blood was isolated at high parasitemia to ensure representation of different parasite stages. One drop of blood was isolated for life cell imaging via fluorescence microscopy.

As shown in figure 19, no C-CAPmCherry signal was observed during early to late ring stages, while the constitutive cytoplasmic GFP signal indicated intact parasites. The first C-CAPmCherry signal was detected in late stage trophozoites and co-localizes with GFP in the cytoplasm (Fig. 19). Furthermore, the C-CAPmCherry signal intensity appeared strongest in schizonts and gametocytes indicating high protein abundance in these stages (Fig. 19). Moreover, the C-CAPmCherry was abundant in single male microgametes (data not shown). The C-CAPmCherry signal abundance in late parasite blood stages confirms the expression data from RT-PCR also on protein level, where *C-CAP* expression could only be detected in 18h old schizonts *in vitro* cultures but not in mixed blood stages (Fig. 7 B).

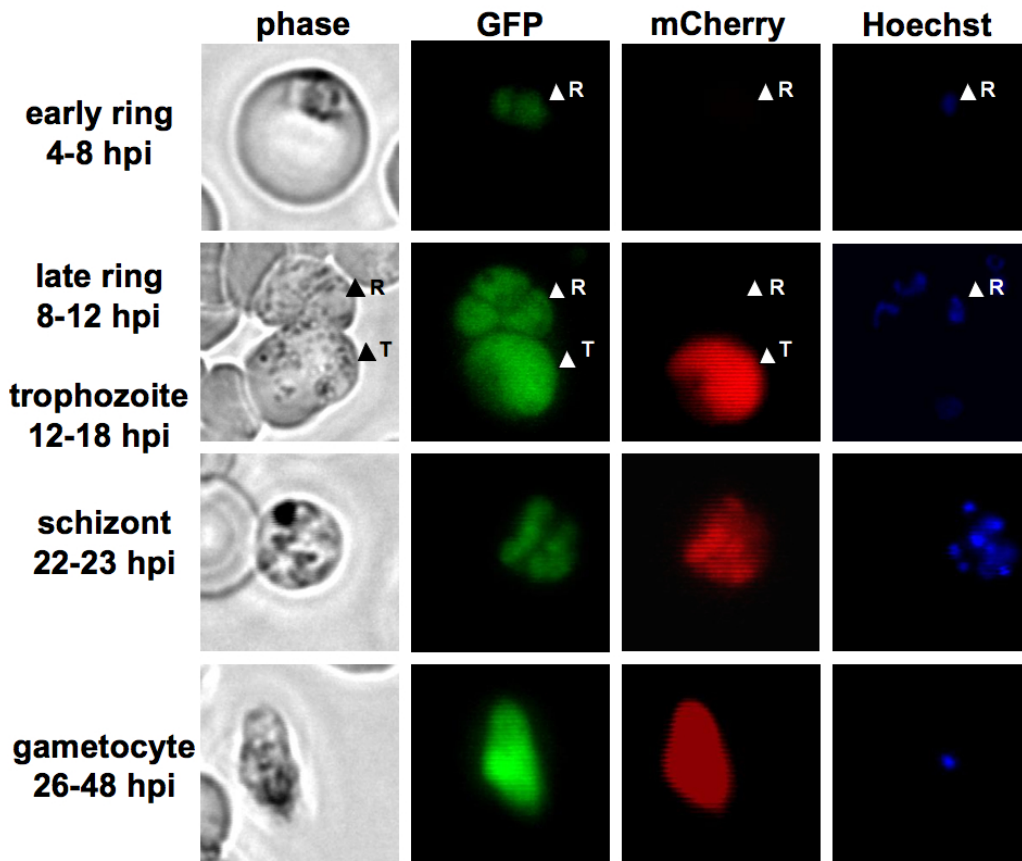


Figure 19: C-CAPmCherry is sequential expressed and exhibits cytoplasmic localization in blood stages.

Live cell imaging was performed on *P. berghei* infected red blood cells (RBCs). Shown are phase contrast images (grey) in the first column, GFP (green) expression and localization of the Anka-507cl host strain in the second column, C-CAPmCherry protein expression and localization (red) in the third column and nuclei were stained with Hoechst 33342 (blue) shown in the fourth column. C-CAPmCherry is not abundant in early and late ring stages (R), first and second row. In trophozoites (T), schizonts and gametocytes C-CAPmCherry is abundant and shows cytoplasmic localization, shown in the second, third and fourth row.

To characterize the expression of *C-CAPmCherry*, the parasites were followed through mosquito stage development. Ookinetes were obtained from 18h *in vitro* cultures, purified with p28 antibody labeled magnetic beads, and kept in complete ookinete medium at room temperature for live cell imaging. As shown in figure 20, ookinetes display a strong C-CAPmCherry signal, with overlapping GFP cytoplasmic stain. The C-CAPmCherry protein is excluded from the crystalloid bodies (Moon *et al.*, 2009) at the posterior end of the ookinetes and from the nucleus (Fig. 20 A, arrows).

To monitor the C-CAPmCherry fluorescence *in vivo* during mosquito development, $\Delta C-CAP::C-CAPmCherry$ parasite infected mice were fed to mosquitoes *A. stephensi* and oocyst development on the mosquito midgut was observed at the indicated time points (Fig. 20 B).

During oocyst development the C-CAPmCherry fluorescence decreases and shows high variability between individual oocysts, but appears independent from oocyst size and age (Fig. 20 B). During the separation of individual sporozoites from the oocyst syncytium at day 12 to 15 post infection, the C-CAPmCherry fusion protein localizes primarily to the syncytium but not within the budding sporozoites. As suggested from the gene expression data (Fig. 7 B), only a very faint C-CAPmCherry fluorescence was observed during life cell imaging on midgut sporozoites (Fig. 20 C). Interestingly a clear punctuated signal in close proximity to the nucleus towards the apical tip of the sporozoite was observed. In all midgut sporozoites this localization was independent from sporozoite motility. A co-localization with specific organelle-markers might reveal the exact organelle identity.

Mature salivary gland sporozoites at day 22 after mosquito infection exhibit a very weak fluorescent C-CAPmCherry signal as compared to the GFP signal intensity. However, the C-CAPmCherry protein appeared uniformly distributed throughout the cell, confirming the cytoplasmic localization of the protein (Fig. 20 C). This pattern was not changed during motility in living sporozoites (Fig. 20 C). The motility of the sporozoites is indicated in figure 20 C. The overlay of individual color channels is shifted, due to the time that is needed for the automated filter change in the microscope.

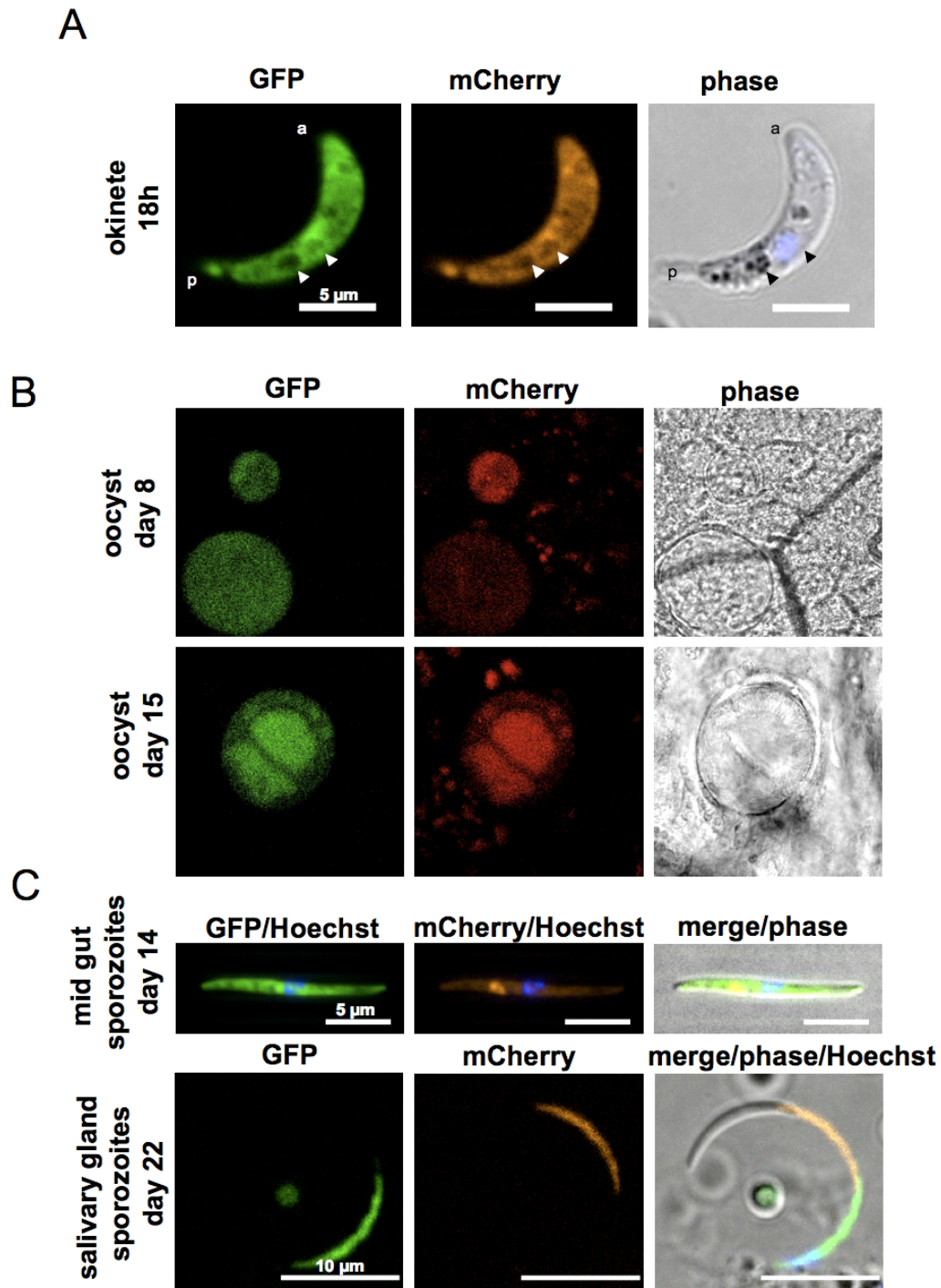


Figure 20: C-CAPmCherry expression and Localization in mosquito stages.

Live cell imaging was performed on all illustrated parasite stages. GFP expression is shown in green, C-CAPmCherry in red, nuclei are stained with Hoechst 33342 (blue) and phase contrast images in grey. **(A)** Ookinetes show cytoplasmic C-CAPmCherry localization like GFP. Polarization of the ookinete is indicated apical (a) and postal (p). Also, mCherry signal is excluded from the nucleus and crystalloid bodies (arrow). **(B)** Midgut associated oocysts at day 8 (top) and 15 (bottom) post infection exhibit weak cytoplasmic C-CAPmCherry signal in the cyst syncytium and is asynchronous intense between oocysts. **(C)** Midgut associated sporozoites at day 14 after infection exhibit a CAPmCherry signal restricted to a dot anterior of the nucleus. **(D)** Salivary gland sporozoites exhibit the weakest cytoplasmic C-CAPmCherry signal observed. The merge image of fluorescent and phase channels demonstrates the motility of the sporozoite.

To observe the $\Delta C-CAP::C-CAPmCherry$ liver stage development in the mammalian host, salivary gland sporozoites were isolated at day 18 after infection from WT and $\Delta C-CAP::C-CAPmCherry$ parasites and used to infect Huh7 cells. Live cell imaging was performed at 24, 48 and 72 hours post infection. The C-CAPmCherry protein was present during entire liver stage development. At 24 hours post infection only a very weak signal was detected which increased during parasite development. The signal peaked at 72 hours, when merozoites were fully developed. Each merozoite showed cytoplasmic C-CAPmCherry distribution. These pictures verify the gene expression analysis in liver stages (Fig. 20 C, B), where *C-CAP* expression increases during development and was the highest in merozoite stage at 72 hours. Also the protein abundance appears to increase, accordingly.

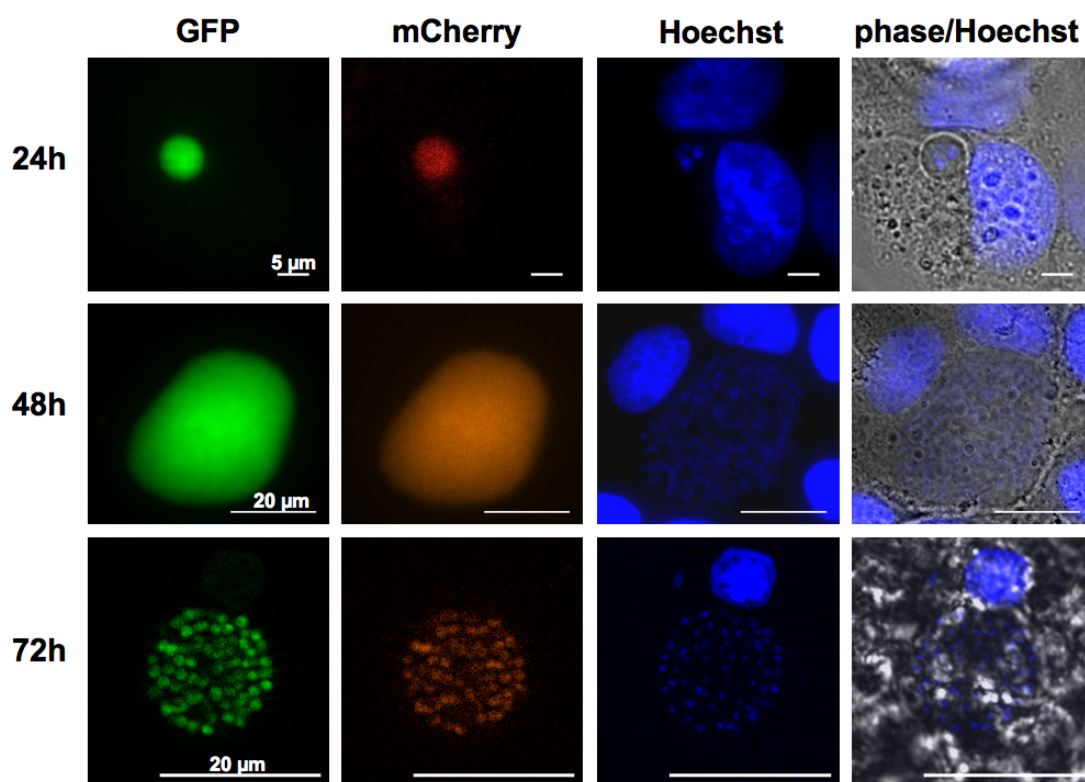


Figure 21: C-CAPmCherry expression and localization in liver stages.

Live cell imaging was performed on sporozoite infected Huh7 cells *in vitro* at 24, 48 and 72 hours after infection. GFP expression is shown in green (first column), C-CAPmCherry in red (second column), nuclei are stained with Hoechst 33342 (blue, third column) and micrographs merge with the phase contrast in grey (forth column). The weakest C-CAPmCherry signal was observed at 24 hours post infection, which increases over time during development up to 72 hours and exhibit cytoplasmic localization during all observed time points.

Taken together, parasites expressing the C-CAPmCherry fusion protein were able to complete the *Plasmodium* life cycle indistinguishable from WT parasites. The C-CAP protein abundance was detected via mCherry fluorescence. The strongest fluorescence was observed

in blood stages, including late trophozoites, schizonts and gametocytes. During mosquito stage development only ookinetes show considerable mCherry signal intensity, which dramatically decreases during further sporozoite development. In hepatocytic stages the C-CAPmCherry fluorescence increases during maturation and was the strongest in merosomes. The differential protein abundance correlate with quantitative gene expression data. Localization of C-CAPmCherry was uniformly cytoplasmic in all stages, except in midgut sporozoites, where a distinct signal in close proximity to the nucleus was observed

3.1.5.3. C-CAPmCherry protein abundance

To test the C-CAPmCherry protein abundance, merozoites, gametocytes, ookinetes and sporozoite stages were collected from $\Delta C-CAP::C-CAPmCherry$ parasites and analyzed by western blot. The fusion protein was nicely detected as a distinct band in merozoites, gametocytes and ookinetes with its predicted molecular size of 44 kDa (Fig. 22). The molecular weight was calculated by summation of the weight of C-CAP (17 kDa) and the weight of mCherry (26 kDa), respectively. In both sporozoite stages only a very weak, close to background signal was detected, despite of high parasite input (150.000 spz./sample). The unspecific bands as seen in midgut sporozoites represent mosquito material, as shown in the control sample (Fig. 22).

Taken together, western blot analysis confirmed the abundance of the C-CAPmCherry fusion protein with the right size and confirmed the decrease in sporozoites as is was shown by life cell imaging and expression data.



Figure 22: C-CAPmCherry protein abundance.

Western blot analysis using a polyclonal α -mCherry antibody, detected the C-CAPmCherry fusing protein with its predicted molecular size of 44 kDa (red asterisk). Samples of merozoites (mero), gametocytes (gamy), ookinetes (ook, n= 300.000 ook/sample) as well as midgut- (mg) and salivary gland (sg) sporozoites (spz., n= 150.000 spz./sample) were used and separated by an 15 % SDS-PAGE. Uninfected mosquito material (unif. mosq.) was used as specificity control. The molecular weight is indicated at the left.

3.1.6. Trans-species complementation with the *Cyptosporidium parvum*

***CpC-CAP* ortholog**

Apicomplexan C-CAP protein orthologs are highly conserved throughout the phylum. They share 70 % similarity between their deduced amino acid sequences (Fig. N1, A). The crystal structure of the *Cyptosporidium parvum* C-CAP protein was solved by Raimund Hui (SGC, Toronto) and is accessible in the protein data bank (PDB). To combine biochemical and structural insights of the C-CAP protein with experimental genetics in the model rodent parasite *P. berghei*, trans-species complementation with the *Cyptosporidium parvum* C-CAP ortholog was performed and thus provides a crucial link between the two complementary lines of research.

3.1.6.1. Generation of *CpC-CAP* complementation parasites

To investigate the functional redundancy between both ortholog C-CAP proteins from *P. berghei* and *C. parvum* *in vivo*, the *C. parvum* C-CAP coding sequence (cds) was introduced into the *P. berghei* *c-cap*(-) background. For complementation, the conserved C-terminal *C. parvum* C-CAP coding sequence (amino acids 34-552) was used. The DNA was amplified by RT-PCR from *C. parvum* cDNA (cdg5_440) with C1 and C3 primers as indicated (Fig. 23 B, Tab. 2) resulting in a fragment of 519 bp length. Subsequently, the amplicon was sequenced and ligated into the B3D+C-CAP knockout plasmid (Fig. 8 A), which contains the 5'UTR and 3'UTR of the endogenous *P. berghei* C-CAP gene for homologous recombination and the marker cassette *Tgdhfr/ts* cassette for selection (Fig. 23 B). The *P. berghei* ANKA-507cl GFP expressing strain (Janse *et al.* 2006) was transfected with the *SacII* / *KpnI* linearized B3D+CpC-CAP complementation plasmid. Pyrimethamine resistant parasites *Cpc-cap* (Δ PbC-CAP::*CpC-CAP*) were cloned *in vivo* by limited dilutions.

Successful integration of the replacement plasmid was confirmed by genotyping with diagnostic PCR primers (Fig. 23 A, Tab. 2). The 5'UTR and 3'UTR recombination events were confirmed by amplification of test'5 with 2530 bp and test'3 with 1025 bp in *Cpc-cap* parasites but not in the wild-type ANKA-507cl GFP parasites (Fig. 23 B). The absence of the wild-type locus in Δ PbC-CAP::*CpC-CAP* parasites was controlled by the absence of amplification of the 2752 bp fragment, thus confirming the clonality of the *Cpc-cap* strain. Moreover, integration of *CpC-CAP* was confirmed by locus amplification of 519 bp with C1 and C3 primers, amplifying the CDS of *CpC-CAP* (Fig. 23 B).

Taken together, the integration of the ortholog *C. parvum* *C-CAP* gene into the *P. berghei* *C-CAP* knockout parasites resulted in viable *P. berghei* blood stage parasites.

A

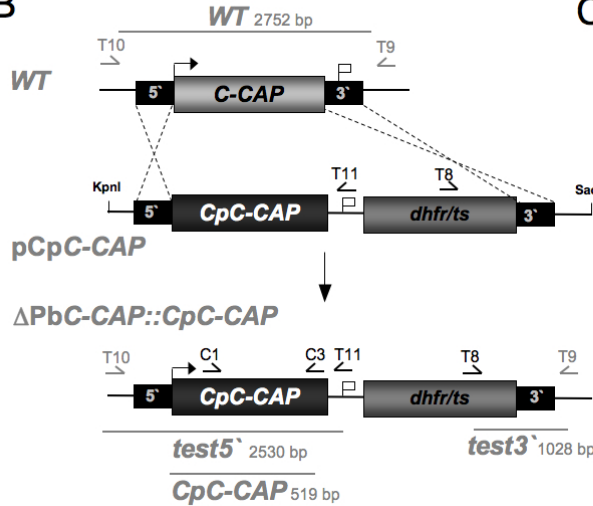
```

PbCAP  -----LNFKDNQWEVCNYKN-EKIIKLEKVELNNSVNIENCENTTFTIENHFKSLQIQNGKCSIVLNLISSIEIIDCKKIK 78
PfCAP  -----MTSEGSIQLEKDDQWDVINYKD-GKIVKLSQVELNNAVINYNCENTTFTVIENNKFSLQIEKCVKNVVLNLISSIEIINSKKVK 84
TgCAP  --TMAKTGAELHLHGDTWRVCNFDKDDIIKIDSATMKQKQVIRDCKGVGIQIES-KVNSVIDNCDNLRLCVNSLISGAEFVNCRKIK 122
CpCAP  --QVVTNGSPKVELQKDTYLVNHN-CADPTLSEGSIKNKVSVRCSQNSRIIVEQ-KVNSIFIENCVGCIPLVNGVISSIEIV-CDDIK 101
Srv2p  GSTLKTRRPPRKELVGNKWFIBNYENETESLVIDAN-KDESIIFIGKCSQVVOIKG-KVNAISLSETESCSVVLDSISGMDVIKSNKFG 448

PbCAP  IOVLGKSSSISIDKCI GVEIYLSKDNTESEFTTALSSEMNVHFE-KNGE---WKEITIEPQYQ--HTLCGGKLNTRVSDLYNY 158
PfCAP  IOVLGKSSSISIDKCTGVEFVLSKENVECEPTTALSSEMNIHIQQQDEE---WTEITIEPQYQ--HLENGKLTTRVSDLYKF 162
TgCAP  FOVKGTCCHSIAIDKCSGVLDLVSKESKDVETTSKSGEMNLNFPKTDDEEDGDWAEVPIPEQFH--HNIKNGVLHTRVSELYSC 203
CpCAP  LQMTGIVPFTISLDKSNKVNIVTSKEGKNVEVYSSKSEMNLFF--GEEEG-WKELAIPQFVTKYNESKGLKESMVSPLYG- 180
Srv2p  IOVNHSLPQISIDKSDGNIYLSKESLNTETITSCSTAINVNLFIGEDDD--YVEFPIPEQMK--HSFADGKFKSAVFEHAG- 526

```

B



C

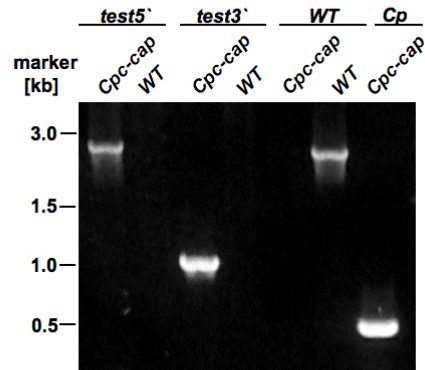


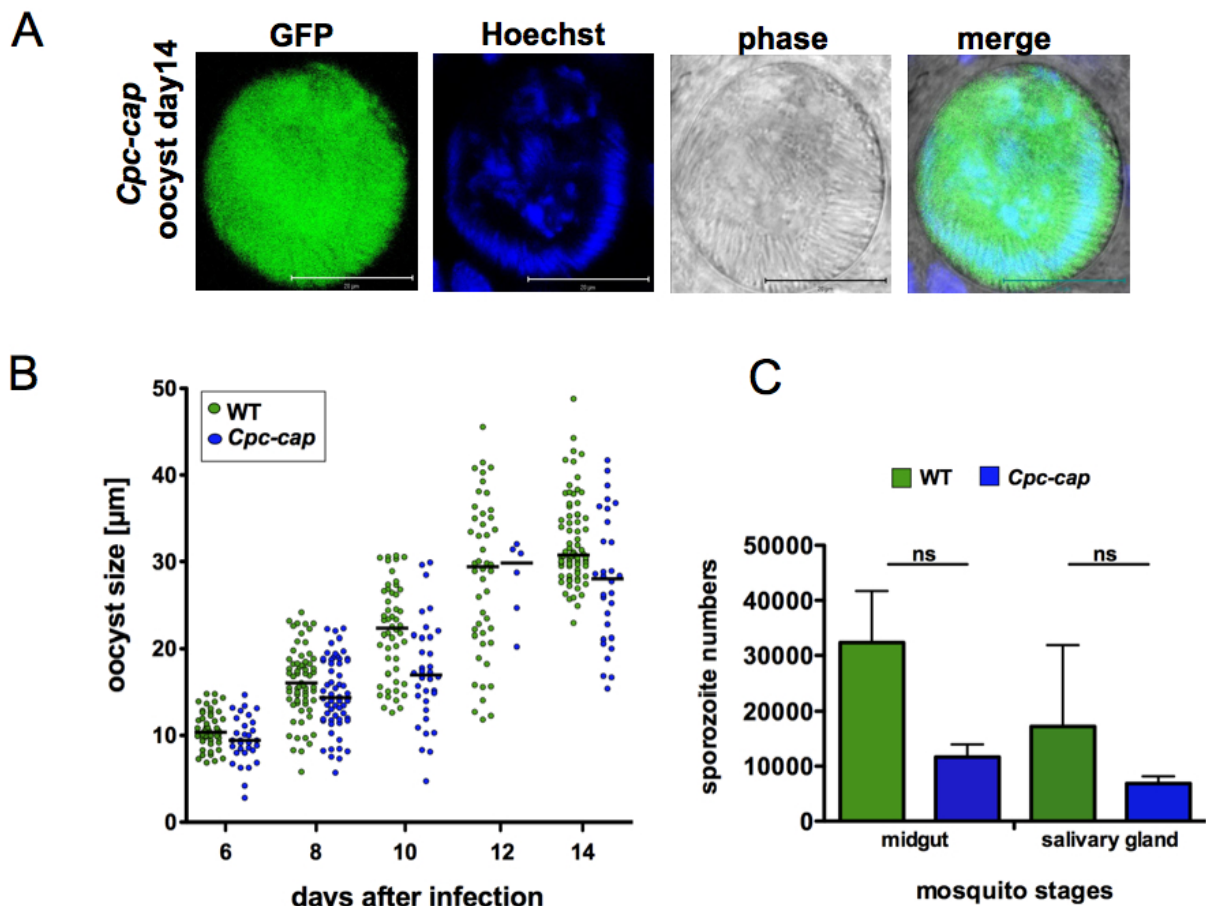
Figure 23: Trans-species complementation in *P. berghei* parasites with *Cryptosporidium parvum* C-CAP.

(A) Sequence alignment of apicomplexan C-CAP actin-binding domain (red residues) orthologs from *T. gondii* (TgCAP; gi 211961913), *C. parvum* (CpCAP; gi 66357652), *P. berghei* (PbCAP; gi 68074593), and *P. falciparum* (PfCAP; gi 124505741) with *S. cerevisiae* (Srv2p/ScCAP; gi 6324191). Highly conserved residues are shaded in grey. (B) Replacement strategy to generate a *P. berghei* population that contains the orthologous *C. parvum* C-CAP cDNA under the control of the *P. berghei* endogenous regulatory promoter sequences (Δ PbC-CAP::CpC-CAP). Integration was facilitated by double homologous recombination in the C-CAP knockout (*c-cap*(-)) background. Diagnostic primers and PCR products are indicated by arrows, which hybridize the genomic locus (grey) or the vector (black) and bars indicating the fragment size. (C) Genotyping of the *Cpc-cap* parasites using PCR with specific primers as indicated in A, confirmed the specific test5' (2053 bp) and test3' (1028 bp) fragment amplification and genomic integration. No residual WT parasites (WT, 2752 bp) were found in the *Cpc-cap* line, thus confirming clonality. The *CpC-CAP* locus was detected at 519 bp size.

3.1.6.2. *Cryptosporidium parvum* C-CAP reverts the defects of the *Plasmodium berghei* C-CAP knockout phenotype.

As expected from the non-vital role of C-CAP in blood stages the *Cpc-cap* complementation parasites showed normal blood stage development. To follow life cycle progression of *Cpc-cap* parasites and to investigate the potential rescue of the *c-cap*(-) defects, *A. stephensi* mosquitoes were infected and the development of oocysts was documented by microscopy in comparison to wild type parasites.

Oocyst numbers were counted at day 10 post mosquito infection and did not show significant differences to wild-type parasites (Fig. 24 C). The oocyst development was analyzed at day 6, 8, 10, 12 and 14 using a confocal microscope and oocyst size was measured. As indicated, in figure 24 B the oocyst size increased over time similar to WT and no significant differences could be detected between WT and *Cpc-cap* by students t-test. Importantly, sporozoite development inside the oocyst could be observed microscopically at day 14 (Fig. 24 A). Quantification of midgut-and salivary gland associated sporozoites at day 14 and 17 revealed complete parasite development in the mosquito. *Cpc-cap* infected mosquitoes typically displayed a trend towards fewer sporozoites compared to WT, but differences were not significant (Fig. 24 C). Accordingly, when transmitted naturally by mosquito bite to naïve C65Bl6 mice, *Cpc-cap* sporozoites consistently induce patent blood stage infections three days after inoculation. This prepatent period was indistinguishable from WT sporozoite infections, and indicates a normal transmission rate and liver stage development of *Cpc-cap* parasites.



D

population	ookinetes	oocyst	natural transmission
<i>Cpc-cap</i>	++	175 ± 39	yes positive day 3
WT	++	223 ± 55	yes positive day 3

Figure 24: *Cryptosporidium parvum* C-CAP rescues the *c-cap*(-) defects.

(A) Restoration of sporozoite formation in *Cpc-cap* parasites. Midgut associated oocysts (day 14) of *Cpc-cap* detected microscopically by endogenous expressed GFP (green). Nuclei are stained with Hoechst 33342 (blue). Phase contrast images are shown (grey) as well as merge of all channels. Scale bars, 20 µm (B) Quantification of oocyst development of *Cpc-cap* (blue) and wild type (WT, green) parasites. Both parasite populations show comparable size increases as oocysts mature inside the mosquito vector. Each data point represents the oocyst size from randomly selected oocysts of parasite- infected midguts (n= 4). Data are from two independent feedings of WT and *Cpc-cap* each. Horizontal lines indicate the median sizes of each group. (C) Sporozoite numbers of WT (green) and *Cpc-cap* (blue) infected *Anopheles stephensi* mosquitoes. Data are from five independent feeding experiments. Differences are statistically non-significant by students t-test (p= 0.4 and 0.13) for midgut and salivary gland sporozoites.

(D) Complete life cycle progression and natural transmission of *Cpc-cap* parasites compared to WT.

In conclusion, *ΔPbC-CAP::CpC-CAP* parasites (*Cpc-cap*) develop normally in the mosquito host as reflected by typical oocyst maturation and sporozoite development. Furthermore, they display regular blood- and liver- stage development in the vertebrate host.

These results demonstrate that a trans-species complementation of the C-CAP protein between *P. berghei* and its ortholog from *C. parvum* rescues the corresponding defect in *c-cap*(-) knockout parasites. Furthermore, this finding confirms a gene specific phenotype of the *c-cap*(-) mutant and excludes pleiotropic effects. Finally, these results identify *CpC-CAP* and *PbC-CAP* as true functional homologues.

3.1.6.3. Mutagenesis of *CpC-CAP*

The apparent functional redundancy of the *P. berghei* C-CAP and the *C. parvum* C-CAP proteins in *P. berghei*, prompted us to analyze the molecular function *in vivo* by site-directed mutagenesis on the *CpC-CAP* protein. The mutants were generated by Julia Sattler (Sattler, PhD thesis, 2010). First, conserved residues of position D117/K118, that mediate G-actin binding was mutated with charge-to-alanine substitutions to influence the function by impaired actin interaction. Second, mutations affecting the homodimer structure were introduced, leading to a premature termination of the *CpC-CAP* protein and the loss of the dimer structure (Fig. 25 A, B).

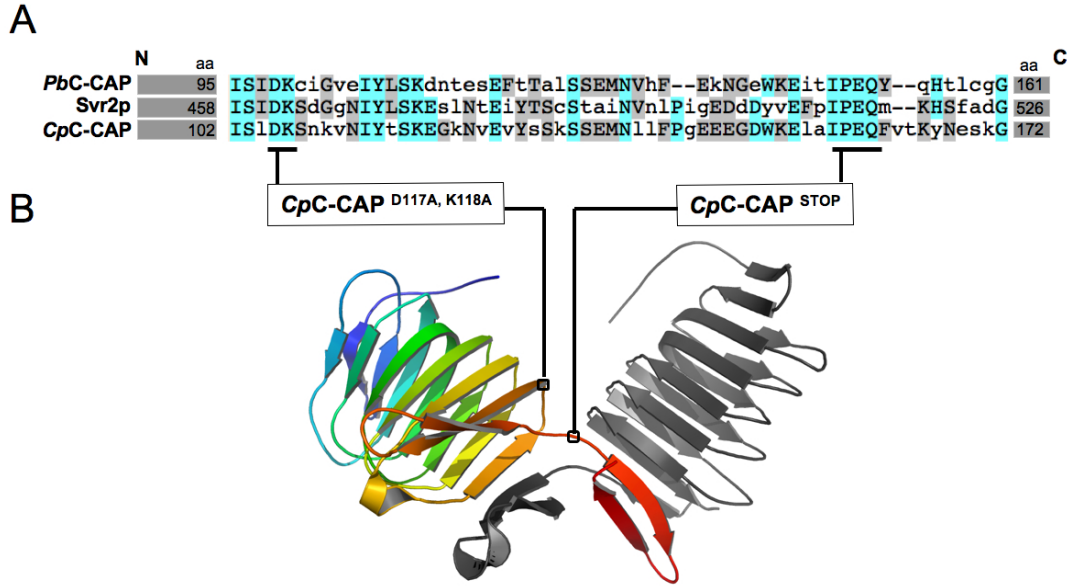


Figure 25: Mutagenesis of the *CpC-CAP* protein.

(A) Sequence alignment of apicomplexan C-CAP orthologs actin-binding domains from *P. berghei* (*PbCAP*; gi 68074593, aa 95-151) with *S. cerevisiae* (*Svr2p/ScCAP*; gi 6324191, aa 458-518) and *C. parvum* (*CpCAP*; gi 66357652, aa 102-163). Identical residues are shaded in blue and similar residues are printed in grey. Positions of mutagenesis are marked with a black bars and residue substitutions are described below. (B) Overview of the *CpC-CAP* protein dimer, one monomer (rainbow color) and the second monomer (grey) creating a dimer interface by domain swapping. Positions and names of mutations are indicated on the structure. *CpC-CAP*^{D117A, K118A} influences the actin interaction and *CpC-CAP*^{STOP} prevents dimerization.

Both mutants were analyzed for their ability to complement the *c-cap*(-) defects. For phenotypic analysis in *P. berghei* the cds of *CpC-CAP*^{D117A, K118A} and *CpC-CAP*^{STOP} mutant proteins were amplified by PCR from their expression vectors with specific primers C1/ C3 for *CpC-CAP*^{D117A, K118A} and C1/C4 for *CpC-CAP*^{STOP} (Tab. 2) and used to replace the *CpC-CAP* in the $\Delta PbC-CAP::CpC-CAP$ complementation vector (Fig. 26 A). The resulting constructs $\Delta PbC-CAP::CpC-CAP$ ^{D117A, K118A} and $\Delta PbC-CAP::CpC-CAP$ ^{STOP} were sequenced, *KpnI/SacII* linearized and transfected into the *P. berghei* ANKA-507cl GFP strain (Janse et al.) Genotyping of clonal parasite lines was performed by diagnostic PCR (Fig. 26 A, Tab. 2), and confirmed successful integration of the 5'UTR and the 3'UTR (Fig. 26 B). None of these fragments could be amplified in WT parasites, confirming the specificity. Locus amplification using primers C1/C3 and C1/C4 revealed specific fragments for *CpC-CAP*^{D117A, K118A} and *CpC-CAP*^{STOP} parasite lines (Fig. 26 B). The WT locus with a size of 2752 bp could only be detected in wild type parasites and was absent in mutant parasites, confirming clonality of the parasite lines.

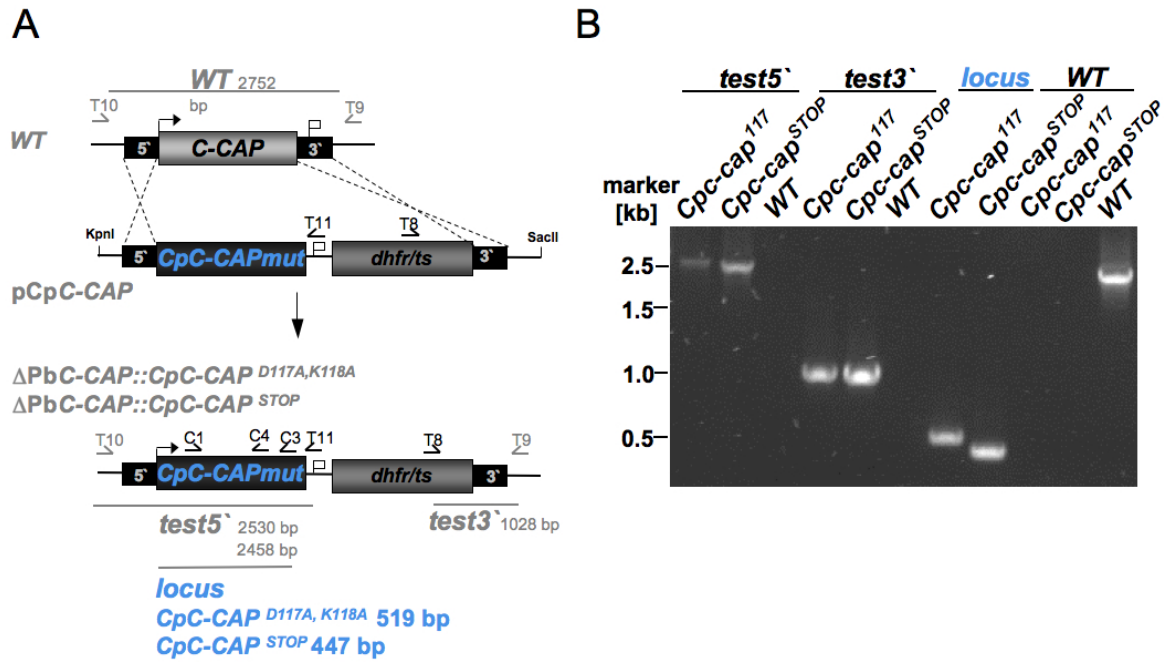


Figure 26: Generation of mutant *Cpc-cap*^{D117A, K118A} and *Cpc-cap*^{STOP} parasites.

(A) Replacement strategy to generate *P. berghei* populations that contain the mutated *C. parvum* C-CAP ORF under the control of the *P. berghei* endogenous promoter sequence. Incorporation was facilitated by double homologous recombination in the *PbC-CAP* knockout background. Diagnostic primers and PCR products are indicated by arrows, that hybridize with the genomic locus (grey) or within the vector (black). Bars indicate the predicted fragments. (B) Genotyping of the *Cpc-cap*^{D117A, K118A} and *Cpc-cap*^{STOP} parasites using PCR with specific primers as indicated in A, confirmed the specific 5'test (2530 bp, 2458 bp) and 3'test (1028 bp) fragment amplification and genomic integration. No residual WT parasites (WT, 2752 bp) were detected in *Cpc-cap*^{D117A, K118A} and *Cpc-cap*^{STOP} mutants, confirming clonality. Specific locus amplification of *Cpc-cap*^{D117A, K118A} (519 bp) and *Cpc-cap*^{STOP} (447 bp) confirmed presence of the altered gene locus.

Phenotypic analysis revealed normal blood stage and ookinete development of both *Cpc-cap*^{D117A, K118A} and *Cpc-cap*^{STOP} mutant parasites (Fig. 27 B). Both were fed to *A. stephensi* and oocyst development was characterized in comparison to WT, *c-cap*(-), and *Cpc-cap* parasites in three independent feedings experiments (Fig. 27 B).

Interestingly, the actin binding mutant *Cpc-cap*^{D117A, K118A} developed normal in mosquitoes. Oocyst formation was comparable to *Cpc-cap* and WT parasites (Fig. 27 A, B). Quantification of midgut- and salivary gland associated sporozoites (5631 ± 2231) revealed equivalent numbers to *Cpc-cap* parasites (6853 ± 2915) and confirmed normal life cycle progression in the mosquito host. Natural transmission to two C65/Bl6 mice was tested and resulted in normal prepatency of three days (Fig. 27 B). These results show that the mutant *CpC-CAP*^{D117A, K118A} protein is able to complement the specific C-CAP function in *c-cap*(-) knockout parasites *in vivo*, despite of reduced actin binding activity *in vitro* (Sattler, PhD thesis, 2010).

In contrast the *Cpc-cap*^{STOP} mutant could not complement the *c-cap*(-) knockout defects.

Only few oocysts were detected, no oocyst growth and maturation, including sporozoite development, could be observed (Fig. 27 A, B). This phenotype resembles the characteristic defects of those observed in *c-cap*(-) parasites (Fig. 27 A, B).

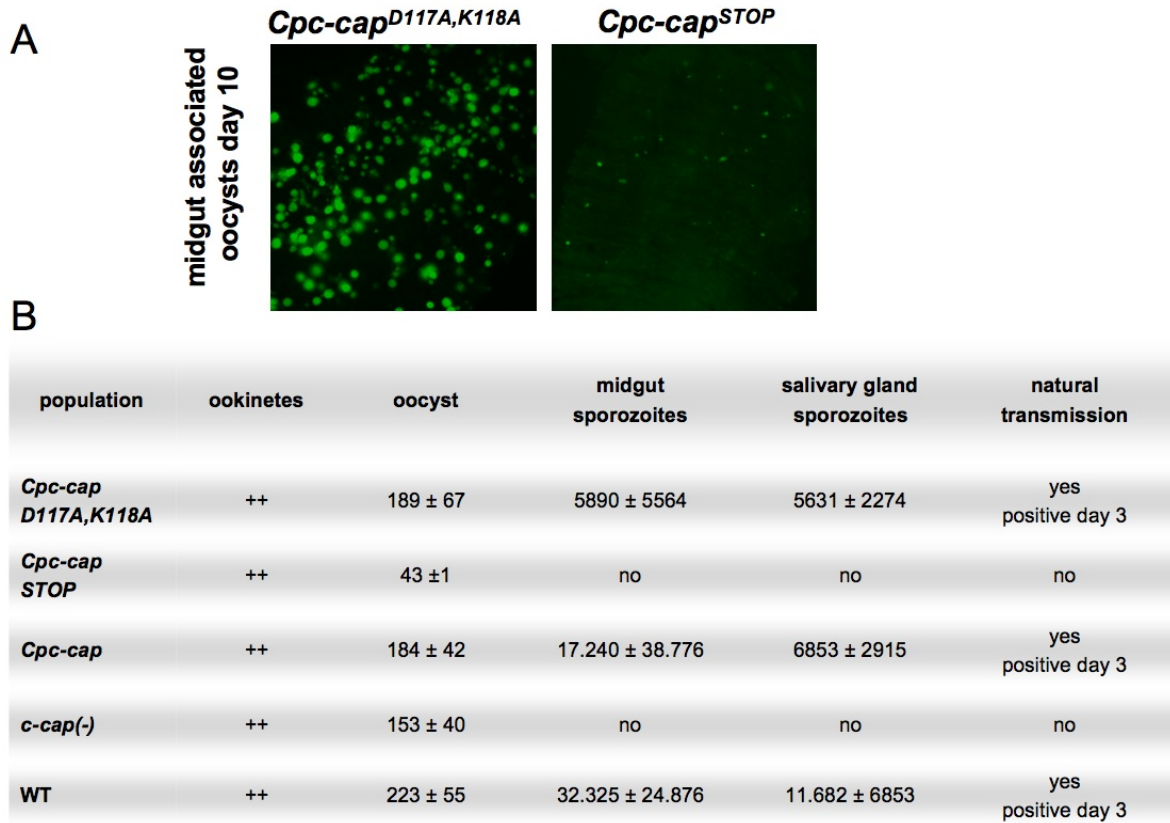


Figure 27: Phenotypic analysis of *Cpc-cap*^{D117A, K118A} and *Cpc-cap*^{STOP} parasites.

(A) Midgut- associated oocysts at day 10 after mosquito infection are detected by endogenous GFP expression (green). Note, that *Cpc-cap*^{D117A, K118A} oocysts develop normal, while *Cpc-cap*^{STOP} oocysts are reduced in numbers and size. (B) Table showing the life cycle progression of the mutants *Cpc-cap*^{D117A, K118A}, *Cpc-cap*^{STOP} in comparison to *Cpc-cap*, *c-cap*(-) and WT parasites. *Cpc-cap*^{D117A, K118A} complements the *c-cap*(-) defects and sporozoite development is restored, while *Cpc-cap*^{STOP} does not, and exhibits characteristic defects of *c-cap*(-).

3.1.6.4. The CpC-CAP^{STOP} mutant protein is degraded *in vivo*

To verify the protein abundance of both mutants *in vivo*, western blot analysis was performed on ookinete stages. *In vitro* cultured ookinetes were purified with p28-antibody labeled magnetic beads and total protein samples were prepared for western blotting. Ookinete proteins were separated on 15 % SDS-PAGE and blotted to polyvinylidene difluoride (PVDF) membrane. Specific protein detection was achieved with the primary CpCAP antibody and the

secondary horseradish peroxidase (HRP)-conjugated anti- rabbit antibody (1: 5000 of dilution, each).

In western blots the wild type *CpC-CAP* protein was detected as a distinct band with a predicted size of 17.8 kDa (Fig. 28 A). No band could be detected in WT ookinete lysate, confirming the specificity of the primary antibody in western blots. A prominent protein band could be detected with a molecular mass of 17.8 kDa in *Cpc-cap*^{D117A, K118A} ookinetes, which is similar to the molecular mass of *CpC-CAP*. In contrast, no such protein band was observed in *Cpc-cap*^{STOP} mutant ookinetes. In both samples the same amount of protein input of 500.000 ookinetes was used as indicated by the equal intensity of unspecific bands (Fig. 28 A). Additionally, a very faint band below 15 kDa was recognized in this mutant, which might indicate protein degradation *in vivo*. To ensure that the primary antibody does recognize the mutant *CpC-CAP*^{STOP} protein, a control western blot using the recombinant proteins *CpCAP*, *CpC-CAP*^{D117A, K118A}, *CpC-CAP*^{STOP} and others was performed. All recombinant *C. parvum* CAP proteins, were recognized by the same primary *CpC-CAP* antibody (Fig. 28 B).

Taken together these results demonstrate that the *CpC-CAP* and its mutant *CpC-CAP*^{D117A, K118A} proteins are abundant in the parasite, whereas the truncated *CpC-CAP*^{STOP} protein appears to be degraded. The similarity of the defective oocyst development between *c-cap*(-) and *Cpc-cap*^{STOP} parasites can thus be explained by the absence of significant levels of *CpC-CAP*^{STOP} protein.

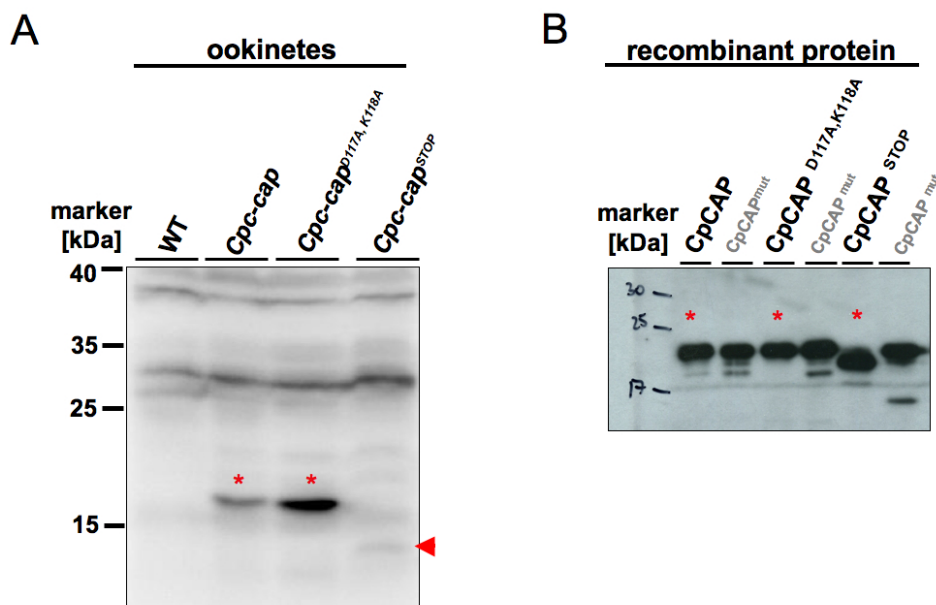


Figure 28: Protein abundance of *CpC-CAP* and its mutants *in vivo*.

(A) Western blot analysis of whole protein samples of cultured ookinetes from wild type (WT), the complementation *Cpc-cap* and the mutant parasites *Cpc-cap*^{D117A, K118A} and *Cpc-cap*^{STOP}. Species and amount of sample input are indicated on the top. Samples were separated using 15 % SDS-PAGE,

blotted onto a polyvinylidene fluoride (PVDF) membrane and detected by specific antibody reaction of anti *CpC-CAP* (rabbit) and anti rabbit horse radish peroxidase (HRP) conjugated antibodies. The molecular mass is indicated on the left. The *CpC-CAP* and *CpC-CAP*^{D117A, K118A} proteins are abundant in ookinetes (asterisk), whereas the *CpC-CAP*^{STOP} protein could not be detected at the right size but only at lower (arrowhead) apparent molecular weight, indicating degradation *in vivo*. No signal was found in WT parasites, confirming the specificity of the primary polyclonal anti *CpC-CAP* antibody. **(B)** Control western blot analysis to test the specificity of the generated primary anti *CpC-CAP* rabbit antibody on selected recombinant *CpC-CAP* proteins. The *CpC-CAP*, *CpC-CAP*^{D117A, K118A}, and *CpC-CAP*^{STOP} proteins (asterisk, black name), are recognized by the antibody, confirming recognition of mutant proteins.

3.1.7. Profilin could not rescue the *c-cap(-)* defects

Previous genetic studies in *S. cerevisiae* provided evidence for a functional redundancy between Srv2/CAP and profilin (Vojtek *et al.*, 1991). Overexpression of profilin is able to suppress the morphological and nutritional defects of cells lacking Srv2/CAP. Additionally, yeast cells lacking profilin, resemble the phenotype of CAP deficient cells, indicating that both proteins are involved in similar cellular processes and are able to complement each others function (Vojtek *et al.*, 1991). Their molecular interaction facilitates actin turnover (Bertling *et al.*, 2007). Since

c-cap(-) parasites exhibit no striking phenotype in blood- and ookinete stage parasites, complementation of C-CAP function by functional related actin binding proteins is plausible.

This prompted me to test whether the G-actin binding protein profilin is able to rescue the *c-cap(-)* defects during oocyst maturation in *P. berghei*. Using reverse genetics, the endogenous *C-CAP* was replaced by *profilin* and the selection marker *Tgdhfr/ts* by homologous recombination (Fig. 29 A). *Profilin* was amplified with primers P1 and P2 from *P. berghei* schizont cDNA (Fig. 29 A, Tab. 2), to exclude the three introns, and the resulting PCR amplicon of 525 bp, was subsequently ligated into the B3D+*C-CAP* knockout plasmid (Fig. 8 A). Transfection was performed with 10 µg of *KpnI* / *SacII* linearized replacement vector on the GFP expressing *P. berghei* Anka-507cl parasite line (Janse *et al.*, 2006) and clonal parasite lines where obtained. Primers T10/T11 and T8/T9 were used for genotyping (Fig. 29 A, Tab. 2) and successfully amplified test5` (2842 bp) and test3` (1028bp) in Δ *PbC-CAP::Pbprofilin* parasites, but not in *WT* (Fig. 29 B). Specific integration of *Profilin* into the *C-CAP* locus was shown by PCR using primers T10/P2 (Fig. 29 A, Tab. 2) and resulted in test5` locus amplification (1613 bp) (Fig. 29 B). Clonality of Δ *PbC-CAP::Pbprofilin* parasites was confirmed by absence of the *WT* signal (2752 bp), which was still detectable in parental parasites (Fig. 29 B).

For phenotypic analysis clonal $\Delta PbC-CAP::Pbprofilin$ parasites were fed to *A. stephensi* mosquitoes and oocyst maturation and sporozoite development was monitored. Two independent feedings showed that $\Delta PbC-CAP::Pbprofilin$ parasites exhibit reduced oocyst numbers per midgut and are arrested during oocyst maturation, comparable to the *c-cap(-)* phenotype (Fig. 29 C). No sporozoites were detected at day 17 and 27 after feeding (data not shown). These results demonstrate, that substitution of C-CAP with Profilin was not successful and indicates a distinct function for both proteins during oocyst maturation. In $\Delta PbC-CAP::Pbprofilin$ parasites profilin is expressed from two copies. First, under its endogenous *Profilin* promoter and second under the promoter of *C-CAP*, which should result in enhanced profilin transcription in schizonts, ookinetes and young oocysts (day 6) (Fig. 7 B). To test increased profilin transcription and protein abundance, qRT-PCR and Western Blot were performed on merozoites and ookinetes from $\Delta PbC-CAP::Pbprofilin$ and *WT* parasites. Quantitative RT-PCR with profilin specific primers X1/X2 (Tab. 3), which do not differentiate between both profilin proteins, were used for amplification and normalized against GFP expression of the *P. berghei* Anka-507cl strain. No significant differences of profilin expression between WT and $\Delta PbC-CAP::Pbprofilin$ parasites could be determined in merozoites and ookinetes. Western blot analysis was not sensitive enough to detect altered protein levels between both parasite strains (data not shown).

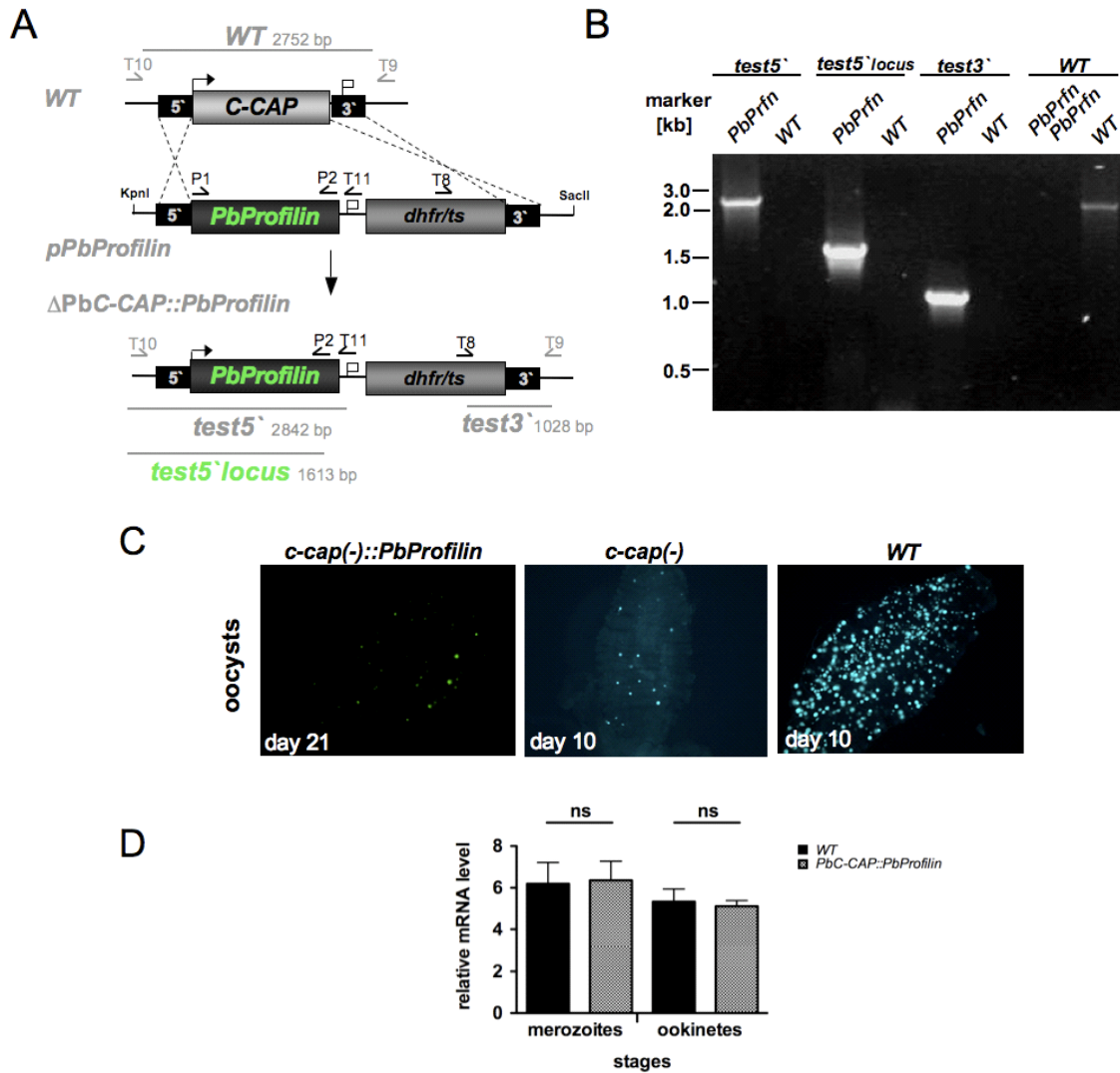


Figure 29: Profilin does not complement the C-CAP function during oocyst maturation.

(A) Replacement strategy to generate *P. berghei* populations, that incorporate *P. berghei profilin* under the control of the endogenous *C-CAP* promoter sequence in the *C-CAP* knockout background (Δ *PbC-CAP::Pbprofilin*). Double homologous recombination was facilitated by 5'UTR and 3'UTR of *C-CAP*.

Diagnostic primers and PCR products are indicated by arrows that hybridize to the genomic locus (grey), or the vector (black). The bars indicate the fragment sizes. (B) Genotyping of the Δ *PbC-CAP::Pbprofilin* parasites using PCR with specific primers (as indicated in A) confirmed the specific 5'test (2842 bp) and 3'test (1028 bp) fragment amplification and genomic integration. No residual *WT* *C-CAP* locus (2752 bp) was detected in Δ *PbC-CAP::Pbprofilin* parasites confirming clonality. Specific 5'locus amplification (1613 bp) confirmed *Profilin* integration into the *C-CAP* locus. (C) Representative fluorescence images of mosquito midguts infected with Δ *PbC-CAP::Pbprofilin*, *c-cap(-)* and *WT* parasites at day 21, and 10 after inoculation. Oocysts are visualized by GFP fluorescence of the *P. berghei* Anka-507cl strain indicating reduced oocyst numbers and reduced oocyst size compared to wild type parasites. (D) qRT-PCR of *profilin* expression in merozoites and ookinetes of *WT* and Δ *PbC-CAP::Pbprofilin* parasites. No significantly elevated levels of *profilin* mRNA in were detected in Δ *PbC-CAP::Pbprofilin* parasites. Students t-test was used to define significance of $p < 0,05$.

3.2. Characterization of the G-actin binding proteins profilin, actin depolymerizing factor 1 and 2 (ADF1, ADF2) in *Plasmodium*

In apicomplexan parasites only a minimal repertoire of G-actin binding proteins is known to regulate actin turnover. In addition to C-CAP, profilin and the actin depolymerizing factors 1 and 2 (ADF1, ADF2) were identified to bind to monomeric actin. Interestingly, they differ significantly in structure and function from their orthologs in other phyla (Kursula *et al.*, 2008; Schuler *et al.*, 2005a; Schuler and Matuschewski, 2006b). In order to understand the function and interplay between these unique proteins during life cycle progression of *Plasmodium*, the mRNA expression levels, protein abundance and subcellular localization were characterized in *P. berghei*.

3.2.1. Gene expression and protein abundance of G-actin binding proteins decrease during sporozoite development in *P. berghei*

First, the role of the two G-actin binding proteins profilin and ADF1 will be discussed, followed by consideration of the ADF2 protein. Profilin and ADF1 perform essential function during blood stage development in *P. berghei* (Kursula *et al.*, 2008, Schuler *et al.*, 2005a). In order to characterize the importance of profilin and ADF1 in non-erythrocytic stages, their gene expression was quantified throughout the life cycle of *P. berghei* using qRT-PCR with specific primers X1/X2 for *profilin* and X3/X4 for *ADF1* (Tab. 3). Expression values were normalized against constitutive *GFP* expression of the host Anka-507cl with X7/X8 primers (Tab. 3). Expression data verified the high *profilin* transcript abundance in merozoites and ookinetes (Fig. 30 A). However, in contrast to published data (Kursula *et al.*, 2008), *profilin* transcripts decreased drastically in midgut- and salivary gland sporozoites and were detected at background levels (Fig. 30 A). During liver stage development *profilin* gene transcription increases again and reaches high levels at 72 hours post infection (Fig. 30 A). The same dynamic expression pattern was observed for *ADF1* transcript abundance (Fig. 30 B). High expression levels were detected in merozoites, ookinetes and during liver stage development at 24 and 72 hours after infection (Fig. 30 B). Similar to *profilin*, *ADF1* expression diminishes during sporozoite development by 81.6 % compared to high expression in ookinete stages. Quantification of *ADF2* gene expression with primers X5/X6 (Tab. 3) by qRT-PCR, revealed that *ADF2* mRNA is only minimally transcribed throughout all stages analyzed (Fig. 30 A). Merozoites contained the highest levels of *ADF2* mRNA, not more than 4 % and 7 % of the

profilin and *ADF1* mRNA levels, respectively (Fig. 30 C). During sporozoite stages expression decreases close to background (Fig. 30 C). Taken together, *ADF1* and *profilin* represent the highest transcribed G-actin binding proteins, followed by *C-CAP* gene expression, (Fig. 7 B) and *ADF2* gene expression with the lowest level.

Protein abundance of all three proteins was investigated by western blot analysis on *P. berghei* wild type protein samples. Endogenous proteins were detected with the primary polyclonal rabbit anti-*P. falciparum* profilin, anti-*P. berghei* ADF1 and anti-*P. berghei* ADF2 antibodies (Tab. 1). The proteins were further traced by chemiluminescence, facilitated by the secondary anti-rabbit HRP conjugated antibody (Tab. 1).

Profilin with an apparent molecular weight of 19 kDa was clearly detected in merozoites, gametocytes and ookinetes (Fig. 30 D I.). Interestingly, no profilin protein was found in midgut- and salivary gland sporozoites (Fig. 30 D I.). Sufficiently high protein input was confirmed in all stages. The protein amount was controlled by robust detection of the 50 kDa α -tubulin protein in merozoites and gametocytes and with detection of the circumsporozoite protein (CSP) in ookinetes with a 52 kDa band and in sporozoite stages with a double band of 52 kDa and 44 kDa, respectively (Fig. 30 D II.) (Yoshida *et al.*, 1981). The ADF1 protein abundance was confirmed in merozoites, gametocytes, ookinetes and sporozoites with a predicted molecular size of 14 kDa (Fig. 30 E I.). However, despite of high parasite input as controlled by CSP protein detection, (Fig. 30 B II.), the amount of ADF1 protein strongly decreased in sporozoite stages (Fig. 30 E I.). The recombinant PbADF1 protein migrated with the same molecular weight of 14 kDa like the endogenous ADF1 in parasite samples (Fig. 30 E II.). The extremely weak transcribed ADF2 protein was not detected in merozoites, gametocytes, ookinetes and sporozoite stages in western blot analysis using the same wild type samples as for ADF1 detection. The recombinant *P. berghei* ADF2 protein was recognized with a molecular mass of 16 kDa and confirmed functionality of the used antibody (Fig. 30 E I.). The specificity of all antibodies was confirmed with uninfected mosquito midgut material (Fig. 30 D - F I.).

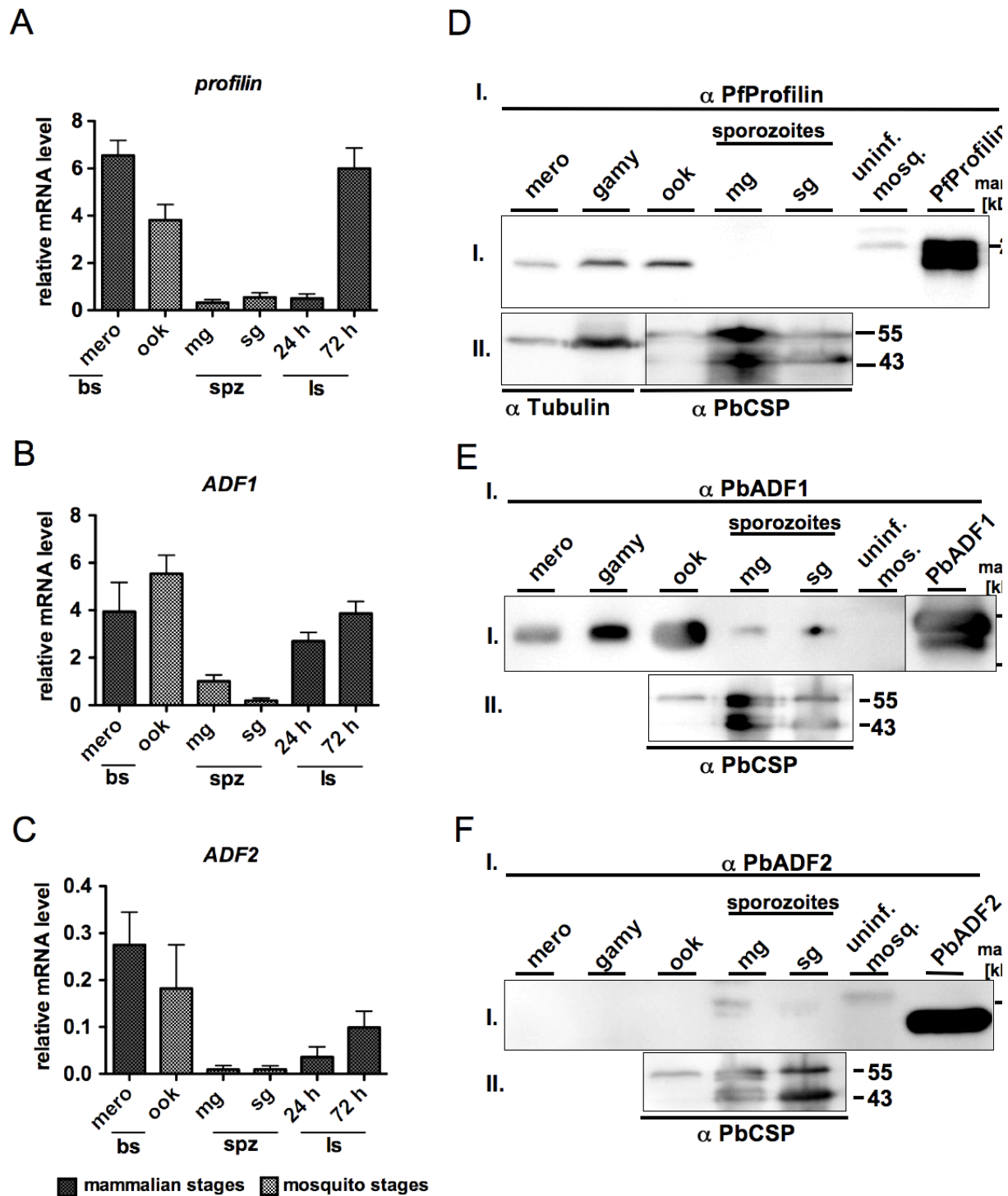


Figure 30: Gene expression and protein abundance of profilin, actin depolymerizing factor 1(ADF1) and 2 (ADF2).

(A-C) Expression profiling by quantitative RT-PCR of *Pbprofilin*, *PbADF1* and *PbADF2* in merozoites (mero), ookinets (ook), midgut (mg), salivary gland (sg) sporozoites (spz) and liver stages (ls) at 24 and 72 hours post infection. Relative mRNA levels were normalized to constitutive GFP expression of the Anka-507cl strain. The mRNA levels of *profilin* and *ADF1* are most abundant in merozoites, ookinets and late liver stages. In sporozoite stages the expression declines drastically for both genes (A, B). The *ADF2* mRNA is very weakly expressed (C). (D-F) Western blot analysis was done for merozoites (mero), gametocytes (gamy), ookinets (ook), midgut- (mg) salivary (sg) gland sporozoites (spz), uninfected mosquito material and on recombinant proteins *P. falciparum* profilin, *P. berghei* ADF1 and *P. berghei* ADF2. (D) Detection of profilin with a molecular size of 19 kDa using

primary rabbit PfProfilin antibody and secondary rabbit HRP conjugated antibody. Protein was abundant in merozoites, gametocytes and ookinetes, but not in sporozoites. For loading control the membrane was cut as indicated (dashed line) and probed with antisera for α -Tubulin and α -CSP. **(E)** The ADF1 protein was recognized by the rabbit anti *P. berghei* ADF1 antibody with a molecular weight of 13.9 kDa. **(F)** Detection of the ADF2 protein was not possible in all parasite samples. **(D-F)** To control protein loading tubulin (50 kDa) detection was used in merozoites and gametocytes, CSP detection was used for ookinetes (52 kDa), and sporozoites (double band of 52 kDa and 44 kDa) (Yoshida *et al.*, 1981).

Taken together, the western blot analysis revealed substantial amounts of the G-actin binding proteins profilin and ADF1 in blood stage merozoites and ookinetes. Surprisingly, no profilin and only very low amounts of ADF1 protein were detected in sporozoite stages. The ADF2 protein concentration was below the detection limit of western blot analysis. The dynamic fluctuation of the protein amount correlates with the gene expression data.

3.2.2. Profilin and ADF1 localize to the cytoplasm

Indirect immuno-fluorescence (IFA) of profilin and ADF2 was performed to investigate the localization and abundance of the proteins in different life cycle stages of *P. berghei* (Fig. 32 A, B). The same antibodies as for WB were used for IFA to ensure specificity for endogenous profilin and ADF1 detection (Fig. 30 D I., E I.) In ookinetes, profilin and ADF1 exhibit clear cytoplasmic localization with an accumulated signal next to the nucleus (Fig. 31 A, B). Profilin displays a dotted distribution in the cytoplasm, whereas ADF1 is continuously distributed throughout the cytoplasm and clearly excluded from the crystalloid bodies similar to C-CAPmCherry (Fig. 19 A). In salivary gland sporozoites no specific profilin signal and only a very faint ADF1 signal was observed by IFA (Fig. P1, A, B), confirming the low protein abundance as shown in western blot (Fig. 30 D I., E I.). CSP, instead, displayed the characteristic staining of the outer pellicule (Fig. 30 A, B). Localization of profilin and ADF1 was also observed during liver stage development at 24 and 72 hours post infection. Both proteins displayed cytoplasmic distribution and co-localize with the heat shock protein 70 (Hsp70) (Fig. 31 A, B). The cytoplasmic Hsp70 protein was used for specific parasite identification and as a control for successful IFA process. In merozoites stages (72 hours) profilin and ADF1 are distributed to each single merosome and maintained cytoplasmic. Together, these results confirmed stage-specific profilin and ADF1 protein abundance in ookinetes and liver stages. Thus far, all monitored G-actin binding proteins exhibit cytoplasmic localization.

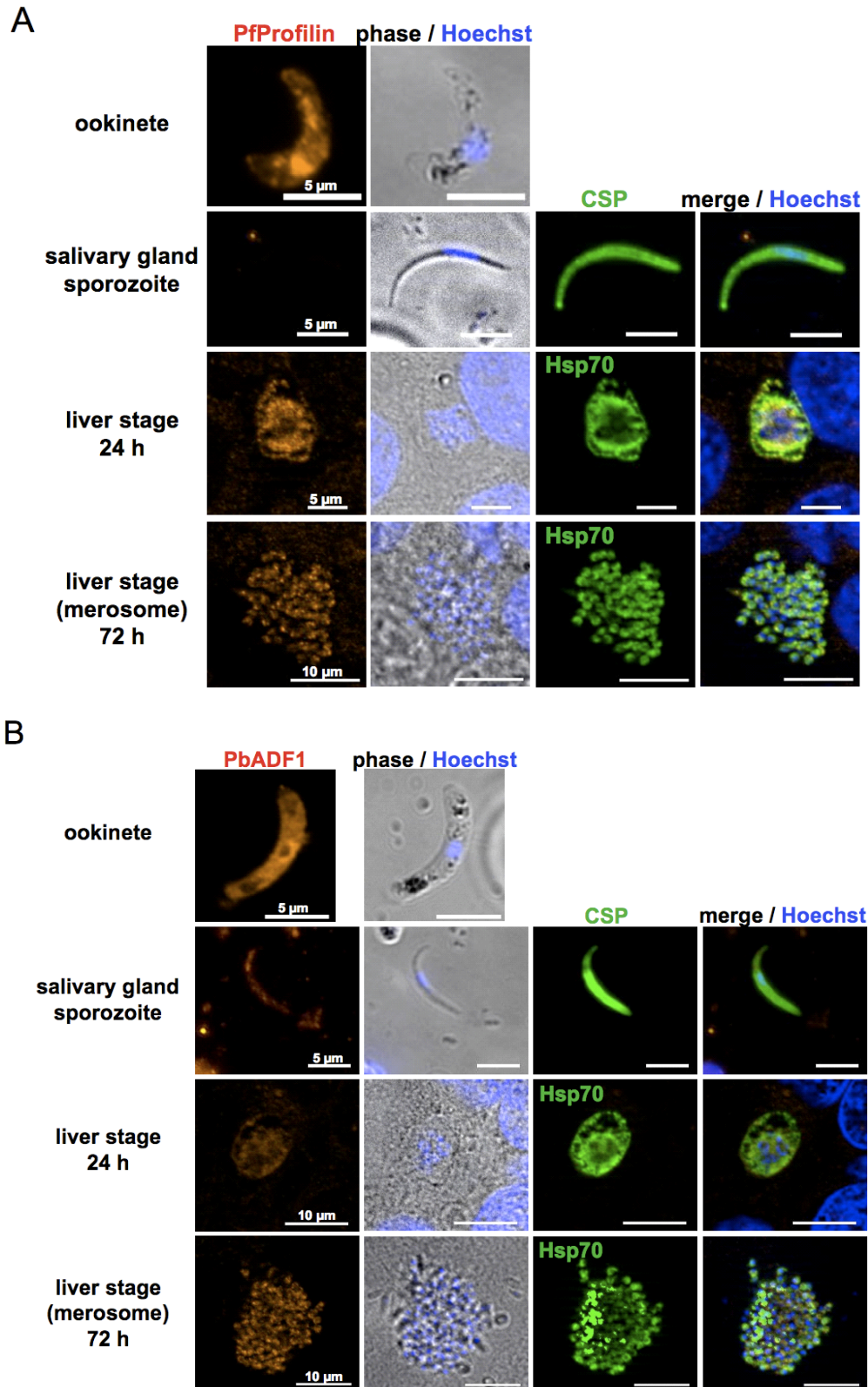


Figure 31: Localization of profilin and ADF1 during life cycle progression of the parasite.

Indirect immuno-fluorescence (IFA) shows the subcellular localization of profilin (**A**) with anti-*P. falciparum* profilin antibody and ADF1 (**B**) with anti-*P. berghei* ADF1 antibody in the red channel. The DNA was stained with Hoechst 33342 in blue and merged with the phase contrast in grey. Sporozoites were co-stained with anti-circumsporozoite protein (CSP) antibody (green) and liver stages with anti heat shock protein 70 (Hsp70) antibody (green). Both G-actin binding proteins localize cytoplasmic and co-localize with Hsp70 in liver stages.

3.2.2.1. A subpopulation of profilin is localized to the plasma membrane in ookinetes

P. berghei profilin and its ortholog in *T. gondii* share 42 % identity between their deduced amino acid sequences (Plattner *et al.*, 2009). Therefore, the α -TgProfilin antibody was tested in western blot for specificity and cross-reactivity against *P. berghei* proteins and subsequently used for subcellular localization of profilin in ookinetes.

Western blot analysis confirmed the cross-reactivity of the *T. gondii* antibody with the *P. berghei* profilin and recognized it with the expected size of 19 kDa in merozoites, gametocytes and ookinetes (Fig. 32 A, I.). No profilin protein was detected in sporozoite stages, confirming the previous results (Fig. 30 D I.). Clear cross-reactivity of the *T. gondii* antibody with the recombinant *P. falciparum* profilin was also shown and specific recognition of the 17 kDa *T. gondii* profilin could be demonstrated (Fig. 32 A I.). Interestingly, ookinetes displayed an unexpected peripheral profilin localization to the outer pellicule of the parasite cell (Fig. 32 B). In contrast, the same antibody was tested in IFA on *T. gondii* parasites and revealed cytoplasmic localization of endogenous profilin (Fig. 32 B), which is consistent with published data (Plattner *et al.*, 2008). Together these results indicate that two distinct profilin populations may exist inside the *Plasmodium* ookinete, which are recognized by different profilin antibodies.

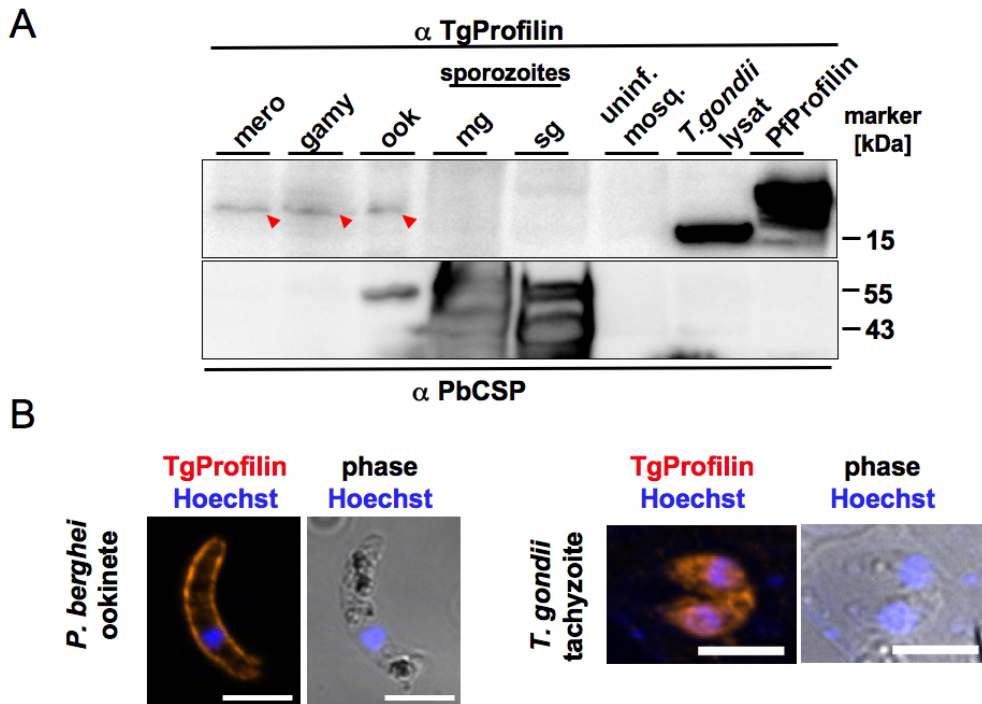


Figure 32: Detection of a profilin subpopulation in ookinetes by an anti *Toxoplasma gondii* profilin antibody.

(A) Western blot analysis of profilin in merozoites (mero), gametocytes (gamy), ookinetes (ook) and midgut (mg) and salivary gland (sg) sporozoites (spz), using the anti-*T. gondii* profilin antibody, revealed cross-reaction with *P. berghei* profilin (19 kDa) in the samples (red arrow), and with the recombinant *P. falciparum* (19 kDa). The *T. gondii* profilin was detected with predicted molecular size of 17 kDa. No profilin was detected in sporozoite stages, despite of high protein input detected by CSP protein in the loading control. **(B)** IFA detecting *P. berghei* profilin in ookinetes with anti-TgProfilin antibody shown in red and DNA stained with Hoechst in blue, revealed clear localization of profilin to the parasite pellicule. IFA of profilin in *T. gondii* tachyzoites using the same antibody, revealed cytoplasmic localization, as published (Plattner *et al.* 2008). Phase and merge with DNA Hoechst stain are shown in blue.

3.2.3. Stage-specific overexpression and tagging of *P. berghei* C-CAP and profilin

The unexpected differential gene expression and stage-specific protein abundance of the G-actin binding proteins during the *Plasmodium* life cycle, prompted us to further investigate the function of C-CAP and profilin proteins. To interrogate the influence of temporal changes in gene expression of C-CAP and profilin on the parasite phenotype, both proteins were expressed under the control of a sporozoite-specific promoter. In addition, both proteins were fused N-terminal to a triple Flag-tag to facilitate Co-immuno-precipitation (Co-IP) for the identification of novel interaction partners *in vivo* and to confirm localization.

Stage-specific overexpression of C-CAP and profilin during the sporozoite stage, was achieved by the circumsporozoite protein (CSP) promoter (Thathy *et al.*, 2002) Ookinete specific overexpression was realized by the promoter of the circumsporozoite- and

trombospondin related sporozoite protein (CTRP) (Dessens *et al.*, 1999). Together, four parasite strains were constructed where *C-CAP* and *profilin* are Flag-tagged and expressed under the control of the *CSP* or *CTRP* promoter, respectively (Fig. 33).

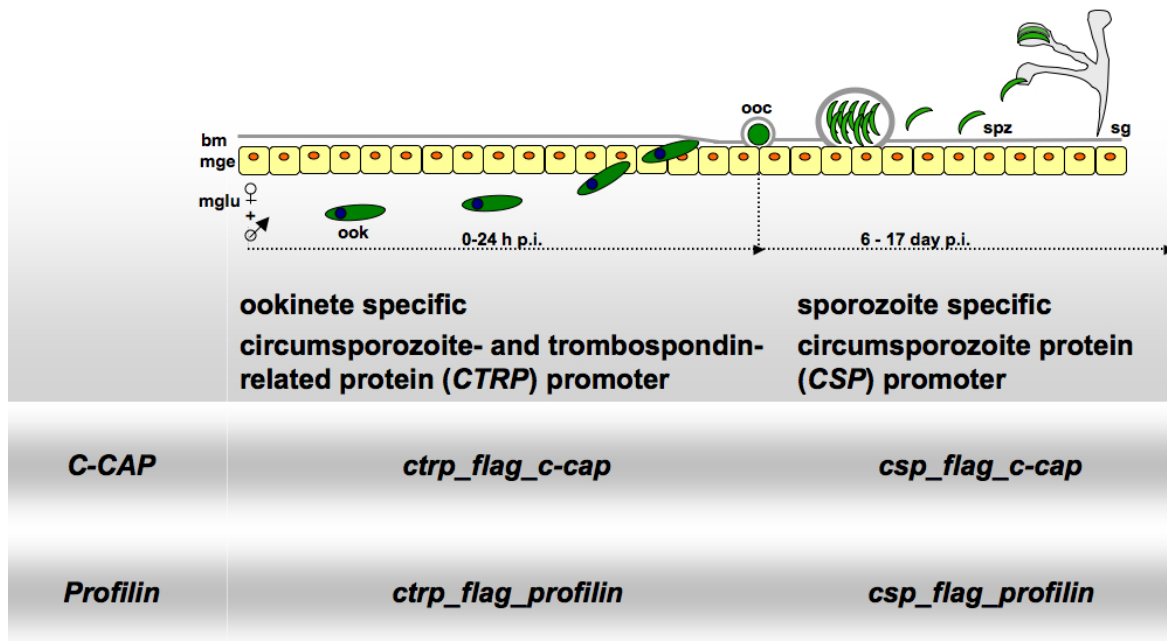


Figure 33: Overview of promoter and gene combinations for generation of recombinant parasites that overexpress *C-CAP* or *profilin* under stage-specific promoters.

The chart indicates promoter specific activity during the *Plasmodium berghei* life cycle inside the mosquito host. After fertilization of male and female microgametes the motile zygote/ookinete (ook) is formed, which traverses during the midgut epithelium (mge) and settles under the basal membrane (bm) to transform into an oocyst (ooc). Sporozoites (spz) develop inside the oocyst and egress into the hemocoel to invade the salivary glands (sg). A signature protein of ookinetes is the circumsporozoite and trombospondin related sporozoite related protein (CTRP). Further oocyst maturation and sporozoite development is correlated with the expression of the circumsporozoite protein (CSP). The G-actin binding proteins examined in this study are indicated in the left column and the resulting promoter and gene combinations are shown below the respective stages.

3.2.3.1. Genetic strategy and generation of parasites with stage-specific overexpression of *Flag*- tagged *C-CAP* or *profilin*

First, the promoter swap along with the generation of mutant parasites and their genotyping strategy is discussed for all four parasite strains in this chapter. The phenotypic analysis will be presented in the following chapters.

To create the expression vectors, the promoter sequences of *CTRP* and *CSP* were amplified from gDNA, with primers CTRP prom for/CTRP prom rev and CS prom for /CS prom rev (Tab. 2) resulting in promoter length of 180 1bp for *CTRP* and 1534 bp for *CSP* (Fig. 34 A). Promoter fragments were subsequently ligated into the B3D vector backbone. The triple

Flag-tag (69 bp) was inserted downstream the promoter followed by the coding sequence of either *C-CAP* or *profilin*. For systematically targeting *P. berghei* *C-CAP* gene the coding sequence, including the intron (829 bp) and the additional *C-CAP* 3'UTR (801 bp) were amplified from gDNA with primers B20 and B23 (Tab. 2). The *profilin* coding sequence, containing the three introns, with a length of 1210 bp and additional 978 bp of the 3'UTR was amplified from gDNA with primers B21/B22 (Tab. 2). Both gene sequences were ligated in frame to the upstream triple *Flag*-tag (Fig. 34 A, C). After sequencing the *CTRP/CSP_Flag_C-CAP* and *CTRP/CSP_Flag_profilin* regions expression plasmids were linearized. Transfection was done with the *P. berghei* Anka strain followed by cloning of pyrimethamine resistant parasites.

Diagnostic genotyping of *ctrp_flag_c-cap* and *csp_flag_c-cap* parasites for 5'UTR and 3'UTR integration was performed with primers B20/T11 and FLAGfor/T9 (Fig. 34 A, Tab. 2) resulting in successful amplification of test5' and test3' in parasite transfectants but not in the wild type strain (Fig. 34 B). Specific recombination between the promoter and the tagged *C-CAP* was tested with promoter specific primers CTRP prom test/CSP prom test and B23 (Fig. 34 A, Tab. 2) and resulted in amplification of 1887 bp in *CTRPprom test* and 1790 bp in *CSPprom test*, respectively but not in WT (Fig. 34 B). *WT* locus amplification of 2752 bp with T9/T10 primers (Tab. 2) was successful in wild type but not in recombinant parasites and confirms clonality of *ctrp_flag_c-cap* and *csp_flag_c-cap* parasites (Fig. 34 B).

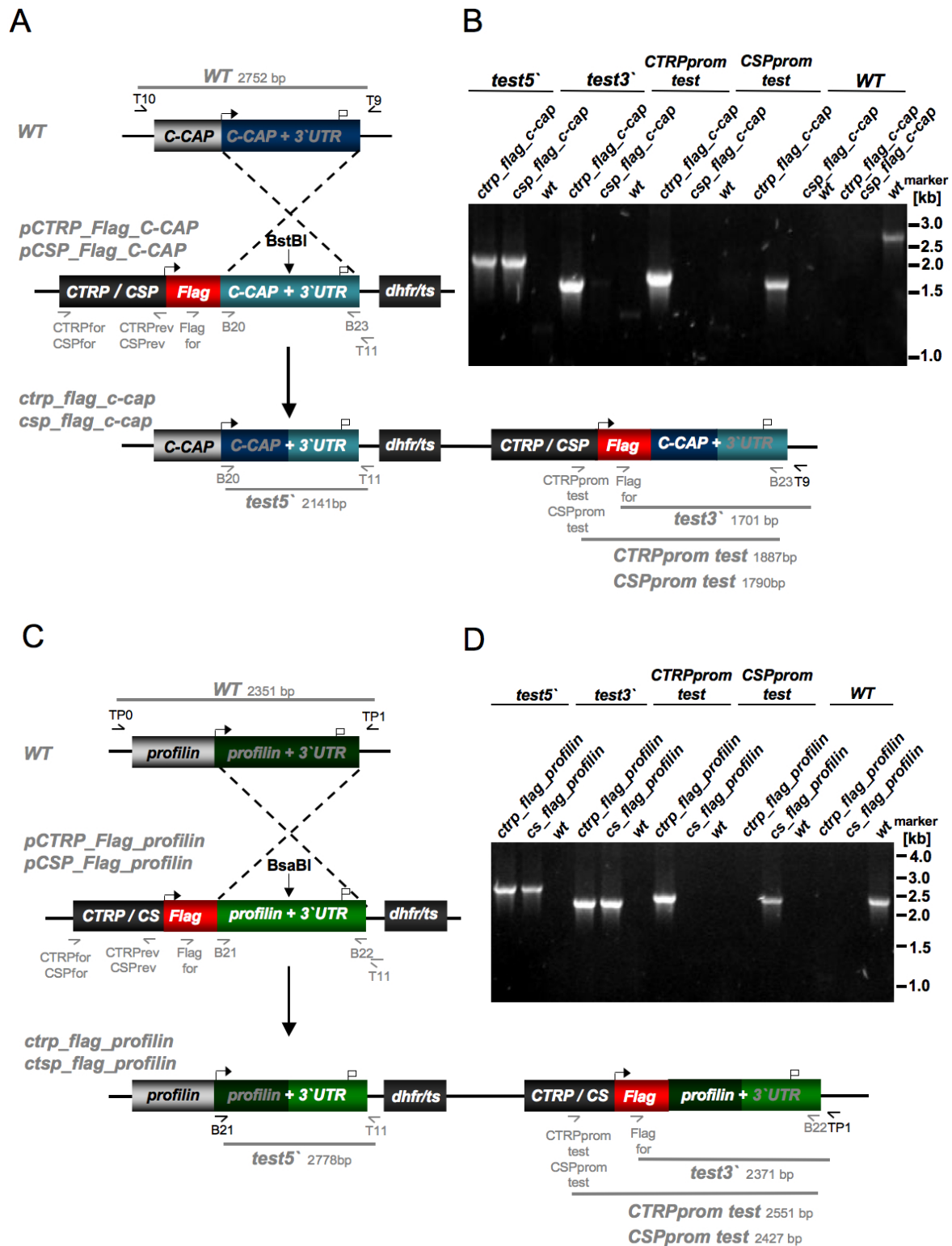


Figure 34: Generation of recombinant parasites expressing *Flag*-tagged *C-CAP* and *profilin* under control of the *CTRP* or *CSP* promoters.

(A, C) Genetic strategy to generate *P. berghei* parasites which express *Flag*-*C-CAP* and *Flag*-*profilin*, under the control of the circumsporozoite and thrombospondin related sporozoite protein (CTRP) and circumsporozoite protein (CSP) promoters. The promoter sequences are shaded in dark grey, the triple *Flag*-tag is shaded in red and the *C-CAP* coding sequence and 3' UTR is shaded in dark blue (genomic locus) or light blue (plasmid origin). The *profilin* sequence is shown in light green (plasmid origin) or dark green (genomic locus). Plasmids were linearized with *Bst*BI or *Bsa*BI, respectively (arrow) to facilitate insertion. Dashed lines indicate homologous recombination sides. Primers used for cloning

and diagnostic genotyping are indicated as arrows in black (hybridization with the gDNA) or in grey (hybridization with the plasmid). Amplified PCR fragment lengths are indicated as lines. **(B)** Genotyping of *ctrp_flag_c-cap* and *csp_flag_c-cap* parasites using PCR with primers as indicated in A, confirmed the specific test5' (2114 bp) and test3' (1701 bp) fragment integration. Specific promoter combination with the *C-CAP* ORF, was confirmed by specific CTRPprom test (1887 bp) and CSPpromtest (1790 bp). The absence of the WT locus amplification (2752 bp) in the two clonal *ctrp_flag_c-cap* and *csp_flag_c-cap* parasites, but not in WT confirmed clonality. **(D)** Genotyping of *ctrp_flag_profilin* and *csp_flag_profilin* parasites with PCR confirmed specific test5' (2778 bp) and test3' (2371 bp) integration. Recombination was shown by amplification of CTRPprom test (2551 bp) and CSPprom test (2427 bp) fragments. Clonality was confirmed by absence of WT locus amplification in transgenic parasite strains, but not in wild type (2351 bp).

Genotyping by PCR of *ctrp_flag_profilin* and *csp_flag_profilin* parasites for specific 5'UTR and 3'UTR integration was performed with B21/T11 and Flagfor/TP0 primers (Fig. 34 C, Tab. 2) and results in amplification of test5' and test3' specifically in transfected parasites (Fig. 34 D). Recombination between the promoters and *profilin* was tested with the primers CTRPprom test/CSPprom test and B22 (Fig. 34 C Tab. 2) and resulted in predicted amplification of 2551 bp in *CTRPprom test* and 2427 bp in *CSPprom test* in transfectants, but not in wild type parasites (Fig. 34 D). Clonality of the recombinant parasite strains was confirmed with primers TP1/TP0 (Fig. 34 C, Tab. 2) and resulted in *WT* locus amplification of 2351 bp in wild type parasites only (Fig. 34 D).

3.2.4. Phenotypic analysis of *csp/ctrp_flag_c-cap/profilin* recombinant parasites

For phenotypic analysis all four clonal parasite lines were fed to *A. stephensi*. The presence and localization of the Flag-tagged fusion proteins C-CAP and profilin was monitored by western blot analysis and IFA using the anti-Flag antibody. Sporozoite numbers, motility and transmission to mice were determined subsequently.

3.2.4.1. Transgenic parasites that overexpress *C-CAP* or *profilin* in the ookinete stage display normal life cycle progression

Indirect immuno-fluorescence in parasites overexpressing either the C-CAP or the profilin-Flag fusion protein under the *CTRP* promoter, display a clear Flag-signal only in ookinetes (Fig. 35 A, C). No Flag-signal was detected in oocysts at day 14 and midgut- and salivary gland sporozoites at day 14 and 22 after feeding (Fig. 35 A, C). Consistent with our previous localization of C-CAP (Fig. M3, A) and profilin (Fig. 32 A), both Flag-fusion proteins exhibit cytoplasmic localization with slightly stronger signal next to the nucleus (Fig. 35 A, C). Western blot analysis confirmed Flag-fusion protein abundance only in ookinetes for Flag-C-CAP with a predicted molecular weight of 21.3 kDa (Fig. 35 B I.), and for Flag-profilin with

a molecular weight of 22.11 kDa (Fig. 35 D I.). The protein input was controlled by detection of α -Tubulin (50 kDa) in ookinetes and the CSP protein (52/44 kDa) in sporozoite stages and revealed substantial amounts of parasite proteins (Fig. 35 B and D II.).

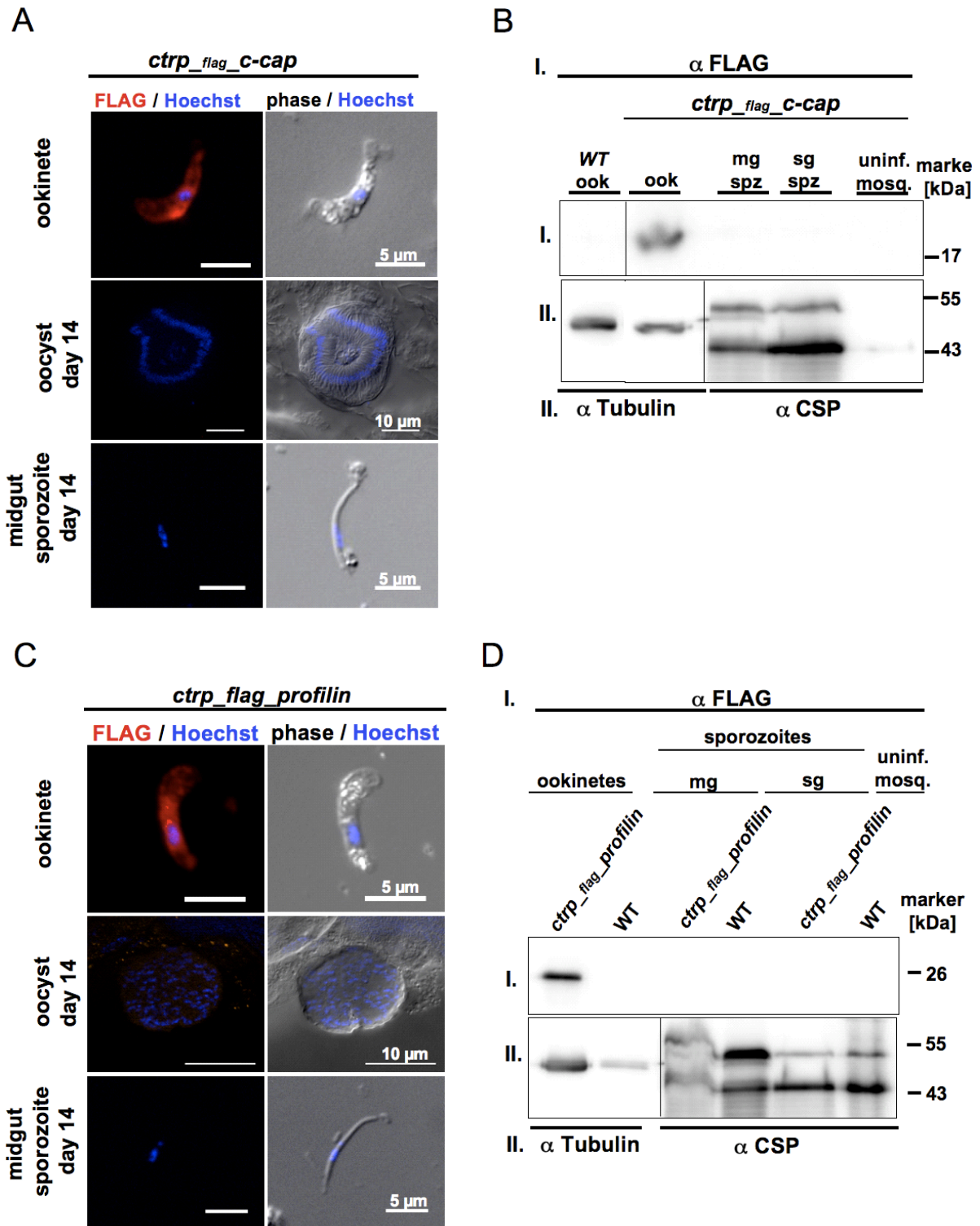


Figure 35: Localization and protein abundance of the Flag-C-CAP and Flag-profilin fusion proteins expressed under control of the *CTRP* promoter.

(A, C) Indirect immuno-fluorescence (IFA) on ookinete stage, oocyst and midgut sporozoites at day 14 post infection, detecting the Flag epitope of c-cap (A) and profilin (C) only in ookinetes with cytoplasmic localization. The Flag-signal is shown in red and DNA in blue. **(B, D)** Western blot analysis for detection of the Flag-c-cap fusion protein (B) and Flag-profilin (D) in ookinetes (ook), mixed blood stages (mix. bs), midgut- (mg) and salivary gland (sg) sporozoite stages (spz) and uninfected mosquito material (uninf. mosq.). Wild type samples are indicated (WT). Protein input was controlled (B, D, II.) by detection of tubulin (50 kDa) and CSP (44/52 kDa). Molecular weights are indicated on the right.

These results clearly demonstrate the successful stage specific overexpression of *C-CAP* and the *profilin* in ookinetes, regulated by the *CTRP* promoter. Thus far, no phenotypic differences between parasite strains and the WT parasites could be observed and hence implicate functionality of the Flag-fusion proteins.

Following the life cycle progression of the transgene parasites, sporozoite numbers were counted for midgut and salivary gland sporozoites. Both parasites developed comparable amounts of midgut sporozoites as compared to WT (Fig. 36 A). Both parasites develop adequate or higher amount of salivary gland sporozoites per mosquito with 3300 for *ctrp_flag_c-cap* parasites and 20.700 sporozoites for *ctrp_flag_profilin* parasites as compared to WT with 8200 sporozoites (Fig. 36 A). The transmission competence of salivary gland sporozoites from both transgene sporozoites was tested in comparison to WT, by intravenous injection of 5000 sporozoites into groups of three C75/B16 mice. Parasitemia was monitored daily by Giemsa-stained blood smears and revealed normal prepatent period of three days for all parasite populations (data not shown). Furthermore, motility of both transgene parasites was investigated with gliding assays on glass slides and subsequent indirect immuno-fluorescence against the CSP protein to detect sporozoite trails. Both parasites displayed normal gliding motility (Fig. 36 B).

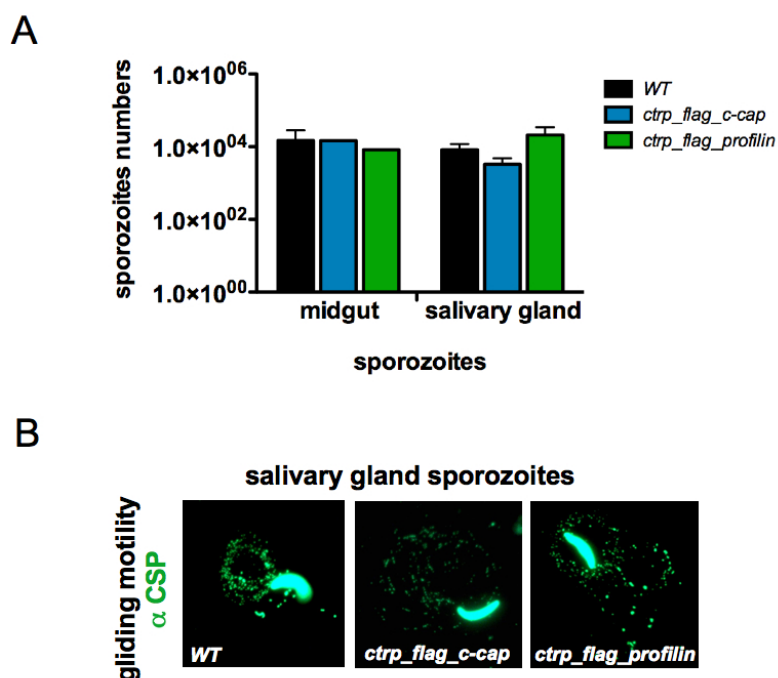


Figure 36: Phenotypic analysis of sporozoite development and motility in parasites expressing c-cap and profilin under the *CTRP* promoter.

(A) Sporozoite numbers per mosquito were counted for midgut- (n=1 for *ctrp_flag_cap/profilin* and n=2 for WT) and salivary gland sporozoites (n=2) in n independent feeding experiments each. (B) Motility of salivary gland sporozoites was tested in gliding assays and subsequent IFA to detect CSP in the sporozoite trails. All sporozoite populations exhibit productive gliding motility.

Together, these results show that overexpression of the G-actin binding proteins C-CAP and profilin during ookinete stages, where these genes are abundantly expressed (Fig. 7 B and Fig. 30 A), does not influence the parasite development. Normal life cycle progression of these transgene parasites was confirmed by regular amounts of motile transmission competent sporozoites are formed in the mosquito and infection leads to normal liver stage development. Furthermore, the functional Flag-tagged C-CAP and profilin can now be used for co-immunoprecipitation to identify interacting proteins.

3.2.4.2. Transgenic parasites that overexpress *C-CAP* or *profilin* under control of the *CSP* promoter exhibit ectopic protein expression, resulting in ablated salivary gland invasion of sporozoites

Both parasite lines *ctrp_flag_profilin* and *csp_flag_profilin* were investigated for their profilin content during ookinete stages by western blot analysis. Endogenous profilin with a molecular size of 19 kDa was detected in ookinetes in WT and both transfected parasite strains (Fig. 37 II.). As expected from the genetic strategy, the additional profilin copy, expressed under control of the *CTRP* and *CSP* promoter was recognized by the α -PfProfilin and the α Flag-antibody with a molecular size of 22 kDa (Fig. 37 I., II.). This result confirmed the

overexpression and presence of two profilin populations in both transfected strains. The protein input was controlled by detection of equal amount of the CSP protein (Fig. 37 III.).

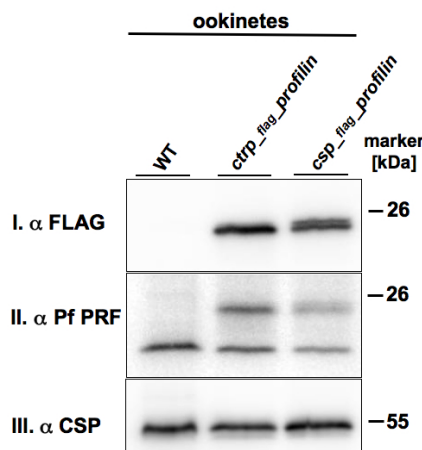


Figure 37: Detection of two profilin populations in ookinetes, indicating functional overexpression of the protein under the *CTRP* and *CSP* promoter.

Western blot analysis of ookinetes from WT, *ctrp_flag_profilin* and *csp_flag_profilin* parasite strains, show clear detection of endogenous profilin (19 kDa) and the additional expressed Flag-profilin fusion protein (22kDa)(II.). Flag specific recognition of the fusion proteins is shown (I.) and protein input was controlled with detection of the CSP protein (55 kDa) (III.).

Indirect immuno-fluorescence detecting the Flag epitope of the profilin-Flag fusion protein confirms again cytoplasmic localization in ookinetes (Fig. 38 C). The ectopic expression of either the C-CAP or the profilin protein during sporozoite maturation is visualized by IFA in oocysts, midgut- and hemocoel sporozoites at day 14 and day 27 of parasite development (Fig. 38 A, C). Both Flag-fusion proteins localize to the immature sporozoites inside the oocyst. In midgut sporozoites the Flag- signal exhibits cytoplasmic localization. Hemocoel sporozoites at day 23 of development display atypical peripheral protein localization for Flag-C-CAP and Flag-profilin (Fig. 38 A, C).

Western blot analysis confirmed the antibody specificity and detected the flag-profilin protein with a distinct band with a molecular weight of 22 kDa in ookinetes, midgut and salivary gland sporozoites (Fig. 38 D). These results demonstrate successful ectopic overexpression and detection of C-CAP and profilin during sporozoite development, in stages where usually both proteins are very low expressed. The localization of the protein changes from cytoplasmic pattern in ookinetes and midgut sporozoites to peripheral localization in hemocoel sporozoites.

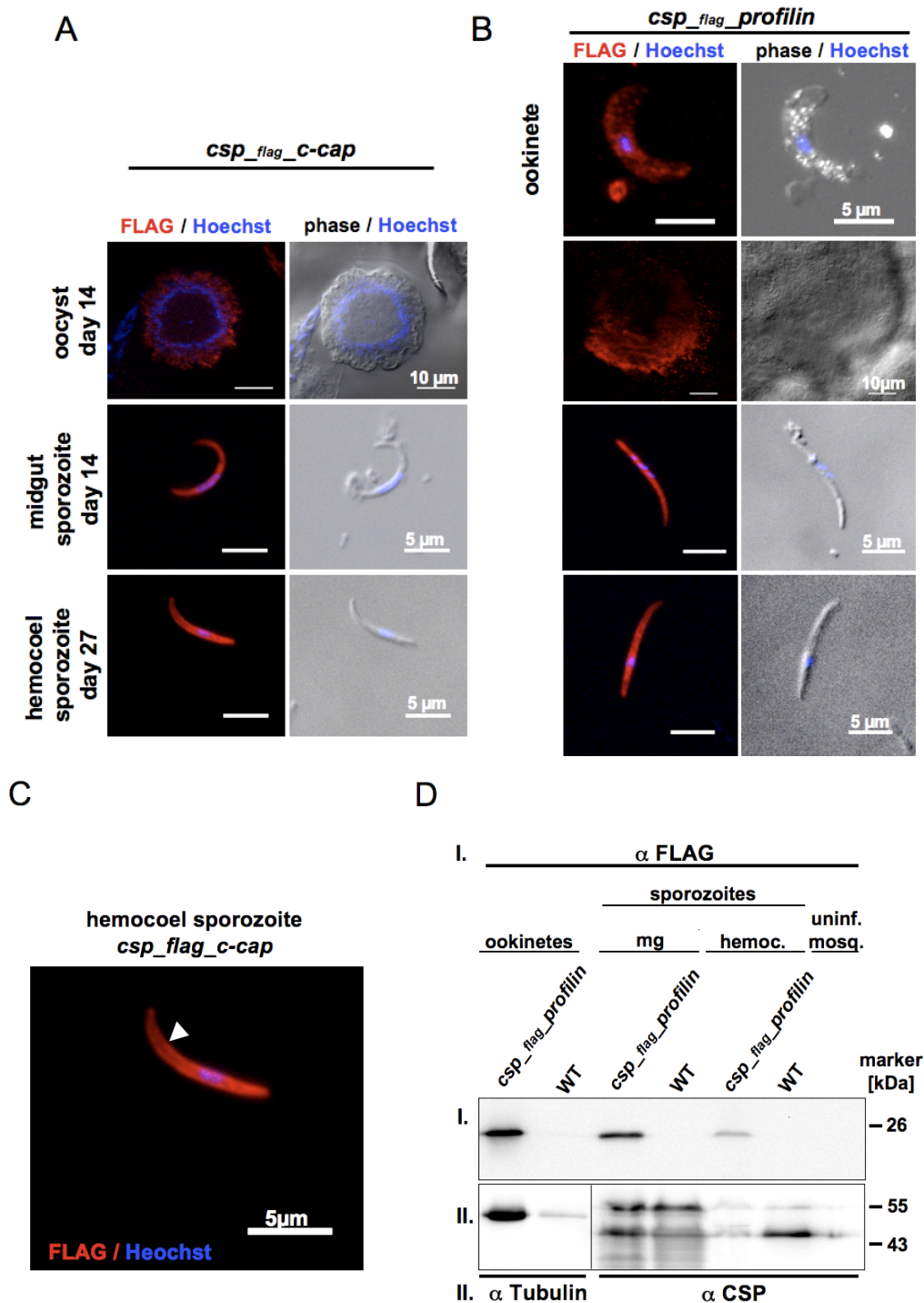


Figure 38: Localization and protein abundance of the Flag-C-CAP and Flag-profilin fusion proteins expressed under control of the CSP promoter.

(A, B) IFA in ookinetes, oocyst and midgut sporozoites, at day 14 and hemocoel sporozoites at day 27 of development. Localization of the Flag-C-CAP fusion protein (A) and the Flag-profilin protein (B) is shown in red. DNA was stained with Hoechst 3361 shown in blue and merged with phase contrast. Note that the fusion proteins exhibit ectopic expression in sporozoite stages. (C) Detail of the peripheral localization of the Flag-C-CAP protein in hemocoel sporozoites. (D) Western blot analysis shows ectopic protein abundance of Flag-profilin in sporozoites with the predicted molecular size of the fusion protein (22 kDa) thereby confirming the CSP promoter activity. The blot was cut for detection of Tubulin and CSP protein in the loading control (D II.).

Despite high C-CAP and profilin abundance the recombinant parasites were able to develop sporozoites (Fig. 38), indicating that both proteins do not interfere with sporozoite formation. For further phenotypic analysis sporozoite numbers were counted. In the case of *csp_flag_c-cap* parasites only low numbers of 2796 ± 2040 sporozoites per mosquito were counted from three independent feeding experiments, as compared to *csp_flag_profilin* and wild type parasites, which developed similar sporozoite numbers of 11.426 ± 6341 and 14.707 ± 18.975 per mosquito (Fig. 39 A). Interestingly, no sporozoites were found in the salivary glands of mosquitoes infected with *csp_flag_c-cap* or *csp_flag_profilin* (Fig. 39 A) in three independent feeding experiments. To investigate the competence of midgut sporozoites to egress from the oocysts into the hemocoel, hemocoel sporozoites were prepared and numbers were determined. Mosquitoes infected with *csp_flag_c-cap* or *csp_flag_profilin* developed 1390 ± 1088 and 800 ± 424 parasites per mosquito and represented less but substantial sporozoite numbers as seen in WT hemocoel sporozoites (4875 ± 3872) (Fig. 39 A). Thus might implicate a slight impaired oocyst egress capacity in both mutant parasites.

Gliding assays of hemocoel sporozoites from both transgene parasites did not reveal major differences (Fig. 39 B). In all hemocoel sporozoites samples small and diffuse CSP accumulations roughly comparable to CSP trails of salivary gland sporozoites were detected by IFA. Interestingly, only in wild type samples sporozoites were found close to CSP trails, whereas in both transgene parasites no sporozoites were found in connection to “mini” trails (Fig. 39 B).

Together these results show that ectopic overexpression of the C-CAP and the profilin protein does not interfere with the sporozoite formation *per se*, but leads to compromised sporozoite oocyst egress and complete abolishment of salivary gland invasion.

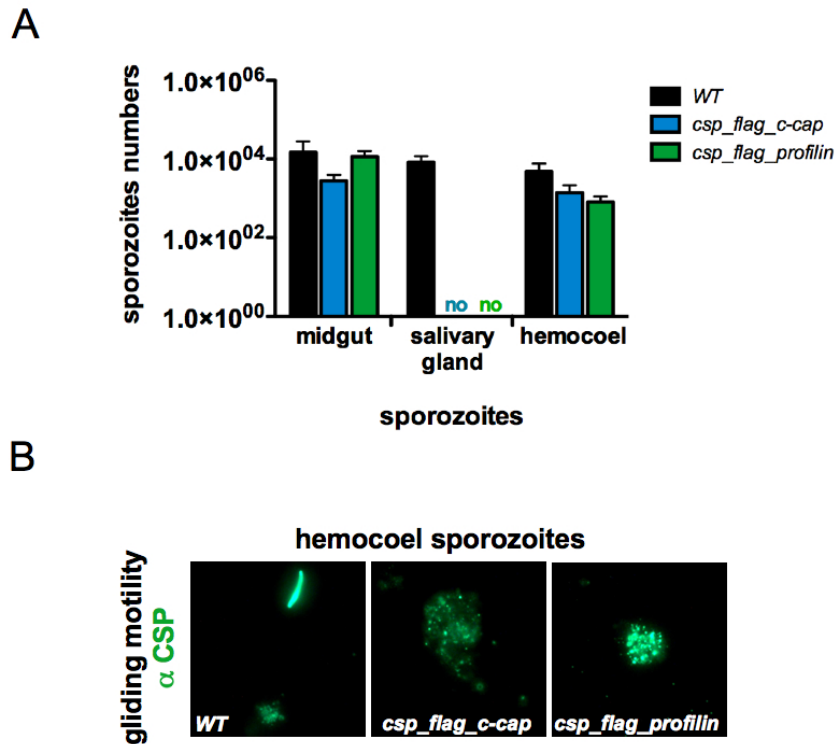


Figure 39: Phenotypic analysis of sporozoite development in parasites with ectopic overexpression of c-cap and profilin under the *CSP* promoter.

(A) Sporozoite numbers were counted from midgut- ($n=2$), salivary gland- ($n=3$) and hemocoel sporozoites ($n=3$) in n independent feeding experiments. All parasites developed midgut sporozoites, but no sporozoites were found in salivary glands of mosquitoes infected with either *csp_flag_c-cap* or *csp_flag_profilin* parasites. However, these parasites form less but substantial amounts of hemocoel sporozoites, indicating slight impairment of oocyst egress and complete inability of salivary gland invasion. Sporozoite number differences were tested by students t-test, and were not significant ($p < 0.5$) (B) Motility of hemocoel sporozoites was investigated by gliding assays on glass slides and subsequent CSP (green) detection by IFA. All hemocoel sporozoites display incomplete gliding as indicated by the “mini” CSP trails or CSP accumulations. Only in WT parasites sporozoites were found associated to trails.

4. Discussion

In this study I characterized the function of the G-actin binding protein cyclase-associated protein C-CAP in the rodent malarial parasite *Plasmodium berghei*. By employing experimental genetics and molecular biological approaches, I discovered previously unrecognized C-CAP functions essential for oocyst maturation.

My work on the three G-actin binding proteins profilin, and actin depolymerization factor 1 and 2 (ADF1, ADF2), yielded unexpected results regarding the sporozoite stage, which indicate that sporozoites exhibit an actin-dynamic regulation that is distinct than merozoites and ookinetes.

4.1. The cellular function of C-CAP in *Plasmodium*

C-CAP gene expression profiling throughout the different life cycle stages of *P. berghei* revealed moderate mRNA levels as compared to the two other G-actin binding proteins, profilin and ADF1. Blood stage merozoites, ookinetes and liver stage merozoites exhibited most abundant C-CAP transcripts indicating possible functions in invasion and motility. Unexpectedly, C-CAP expression dropped to background levels during sporozoite development. The cellular function of C-CAP was addressed by reverse genetics, where the endogenous C-CAP gene locus was deleted by homologous recombination. The C-CAP gene deletion resulted in viable blood stages, demonstrating a non-essential function in this stage of the life cycle. Furthermore, growth curve analysis revealed no differences between wild type and *c-cap*(-) parasites in mice.

These results indicate that lack of C-CAP has no measurable impact on replication, growth and invasion of the parasites during the asexual life cycle, despite their actin-dependence (Field *et al.*, 1993; Miller *et al.*, 1979; Mizuno *et al.*, 2002; Smythe *et al.*, 2008). One plausible explanation is that the cellular role can be compensated by functional redundancy of G-actin binding proteins, like profilin or ADF1, that both exhibiting G-actin sequestering activity (Huttu *et al.*, 2011; Kursula *et al.*, 2008; Schuler *et al.*, 2005a; Wong *et al.*). *In vivo* analysis in mice does not permit high resolution of the spatiotemporal parasite activity. Therefore it cannot be excluded that minor defects during invasion occur in *c-cap*(-) parasites. Due to the lack of a reliable *in vitro* culturing system where invasion assays could be performed for *P. berghei* asexual blood stages, live cell imaging of the invasion process and flow cytometry-based analysis of the parasite replication could be used in the future for more exact parasitemia measurements in mice.

Sexual gametocyte differentiation and subsequent ookinete development was not affected in *c-cap(-)* parasites, despite high *C-CAP* expression and protein abundance in these stages. The cellular architecture of *c-cap(-)* ookinetes was indistinguishable from wild type, as judged by localization of cytoskeletal components, for instance tubulin, DNA integrity and Giemsa-staining (data not shown). Ookinetes employ an equal actomyosin-based motor as described in merozoites. Their motility is susceptible to actin stabilizing and destabilizing drugs, resulting in velocity reduction in a concentration specific manner (Siden-Kiamos *et al.*, 2006). The integrity of motor components in *c-cap(-)* ookinetes for myosinA and actin was not influenced (data not shown). However, *in vitro* analysis of ookinete motility revealed a significant decrease in velocity as compared to wild type. This is the first indication for a role of C-CAP in parasite motility. The speed reduction is consistent with temporal disorganization of the actin-skeleton. Referring to the G-sequestering activity of C-CAP, a delayed G-actin turnover leads to impairment of fast retrieval of polymerization-competent ATP-actin in motile ookinetes, which in turn retards ookinete velocity in *c-cap(-)* parasites. Nevertheless, *c-cap(-)* parasites employed all motility patterns known to date (Siden-Kiamos *et al.*, 2006) and were able to successfully traverse the mosquito midgut of *A. stephensi* and transform into oocysts. These results show that *C-CAP* is also not vital for ookinete formation and motility. Its absence can perhaps again be compensated by functionally redundant proteins. To correlate the *in vitro* motility with the *in vivo* situation, mosquitoes were infected with *c-cap(-)*, revealing reduced oocyst numbers. *In vivo* the ookinete has to traverse the peritrophic membrane and the midgut epithelium. Therefore, it is likely that reduced speed *in vitro* translates into reduction of successful transmigration events *in vivo*. Slower parasites might be digested in the blood meal or inactivated by defense factors of the mosquito host (Lehane *et al.*, 2004; Levashina, 2004). This hypothesis could be assessed by TEP1 staining, which recognizes ookinetes that are opsonized by the mosquito immune factor (Blandin *et al.*, 2008) and are therefore prone to be eliminated.

The most important finding of this study is the essential function of *C-CAP* for oocyst maturation and sporozoite formation. *C-cap(-)* parasites are completely aborted during oocyst development and do not form sporozoites. These results strongly support a stage-specific and non-redundant function of C-CAP. Initial growth and first mitotic divisions of DNA appear unaltered until day 6 of development. Subsequent development differs significantly from wild type parasites. Oocysts are arrested in growth and are ~50 % smaller in size at day 14 after infection. Furthermore, mitotic divisions are aborted, indicating a DNA condensation and segregation defect (Fig. 12). During *c-cap(-)* persistence in the midgut, oocysts undergo cell

death as indicated by life/death stain, vacuolization of the cysts, and loss of GFP expression. Transmission electron microscopy data revealed a more detailed phenotype of *c-cap(-)* parasites during development. At day 6, plasma membrane invaginations of the inner oocyst-wall, known as membrane retractions, occur in wild type oocysts (Baton and Ranford-Cartwright, 2005; Menard *et al.*, 1997; Terzakis *et al.*, 1967; Vanderberg, 1974) but are undetectable in the *c-cap(-)* mutants. Also, signs of deficient DNA segregation are visible (Fig. 16). Later, the defined oocyst compartmentation into blastomers and sporozoites is absent in *c-cap(-)* parasites (Fig. 17). This defect is likely due to the lack of inner membranes that define specialized compartments in the resulting sporozoite. Taken together, *c-cap(-)* parasites exhibited an unexpected phenotype, which possibly revealed a novel actin-dependent role during oocyst maturation.

4.1.1. The role of C-CAP during oocyst maturation

The spatiotemporal organization of the developing oocyst is difficult to assess and not much research has been done on this unique extracellular replication phase of the parasite. Thus far, it is clear that the motile tetraploid ookinetes transform into highly replication-competent and metabolically active oocysts. This transformation happens at 18 - 24 hours after blood meal (Adini and Warburg, 1999) and is characterized by drastic morphological changes. The microtubuli cytoskeleton and the apical complex disassemble to form the round shape of the cyst. A young oocyst undergoes a dramatic increase in volume, characterized by a 10-fold growth in diameter (from ~5 μm to ~50 μm), and several simultaneous mitotic divisions that produce 2.000 - 8.000 haploid nuclei (Canning and Sinden, 1973). It was shown that oocyst growth relies on nutrient uptake from surrounding compartments like the hemocoel, for instance the essential amino acid leucine (Vanderberg and Rhodin, 1967). In all life cycle stages hexoses are essential for *Plasmodium* and the corresponding transporters have been localized to the oocyst periphery, indicating import of hexoses, such as fructose or glucose (Blume *et al.*, 2010; Slavic *et al.*, 2010). Considering that the type II fatty acid synthesis (FASII) pathway is not essential for sporozoite development (Vaughan *et al.*, 2009), it is not surprising that oocysts ingest lipids from the host to build up membranes necessary for sporozoite development. Lipophorins (Lp), the main lipid carrier in the mosquito, are important factors for oocyst maturation in *A. gambiae* (Mendes *et al.*, 2008; Rono *et al.*), and can be taken up by the oocysts (Atella *et al.*, 2009). However, the uptake mechanism through the dense fibrous capsule remains elusive. The fact that *c-cap(-)* oocysts do not grow and exhibit no inner membranes for compartmentation, may suggest a direct or indirect defect in

nutrient and/or lipid uptake. The membrane invagination process observed in wild type parasites might contribute to this uptake (Fig. 16, 17). Membrane invaginations, filled with capsule components, extend into the cytoplasm and appear to ultimately bud off as electron dense, round bodies. Such invaginations and budding processes are absent in *c-cap(-)* mutants. Endocytosis is an actin-dependent process (Smythe and Ayscough, 2006) and has been described in *Plasmodium* blood stages (Smythe *et al.*, 2008). Whether these invaginations are endocytic vesicles and reflect actin-dependent endocytosis in developing oocysts requires further research. Besides this “endocytosis-like” process, actin and its binding proteins are required for numerous fundamental cellular functions. For instance, membrane retraction during cytokinesis is mediated by F-actin filament action in the contractile ring (Kamasaki *et al.*, 2007). It has been shown that the genesis of cell polarity in yeast and *Drosophila* is controlled by spatial regulation of actin filaments and mRNA determinants by CAP (Baum *et al.*, 2000; Kamasaki *et al.*, 2005). Furthermore, the positioning of the mitotic spindle during nuclear division depends on actin (Azoury *et al.*, 2008; Dumont *et al.*, 2007). Dysfunction of these processes is also consistent with the observed ultra structural defects of *c-cap(-)* oocysts. To further dissect the questions of whether nutrient uptake, membrane retraction, and nuclear division are actin dependent processes in *Plasmodium* oocysts, axenic oocyst-culture may be performed (Al-Olayan *et al.*, 2002; Warburg and Miller, 1992; Warburg and Schneider, 1993). This *in vitro* culture system would allow application of inhibitors that interfere either with the actin or the tubulin cytoskeleton. However, the *in vitro* culturing of oocysts remains to be optimized (data not shown). Additionally, immuno electron microscopy may help to detect the localization of actin. Finally endosomal markers would further contribute to solve this question.

The *c-cap(-)* oocysts were tested for expression and localization of other factors essential for sporozoite development, such as the circum sporozoite protein (CSP) (Menard *et al.*, 1997) and the CAP380 protein (Srinivasan *et al.*, 2008). However, no differences in expression timing and localization could be detected in *c-cap(-)* and wild type oocysts (Fig. 14). This finding indicates a CSP and CAP380- independent mechanism of sporozoite development abortion.

The subcellular localization of the C-CAP protein was addressed by expression of a C-CAP mCherry fusion protein, which was integrated into a knockout background. The *c-cap(-)* phenotype could be rescued by the *c-capmCherry* expression throughout the complete parasite life cycle. This further confirms a C-CAP-specific phenotype of *c-cap(-)* parasites. Life cell imaging displayed clear cytoplasmic localization in all observed stages (Fig. 19-21) and signal

intensity reflected mRNA expression data well. The cytoplasmic C-CAPmCherry localization supports its G-actin sequestering function (Julia Sattler, dissertation), because G-actin is highly abundant in the parasite cytoplasm (Dobrowolski and Sibley, 1997; Field *et al.*, 1993). Furthermore, the lack of the N-terminal and the P2 domain (Schuler and Matuschewski, 2006b), which confers localization to cortical actin patches in yeast and human (Freeman *et al.*, 1996; Freeman and Field, 2000; Lila and Drubin, 1997), is consistent with the cytoplasmic pattern of C-CAPmCherry.

4.2. C-CAP but not its actin-sequestering activity is essential in oocysts

4.2.1. Complementation with *Cryptosporidium parvum* C-CAP (CpC-CAP)

The successful functional complementation of the *Plasmodium* C-CAP loss of function mutant by its ortholog from *C. parvum* provided us with a crucial link for the biochemical activity and cellular role *in vivo*. The *C. parvum* C-CAP complementation was achieved by introduction of the CpC-CAP coding sequence into the knockout vector, with the *C. parvum* transgene being expressed under the control of endogenous C-CAP promoter. Successful genomic integration resulted in viable blood stages, indicating tolerance of the *C. parvum* transgene by *Plasmodium*. Complemented parasites progressed throughout the entire life cycle. Oocyst maturation and sporozoite development could be restored and resulted in infection-competent sporozoites. These results confirmed that, both proteins are functionally redundant, most likely through its G-actin sequestering activity.

To specifically link G-actin sequestering activity to the cellular function, mutagenesis on CpC-CAP was performed. The mutations were predicted to either interfere with the actin binding capacity (CpC-CAP^{D117A, K118A}) or with the dimerization (CpC-CAP^{STOP}). Phenotypic analysis throughout mosquito development revealed that the actin-binding impaired CpC-CAP^{D117A, K118A} protein still rescued the *c-cap*(-) parasites, whereas the dimerization mutant in CpC-CAP^{STOP} parasites did not. This strongly favors an actin-sequestering independent function of C-CAP in oocysts. However, several caveats need to be considered during interpretation of the CpC-CAP^{D117A, K118A} mutant: (i) the selected mutation may not be entirely sufficient to disrupt actin interaction *in vivo* as it has been shown in the *in vitro* assay (Julia Sattler, dissertation), (ii) *in vitro* analysis has been done with rabbit muscle actin, which structurally differs from the apicomplexan actin or (iii) the *c-cap*(-) defect relies entirely on an actin-independent process and involves new interaction partners and novel physiological

functions of the C-CAP protein. Western blot analysis suggests that the *CpC-CAP^{STOP}* mutant did not complement due to degradation of the truncated *CpC-CAP^{STOP}* protein by the parasite. The truncation possibly leads to misfolding of the protein and subsequent proteasome targeting. Thus, the mutational analysis did not yet provide validation for the essential interaction of *CpC-CAP* and actin *in vivo* and favors an actin-sequestering independent function. Additional mutants of the *CpC-CAP* protein were characterized for inhibition of its actin-binding activity, complex formation and abolishment of actin-sequestering activity (Julia Sattler, dissertation). Using these mutants for further complementation experiments might facilitate the dissection of the multiple functions *in vivo*.

4.2.2. *C-cap(-)* mutants can not be complemented by *profilin*

To further investigate the role of C-CAP during oocyst maturation, I attempted the complementation with profilin overexpression. Both proteins share a common G-actin sequestering activity (Kursula *et al.*, 2007; Sattler *et al.*, 2010), and interestingly, *C-CAP* loss of function mutants in *S. cerevisiae* can be complemented by *profilin* overexpression (Haarer *et al.*, 1993; Vojtek *et al.*, 1991). Expression of *profilin* from the endogenous *C-CAP* locus was well tolerated by blood stages and ookinetes, but failed to complement the *c-cap(-)* specific defects during oocyst development. This result further supports the conclusion that the G-actin sequestering function of C-CAP may not be crucial in oocysts. However, these experiments do not exclude redundant functions between profilin and C-CAP in merozoites or ookinetes, which suffer no or undetectable defects upon *C-CAP* deletion.

4.3. C-CAP and potential actin-independent processes in oocysts

To address a potential “actin-independent” function of C-CAP in *Plasmodium*, Co-immuno precipitation (Co-IP) and subsequent mass spectrum analysis could be performed in order to identify potential interacting proteins. Parasites overexpressing a Flag-tag C-CAP fusion protein in ookinetes, were constructed. These parasites exhibited normal life cycle progression and the characteristic cytoplasmic localization of C-CAP (Fig. 35, 36). These results indicate functionality of the fusion protein and provide a tool for future C-CAP Co-immunoprecipitation experiments.

Potential interaction candidates might include actin II, actin related proteins (ARP), and actin like proteins (ALP), which share the common actin-fold and an overall sequence similarity with actin (Frankel and Mooseker, 1996; Wesseling *et al.*, 1989). *Plasmodium* species express a second actin, termed actinII, which is essential for exflagellation of male gametocytes

(Wesseling *et al.*, 1989, Siden-Kiamos, unpublished). Whether actinII plays a role during oocyst maturation has not been investigated. ARPs are required for a variety of biochemical and structural roles in higher eukaryotic cells, including actin polymerization and branch formation (Frankel and Mooseker, 1996; Machesky *et al.*, 1994; Mahaffy and Pollard, 2006), vesicle transport along microtubuli (Schroer and Sheetz, 1991), cell division (Karki and Holzbaur, 1999), and chromatin remodeling (Shen *et al.*, 2003; Szerlong *et al.*, 2003). In apicomplexa, 10 distinct ARPs have been identified (Gordon and Sibley, 2005). The Arp1 protein is the most conserved member and functions as an integral component of the dynactin complex in eukaryotic cells. It also shares the ATPase activity and the capacity to form short filaments rods of ~40 nm, with actin. A *Plasmodium* homologue, Arp1, is expressed throughout the parasite life cycle and is essential during blood stage development (Siden-Kiamos *et al.*, 2010). Also, six unique species-specific actin-like proteins (ALP) have been identified in apicomplexa, which share no known homologues in other species. The ALP1 protein is dynamically associated with the IMC and exerts a role in daughter cell formation in *Toxoplasma gondii* (Gordon and Sibley, 2008). Possibly, ARP and/or ALPs may be capable to function stage-specifically in *Plasmodium* in otherwise actin-dependent processes.

Another attractive hypothesis is that C-CAP may be a bi-functional molecule that may interact with the actin cytoskeleton and the tubulin cytoskeleton in a stage-specific manner. The G-actin binding capacity was already characterized, and relies on the highly conserved tertiary domain structure, called CARP domain. CARP domains representing tandem repeats, which are shared between the cyclase-associated proteins (CAP), the X-linked retinitis pigmentosa (RP2) proteins and the tubulin cofactor C (TBCC) (Dodatko *et al.*, 2004; Kuhnel *et al.*, 2006). The latter two proteins participate in tubulin biogenesis in eukaryotes. TBCC functions, along with the tubulin cofactors A- D, in assembly of the alpha- and beta- tubulin heterodimer in higher eukaryotic cells (Kirik *et al.*, 2002; Kortazar *et al.*, 2007). Databank research revealed that most tubulin cofactors are encoded by the *Plasmodium* genome (data not shown). The CARP domain is clearly shared between the C-CAP and the TBCC (PBANKA_121410) protein in *P. berghei*. It is thus plausible that both proteins are able to mutually interact via their tertiary structure (Dodatko *et al.*, 2004), creating dimers, and link the cytoskeleton assembly.

4.4. Conservation of the N-terminal part of C-CAP in *Plasmodium* parasites

Initial homology searches in the *Plasmodium* genome and annotation studies of the *C-CAP* gene confirmed an N-terminal truncation, in comparison to CAP proteins in higher eukaryotes (Schuler and Matuschewski, 2006b). However, in the course of annotation updates at the *Plasmodium* genome data bank (PlasmoDB) I identified a protein, which might represent a candidate for the missing N-terminal part in *Plasmodium*. The conserved gene with unknown function (PBANKA_020790, named here *N-CAP*) besides 758 base pairs upstream of the *C-CAP* coding sequence (PBANKA_020800) on the second chromosome of the *Plasmodium berghei* Anka strain. The gene encodes for a 140 amino acid protein with a predicted molecular size of 16,5 kDa. It contains an N-terminal signal peptide (1-21 aa) and two transmembrane domains (TM1 4-26 aa, TM2 88-110 aa). Very interestingly, both genes (*N-CAP* and *C-CAP*) are encoded by two independent open reading frames (ORFs) and represent two distinct proteins in all *Plasmodium* species, except in *P. vivax*. In *P. vivax* one single ORF fuses both genes (PVX_081500) and encodes for one protein, which contains the N-terminal uncharacterized domain and the C-terminal C-CAP domain. Both domains are connected by a linker of 9 x DQRN repeats. The possibility exists that both proteins interact with each other, as if corresponding homologs are transcribed as one gene. Blast searches with the *P. berghei* N-terminal domain did not reveal any predicted homolog in higher eukaryotes. Taking into account that the N-terminal cyclase-associated domain in yeast is not conserved among higher eukaryotes (Hubberstey and Mottillo, 2002), it is therefore plausible that apicomplexa encode the N-terminus as a separate protein with distinct functions.

4.5. A brief conclusion of C-CAP

Taken together, C-CAP is the first characterized G-actin binding protein displaying essential roles during oocyst maturation of the malarial parasite. Defects in this extracellular replication phase, includes attenuation of oocyst growth, of compartmentation, nuclear divisions, and the complete lack of sporozoite development. To what extent the G-actin sequestering activity influences these cellular processes in *Plasmodium* remains to be studied. Motile processes such as invasion and transmigration, displayed by merozoites and ookinetes, do not vitally depend on C-CAP. Proteins with likely redundant functions, like profilin or ADF1/2 can potentially compensate for the loss of C-CAP in these motile stages. The cytoplasmic localization of the C-CAPmCherry protein supports a physiological G-actin sequestering

activity. Trans-species complementation with the *C. parvum* C-CAP proved functional redundancy between apicomplexan CAP proteins. Establishment of the precise cellular defect during oocyst maturation and the exploration of potential biological interaction partners of C-CAP, will open new avenues to understand the relevance of the cytoskeleton during *Plasmodium* differentiation.

4.6. The characterization of the G-actin binding proteins profilin, ADF1 and ADF2

Profilin and ADF/cofilins are key regulators of actin dynamics in eukaryotic cells. Despite their distinct functions on the actin filaments, they regulate the constant cellular actin turnover. *Profilin* and *ADF1* perform essential roles during blood stage development of *Plasmodium berghei* parasites (Kursula *et al.*, 2008; Schuler *et al.*, 2005a), whereas ADF2 is not essential and deletion causes only minor defects during oocyst maturation and liver stage development (Doi *et al.*, 2010).

I characterized their protein abundance throughout the *Plasmodium* life cycle via expression profiling by quantitative RT-PCR, western blotting and indirect immuno microscopy.

Profilin and *ADF1* mRNA levels are clearly the most abundant amongst the *Plasmodium* G-actin binding proteins, which further emphasizes their importance. In accordance with previous data *ADF2* mRNA exhibited the lowest expression levels (Schüler *et al.*, 2005a). All G-actin binding proteins, including C-CAP, displayed a similar expression pattern. The highest expression is observed in merozoites, ookinetes and late liver stages, indicating a potential role during invasion, egress and motility. Interestingly, mRNA levels of all G-actin binding proteins decrease dramatically by 8 to 30 fold during sporozoite development. *Profilin* and *ADF1* transcripts were previously detected in salivary gland sporozoites by RT-PCR (Kursula *et al.*, 2008; Schuler *et al.*, 2005a). However, quantitative RT-PCR revealed a significant downregulation of mRNA in sporozoites, which was not found in previous studies by conventional RT-PCR.

This findings suggests that *Plasmodium* downregulates the expression of the main G-actin binding proteins, profilin, ADF1 and C-CAP, in sporozoites. This result was very surprising, considering the exceptional motility of salivary gland sporozoites and the essentiality of *ADF1* and *profilin* in blood stages. The absence of the profilin protein in midgut- and mature salivary- gland sporozoites was confirmed by western blot analysis. In contrast, the ADF1 protein is detectable in sporozoites. However, transcriptional downregulation led to significantly less protein in sporozoites as compared to ookinetes. Because both transcripts are

expressed at similar levels, this raises the possibility of an additional control of gene expression, i.e. translational silencing of profilin but not of ADF1. The ADF2 protein was not detected in any of the observed stages, which is in agreement with the overall low mRNA levels.

Localization of profilin and ADF1 by immuno fluorescence assays exhibited cytoplasmic distribution that is comparable to C-CAPmCherry. Analogous cytoplasmic localization for ADF1 and profilin has already been shown in *T. gondii* intracellular tachyzoites (Mehta and Sibley, ; Plattner *et al.*, 2008) and *P. falciparum* merozoites (Wong *et al.*). These results are in good agreement with the G-actin sequestering function of both proteins, which is expected to mainly occur in the cytoplasm. Also, the fluorescence signal intensity reflects the respective expression and protein abundance pattern.

Taken together, my results suggest that *Plasmodium* tightly regulates expression and protein abundance in sporozoites. Despite of mRNA downregulation, ADF1 was the only detected G-actin binding protein in this stage. However, I cannot formally exclude very low profilin, ADF2 and C-CAP protein levels, due to the detection limit by western blot analysis. ELISA or proteomic analysis in sporozoite stages would complete my results. Due to the lack of a robust conditional knock out system in *Plasmodium*, genetic evaluation using a promoter exchange strategy may be necessary to specifically delete profilin and other G-actin binding proteins with exception of asexual stages. Further support for the absence of profilin in sporozoites comes from genetically engineered *Plasmodium berghei* parasites that express a fusion protein of *T. gondii* profilin with GFP under the *profilin* endogenous promoter. A prominent GFP signal was readily observed in blood stages, whereas no GFP signal was detected in sporozoites (Katja Müller, personnel communication). This observation further supports the notion that the profilin expression is downregulated and the protein is not abundant in sporozoites.

4.7. The two states of profilin

Interestingly, profilin exhibits a second distinct localization to the periphery of ookinete cells that can be visualized by a polyclonal α *T. gondii* profilin antibody. The *T. gondii* profilin antibody specifically recognizes *P. berghei* and *P. falciparum* profilin, as demonstrated by western blot. It thus appears that the antibody can distinguish between cytosolic and membrane-associated profilin in cells.

In higher eukaryotes profilin regulates the phospholipid metabolism by binding with high affinity to phosphatidy inositol phosphates PI(4,5)P₂ and PI(3,4,5)P₃ at the cell membrane and

inhibiting their cleavage into inositol trisphosphate (IP₃) and diacylglycerol (DAG) by competing with phospholipase C γ 1 (PLC) (Nishizuka, 1986). The profilin::PIP_{2/3} complex interferes with the actin-binding and sequestering activity of profilin. The activation of PLC allows hydrolysis of the complex and releases profilin into the cytoplasm (Goldschmidt-Clermont *et al.*, 1991). In contrast, *P. falciparum* profilin does neither bind to PI(4,5)P₂, nor PI(3,4,5)P₃, but interacts selectively with their precursor molecules phosphoinositol monophosphates (PIPs) and phosphatidyl acid (PA) *in vitro* (Kursula *et al.*, 2008). This binding specificity is likely conferred by the rudimentary structure of the non-conserved PIP binding residues (Kursula *et al.*, 2008). Whether these results can be extrapolated to *in vivo* conditions remains to be seen, particularly since the phosphoinositide profile changes during the intra-erythrocytic development of *P. falciparum* (Tawh *et al.*). It is conceivable, that the minidomain of *P. falciparum* profilin structure determines its function in the phospholipid-metabolism and actin-binding capacity. One attractive hypothesis is that resting cells contain a high amount of profilin::PIP complexes, associated with the plasma membrane and inhibiting fast spontaneous actin filament assembly. After activation of PLC and concomitant hydrolysis of PIP, profilin is released into the cytoplasm to promote actin polymerization, which in turn leads to initiation and/or reinforcement of motility. In intracellular *T. gondii* tachyzoites profilin localizes to the cytoplasm, confirming the findings by Plattner *et al.* (2008). The profilin localization in extracellular *T. gondii* tachyzoites, however, was not clear and needs to be re-examined (Plattner *et al.*, 2008). It would therefore, be interesting to link the spatiotemporal regulation of profilin to motility in the parasite. Time lapse microscopy of moving parasites expressing labeled profilin, combined with inhibition of PLC activity could help to solve this question.

4.8. Overexpression of *C-CAP* and *profilin*

The unexpected absence of profilin and C-CAP in sporozoites, prompted me to test the influence of both proteins in these stages. Therefore, I separately placed both genes under the control of the circum sporozoite protein (*CSP*) promoter and generated stable integrations in clonal parasite lines. This strategy resulted in transgenic parasites expressing two copies of either *C-CAP* or *profilin*, under (i) the endogenous and (ii) the *CSP* promoter. Additional Flag-tagging of both proteins facilitated protein detection by western blot and localization by IFA. Furthermore, the Flag-tag will allow Co-IP experiments and the identification of interaction partners. Control parasites, which overexpress *C-CAP* or *profilin* under the

circumsporozoite- and trombospodin related sporozoite protein (*CTRP*) promoter in ookinetes, where analyzed in parallel.

The introduction of a second copy of either *C-CAP* or *profilin* was well tolerated by the parasites, as revealed by the viability of clonal blood stages.

4.8.1. Overexpression of *C-CAP* and *profilin* in ookinetes does not influence the parasite development in mosquitoes

Ookinete-specific overexpression does not alter the cytoplasmic subcellular localization of the Flag-tagged C-CAP and profilin (Fig. 35). The activity of the *CTRP* promoter is strictly confined to ookinetes, as oocysts and sporozoites did not show any detectable Flag-signal. As predicted, phenotypic characterization displayed normal development of sporozoites, motility and infectivity. These results demonstrate that increasing the amount of C-CAP or profilin protein in stages where both proteins are highly abundant does not interfere with the parasite development. Furthermore, the parasites efficiently downregulate and degrade these proteins, as no residual Flag-signal was detected after ookinete stages. Whether protein overexpression has a minor influence on ookinete motility still needs to be examined. But the fact that *ctrp_flag c-cap/profilin* parasites yield similar amounts of midgut sporozoites, already excludes a major defect in ookinete motility.

4.8.2. Ectopic overexpression in sporozoites abolished salivary gland invasion

The ectopic overexpression of *profilin* and *C-CAP* under the *CSP* promoter was shown by IFA and confirmed by western blotting for profilin. Again, profilin localized to the cytosol of ookinetes. The ectopic expression in midgut sporozoites exhibited cytoplasmic distribution for both proteins as well. However, hemocoel sporozoites displayed a distinct peripheral localization of both proteins (Fig. 37). Transgenic parasites exhibited comparable numbers of midgut sporozoites in the case of profilin overexpression and less numbers for *C-CAP* overexpression. No sporozoites were found in the salivary glands of the mosquitoes and only low numbers of hemocoel sporozoites were counted. These results indicate that ectopic overexpression of *C-CAP* and *profilin* did not influence sporozoite differentiation *per se*, but that sporozoites are impaired in egress from the oocyst and unable to invade the salivary glands. Both observations strongly suggest a motility defect. Motility assays, however, were not yet conclusive at this stage. To further dissect the phenotype, live cell imaging documenting the behavior of hemocoel sporozoites should be performed in the future.

Infectivity can be tested *in vitro* by sporozoite infection of Huh7 cells or *in vivo* by infection experiments to mice. The *CSP* promoter is also active in early liver stages (Singh *et al.*, 2007) and will drive subsequent ectopic expression of *C-CAP* and *profilin*. Whether the peripheral localization in hemocoel sporozoites explains impaired motility requires further investigations. It seems plausible that over saturation of profilin and C-CAP in sporozoites perturbs the equilibrium of actin-turnover and thereby interferes with fast motility. Profilin may bind to various PIP molecules at the membrane and probably inhibits actin filament polymerization. C-CAP saturation may also negatively influence actin polymerization *via* its sequestering activity. It would therefore be helpful to compare the actin localization in sporozoites of both mutants to corroborate actin-specific effects on the motility of these sporozoites.

4.9. Conclusions and the “minimalistic model” for actin regulation in motile sporozoites

This study examined the repertoire of G-actin binding proteins in *Plasmodium* and their contribution to parasite motility. In this regard the sporozoite stage apparently stands out in terms of gliding, invasion, and in terms of actin-regulation. ADF1, ADF2, profilin and C-CAP are most abundant at transcriptomic and proteomic levels in merozoites, ookinetes, and liver stage merozoites suggesting a role in invasion and motility. Surprisingly, my study demonstrated, that all G-actin binding proteins are tightly down regulated in sporozoites. Profilin is, irrespective of its importance for blood stages, not present in sporozoites. The second essential protein, ADF1, is the only detectable G-actin binding protein in this stage. ADF2 and C-Cap are also most likely not abundant, considering the low expression and the live cell imaging data. Furthermore, overexpression of *profilin* and *C-CAP* lead to complete disruption of salivary gland invasion, most likely due to interference with actin-dependent motility.

The combined results strongly favor a hypothesis that places ADF1 as the major actin regulator in sporozoites. It has been shown, that ADF1 is necessary to achieve actin-sequestering activity in *Plasmodium* and *Toxoplasma*, despite only minimal F-actin binding capacity (Mehta and Sibley, ; Wong *et al.*). ADF1 also promotes nucleotide exchange on actin (Schuler *et al.*, 2005a) and ADF/cofilin is able to nucleate actin at high local concentrations (Andrianantoandro and Pollard, 2006). Considering the narrow space between the IMC and the plasma membrane of about 20nm, where the motor machinery, the anchoring proteins, and the F-actin turnover are located, it seems particularly efficient to employ few multifunctional

proteins instead of many specialized proteins. ADF1 in *Plasmodium* seems to exhibit all essential functions necessary for enhancing actin turnover in the absence of competing proteins like profilin. High ADF1 concentrations at the local force traction sides of the gliding sporozoite promote filament nucleation at the barbed end of the actin filament. Formin activity for nucleation cannot be excluded, but no data are available for sporozoites. The short actin filaments are stabilized by the capping protein (Ganter *et al.*, 2009) and thereby ensure the movement of the myosin motor protein along the filament. Severing and depolymerization at the pointed end as well as the nucleotide exchange on actin can again be facilitated by ADF1. According to this model, phosphorylated ADF/cofilin promotes chemotaxis by activation of Phospholipase D1 (PDL1) (Han *et al.*, 2007; Lehman *et al.*, 2006), which could be one mechanism that directs sporozoites through their final destination in the liver. This “minimalistic model” can explain the central aspects for efficient actin-regulation in sporozoites that leads to fast and long-lasting motility.

Actin regulation in the other motile and invasive stages appears to involve a broader spectrum of G-actin binding proteins and resembles other apicomplexan parasites, such as *T. gondii* more closely.

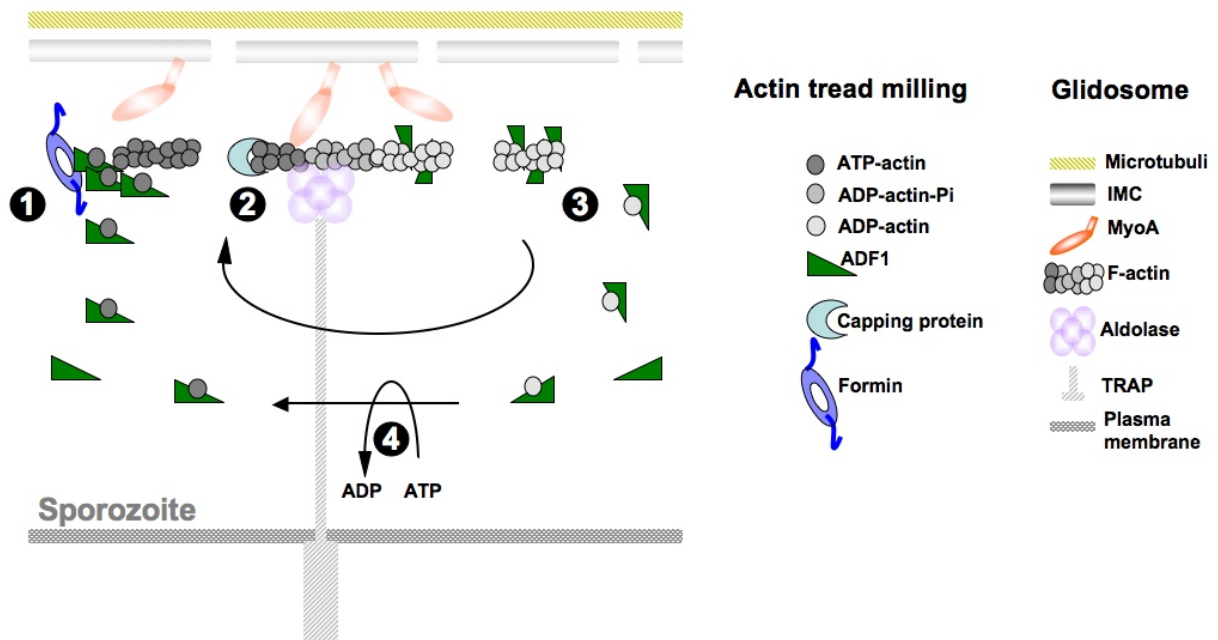


Figure 40: The “minimalistic model” for actin regulation in sporozoites.

The actin-depolymerizing factor (ADF1) as the main player of actin turnover. 1) At high concentrations ADF1 facilitates actin filament nucleation, perhaps supported by formin. 2) Short actin stubs are stabilized by the capping protein (CP), to facilitate the power stroke of MyosinA (MyoA). 3) ADF1 can interact with F-actin and promote severing into short actin fragments and ADP-actin monomers. 4) ADF1 enhances nucleotide exchange on actin to replenish the ATP-actin pool for further rounds of polymerization.

5. References

- Abrahamsen, M.S., Templeton, T.J., Enomoto, S., Abrahante, J.E., Zhu, G., Lancto, C.A., Deng, M., Liu, C., Widmer, G., Tzipori, S., Buck, G.A., Xu, P., Bankier, A.T., Dear, P.H., Konfortov, B.A., Spriggs, H.F., Iyer, L., Anantharaman, V., Aravind, L., and Kapur, V. (2004) Complete genome sequence of the apicomplexan, *Cryptosporidium parvum*. *Science* **304**: 441-445.
- Adini, A., and Warburg, A. (1999) Interaction of *Plasmodium gallinaceum* ookinetes and oocysts with extracellular matrix proteins. *Parasitology* **119** (Pt 4): 331-336.
- Adl, S.M., Simpson, A.G., Farmer, M.A., Andersen, R.A., Anderson, O.R., Barta, J.R., Bowser, S.S., Brugerolle, G., Fensome, R.A., Fredericq, S., James, T.Y., Karpov, S., Kugrens, P., Krug, J., Lane, C.E., Lewis, L.A., Lodge, J., Lynn, D.H., Mann, D.G., McCourt, R.M., Mendoza, L., Moestrup, O., Mozley-Standridge, S.E., Nerad, T.A., Shearer, C.A., Smirnov, A.V., Spiegel, F.W., and Taylor, M.F. (2005) The new higher level classification of eukaryotes with emphasis on the taxonomy of protists. *J Eukaryot Microbiol* **52**: 399-451.
- Aikawa, M., Miller, L.H., Johnson, J., and Rabbege, J. (1978) Erythrocyte entry by malarial parasites. A moving junction between erythrocyte and parasite. *J Cell Biol* **77**: 72-82.
- Al-Olayan, E.M., Beetsma, A.L., Butcher, G.A., Sinden, R.E., and Hurd, H. (2002) Complete development of mosquito phases of the malaria parasite in vitro. *Science* **295**: 677-679.
- Aly, A.S., and Matuschewski, K. (2005) A malarial cysteine protease is necessary for *Plasmodium* sporozoite egress from oocysts. *J Exp Med* **202**: 225-230.
- Amino, R., Thiberge, S., Martin, B., Celli, S., Shorte, S., Frischknecht, F., and Menard, R. (2006) Quantitative imaging of *Plasmodium* transmission from mosquito to mammal. *Nat Med* **12**: 220-224.
- Amino, R., Giovannini, D., Thiberge, S., Gueirard, P., Boisson, B., Dubremetz, J.F., Prevost, M.C., Ishino, T., Yuda, M., and Menard, R. (2008) Host cell traversal is important for progression of the malaria parasite through the dermis to the liver. *Cell Host Microbe* **3**: 88-96.
- Andrianantoandro, E., and Pollard, T.D. (2006) Mechanism of actin filament turnover by severing and nucleation at different concentrations of ADF/cofilin. *Mol Cell* **24**: 13-23.
- Atella, G.C., Bittencourt-Cunha, P.R., Nunes, R.D., Shahabuddin, M., and Silva-Neto, M.A. (2009) The major insect lipoprotein is a lipid source to mosquito stages of malaria parasite. *Acta Trop* **109**: 159-162.
- Azoury, J., Lee, K.W., Georget, V., Rassinier, P., Leader, B., and Verlhac, M.H. (2008) Spindle positioning in mouse oocytes relies on a dynamic meshwork of actin filaments. *Curr Biol* **18**: 1514-1519.
- Balcer, H.I., Goodman, A.L., Rodal, A.A., Smith, E., Kugler, J., Heuser, J.E., and Goode, B.L. (2003) Coordinated regulation of actin filament turnover by a high-molecular-weight Srv2/CAP complex, cofilin, profilin, and Aip1. *Curr Biol* **13**: 2159-2169.
- Bamburg, J.R. (1999) Proteins of the ADF/cofilin family: essential regulators of actin dynamics. *Annu Rev Cell Dev Biol* **15**: 185-230.
- Bannister, L.H., and Mitchell, G.H. (1995) The role of the cytoskeleton in *Plasmodium falciparum* merozoite biology: an electron-microscopic view. *Ann Trop Med Parasitol* **89**: 105-111.
- Barragan, A., and Sibley, L.D. (2003) Migration of *Toxoplasma gondii* across biological barriers. *Trends Microbiol* **11**: 426-430.

- Baton, L.A., and Ranford-Cartwright, L.C. (2005) Spreading the seeds of million-murdering death: metamorphoses of malaria in the mosquito. *Trends Parasitol* **21**: 573-580.
- Baum, B., Li, W., and Perrimon, N. (2000) A cyclase-associated protein regulates actin and cell polarity during *Drosophila* oogenesis and in yeast. *Curr Biol* **10**: 964-973.
- Baum, J., Papenfuss, A.T., Baum, B., Speed, T.P., and Cowman, A.F. (2006a) Regulation of apicomplexan actin-based motility. *Nat Rev Microbiol* **4**: 621-628.
- Baum, J., Richard, D., Healer, J., Rug, M., Krnajska, Z., Gilberger, T.W., Green, J.L., Holder, A.A., and Cowman, A.F. (2006b) A conserved molecular motor drives cell invasion and gliding motility across malaria life cycle stages and other apicomplexan parasites. *J Biol Chem* **281**: 5197-5208.
- Baum, J., Gilberger, T.W., Frischknecht, F., and Meissner, M. (2008a) Host-cell invasion by malaria parasites: insights from *Plasmodium* and *Toxoplasma*. *Trends Parasitol* **24**: 557-563.
- Baum, J., Tonkin, C.J., Paul, A.S., Rug, M., Smith, B.J., Gould, S.B., Richard, D., Pollard, T.D., and Cowman, A.F. (2008b) A malaria parasite formin regulates actin polymerization and localizes to the parasite-erythrocyte moving junction during invasion. *Cell Host Microbe* **3**: 188-198.
- Bearer, E.L. (1991) Direct observation of actin filament severing by gelsolin and binding by gCap39 and CapZ. *J Cell Biol* **115**: 1629-1638.
- Bergman, L.W., Kaiser, K., Fujioka, H., Coppens, I., Daly, T.M., Fox, S., Matuschewski, K., Nussenzweig, V., and Kappe, S.H. (2003) Myosin A tail domain interacting protein (MTIP) localizes to the inner membrane complex of *Plasmodium* sporozoites. *J Cell Sci* **116**: 39-49.
- Bertling, E., Quintero-Monzon, O., Mattila, P.K., Goode, B.L., and Lappalainen, P. (2007) Mechanism and biological role of profilin-Srv2/CAP interaction. *J Cell Sci* **120**: 1225-1234.
- Billker, O., Shaw, M.K., Margos, G., and Sinden, R.E. (1997) The roles of temperature, pH and mosquito factors as triggers of male and female gametogenesis of *Plasmodium berghei* in vitro. *Parasitology* **115** (Pt 1): 1-7.
- Blanchoin, L., and Pollard, T.D. (1999) Mechanism of interaction of *Acanthamoeba* actophorin (ADF/Cofilin) with actin filaments. *J Biol Chem* **274**: 15538-15546.
- Blanchoin, L., Robinson, R.C., Choe, S., and Pollard, T.D. (2000) Phosphorylation of *Acanthamoeba* actophorin (ADF/cofilin) blocks interaction with actin without a change in atomic structure. *J Mol Biol* **295**: 203-211.
- Blanchoin, L., and Pollard, T.D. (2002) Hydrolysis of ATP by polymerized actin depends on the bound divalent cation but not profilin. *Biochemistry* **41**: 597-602.
- Blandin, S.A., Marois, E., and Levashina, E.A. (2008) Antimalarial responses in *Anopheles gambiae*: from a complement-like protein to a complement-like pathway. *Cell Host Microbe* **3**: 364-374.
- Blume, M., Hliscs, M., Rodriguez-Contreras, D., Sanchez, M., Landfear, S., Lucius, R., Matuschewski, K., and Gupta, N. A constitutive pan-hexose permease for the *Plasmodium* life cycle and transgenic models for screening of antimalarial sugar analogs. *Faseb J* **25**: 1218-1229.
- Bubb, M.R., Senderowicz, A.M., Sausville, E.A., Duncan, K.L., and Korn, E.D. (1994) Jasplakinolide, a cytotoxic natural product, induces actin polymerization and competitively inhibits the binding of phalloidin to F-actin. *J Biol Chem* **269**: 14869-14871.
- Burkhard, P., Stetefeld, J., and Strelkov, S.V. (2001) Coiled coils: a highly versatile protein folding motif. *Trends Cell Biol* **11**: 82-88.

- Buscaglia, C.A., Coppens, I., Hol, W.G., and Nussenzweig, V. (2003) Sites of interaction between aldolase and thrombospondin-related anonymous protein in plasmodium. *Mol Biol Cell* **14**: 4947-4957.
- Buscaglia, C.A., Hol, W.G., Nussenzweig, V., and Cardozo, T. (2007) Modeling the interaction between aldolase and the thrombospondin-related anonymous protein, a key connection of the malaria parasite invasion machinery. *Proteins* **66**: 528-537.
- Bushell, E.S., Ecker, A., Schlegelmilch, T., Goulding, D., Dougan, G., Sinden, R.E., Christophides, G.K., Kafatos, F.C., and Vlachou, D. (2009) Paternal effect of the nuclear formin-like protein MISFIT on Plasmodium development in the mosquito vector. *PLoS Pathog* **5**: e1000539.
- Caldwell, J.E., Heiss, S.G., Mermall, V., and Cooper, J.A. (1989) Effects of CapZ, an actin capping protein of muscle, on the polymerization of actin. *Biochemistry* **28**: 8506-8514.
- Canning, E.U., and Sinden, R.E. (1973) The organization of the ookinete and observations on nuclear division in oocysts of Plasmodium berghei. *Parasitology* **67**: 29-40.
- Carlier, M.F., and Pantaloni, D. (1986) Direct evidence for ADP-Pi-F-actin as the major intermediate in ATP-actin polymerization. Rate of dissociation of Pi from actin filaments. *Biochemistry* **25**: 7789-7792.
- Carlier, M.F. (1990) Actin polymerization and ATP hydrolysis. *Adv Biophys* **26**: 51-73.
- Carlier, M.F., and Pantaloni, D. (1997) Control of actin dynamics in cell motility. *J Mol Biol* **269**: 459-467.
- Carlsson, L., Nystrom, L.E., Sundkvist, I., Markey, F., and Lindberg, U. (1977) Actin polymerizability is influenced by profilin, a low molecular weight protein in non-muscle cells. *J Mol Biol* **115**: 465-483.
- Chaudhary, A., Chen, J., Gu, Q.M., Witke, W., Kwiatkowski, D.J., and Prestwich, G.D. (1998) Probing the phosphoinositide 4,5-bisphosphate binding site of human profilin I. *Chem Biol* **5**: 273-281.
- Chaudhry, F., Little, K., Talarico, L., Quintero-Monzon, O., and Goode, B.L. A central role for the WH2 domain of Srv2/CAP in recharging actin monomers to drive actin turnover in vitro and in vivo. *Cytoskeleton (Hoboken)* **67**: 120-133.
- Cintra, W.M., and De Souza, W. (1985) Immunocytochemical localization of cytoskeletal proteins and electron microscopy of detergent extracted tachyzoites of Toxoplasma gondii. *J Submicrosc Cytol* **17**: 503-508.
- Cooper, J.A. (1987) Effects of cytochalasin and phalloidin on actin. *J Cell Biol* **105**: 1473-1478.
- Cooper, J.A., and Sept, D. (2008) New insights into mechanism and regulation of actin capping protein. *Int Rev Cell Mol Biol* **267**: 183-206.
- Coppi, A., Natarajan, R., Pradel, G., Bennett, B.L., James, E.R., Roggero, M.A., Corradin, G., Persson, C., Tewari, R., and Sinnis, P. The malaria circumsporozoite protein has two functional domains, each with distinct roles as sporozoites journey from mosquito to mammalian host. *J Exp Med* **208**: 341-356.
- Daher, W., Plattner, F., Carlier, M.F., and Soldati-Favre, D. Concerted action of two formins in gliding motility and host cell invasion by Toxoplasma gondii. *PLoS Pathog* **6**.
- Daher, W., and Soldati-Favre, D. (2009) Mechanisms controlling glideosome function in apicomplexans. *Curr Opin Microbiol* **12**: 408-414.
- de Koning-Ward, T.F., Fidock, D.A., Thathy, V., Menard, R., van Spaendonk, R.M., Waters, A.P., and Janse, C.J. (2000) The selectable marker human dihydrofolate reductase enables sequential genetic manipulation of the Plasmodium berghei genome. *Mol Biochem Parasitol* **106**: 199-212.

- Deeks, M.J., Rodrigues, C., Dimmock, S., Ketelaar, T., Maciver, S.K., Malho, R., and Hussey, P.J. (2007) Arabidopsis CAP1 - a key regulator of actin organisation and development. *J Cell Sci* **120**: 2609-2618.
- Dessens, J.T., Beetsma, A.L., Dimopoulos, G., Wengelnik, K., Crisanti, A., Kafatos, F.C., and Sinden, R.E. (1999) CTRP is essential for mosquito infection by malaria ookinetes. *Embo J* **18**: 6221-6227.
- Dessens, J.T., Mendoza, J., Claudianos, C., Vinetz, J.M., Khater, E., Hassard, S., Ranawaka, G.R., and Sinden, R.E. (2001) Knockout of the rodent malaria parasite chitinase pbCHT1 reduces infectivity to mosquitoes. *Infect Immun* **69**: 4041-4047.
- Dobrowolski, J., and Sibley, L.D. (1997) The role of the cytoskeleton in host cell invasion by *Toxoplasma gondii*. *Behring Inst Mitt*: 90-96.
- Dobrowolski, J.M., and Sibley, L.D. (1996) *Toxoplasma* invasion of mammalian cells is powered by the actin cytoskeleton of the parasite. *Cell* **84**: 933-939.
- Dodatko, T., Fedorov, A.A., Grynberg, M., Patskovsky, Y., Rozwarski, D.A., Jaroszewski, L., Aronoff-Spencer, E., Kondraskina, E., Irving, T., Godzik, A., and Almo, S.C. (2004) Crystal structure of the actin binding domain of the cyclase-associated protein. *Biochemistry* **43**: 10628-10641.
- Doi, Y., Shinzawa, N., Fukumoto, S., Okano, H., and Kanuka, H. ADF2 is required for transformation of the ookinete and sporozoite in malaria parasite development. *Biochem Biophys Res Commun* **397**: 668-672.
- Drees, B.L., Sundin, B., Brazeau, E., Caviston, J.P., Chen, G.C., Guo, W., Kozminski, K.G., Lau, M.W., Moskow, J.J., Tong, A., Schenkman, L.R., McKenzie, A., 3rd, Brennwald, P., Longtine, M., Bi, E., Chan, C., Novick, P., Boone, C., Pringle, J.R., Davis, T.N., Fields, S., and Drubin, D.G. (2001) A protein interaction map for cell polarity development. *J Cell Biol* **154**: 549-571.
- Drenckhahn, D., and Pollard, T.D. (1986) Elongation of actin filaments is a diffusion-limited reaction at the barbed end and is accelerated by inert macromolecules. *J Biol Chem* **261**: 12754-12758.
- Dumont, J., Million, K., Sunderland, K., Rassinier, P., Lim, H., Leader, B., and Verlhac, M.H. (2007) Formin-2 is required for spindle migration and for the late steps of cytokinesis in mouse oocytes. *Dev Biol* **301**: 254-265.
- Evangelista, M., Pruyne, D., Amberg, D.C., Boone, C., and Bretscher, A. (2002) Formins direct Arp2/3-independent actin filament assembly to polarize cell growth in yeast. *Nat Cell Biol* **4**: 260-269.
- Evangelista, M., Zigmond, S., and Boone, C. (2003) Formins: signaling effectors for assembly and polarization of actin filaments. *J Cell Sci* **116**: 2603-2611.
- Fagarasanu, A., and Rachubinski, R.A. (2007) Orchestrating organelle inheritance in *Saccharomyces cerevisiae*. *Curr Opin Microbiol* **10**: 528-538.
- Fedor-Chaiken, M., Deschenes, R.J., and Broach, J.R. (1990) SRV2, a gene required for RAS activation of adenylate cyclase in yeast. *Cell* **61**: 329-340.
- Fedorov, A.A., Magnus, K.A., Graupe, M.H., Lattman, E.E., Pollard, T.D., and Almo, S.C. (1994) X-ray structures of isoforms of the actin-binding protein profilin that differ in their affinity for phosphatidylinositol phosphates. *Proc Natl Acad Sci U S A* **91**: 8636-8640.
- Field, J., Vojtek, A., Ballester, R., Bolger, G., Colicelli, J., Ferguson, K., Gerst, J., Kataoka, T., Michaeli, T., Powers, S., and et al. (1990) Cloning and characterization of CAP, the *S. cerevisiae* gene encoding the 70 kd adenylyl cyclase-associated protein. *Cell* **61**: 319-327.
- Field, S.J., Pinder, J.C., Clough, B., Dluzewski, A.R., Wilson, R.J., and Gratzer, W.B. (1993) Actin in the merozoite of the malaria parasite, *Plasmodium falciparum*. *Cell Motil Cytoskeleton* **25**: 43-48.

- Forney, J.R., Vaughan, D.K., Yang, S., and Healey, M.C. (1998) Actin-dependent motility in *Cryptosporidium parvum* sporozoites. *J Parasitol* **84**: 908-913.
- Frankel, S., and Mooseker, M.S. (1996) The actin-related proteins. *Curr Opin Cell Biol* **8**: 30-37.
- Freeman, N.L., Lila, T., Mintzer, K.A., Chen, Z., Pahk, A.J., Ren, R., Drubin, D.G., and Field, J. (1996) A conserved proline-rich region of the *Saccharomyces cerevisiae* cyclase-associated protein binds SH3 domains and modulates cytoskeletal localization. *Mol Cell Biol* **16**: 548-556.
- Freeman, N.L., and Field, J. (2000) Mammalian homolog of the yeast cyclase associated protein, CAP/Srv2p, regulates actin filament assembly. *Cell Motil Cytoskeleton* **45**: 106-120.
- Frevert, U., Engelmann, S., Zougbede, S., Stange, J., Ng, B., Matuschewski, K., Liebes, L., and Yee, H. (2005) Intravital observation of *Plasmodium berghei* sporozoite infection of the liver. *PLoS Biol* **3**: e192.
- Frischknecht, F., Baldacci, P., Martin, B., Zimmer, C., Thiberge, S., Olivo-Marin, J.C., Shorte, S.L., and Menard, R. (2004) Imaging movement of malaria parasites during transmission by *Anopheles* mosquitoes. *Cell Microbiol* **6**: 687-694.
- Galletta, B.J., and Cooper, J.A. (2009) Actin and endocytosis: mechanisms and phylogeny. *Curr Opin Cell Biol* **21**: 20-27.
- Gandhi, M., and Goode, B.L. (2008) Coronin: the double-edged sword of actin dynamics. *Subcell Biochem* **48**: 72-87.
- Ganter, M., Schuler, H., and Matuschewski, K. (2009) Vital role for the *Plasmodium* actin capping protein (CP) beta-subunit in motility of malaria sporozoites. *Mol Microbiol* **74**: 1356-1367.
- Gardner, M.J., Hall, N., Fung, E., White, O., Berriman, M., Hyman, R.W., Carlton, J.M., Pain, A., Nelson, K.E., Bowman, S., Paulsen, I.T., James, K., Eisen, J.A., Rutherford, K., Salzberg, S.L., Craig, A., Kyes, S., Chan, M.S., Nene, V., Shallom, S.J., Suh, B., Peterson, J., Angiuoli, S., Pertea, M., Allen, J., Selengut, J., Haft, D., Mather, M.W., Vaidya, A.B., Martin, D.M., Fairlamb, A.H., Fraunholz, M.J., Roos, D.S., Ralph, S.A., McFadden, G.I., Cummings, L.M., Subramanian, G.M., Mungall, C., Venter, J.C., Carucci, D.J., Hoffman, S.L., Newbold, C., Davis, R.W., Fraser, C.M., and Barrell, B. (2002) Genome sequence of the human malaria parasite *Plasmodium falciparum*. *Nature* **419**: 498-511.
- Gerst, J.E., Ferguson, K., Vojtek, A., Wigler, M., and Field, J. (1991) CAP is a bifunctional component of the *Saccharomyces cerevisiae* adenylate cyclase complex. *Mol Cell Biol* **11**: 1248-1257.
- Gieselmann, R., and Mann, K. (1992) ASP-56, a new actin sequestering protein from pig platelets with homology to CAP, an adenylate cyclase-associated protein from yeast. *FEBS Lett* **298**: 149-153.
- Gohla, A., and Bokoch, G.M. (2002) 14-3-3 regulates actin dynamics by stabilizing phosphorylated cofilin. *Curr Biol* **12**: 1704-1710.
- Gohla, A., Birkenfeld, J., and Bokoch, G.M. (2005) Chronophin, a novel HAD-type serine protein phosphatase, regulates cofilin-dependent actin dynamics. *Nat Cell Biol* **7**: 21-29.
- Goldschmidt-Clermont, P.J., Machesky, L.M., Doberstein, S.K., and Pollard, T.D. (1991) Mechanism of the interaction of human platelet profilin with actin. *J Cell Biol* **113**: 1081-1089.
- Goldschmidt-Clermont, P.J., Furman, M.I., Wachsstock, D., Safer, D., Nachmias, V.T., and Pollard, T.D. (1992) The control of actin nucleotide exchange by thymosin beta 4 and profilin. A potential regulatory mechanism for actin polymerization in cells. *Mol Biol Cell* **3**: 1015-1024.

- Gordon, J.L., and Sibley, L.D. (2005) Comparative genome analysis reveals a conserved family of actin-like proteins in apicomplexan parasites. *BMC Genomics* **6**: 179.
- Gottwald, U., Brokamp, R., Karakesisoglou, I., Schleicher, M., and Noegel, A.A. (1996) Identification of a cyclase-associated protein (CAP) homologue in Dictyostelium discoideum and characterization of its interaction with actin. *Mol Biol Cell* **7**: 261-272.
- Haarer, B.K., Petzold, A.S., and Brown, S.S. (1993) Mutational analysis of yeast profilin. *Mol Cell Biol* **13**: 7864-7873.
- Han, L., Stope, M.B., de Jesus, M.L., Oude Weernink, P.A., Urban, M., Wieland, T., Roskopf, D., Mizuno, K., Jakobs, K.H., and Schmidt, M. (2007) Direct stimulation of receptor-controlled phospholipase D1 by phospho-cofilin. *Embo J* **26**: 4189-4202.
- Heintzelman, M.B., and Schwartzman, J.D. (1997) A novel class of unconventional myosins from Toxoplasma gondii. *J Mol Biol* **271**: 139-146.
- Herm-Gotz, A., Weiss, S., Stratmann, R., Fujita-Becker, S., Ruff, C., Meyhofer, E., Soldati, T., Manstein, D.J., Geeves, M.A., and Soldati, D. (2002) Toxoplasma gondii myosin A and its light chain: a fast, single-headed, plus-end-directed motor. *Embo J* **21**: 2149-2158.
- Higashida, C., Miyoshi, T., Fujita, A., Ocegüera-Yanez, F., Monypenny, J., Andou, Y., Narumiya, S., and Watanabe, N. (2004) Actin polymerization-driven molecular movement of mDia1 in living cells. *Science* **303**: 2007-2010.
- Higgs, H.N., and Pollard, T.D. (2001) Regulation of actin filament network formation through ARP2/3 complex: activation by a diverse array of proteins. *Annu Rev Biochem* **70**: 649-676.
- Hliscs, M., Sattler, J.M., Tempel, W., Artz, J.D., Dong, A., Hui, R., Matuschewski, K., and Schuler, H. Structure and function of a G-actin sequestering protein with a vital role in malaria oocyst development inside the mosquito vector. *J Biol Chem* **285**: 11572-11583.
- Hubberstey, A., Yu, G., Loewith, R., Lakusta, C., and Young, D. (1996) Mammalian CAP interacts with CAP, CAP2, and actin. *J Cell Biochem* **61**: 459-466.
- Hubberstey, A.V., and Mottillo, E.P. (2002) Cyclase-associated proteins: CAPacity for linking signal transduction and actin polymerization. *Faseb J* **16**: 487-499.
- Huttu, J., Singh, B.K., Bhargav, S.P., Sattler, J.M., Schuler, H., and Kursula, I. Crystallization and preliminary structural characterization of the two actin-depolymerization factors of the malaria parasite. *Acta Crystallogr Sect F Struct Biol Cryst Commun* **66**: 583-587.
- Isenberg, G., Aebi, U., and Pollard, T.D. (1980) An actin-binding protein from Acanthamoeba regulates actin filament polymerization and interactions. *Nature* **288**: 455-459.
- Ishino, T., Orito, Y., Chinzei, Y., and Yuda, M. (2006) A calcium-dependent protein kinase regulates Plasmodium ookinete access to the midgut epithelial cell. *Mol Microbiol* **59**: 1175-1184.
- Janse, C.J., Franke-Fayard, B., and Waters, A.P. (2006a) Selection by flow-sorting of genetically transformed, GFP-expressing blood stages of the rodent malaria parasite, Plasmodium berghei. *Nat Protoc* **1**: 614-623.
- Janse, C.J., Ramesar, J., and Waters, A.P. (2006b) High-efficiency transfection and drug selection of genetically transformed blood stages of the rodent malaria parasite Plasmodium berghei. *Nat Protoc* **1**: 346-356.
- Jewett, T.J., and Sibley, L.D. (2003) Aldolase forms a bridge between cell surface adhesins and the actin cytoskeleton in apicomplexan parasites. *Mol Cell* **11**: 885-894.
- Jockusch, B.M., Murk, K., and Rothkegel, M. (2007) The profile of profilins. *Rev Physiol Biochem Pharmacol* **159**: 131-149.
- Johnson, T.M., Rajfur, Z., Jacobson, K., and Beckers, C.J. (2007) Immobilization of the type XIV myosin complex in Toxoplasma gondii. *Mol Biol Cell* **18**: 3039-3046.

- Kadota, K., Ishino, T., Matsuyama, T., Chinzei, Y., and Yuda, M. (2004) Essential role of membrane-attack protein in malarial transmission to mosquito host. *Proc Natl Acad Sci U S A* **101**: 16310-16315.
- Kaksonen, M., Toret, C.P., and Drubin, D.G. (2006) Harnessing actin dynamics for clathrin-mediated endocytosis. *Nat Rev Mol Cell Biol* **7**: 404-414.
- Kamasaki, T., Arai, R., Osumi, M., and Mabuchi, I. (2005) Directionality of F-actin cables changes during the fission yeast cell cycle. *Nat Cell Biol* **7**: 916-917.
- Kamasaki, T., Osumi, M., and Mabuchi, I. (2007) Three-dimensional arrangement of F-actin in the contractile ring of fission yeast. *J Cell Biol* **178**: 765-771.
- Karki, S., and Holzbaur, E.L. (1999) Cytoplasmic dynein and dynactin in cell division and intracellular transport. *Curr Opin Cell Biol* **11**: 45-53.
- Kato, T., Watanabe, N., Morishima, Y., Fujita, A., Ishizaki, T., and Narumiya, S. (2001) Localization of a mammalian homolog of diaphanous, mDia1, to the mitotic spindle in HeLa cells. *J Cell Sci* **114**: 775-784.
- Kirik, V., Mathur, J., Grini, P.E., Klinkhammer, I., Adler, K., Bechtold, N., Herzog, M., Bonneville, J.M., and Hulskamp, M. (2002) Functional analysis of the tubulin-folding cofactor C in *Arabidopsis thaliana*. *Curr Biol* **12**: 1519-1523.
- Kobielak, A., Pasolli, H.A., and Fuchs, E. (2004) Mammalian formin-1 participates in adherens junctions and polymerization of linear actin cables. *Nat Cell Biol* **6**: 21-30.
- Kortazar, D., Fanarraga, M.L., Carranza, G., Bellido, J., Villegas, J.C., Avila, J., and Zabala, J.C. (2007) Role of cofactors B (TBCB) and E (TBCE) in tubulin heterodimer dissociation. *Exp Cell Res* **313**: 425-436.
- Kovar, D.R., Kuhn, J.R., Tichy, A.L., and Pollard, T.D. (2003) The fission yeast cytokinesis formin Cdc12p is a barbed end actin filament capping protein gated by profilin. *J Cell Biol* **161**: 875-887.
- Kovar, D.R., Wu, J.Q., and Pollard, T.D. (2005) Profilin-mediated competition between capping protein and formin Cdc12p during cytokinesis in fission yeast. *Mol Biol Cell* **16**: 2313-2324.
- Kudryashev, M., Lepper, S., Baumeister, W., Cyrklaff, M., and Frischknecht, F. Geometric constrains for detecting short actin filaments by cryogenic electron tomography. *PMC Biophys* **3**: 6.
- Kuhnel, K., Veltel, S., Schlichting, I., and Wittinghofer, A. (2006) Crystal structure of the human retinitis pigmentosa 2 protein and its interaction with Arl3. *Structure* **14**: 367-378.
- Kursula, I., Kursula, P., Ganter, M., Panjekar, S., Matuschewski, K., and Schuler, H. (2008) Structural basis for parasite-specific functions of the divergent profilin of *Plasmodium falciparum*. *Structure* **16**: 1638-1648.
- Lambrechts, A., Verschelde, J.L., Jonckheere, V., Goethals, M., Vandekerckhove, J., and Ampe, C. (1997) The mammalian profilin isoforms display complementary affinities for PIP2 and proline-rich sequences. *Embo J* **16**: 484-494.
- Lassing, I., and Lindberg, U. (1985) Specific interaction between phosphatidylinositol 4,5-bisphosphate and profilactin. *Nature* **314**: 472-474.
- Lee, L., Klee, S.K., Evangelista, M., Boone, C., and Pellman, D. (1999) Control of mitotic spindle position by the *Saccharomyces cerevisiae* formin Bni1p. *J Cell Biol* **144**: 947-961.
- Lehane, M.J., Aksoy, S., and Levashina, E. (2004) Immune responses and parasite transmission in blood-feeding insects. *Trends Parasitol* **20**: 433-439.
- Lehman, N., Di Fulvio, M., McCray, N., Campos, I., Tabatabaian, F., and Gomez-Cambronero, J. (2006) Phagocyte cell migration is mediated by phospholipases PLD1 and PLD2. *Blood* **108**: 3564-3572.

- Lemgruber, L., Kloetzel, J.A., Souza, W., and Vommoro, R.C. (2009) Toxoplasma gondii: further studies on the subpellicular network. *Mem Inst Oswaldo Cruz* **104**: 706-709.
- Levashina, E.A. (2004) Immune responses in Anopheles gambiae. *Insect Biochem Mol Biol* **34**: 673-678.
- Lila, T., and Drubin, D.G. (1997) Evidence for physical and functional interactions among two Saccharomyces cerevisiae SH3 domain proteins, an adenyl cyclase-associated protein and the actin cytoskeleton. *Mol Biol Cell* **8**: 367-385.
- Loisel, T.P., Boujemaa, R., Pantaloni, D., and Carlier, M.F. (1999) Reconstitution of actin-based motility of Listeria and Shigella using pure proteins. *Nature* **401**: 613-616.
- Machesky, L.M., Atkinson, S.J., Ampe, C., Vandekerckhove, J., and Pollard, T.D. (1994) Purification of a cortical complex containing two unconventional actins from Acanthamoeba by affinity chromatography on profilin-agarose. *J Cell Biol* **127**: 107-115.
- Machesky, L.M., Mullins, R.D., Higgs, H.N., Kaiser, D.A., Blanchoin, L., May, R.C., Hall, M.E., and Pollard, T.D. (1999) Scar, a WASp-related protein, activates nucleation of actin filaments by the Arp2/3 complex. *Proc Natl Acad Sci U S A* **96**: 3739-3744.
- Mahaffy, R.E., and Pollard, T.D. (2006) Kinetics of the formation and dissociation of actin filament branches mediated by Arp2/3 complex. *Biophys J* **91**: 3519-3528.
- Mann, T., and Beckers, C. (2001) Characterization of the subpellicular network, a filamentous membrane skeletal component in the parasite Toxoplasma gondii. *Mol Biochem Parasitol* **115**: 257-268.
- Martin, S.G., and Chang, F. (2006) Dynamics of the formin for3p in actin cable assembly. *Curr Biol* **16**: 1161-1170.
- Maruyama, K., and Obinata, T. (1965) Presence of Beta-Actinin in the Soluble Fraction of the Muscle Cells of the Chick Embryo. *J Biochem* **57**: 575-577.
- Mattila, P.K., Quintero-Monzon, O., Kugler, J., Moseley, J.B., Almo, S.C., Lappalainen, P., and Goode, B.L. (2004) A high-affinity interaction with ADP-actin monomers underlies the mechanism and in vivo function of Srv2/cyclase-associated protein. *Mol Biol Cell* **15**: 5158-5171.
- Matuschewski, K., Mota, M.M., Pinder, J.C., Nussenzweig, V., and Kappe, S.H. (2001) Identification of the class XIV myosins Pb-MyoA and Py-MyoA and expression in Plasmodium sporozoites. *Mol Biochem Parasitol* **112**: 157-161.
- Matuschewski, K., Nunes, A.C., Nussenzweig, V., and Menard, R. (2002) Plasmodium sporozoite invasion into insect and mammalian cells is directed by the same dual binding system. *Embo J* **21**: 1597-1606.
- McGough, A., Pope, B., Chiu, W., and Weeds, A. (1997) Cofilin changes the twist of F-actin: implications for actin filament dynamics and cellular function. *J Cell Biol* **138**: 771-781.
- Mehta, S., and Sibley, L.D. Actin depolymerizing factor controls actin turnover and gliding motility in Toxoplasma gondii. *Mol Biol Cell* **22**: 1290-1299.
- Mehta, S., and Sibley, L.D. Toxoplasma gondii actin depolymerizing factor acts primarily to sequester G-actin. *J Biol Chem* **285**: 6835-6847.
- Meissner, M., Schluter, D., and Soldati, D. (2002) Role of Toxoplasma gondii myosin A in powering parasite gliding and host cell invasion. *Science* **298**: 837-840.
- Menard, R., and Janse, C. (1997) Gene targeting in malaria parasites. *Methods* **13**: 148-157.
- Menard, R., Sultan, A.A., Cortes, C., Altszuler, R., van Dijk, M.R., Janse, C.J., Waters, A.P., Nussenzweig, R.S., and Nussenzweig, V. (1997) Circumsporozoite protein is required for development of malaria sporozoites in mosquitoes. *Nature* **385**: 336-340.
- Mendes, A.M., Schlegelmilch, T., Cohuet, A., Awono-Ambene, P., De Iorio, M., Fontenille, D., Morlais, I., Christophides, G.K., Kafatos, F.C., and Vlachou, D. (2008) Conserved

- mosquito/parasite interactions affect development of *Plasmodium falciparum* in Africa. *PLoS Pathog* **4**: e1000069.
- Miller, L.H., Aikawa, M., Johnson, J.G., and Shiroishi, T. (1979) Interaction between cytochalasin B-treated malarial parasites and erythrocytes. Attachment and junction formation. *J Exp Med* **149**: 172-184.
- Mizuno, Y., Makioka, A., Kawazu, S., Kano, S., Kawai, S., Akaki, M., Aikawa, M., and Ohtomo, H. (2002) Effect of jasplakinolide on the growth, invasion, and actin cytoskeleton of *Plasmodium falciparum*. *Parasitol Res* **88**: 844-848.
- Mockrin, S.C., and Korn, E.D. (1980) Acanthamoeba profilin interacts with G-actin to increase the rate of exchange of actin-bound adenosine 5'-triphosphate. *Biochemistry* **19**: 5359-5362.
- Moon, R.W., Taylor, C.J., Bex, C., Schepers, R., Goulding, D., Janse, C.J., Waters, A.P., Baker, D.A., and Billker, O. (2009) A cyclic GMP signalling module that regulates gliding motility in a malaria parasite. *PLoS Pathog* **5**: e1000599.
- Moriyama, K., and Yahara, I. (2002) Human CAP1 is a key factor in the recycling of cofilin and actin for rapid actin turnover. *J Cell Sci* **115**: 1591-1601.
- Morrison, D.A. (2009) Evolution of the Apicomplexa: where are we now? *Trends Parasitol* **25**: 375-382.
- Morrisette, N.S., and Roos, D.S. (1998) *Toxoplasma gondii*: a family of apical antigens associated with the cytoskeleton. *Exp Parasitol* **89**: 296-303.
- Morrisette, N.S., and Sibley, L.D. (2002) Cytoskeleton of apicomplexan parasites. *Microbiol Mol Biol Rev* **66**: 21-38; table of contents.
- Moseley, J.B., Sagot, I., Manning, A.L., Xu, Y., Eck, M.J., Pellman, D., and Goode, B.L. (2004) A conserved mechanism for Bni1- and mDia1-induced actin assembly and dual regulation of Bni1 by Bud6 and profilin. *Mol Biol Cell* **15**: 896-907.
- Mota, M.M., Pradel, G., Vanderberg, J.P., Hafalla, J.C., Frevert, U., Nussenzweig, R.S., Nussenzweig, V., and Rodriguez, A. (2001) Migration of *Plasmodium* sporozoites through cells before infection. *Science* **291**: 141-144.
- Natarajan, R., Thathy, V., Mota, M.M., Hafalla, J.C., Menard, R., and Vernick, K.D. (2001) Fluorescent *Plasmodium berghei* sporozoites and pre-erythrocytic stages: a new tool to study mosquito and mammalian host interactions with malaria parasites. *Cell Microbiol* **3**: 371-379.
- Nishida, Y., Shima, F., Sen, H., Tanaka, Y., Yanagihara, C., Yamawaki-Kataoka, Y., Kariya, K., and Kataoka, T. (1998) Coiled-coil interaction of N-terminal 36 residues of cyclase-associated protein with adenyl cyclase is sufficient for its function in *Saccharomyces cerevisiae* ras pathway. *J Biol Chem* **273**: 28019-28024.
- Nishizuka, Y. (1986) Studies and perspectives of protein kinase C. *Science* **233**: 305-312.
- Niwa, R., Nagata-Ohashi, K., Takeichi, M., Mizuno, K., and Uemura, T. (2002) Control of actin reorganization by Slingshot, a family of phosphatases that dephosphorylate ADF/cofilin. *Cell* **108**: 233-246.
- Oliferenko, S., Chew, T.G., and Balasubramanian, M.K. (2009) Positioning cytokinesis. *Genes Dev* **23**: 660-674.
- Otomo, T., Tomchick, D.R., Otomo, C., Panchal, S.C., Machius, M., and Rosen, M.K. (2005) Structural basis of actin filament nucleation and processive capping by a formin homology 2 domain. *Nature* **433**: 488-494.
- Otto, I.M., Raabe, T., Rennefahrt, U.E., Bork, P., Rapp, U.R., and Kerkhoff, E. (2000) The p150-Spir protein provides a link between c-Jun N-terminal kinase function and actin reorganization. *Curr Biol* **10**: 345-348.
- Pimenta, P.F., Touray, M., and Miller, L. (1994) The journey of malaria sporozoites in the mosquito salivary gland. *J Eukaryot Microbiol* **41**: 608-624.

- Plattner, F., Yarovinsky, F., Romero, S., Didry, D., Carlier, M.F., Sher, A., and Soldati-Favre, D. (2008) Toxoplasma profilin is essential for host cell invasion and TLR11-dependent induction of an interleukin-12 response. *Cell Host Microbe* **3**: 77-87.
- Pollard, T.D. (1986) Rate constants for the reactions of ATP- and ADP-actin with the ends of actin filaments. *J Cell Biol* **103**: 2747-2754.
- Pollard, T.D., and Borisy, G.G. (2003) Cellular motility driven by assembly and disassembly of actin filaments. *Cell* **112**: 453-465.
- Pollard, T.D. (2007) Regulation of actin filament assembly by Arp2/3 complex and formins. *Annu Rev Biophys Biomol Struct* **36**: 451-477.
- Pradel, G., and Frevert, U. (2001) Malaria sporozoites actively enter and pass through rat Kupffer cells prior to hepatocyte invasion. *Hepatology* **33**: 1154-1165.
- Pruyne, D., Evangelista, M., Yang, C., Bi, E., Zigmond, S., Bretscher, A., and Boone, C. (2002) Role of formins in actin assembly: nucleation and barbed-end association. *Science* **297**: 612-615.
- Pruyne, D., Legesse-Miller, A., Gao, L., Dong, Y., and Bretscher, A. (2004) Mechanisms of polarized growth and organelle segregation in yeast. *Annu Rev Cell Dev Biol* **20**: 559-591.
- Quinlan, M.E., Heuser, J.E., Kerkhoff, E., and Mullins, R.D. (2005) Drosophila Spire is an actin nucleation factor. *Nature* **433**: 382-388.
- Quintero-Monzon, O., Jonasson, E.M., Bertling, E., Talarico, L., Chaudhry, F., Sihvo, M., Lappalainen, P., and Goode, B.L. (2009) Reconstitution and dissection of the 600-kDa Srv2/CAP complex: roles for oligomerization and cofilin-actin binding in driving actin turnover. *J Biol Chem* **284**: 10923-10934.
- Reinhard, M., Giehl, K., Abel, K., Haffner, C., Jarchau, T., Hoppe, V., Jockusch, B.M., and Walter, U. (1995) The proline-rich focal adhesion and microfilament protein VASP is a ligand for profilins. *Embo J* **14**: 1583-1589.
- Riveline, D., Zamir, E., Balaban, N.Q., Schwarz, U.S., Ishizaki, T., Narumiya, S., Kam, Z., Geiger, B., and Bershadsky, A.D. (2001) Focal contacts as mechanosensors: externally applied local mechanical force induces growth of focal contacts by an mDial1-dependent and ROCK-independent mechanism. *J Cell Biol* **153**: 1175-1186.
- Romero, S., Le Clainche, C., Didry, D., Egile, C., Pantaloni, D., and Carlier, M.F. (2004) Formin is a processive motor that requires profilin to accelerate actin assembly and associated ATP hydrolysis. *Cell* **119**: 419-429.
- Rono, M.K., Whitten, M.M., Oulad-Abdelghani, M., Levashina, E.A., and Marois, E. The major yolk protein vitellogenin interferes with the anti-plasmodium response in the malaria mosquito Anopheles gambiae. *PLoS Biol* **8**: e1000434.
- Rosenblatt, J., Peluso, P., and Mitchison, T.J. (1995) The bulk of unpolymerized actin in Xenopus egg extracts is ATP-bound. *Mol Biol Cell* **6**: 227-236.
- Russell, D.G., and Sinden, R.E. (1981) The role of the cytoskeleton in the motility of coccidian sporozoites. *J Cell Sci* **50**: 345-359.
- Saarikangas, J., Zhao, H., and Lappalainen, P. Regulation of the actin cytoskeleton-plasma membrane interplay by phosphoinositides. *Physiol Rev* **90**: 259-289.
- Safer, D., and Nachmias, V.T. (1994) Beta thymosins as actin binding peptides. *Bioessays* **16**: 590.
- Sahoo, N., Beatty, W., Heuser, J., Sept, D., and Sibley, L.D. (2006) Unusual kinetic and structural properties control rapid assembly and turnover of actin in the parasite Toxoplasma gondii. *Mol Biol Cell* **17**: 895-906.
- Sattler, J.M., Ganter, M., Hliscs, M., Matuschewski, K., and Schuler, H. Actin regulation in the malaria parasite. *Eur J Cell Biol*.

- Schafer, D.A., Gill, S.R., Cooper, J.A., Heuser, J.E., and Schroer, T.A. (1994) Ultrastructural analysis of the dynactin complex: an actin-related protein is a component of a filament that resembles F-actin. *J Cell Biol* **126**: 403-412.
- Schmitz, S., Schaap, I.A., Kleinjung, J., Harder, S., Grainger, M., Calder, L., Rosenthal, P.B., Holder, A.A., and Veigel, C. Malaria parasite actin polymerization and filament structure. *J Biol Chem* **285**: 36577-36585.
- Schmitz, S., Grainger, M., Howell, S., Calder, L.J., Gaeb, M., Pinder, J.C., Holder, A.A., and Veigel, C. (2005) Malaria parasite actin filaments are very short. *J Mol Biol* **349**: 113-125.
- Schroer, T.A., and Sheetz, M.P. (1991) Two activators of microtubule-based vesicle transport. *J Cell Biol* **115**: 1309-1318.
- Schuler, H., Mueller, A.K., and Matuschewski, K. (2005a) A Plasmodium actin-depolymerizing factor that binds exclusively to actin monomers. *Mol Biol Cell* **16**: 4013-4023.
- Schuler, H., Mueller, A.K., and Matuschewski, K. (2005b) Unusual properties of Plasmodium falciparum actin: new insights into microfilament dynamics of apicomplexan parasites. *FEBS Lett* **579**: 655-660.
- Schuler, H., and Matuschewski, K. (2006a) Plasmodium motility: actin not actin' like actin. *Trends Parasitol* **22**: 146-147.
- Schuler, H., and Matuschewski, K. (2006b) Regulation of apicomplexan microfilament dynamics by a minimal set of actin-binding proteins. *Traffic* **7**: 1433-1439.
- Shaw, M.K., and Tilney, L.G. (1999) Induction of an acrosomal process in Toxoplasma gondii: visualization of actin filaments in a protozoan parasite. *Proc Natl Acad Sci U S A* **96**: 9095-9099.
- Shen, X., Ranallo, R., Choi, E., and Wu, C. (2003) Involvement of actin-related proteins in ATP-dependent chromatin remodeling. *Mol Cell* **12**: 147-155.
- Sherman, I.W. (1985) Membrane structure and function of malaria parasites and the infected erythrocyte. *Parasitology* **91** (Pt 3): 609-645.
- Siden-Kiamos, I., Ecker, A., Nyback, S., Louis, C., Sinden, R.E., and Billker, O. (2006a) Plasmodium berghei calcium-dependent protein kinase 3 is required for ookinete gliding motility and mosquito midgut invasion. *Mol Microbiol* **60**: 1355-1363.
- Siden-Kiamos, I., Pinder, J.C., and Louis, C. (2006b) Involvement of actin and myosins in Plasmodium berghei ookinete motility. *Mol Biochem Parasitol* **150**: 308-317.
- Silvie, O., Mota, M.M., Matuschewski, K., and Prudencio, M. (2008) Interactions of the malaria parasite and its mammalian host. *Curr Opin Microbiol* **11**: 352-359.
- Sinden, R.E., and Garnham, P.C. (1973) A comparative study on the ultrastructure of Plasmodium sporozoites within the oocyst and salivary glands, with particular reference to the incidence of the micropore. *Trans R Soc Trop Med Hyg* **67**: 631-637.
- Sinden, R.E. (1974) Excystment by sporozoites of malaria parasites. *Nature* **252**: 314.
- Sinden, R.E., Butcher, G.A., and Beetsma, A.L. (2002) Maintenance of the Plasmodium berghei life cycle. *Methods Mol Med* **72**: 25-40.
- Singh, A.P., Buscaglia, C.A., Wang, Q., Levay, A., Nussenzweig, D.R., Walker, J.R., Winzeler, E.A., Fujii, H., Fontoura, B.M., and Nussenzweig, V. (2007) Plasmodium circumsporozoite protein promotes the development of the liver stages of the parasite. *Cell* **131**: 492-504.
- Slavic, K., Straschil, U., Reininger, L., Doerig, C., Morin, C., Tewari, R., and Krishna, S. Life cycle studies of the hexose transporter of Plasmodium species and genetic validation of their essentiality. *Mol Microbiol* **75**: 1402-1413.
- Small, J.V. (1995) Getting the actin filaments straight: nucleation-release or treadmilling? *Trends Cell Biol* **5**: 52-55.

- Smythe, E., and Ayscough, K.R. (2006) Actin regulation in endocytosis. *J Cell Sci* **119**: 4589-4598.
- Smythe, W.A., Joiner, K.A., and Hoppe, H.C. (2008) Actin is required for endocytic trafficking in the malaria parasite *Plasmodium falciparum*. *Cell Microbiol* **10**: 452-464.
- Soldati, D., Foth, B.J., and Cowman, A.F. (2004) Molecular and functional aspects of parasite invasion. *Trends Parasitol* **20**: 567-574.
- Srinivasan, P., Fujioka, H., and Jacobs-Lorena, M. (2008) PbCap380, a novel oocyst capsule protein, is essential for malaria parasite survival in the mosquito. *Cell Microbiol* **10**: 1304-1312.
- Staiger, C.J., Sheahan, M.B., Khurana, P., Wang, X., McCurdy, D.W., and Blanchoin, L. (2009) Actin filament dynamics are dominated by rapid growth and severing activity in the *Arabidopsis* cortical array. *J Cell Biol* **184**: 269-280.
- Starnes, G.L., Coincon, M., Sygusch, J., and Sibley, L.D. (2009) Aldolase is essential for energy production and bridging adhesin-actin cytoskeletal interactions during parasite invasion of host cells. *Cell Host Microbe* **5**: 353-364.
- Sultan, A.A., Thathy, V., Frevert, U., Robson, K.J., Crisanti, A., Nussenzweig, V., Nussenzweig, R.S., and Menard, R. (1997) TRAP is necessary for gliding motility and infectivity of *plasmodium* sporozoites. *Cell* **90**: 511-522.
- Sun, H.Q., Yamamoto, M., Mejillano, M., and Yin, H.L. (1999) Gelsolin, a multifunctional actin regulatory protein. *J Biol Chem* **274**: 33179-33182.
- Svitkina, T.M., Verkhovsky, A.B., McQuade, K.M., and Borisy, G.G. (1997) Analysis of the actin-myosin II system in fish epidermal keratocytes: mechanism of cell body translocation. *J Cell Biol* **139**: 397-415.
- Svitkina, T.M., and Borisy, G.G. (1999) Arp2/3 complex and actin depolymerizing factor/cofilin in dendritic organization and treadmilling of actin filament array in lamellipodia. *J Cell Biol* **145**: 1009-1026.
- Szerlong, H., Saha, A., and Cairns, B.R. (2003) The nuclear actin-related proteins Arp7 and Arp9: a dimeric module that cooperates with architectural proteins for chromatin remodeling. *Embo J* **22**: 3175-3187.
- Tardieux, I., Liu, X., Poupel, O., Parzy, D., Dehoux, P., and Langsley, G. (1998) A *Plasmodium falciparum* novel gene encoding a coronin-like protein which associates with actin filaments. *FEBS Lett* **441**: 251-256.
- Tawk, L., Chicanne, G., Dubremetz, J.F., Richard, V., Payrastre, B., Vial, H.J., Roy, C., and Wengelnik, K. Phosphatidylinositol 3-phosphate, an essential lipid in *Plasmodium*, localizes to the food vacuole membrane and the apicoplast. *Eukaryot Cell* **9**: 1519-1530.
- Terzakis, J.A., Sprinz, H., and Ward, R.A. (1967) The transformation of the *Plasmodium gallinaceum* oocyst in *Aedes aegypti* mosquitoes. *J Cell Biol* **34**: 311-326.
- Thathy, V., Fujioka, H., Gantt, S., Nussenzweig, R., Nussenzweig, V., and Menard, R. (2002) Levels of circumsporozoite protein in the *Plasmodium* oocyst determine sporozoite morphology. *Embo J* **21**: 1586-1596.
- Thathy, V., and Menard, R. (2002) Gene targeting in *Plasmodium berghei*. *Methods Mol Med* **72**: 317-331.
- Tilney, L.G., and Inoue, S. (1985) Acrosomal reaction of the Thyone sperm. III. The relationship between actin assembly and water influx during the extension of the acrosomal process. *J Cell Biol* **100**: 1273-1283.
- Tolliday, N., Bouquin, N., and Li, R. (2001) Assembly and regulation of the cytokinetic apparatus in budding yeast. *Curr Opin Microbiol* **4**: 690-695.

- Tominaga, T., Sahai, E., Chardin, P., McCormick, F., Courtneidge, S.A., and Alberts, A.S. (2000) Diaphanous-related formins bridge Rho GTPase and Src tyrosine kinase signaling. *Mol Cell* **5**: 13-25.
- van Dijk, M.R., Waters, A.P., and Janse, C.J. (1995) Stable transfection of malaria parasite blood stages. *Science* **268**: 1358-1362.
- Vanderberg, J., and Rhodin, J. (1967) Differentiation of nuclear and cytoplasmic fine structure during sporogonic development of *Plasmodium berghei*. *J Cell Biol* **32**: C7-10.
- Vanderberg, J.P. (1974) Studies on the motility of *Plasmodium* sporozoites. *J Protozool* **21**: 527-537.
- Vanderberg, J.P., and Frevert, U. (2004) Intravital microscopy demonstrating antibody-mediated immobilisation of *Plasmodium berghei* sporozoites injected into skin by mosquitoes. *Int J Parasitol* **34**: 991-996.
- Vaughan, A.M., O'Neill, M.T., Tarun, A.S., Camargo, N., Phuong, T.M., Aly, A.S., Cowman, A.F., and Kappe, S.H. (2009) Type II fatty acid synthesis is essential only for malaria parasite late liver stage development. *Cell Microbiol* **11**: 506-520.
- Vaughan, J.A., Noden, B.H., and Beier, J.C. (1992) Population dynamics of *Plasmodium falciparum* sporogony in laboratory-infected *Anopheles gambiae*. *J Parasitol* **78**: 716-724.
- Vedadi, M., Lew, J., Artz, J., Amani, M., Zhao, Y., Dong, A., Wasney, G.A., Gao, M., Hills, T., Brokx, S., Qiu, W., Sharma, S., Diassiti, A., Alam, Z., Melone, M., Mulichak, A., Wernimont, A., Bray, J., Loppnau, P., Plotnikova, O., Newberry, K., Sundararajan, E., Houston, S., Walker, J., Tempel, W., Bochkarev, A., Kozieradzki, I., Edwards, A., Arrowsmith, C., Roos, D., Kain, K., and Hui, R. (2007) Genome-scale protein expression and structural biology of *Plasmodium falciparum* and related Apicomplexan organisms. *Mol Biochem Parasitol* **151**: 100-110.
- Vidali, L., van Gisbergen, P.A., Guerin, C., Franco, P., Li, M., Burkart, G.M., Augustine, R.C., Blanchoin, L., and Bezanilla, M. (2009) Rapid formin-mediated actin-filament elongation is essential for polarized plant cell growth. *Proc Natl Acad Sci U S A* **106**: 13341-13346.
- Vojtek, A., Haarer, B., Field, J., Gerst, J., Pollard, T.D., Brown, S., and Wigler, M. (1991) Evidence for a functional link between profilin and CAP in the yeast *S. cerevisiae*. *Cell* **66**: 497-505.
- Volkman, N., Amann, K.J., Stoilova-McPhie, S., Egile, C., Winter, D.C., Hazelwood, L., Heuser, J.E., Li, R., Pollard, T.D., and Hanein, D. (2001) Structure of Arp2/3 complex in its activated state and in actin filament branch junctions. *Science* **293**: 2456-2459.
- Waller, B.J., and Alberts, A.S. (2003) The formins: active scaffolds that remodel the cytoskeleton. *Trends Cell Biol* **13**: 435-446.
- Wang, W., Goswami, S., Sahai, E., Wyckoff, J.B., Segall, J.E., and Condeelis, J.S. (2005) Tumor cells caught in the act of invading: their strategy for enhanced cell motility. *Trends Cell Biol* **15**: 138-145.
- Warburg, A., and Miller, L.H. (1992) Sporogonic development of a malaria parasite in vitro. *Science* **255**: 448-450.
- Warburg, A., and Schneider, I. (1993) In vitro culture of the mosquito stages of *Plasmodium falciparum*. *Exp Parasitol* **76**: 121-126.
- Watanabe, N., Madaule, P., Reid, T., Ishizaki, T., Watanabe, G., Kakizuka, A., Saito, Y., Nakao, K., Jockusch, B.M., and Narumiya, S. (1997) p140mDia, a mammalian homolog of *Drosophila* diaphanous, is a target protein for Rho small GTPase and is a ligand for profilin. *Embo J* **16**: 3044-3056.
- Watanabe, N., and Higashida, C. (2004) Formins: processive cappers of growing actin filaments. *Exp Cell Res* **301**: 16-22.

- Waters, A.P., Thomas, A.W., van Dijk, M.R., and Janse, C.J. (1997) Transfection of malaria parasites. *Methods* **13**: 134-147.
- Weathersby, A.B. (1952) The role of the stomach wall in the exogenous development of *Plasmodium gallinaceum* as studies by means of haemocoel injections of susceptible and refractory mosquitoes. *J Infect Dis* **91**: 198-205.
- Weaver, A.M., Young, M.E., Lee, W.L., and Cooper, J.A. (2003) Integration of signals to the Arp2/3 complex. *Curr Opin Cell Biol* **15**: 23-30.
- Wegner, A. (1976) Head to tail polymerization of actin. *J Mol Biol* **108**: 139-150.
- Welch, M.D., and Mullins, R.D. (2002) Cellular control of actin nucleation. *Annu Rev Cell Dev Biol* **18**: 247-288.
- Wellington, A., Emmons, S., James, B., Calley, J., Grover, M., Tolia, P., and Manseau, L. (1999) Spire contains actin binding domains and is related to ascidian posterior end mark-5. *Development* **126**: 5267-5274.
- Wesseling, J.G., Snijders, P.J., van Someren, P., Jansen, J., Smits, M.A., and Schoenmakers, J.G. (1989) Stage-specific expression and genomic organization of the actin genes of the malaria parasite *Plasmodium falciparum*. *Mol Biochem Parasitol* **35**: 167-176.
- Wetzel, D.M., Hakansson, S., Hu, K., Roos, D., and Sibley, L.D. (2003) Actin filament polymerization regulates gliding motility by apicomplexan parasites. *Mol Biol Cell* **14**: 396-406.
- Witke, W. (2004) The role of profilin complexes in cell motility and other cellular processes. *Trends Cell Biol* **14**: 461-469.
- Wong, W., Skau, C.T., Marapana, D.S., Hanssen, E., Taylor, N.L., Riglar, D.T., Zuccala, E.S., Angrisano, F., Lewis, H., Catimel, B., Clarke, O.B., Kershaw, N.J., Perugini, M.A., Kovar, D.R., Gulbis, J.M., and Baum, J. Minimal requirements for actin filament disassembly revealed by structural analysis of malaria parasite actin-depolymerizing factor 1. *Proc Natl Acad Sci U S A* **108**: 9869-9874.
- Xu, Y., Moseley, J.B., Sagot, I., Poy, F., Pellman, D., Goode, B.L., and Eck, M.J. (2004) Crystal structures of a Formin Homology-2 domain reveal a tethered dimer architecture. *Cell* **116**: 711-723.
- Yasuda, T., Yagita, K., Nakamura, T., and Endo, T. (1988) Immunocytochemical localization of actin in *Toxoplasma gondii*. *Parasitol Res* **75**: 107-113.
- Yonezawa, N., Nishida, E., Iida, K., Yahara, I., and Sakai, H. (1990) Inhibition of the interactions of cofilin, destrin, and deoxyribonuclease I with actin by phosphoinositides. *J Biol Chem* **265**: 8382-8386.
- Yoshida, N., Potocnjak, P., Nussenzweig, V., and Nussenzweig, R.S. (1981) Biosynthesis of Pb44, the protective antigen of sporozoites of *Plasmodium berghei*. *J Exp Med* **154**: 1225-1236.
- Yuda, M., Sakaida, H., and Chinzei, Y. (1999) Targeted disruption of the *plasmodium berghei* CTRP gene reveals its essential role in malaria infection of the vector mosquito. *J Exp Med* **190**: 1711-1716.

6. Appendix

6.1. Short report

The circum sporozoite protein (CSP) is already expressed in ookinetes

The CSP protein plays crucial roles in sporozoite development and maturation (Menard *et al.*, 1997; Thathy *et al.*, 2002). It furthermore is suggested that this protein interacts with and targets both, the mosquito salivary glands and the mammalian liver cells (Amino *et al.*, 2008; Frevert *et al.*, 2005; Mota *et al.*, 2001; Singh *et al.*, 2007). Thus far it was reported, that CSP protein expression starts at day 6 of oocyst development and first appears at the inner membrane of the oocyst capsule, where it is important for the sporozoite formation and maturation.

During this study the CSP protein was widely used as loading control for sporozoite and ookinete stages in western blot analysis. Consistently, the CSP protein was detected already in ookinetes as a single band with a specific molecular mass of ~52 kDa (Fig. 41 and Fig. 37, 32, 30), which represents the premature, non-cleaved CSP protein (Coppi *et al.*, ; Yoshida *et al.*, 1981). Later, in sporozoite stages the CSP protein matures by proteolytical cleavage and is detected as a double band with molecular sizes of ~52 and ~44 kDa by western blot analysis (Fig. 40).

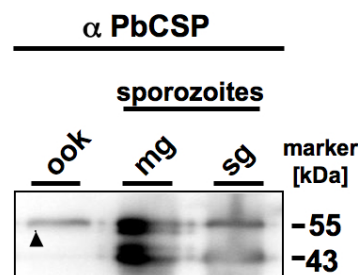


Figure 41. The circumsporozoite protein (CSP) is expressed in ookinetes.

Samples from ookinetes (ook) and midgut- (mg) and salivary gland- (sg) sporozoites were separated in a 15 % SDS-PAGE, blotted on PVDF membrane and detected by α -PbCSP antibody in western blot analysis. Molecular sizes (kDa) are indicated at the left. The premature CSP is detected with 52 kDa (arrow).

The localization and function of the premature CSP protein in ookinetes, is not known thus far.

Interestingly, previous data reveal CSP mRNA expression and the presence of the premature protein in blood stages (Sabine Engelmann, dissertation 2005) and was also discussed by (Natarajan *et al.*, 2001). Since the CSP is important for infection and one of the major vaccine candidates, it is

important to understand the process that leads to the cleavage and protein maturation in sporozoite stages. The contributing protease remains to be identified. My results suggest the use of correlative proteomics between ookinetes and sporozoites may therefore be helpful to identify the CSP-processing maturase.